Optical Pulse Processing Towards Tb/s High-Speed Photonic Systems

A thesis submitted in Partial Fulfilment of the Requirements
for the Degree of Doctor of Philosophy
(Electronic Engineering)

By
Aisling Clarke
B. Eng., MIEEE

School of Electronic Engineering
Faculty of Engineering and Computing
Dublin City University

Research Supervisor
Prof. Liam P. Barry

August 2007

DECLARATION

I hereby certify that this material, which I now submit for assessment on the programme of study leading to the award of Doctor of Philosophy is entirely my own work and has not been taken from the work of others save and to the extent that such work has been cited and acknowledged within the text of my work.

Signed: _____

ID No.: _____

Date: _____

APPROVAL

Name:	Aisling Clarke
Degree:	Doctor of Philosophy (Electronic Engineering)
Title of Thesis:	Optical Pulse Processing Towards Tb/s High-Speed Photonic Systems
Chairperson:	Dr. Sean Marlow
Internal Examiner:	Prof. John Costello
External Examiner:	Prof. Ian Bennion

For my parents and Ray.

Ni heolas go haontios

- There is no knowledge without unity

ACKNOWLEDGEMENTS

This thesis brings to a close four enjoyable years of work and I would like to take this moment to express my gratitude to all those who made it possible for me to complete it.

First and foremost, I would very much like to thank Prof. Liam Barry, my supervisor and guide throughout my PhD, for all the selfless time and effort he has afforded me. Because of his support I have been able to achieve a wonderful goal in my life.

My boyfriend Ray has been a constant pillar of support, encouragement and laughter, which I can not explain in words. I would dearly like to thank him with all my heart for being such a great part of my life.

I owe a great deal to my parents, Bríd and Leo. They continue to inspire me in every way of life and with all their love they have shown me how to succeed in all of life's challenges. Go raibh míle maith agaibh. Many thanks and lots of appreciation must go to my older brothers and sisters, Niamh, Fergal, Deirdre, and Kevin. Their guidance and advice has always spurred me on to make the best choices. Special gratitude must also go to the other members of my family, Clare, Paul, Jiing Tarng, John, Kristen, Jordan, Cian, Genevieve, and Catherine.

I am indebted to all past, present and honouree members of the Radio and Optics Lab: Prince, Ola, Paul, Brendan, Damien, Frank, Celine, Rob, Eoin C., Eoin K., Mark, Krzystof, Doug, Sylwester, Karl, Ciara, and Ling. Thank you so much for your help but most importantly for your friendship. I would also like to thank the staff from the School of Electronic Engineering, and particular mention must go to Pascal Landais, Robert Clare, Ger Considine, and Billy Roarty.

Finally, I would also like to acknowledge the kind hospitality of my colleagues from collaborating Photonics Groups namely Auckland University, University of Limerick, ENSSAT/PERSYST, Bristol University and Tyndall, University College Cork.

Aisling Clarke,
August 2007

TABLE OF CONTENTS

LIST OF FIGURES

LIST OF TABLES

LIST OF ACRONYMS

3R	Reamplify, Reshape, Retime
ASE	Amplified Spontaneous Emission
ASK	Amplitude-Shift Keying
AWG	Arrayed Waveguide Grating
B2B	Back-to-Back
BER	Bit Error Rate
BPF	Bandpass Filter
BSF	Blue Shifted Filtering
CCD	Charge Coupled Device
CCKW	Counter Clockwise
CD	Chromatic Dispersion
CE	Conversion Efficiency
CH	Carrier Heating
CKW	Clockwise
CW	Continuous Wave
DBR	Distributed Bragg Reflector
DC	Direct Current
DCA	Digital Communications Analyser
DCF	Dispersion Compensating Fibre
DFB	Distributed Feedback
DFG	Difference Frequency Generation
DI	Differential Interferometer
DRA	Distributed Raman Amplifier
DSL	Digital Subscriber Line
DWDM	Dense Wavelength Division Multiplexing
EAM	Electro-Absorption Modulator
ECL	External Cavity Laser
ED	Error Detector
EDFA	Erbium Doped Fibre Amplifier
EI	External Injection
ER	Extinction Ratio

FBG	Fibre Bragg Grating
FCA	Free Carrier Absorption
FDM	Frequency Division Multiplexing
FP	Fabry–Pérot
FPA	Fabry–Pérot Amplifier
FROG	Frequency-Resolved Optical Gating
FSK	Frequency-Shift Keying
FTTH	Fibre-to-the-Home
FWHM	Full Width Half Maximum
FWM	Four Wave Mixing
GDR	Group Delay Ripple
GVD	Group Velocity Dispersion
HDTV	High-Definition Television
ICT	Information and Communications Technology
ISI	Inter Symbol Interference
ITU	International Telecommunications Union
L FBG	Linear Fibre Bragg Gratings
LEF	Linewidth Enhancement Factor
$LiNbO_3$	Lithium Niobate
MEMS	Micro-Electro-Mechanical Systems
MPN	Mode Partition Noise
MQW	Multi-Quantum Well
MZI	Mach Zehnder Interferometer
MZM	Mach Zehnder Modulator
NALM	Nonlinear Amplifying Loop Mirror
NL FBG	Nonlinearly Chirped Fibre Bragg Grating
NOLM	Nonlinear Optical Loop Mirror
NRZ	Non Return-to-Zero
ODL	Optical Delay Line
OECD	Organisation for Economic Co-operation and Development
OEO	Optical-Electronic-Optical
OOK	On-Off Keying
OSA	Optical Spectrum Analyser
OSNR	Optical Signal-to-Noise Ratio

OTDM	Optical Time Division Multiplexing
PBS	Polarisation Beam Splitter
PC	Polarisation Controller
PMD	Polarisation Mode Dispersion
PPG	Pulse Pattern Generator
P_{sat}	Saturation Power
PSK	Phase-Shift Keying
PRBS	Pseudo Random Bit Sequence
PROF	Pulse Reformatting Optical Filter
QW	Quantum Well
RF	Radio Frequency
rms	root-mean-square
RSF	Red Shifted Filtering
RZ	Return-to-Zero
SA	Saturable Absorber
SDH	Synchronous Digital Hierarchy
SHB	Spectral Hole Burning
SHG	Second Harmonic Generation
SLA	Semiconductor Laser Amplifier
SLALOM	Semiconductor Laser Amplifier in a Loop Optical Mirror
SMSR	Side Mode Suppression Ratio
SMZI	Symmetric Mach-Zehnder Interferometer
SNR	Signal-to-Noise Ratio
SOA	Semiconductor Optical Amplifier
SONET	Synchronous Optical Network
SPM	Self Phase Modulation
SRS	Stimulated Raman Scattering
TBG	Tunable Bragg Grating
TBP	Time-Bandwidth-Product
TE	Transverse Electric
TM	Transverse Magnetic
TMLL	Tunable Mode-Locked Laser
TOAD	Terahertz Optical Amplifier Demultiplexer
TPA	Two Photon Absorption

TPSR	Temporal Pedestal Suppression Ratio
TWA	Travelling Wave Amplifier
UNI	Ultrafast Nonlinear Interferometer
UV	Ultra-violet
VOA	Variable Optical Attenuator
WDM	Wavelength Division Multiplexing
XGM	Cross Gain Modulation
XPM	Cross Phase Modulation

ABSTRACT – OPTICAL PULSE PROCESSING TOWARDS TB/S HIGH-SPEED PHOTONIC SYSTEMS

Aisling Clarke

B.Eng., MIEEE

Due to the continued growth of high-bandwidth services provided by the internet, there is a requirement to operate individual line rates in excess of 100 Gb/s in next generation optical communications systems. Thus, to implement these high-speed optical networks all-optical processing techniques are necessary for pulse shaping and pulse routing. Two sub-systems (pulse generation and wavelength conversion), which exploit optical processing techniques are explored within this thesis.

Future systems will require high-quality pulse sources and this thesis develops the pulse generation technique of gain switching to provide simple and cost efficient pulse sources. The poor pulse quality typically associated with gain switching is enhanced by developing all-optical methods. The main attribute of the first pulse generation scheme presented is its wavelength tunability over 50 nm. The novelty of the second scheme lies in the ability to design a grating which has a nonlinear chirp profile exactly opposite to the gain-switched pulses. This grating used in conjunction with the gain-switched laser generates transform limited pulses suitable for 80 Gb/s systems. Furthermore the use of a vertical microcavity-based saturable absorber to suppress detrimental temporal pulse pedestals of a pulse source is investigated.

Next generation networks will require routing of data in the optical domain, which can be accomplished by high-speed all-optical wavelength converters. A semiconductor optical amplifier (SOA) is an ideal device to carry out wavelength conversion. In this thesis pulses following propagation through an SOA are experimentally characterised to examine the temporal and spectral dynamics due to the nonlinear response of the SOA. High-speed wavelength conversion is presented using SOA-based shifted filtering. For the first time 80 Gb/s error-free performance was obtained using cross phase modulation in conjunction with blue spectral shifted filtering. In addition an important attribute of this work experimentally examines the temporal profile and phase of the SOA-based shifted filtering wavelength converted signals. Thus the contribution and effect of ultrafast carrier dynamics associated with SOAs is presented.

INTRODUCTION

The continued growth and demand for high-bandwidth to the home and business spurred on by new multimedia applications and file sharing, is stimulating the further development of high-speed optical fibre communications systems. In comparison to other bandwidth providing solutions, optical fibre systems are the top competitor due to its ability to provide almost limitless capacity. Therefore, there is a requirement to develop and research all-optical subsystems that will be required as components in future optical networks. Two such all-optical subsystems are optical pulse sources and wavelength converters. This thesis develops a high quality optical pulse source, investigates its performance in a high-speed test-bed and explores a semiconductor optical amplifier (SOA)-based wavelength conversion scheme in-depth.

Main Contributions

The main contributions of this work are:

- **Development of Optical Techniques to Achieve High Quality Pulse Generation –** Pulse generation techniques based principally on the method of gain switching are demonstrated. The first source exhibits high wavelength tunability, up to 50 nm, with excellent side mode suppression ratio (SMSR) and low jitter, providing a source suitable for future wavelength division multiplexing (WDM) and optical time division multiplexing (OTDM) systems. A second gain switching source is presented which uses a tailor-made nonlinearly chirped grating to achieve transform limited 3.5 ps pulses suitable for use in an 80 Gb/s OTDM system. The novelty of this source lies in the experimental method used to find the chirp profile of the fibre Bragg grating (FBG) to achieve full compensation of the nonlinear chirp of the gain-switched pulse. In addition, we investigated the technique of a vertical microcavity based saturable absorber (SA) to improve the temporal quality of a pulse source. In particular the nonlinear transfer function of the SA results in a large reduction of pulse temporal pedestals which are detrimental to the quality of pulse sources. Thus it is shown that the inclusion of a SA in high-speed pulse source results in an overall system performance enhancement.
- **High-Speed Implementation and Characterisation of an SOA-based Wavelength Conversion Scheme –** 80 Gb/s error-free polarity preserved wavelength conversion was achieved by implementing simple cross gain

modulation (XGM)/cross phase modulation (XPM) in an SOA in conjunction with shifted filtering. In contrast to other similar shifted filtering wavelength conversion schemes, the technique presented is advantageous in that the polarity of the output signal is preserved, the scheme exhibits polarisation independence, and the set-up has a very simple configuration. Optimisation and comparison of the filter placement in order to retain the red or blue spectral components of the filtering assisted schemes is presented. In particular a frequency-resolved optical gating (FROG) characterisation of the wavelength converted signals is given to provide enhanced understanding of the gain and phase dynamics of the SOA which contribute to the shape and performance of the wavelength converted pulses.

Outline of the Thesis

This section outlines the content of this thesis which is divided into six chapters as follows:

- **Chapter 1** outlines the motivation for the development of future high-speed optical communications systems. Future direction points towards the implementation of systems capable of operating at higher bit rates per channel to reduce cost and complexity of networks. Thus all-optical systems may be required to overcome the limited speed of electronics and/or provide a more cost-efficient alternative to electronic processes. An overview of multiplexing schemes which are presently used and which will be used in the future such as electrical time division multiplexing (ETDM), WDM and OTDM are given. As individual line rates increase, all-optical processing may be required to route and regenerate the optical signal, thus the importance of wavelength converters in future networks is discussed.
- **Chapter 2** introduces the requirements that pulse generation methods must meet in order to be suitable for future high-speed systems and discusses the techniques used to measure these ultrashort pulses. Particular emphasis is given to the measurement technique of FROG as this technique is able to retrieve the electric field of the measured pulses. Various pulse generation methods are outlined, but focus is placed on the pulse generation method of gain switching. The poor pulse quality of gain-switched pulses can be improved by optical injection, and the performance enhancement obtained is examined. Finally a wavelength tunable source capable of providing tunability up to 65 nm is presented based on dual Fabry–Pérot lasers and self or external seeding. The

generated pulses exhibit high quality characteristics such as 60 dB SMSR, with low jitter and narrow pulse widths from 15-30 ps.

- **Chapter 3** investigates in detail the effect on system performance of different temporal pedestal suppression ratio (TPSR) levels of a pulse source. A pedestal of varying levels is introduced to a 2 ps pulse source and tested in an 80 Gb/s OTDM system. One method to overcome insufficient TPSR levels is to employ a SA. It is shown how the inclusion of a vertical microcavity based SA improves significantly the TPSR and the overall system performance. The work presented on gain-switched pulse sources in Chapter 2, is further enhanced in this chapter, by processing the generated pulses which involves spectral shaping, temporal compression and chirp compensation. The generation of transform limited short optical pulses, which display excellent spectral and temporal qualities is presented. The pulses are generated by employing a novel technology, based on an externally injected gain-switched laser in conjunction with a nonlinearly chirped grating. The excellent system performance of this source in an 80 Gb/s OTDM system is detailed.
- **Chapter 4** outlines how a semiconductor optical amplifier (SOA) is a promising device to provide all-optical switching due to the large nonlinearity caused by gain saturation. The gain dynamics of an SOA upon the input of a picosecond pulse is presented, and an explanation of how this limits the speed of operation to less than 40 Gb/s is given. A complete experimental characterisation of the temporal and chirp profiles of amplified picosecond pulses following an SOA is characterised by the FROG measurement technique. This study is important to examine the SOA as an amplifier but also to aid the development of SOA-based all-optical processing devices.
- **Chapter 5** initially overviews the various wavelength conversion techniques which are available, with particular emphasis given to the nonlinear processes of XGM, XPM and four wave mixing (FWM) in an SOA. A brief outline is given which explains the effects SOA operating parameters have on wavelength converted pulses following XGM and XPM. To overcome the carrier recovery dynamics of an SOA and the corresponding patterning effects, shifted filtering in conjunction with XGM/XPM can be employed. We examine the different characteristics of the converted pulses by exploiting either XGM or XPM for both blue and red shifted filtering at 10 Gb/s. XPM in conjunction with shifted filtering offers many advantages over XGM, which include preserving the polarity of the input signal and a simple configuration. Therefore we proceeded to concentrate on this scheme and present error-free performance at 80 Gb/s for

the blue-shifted filtering scheme. To examine in detail the shape and chirp attributable to the gain and chirp dynamics and the placement of the filter, a detailed FROG characterisation is carried out of the wavelength converted pulses at repetition rates from 10-80 GHz.

- **Chapter 6** gives a brief summary and analysis of the main points of the work presented in this thesis.

CHAPTER 1 – HIGH-SPEED OPTICAL COMMUNICATIONS SYSTEMS

1.1 Introduction

Optical fibre communications systems provide huge-bandwidth capabilities, and offer many advantages over other communications systems [1]. Statistics reported by the Organisation for Economic Co-operation and Development (OECD) show that the number of broadband subscribers has increased by 33% from June 2005-June 2006 [2]. Presently the largest uptake is digital subscriber line (DSL), however as high-bandwidth consumer products unfold fibre-to-the-home (FTTH) will be required to support the large data transfer rates needed for these high-bandwidth products. In general Internet traffic is becoming more symmetric in that peer-to-peer communications presently accounts for 50-70% of all its traffic [3]. In business, high-bandwidth applications include e-commerce capabilities, video-on-demand and mobile telephony. In the home applications include high-definition television (HDTV), video sharing, and online gaming (which accounted for 10% Internet traffic in 2003) all of which are driving the need to install fibre-to-the-premises. Future applications which will continue to increase the demand for high-bandwidth include telemedicine (home care/health-monitoring), and multimedia connected homes (media PCs will replace numerous electronic devices such as music, HDTV, video phones, etc. which will receive feeds from one central device) [4]. Thus an overall increase in demand for bandwidth in the access and metro networks will in turn result in increased data capacity requirements in the transport/core network. Therefore, it is important for network providers to better utilise their installed fibre networks and to develop the components within these systems so that they can meet consumer demands of increased bandwidth requirements at cost-efficient prices.

One way to exploit the large bandwidth capabilities of optical fibre is to use different multiplexing techniques, where multiple data channels are transmitted simultaneously over a single optical fibre. This chapter will discuss electrical time division multiplexing (ETDM) and the two main optical multiplexing techniques optical time division multiplexing (OTDM) and wavelength division multiplexing (WDM). The push for higher data rates on single wavelength channels, which has historically always left behind the development of high-speed electronics, necessitates the use of OTDM transmitters and receivers until their economically more attractive ETDM equivalents become available [5]. The principal motivation for all-optical networks arises from the

ability of optics and not electronics as being the most cost effective way to tap the multi-Tb/s capacity of the optical fibre, i.e. through the use of optical bypass and optical switching nodes. In doing so the growing demand for bandwidth per user, higher path reliability, and simplified operation and management is fulfilled [6].

1.2 Multiplexing Schemes to Implement High-Speed Systems

Historically, serial optical data transport has proven most attractive because it has the advantage of decreasing the power and space consumption, reducing the complexity of terminals and thus lowering costs and management effort of the fibre network in comparison to parallel WDM systems. This trend has continued to hold true, despite the fact that transmission at higher per-channel bit rates is accompanied by a reduced tolerance to some fibre transmission impairments. As high-speed optoelectronic components mature, implementing ETDM schemes is the preferred option due to the reduced cost in data transmission. However, due to the limited speeds of optical modulators and driver amplifiers, OTDM is an option to achieve large increases in serial channel rates [5]. However new technologies are needed for the implementation of OTDM systems. An alternative multiplexing scheme which has the potential to take full advantage of the terahertz bandwidth of optical fibres is WDM [7]. Thus, a solution to increase the overall capacity of fibre networks will most likely employ WDM, however with increased capacity on each individual wavelength channel. The next data rate of individual wavelength channels will aim to meet the next important bit-rate hierarchy of 160 Gb/s [8].

1.2.1 Electrical Time Division Multiplexing

The choice of serial versus parallel transmission is driven by the overall cost to transmit information across an optical network, which is impacted by aspects such as high-speed hardware availability, transceiver footprint, geographic network dimensions, optical transmission impairments, and wavelength management considerations [9]. Thus these demands can be achieved by implementing the highest speed ETDM schemes. Electronic circuitry for 40 Gb/s is currently available commercially, however electronic circuitry for bit rates of 80 Gb/s and greater is still in development stages [10]. Presently, only few reports of binary modulators operating at bandwidths of 80 GHz and above have been published [9]. Thus one of the first challenges to implementing more efficient optical networks is related to the development of commercial grade broadband high-speed electronics for high-speed transmitter and receivers.

In ETDM, a number of lower speed (baseband) sub-channels are multiplexed together in the time domain using electronics [11]. A simple representation of an ETDM system is illustrated in Figure 1-1. The transmitter consists of a modulator, multiplexer and distributed feedback (DFB) continuous wave (CW) source, where the multiplexed electrical signal is converted into an optical signal. Future networks will most likely use external modulation techniques as they give superior transmission performance in comparison to directly modulated sources (which generate highly chirped pulses). The incoming data tributaries are multiplexed in the electrical domain, electrically amplified and applied to the first modulator. Presently, driver amplifiers lack sufficient bandwidth and can exhibit signal distortions at bit rates >80 Gb/s, thus electro-absorption modulators (EAMs) are more suitable in comparison to Mach Zehnder modulators (MZMs) as a smaller applied voltage is required [9]. The second modulator is optional and can be used to convert the non return-to-zero (NRZ) signal to a return-to-zero (RZ) signal, by gating the NRZ signal by the applied transfer function of the second modulator. To date the highest binary operating rates of ETDM transmitters are 100 and 107 Gb/s [12]. Following transmission in the optical fibre, the signal is detected using a high-speed photodiode. The signal is then electronically demultiplexed into smaller tributary bit rates. In ETDM receivers, a synchronous electrical clock signal has to be recovered from the incoming data signal. Thus far, ETDM receivers have only accomplished 80 Gb/s operation [13].

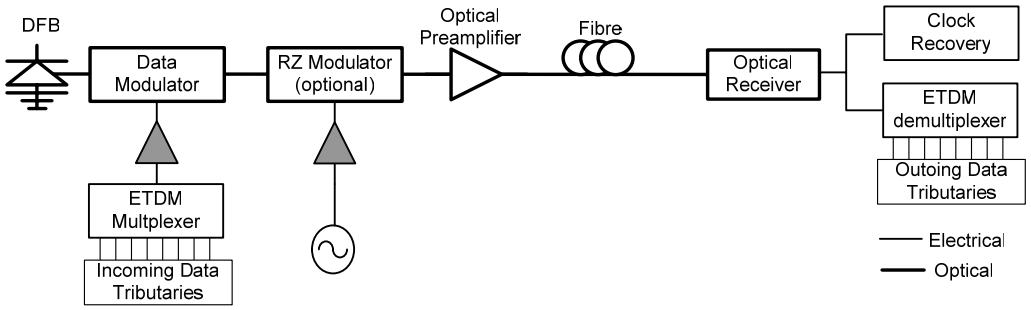

Figure 1-1 A schematic illustration of an ETDM transmitter and receiver system.

Thus, it is clear that present ETDM systems will result in the formation of bottlenecks at the transmitter and receiver and thus will not be capable of meeting the required bandwidth for optical networks.

1.2.2 Wavelength Division Multiplexing

Due to the limited speed of electronics as outlined above, further techniques are required to exceed the bandwidth of a simple point-to-point link. Wavelength division multiplexing (WDM) is one such scheme whereby the simultaneous transmission of

multiple data channels at different wavelengths over a single fibre is enabled (16 channels operating at 10 Gb/s can give an overall data rate of 160 Gb/s) [14,15]. WDM is related to frequency division multiplexing (FDM), the electronic multiplexing scheme and takes advantage of the fact that optical sources have a very narrow spectral linewidth. Figure 1-2 illustrates a WDM multiplexing scheme. Light sources with narrow spectral widths operating at different wavelengths are coupled together and then transmitted along the optical waveguide. At the receiver, a coupler is used to split the data into number of different channels and filters are used to extract the channel at a certain wavelength that holds the requested information. For more efficient multiplexing and demultiplexing new components such as the arrayed waveguide grating (AWG) are replacing the traditional couplers and filters [16,17].

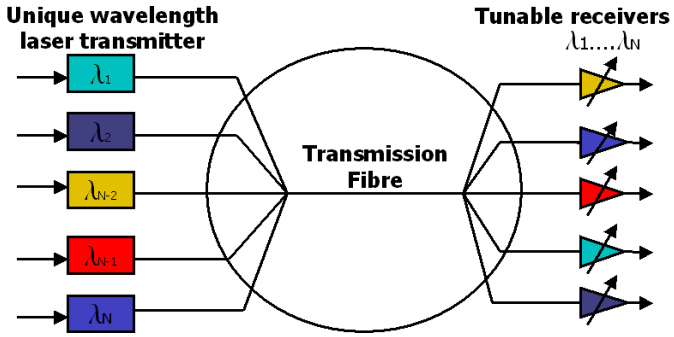

Figure 1-2 A basic illustration of a WDM system.

The advent of the Erbium doped fibre amplifier (EDFA) led to the wide scale deployment of WDM systems [18]. The EDFA allows for the amplification of many wavelength channels over a large span with little detrimental effects, resulting in the redundancy of repeaters. EDFAs dramatically reduced the overall cost of optical systems and enabled very large bandwidth and large transmission distance capabilities in optical networks.

The most important factor in WDM systems is the channel spacing, the wavelength range between two peak wavelength emissions. The ITU-T G.692 standard (Oct 1998) sets out the minimum channel spacing that can be used, which is 50 GHz (corresponding to 0.4 nm at 1550 nm) and sets the starting central channel at a frequency of 196.1 THz (corresponding to 1528.77 nm) for dense WDM (DWDM) [14]. The channel spacing chosen for a specific network is required to take crosstalk effects into account, to ensure that the integrity of each of the independent messages from each wavelength source is maintained for subsequent retrieval at the receiver. Crosstalk can be divided into two categories, linear and nonlinear. Linear crosstalk is due to the inability of WDM optical

components (e.g. the stop-band rejection of optical filters) to prevent some power from the adjacent wavelengths falling on the receiver [19] resulting in the degradation of the receiver sensitivity [20]. Nonlinear mechanisms in fibre can cause coupling of power from one wavelength to another, such as stimulated Raman scattering (SRS) [21]. In addition, mixing of the crosstalk and signal optical fields can result in the generation of interferometric noise at the receiver if both arise from the same laser source or from distinct laser sources whose wavelengths are closely aligned [22,23].

The advent of optically amplified transmission and of DWDM technology has transformed the technology and also the economics of optical network deployments. In less than 10 years, the capacity of a single optical fibre equipped with commercial transmission equipment has increased from a single OC-48 signal, transmitting at a rate of 2.488 Gb/s to 160 OC-192 (9.953 Gb/s) signals, giving an overall data rate of 1.6 Tb/s [24]. The economics of DWDM are driving the development and deployment of a new generation of ultra-long-haul DWDM systems for terrestrial networks that can carry these high-capacity data streams over thousands of kilometres. As the capacity of DWDM systems have exploded, the cost of terminals and regenerators has become an even larger fraction of the total system cost. Minimising the number and the cost of regenerators is now a major economic driver in the design of new equipment and the design of carriers' fibre networks. Therefore increasing the number of channels by decreasing the channel spacing will increase the overall costs. It has the additional expense of higher levels of penalty induced by linear and nonlinear crosstalk [25]. These economic factors are driving increased channel bit-rates from OC-48 (2.448 Gb/s) to OC-192 (9.953 Gb/s), and in the near future, to OC-768 (39.813 Gb/s) to minimise the number of regenerators, transmitters, and receivers. The cost benefit of increasing channel bit-rates is due to the redundancy of expensive optoelectronic regenerators between nodes [26]. However presently, the maximum data rate for each wavelength channel is defined by the maximum speed of electronics, thus a different multiplexing scheme is required to increase the individual channel rates even further.

1.2.3 Optical Time Division Multiplexing

Optical time division multiplexing (OTDM) is one such multiplexing technique that can provide ultra-high bit rates for each individual wavelength channel until high-speed electronics become commercially available, or to fully replace electronics which may not be able to reach speeds in excess of 100 Gb/s [27]. In addition, high-speed OTDM techniques are becoming increasingly important to investigate high-speed optical signal processing and for investigating the ultimate transmission capability of a single channel

[28,29]. OTDM is a very logical approach to investigate transmission issues before the advent of high-speed electronic or optoelectronic components, and can be used for evaluating similar systems carried out using ETDM to find the superior sub-system technology.

OTDM was first proposed by Zhang et al. in a patent disclosure in 1987 [30] and first reported by Tucker et al. in 1988 [31]. The principle behind OTDM involves modulating a number of electrical NRZ data signals onto an optical pulse source to generate optical RZ data channels and then multiplex them together in the temporal domain. Figure 1-3 displays a typical OTDM system. The temporal modulation of OTDM dictates that RZ coding is a requirement for OTDM. Thus an optical pulse source is required to generate very narrow pulses. The pulse width is determined by the overall required data rate and the optimum pulse width has been found to be a third of the bit slot duration (e.g. 2 ps for 160 Gb/s transmission). The pulse train is amplified to overcome the large loss introduced by the coupler, which splits the pulse train into the number of required paths (e.g. 2 ps pulses at 10 GHz, requires 16 paths for 160 Gb/s transmission). The optical pulse train in each path is encoded using electrical NRZ data by a modulator to give RZ data encoded optical pulses. Each path includes a fixed fibre delay so that each data channel is assigned a certain temporal bit slot. Clearly the overall data rate in an OTDM system is determined by the pulse width achievable, therefore emphasizing the importance of developing a high quality optical picosecond pulse source.

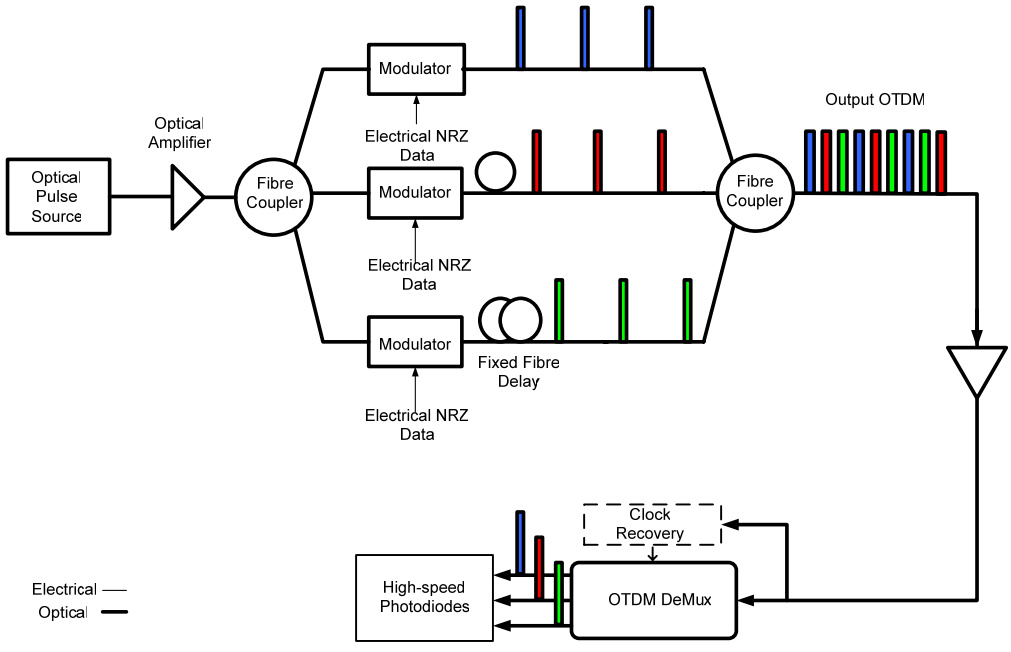

Figure 1-3 A schematic illustration of an OTDM set-up.

At the receiver, an OTDM demultiplexer is required to separate the multiplexed channels to lower bit rates so that they can be detected using high-speed detectors. An ideal candidate for use as an all-optical demultiplexer is a semiconductor optical amplifier (SOA) [32,33]. For successful demultiplexing, a clock signal must be retrieved from the inputted data stream and optical clock recovery has been demonstrated using injection locked laser diodes [34]. One system parameter required for an OTDM signal is a high optical signal-to-noise ratio (OSNR) because of the high density of bits. For 40 Gb/s based systems a receiver will require an OSNR of 24 dB (0.1 nm resolution) in order to achieve a BER performance better than 10^{-9}. Theoretically the OSNR must increase by 6 dB for each factor of four increase in the channel bit rate, to maintain the same noise performance. A summary describing the progression of OTDM single channel achievable rates is given by Nakazawa, which includes a transmission example of a 1.28 Tb/s OTDM system [35].

The overall advantages of implementing OTDM systems are:

- Simple management and control (single stream vs. many wavelength channels).
- A reduced number of transmitters and receivers, and a smaller footprint for networking components used for switching and routing (such as add-drops and cross connects).
- The use of digital regeneration, digital buffering, coding and encryption.

The reduction in component count and complexity (serial rather than parallel) of the network generally leads to an overall improvement of the size, cost, and electrical power consumption of the network. The deployment of high-speed transport reduces the number of paths to monitor and restore in case of hardware failure or malfunction, thus simplifying the provision, operation, administration, and maintenance of the network. It is cheaper to spare one high-speed transponder than several low-speed WDM transponders. Besides these aforementioned advantages of OTDM, there are a number of disadvantages associated with it, such as synchronisation and the elimination of protocol transparency.

1.2.4 Hybrid WDM/OTDM System

One method to overcome the restrictions of implementing OTDM and WDM at their maximum data rates is to use hybrid WDM/OTDM [36,37]. The hybrid approach works by utilising OTDM to enhance the bandwidth of a number of different wavelength channels in a WDM network by putting OTDM coding on top of the channels provided by WDM. This would result in a smaller number of WDM channels each operating at

much higher data rates. These benefits include space advantages in terminal buildings, lower power consumption, less complexity of terminals, and thus lower costs and management effort of the fibre network [38]. Many hybrid applications have been presented, operating at individual line rates of 160 Gb/s for 4 and 8 wavelength channels [38,39]. They exploit the parallelism of WDM architectures and the speed of OTDM [11]. A key requirement for such high-capacity hybrid networks, are optical pulse sources that are able to generate wavelength tunable picosecond pulses.

1.2.5 Modulation Formats for High-Speed Systems

An increasingly important aspect of future all-optical networks is the modulation format of the transmitted data. High-capacity transmission systems are known to suffer from impairments arising from fibre nonlinear effects [40], chromatic dispersion (CD) [41], polarisation mode dispersion (PMD) [42], and amplified spontaneous emission (ASE) [43]. One method to overcome these impairments is to use advanced modulation formats [44]. Modulation formats can be categorised into three main areas: amplitude-shift keying (ASK) or on-off keying (OOK), phase-shift keying (PSK), frequency-shift keying (FSK) or a combination of these. OOK encodes data by turning on or off the amplitude of light and includes NRZ and RZ formats. These formats are the most simple modulation formats to implement in high-speed optical systems. RZ data does not perform well with respect to dispersion, i.e. the broader spectrum of RZ compared to NRZ results in a faster broadening of the data signal. The smaller the duty cycle the faster the eye closes with cumulative dispersion (neglecting nonlinear effects). However, RZ coding generally enables transmission at higher powers, and is not limited by nonlinearity in the fibre to the same extent as NRZ coding [45]. Higher powers provide larger power budget margins that can be used to extend the reach of the system.

Although NRZ is presently the format used in long-haul transmission, RZ coding will most likely be the coding of choice for high bit rate applications due to its superior performance resulting from its inherent receiver sensitivity improvement [46,47], and reduced sensitivity to fibre impairments caused by nonlinearity [45] and PMD [48]. Although RZ coding is more susceptible to CD, (which becomes a limiting factor at bit rates greater than 40 Gb/s in comparison to NRZ coding), RZ coding used in conjunction with more advanced modulation formats (e.g. RZ differential-phase shift keying) will provide overall better tolerance to the combination of system impairments [45]. In addition, data processing and regeneration is simpler to carry out in RZ format in comparison to NRZ. Therefore to implement RZ coding in future systems, the development of high-quality picosecond optical pulse sources are required.

1.3 All-Optical Processing for Future High-Speed Systems

The successful delivery of information through such high-speed networks requires the optical signals to be manipulated or processed in some way; processing applications include amplification, regeneration, retiming, multiplexing, demultiplexing, reshaping and rerouting. Commonly data is processed electronically, which requires optical-electronic-optical (OEO) conversion. Due to the introduction of the EDFA, WDM systems became cost-efficient as optical signals could be optically amplified without electrical conversion over a large wavelength span [18]. Cost reductions and increased flexibility will be the main drivers for the evolution of all-optical transport networks [49]. Electronic processing techniques therefore may not continue to be cost effective when they are scaled up to accommodate the growth in network capacity. In WDM systems, electronic regeneration would require demultiplexing the wavelength channels, detecting and electronically regenerating each individual channel and then transmitting the regenerated signal and multiplexing them together again. Electronic processing would therefore be costly in high-capacity systems with large channel counts. In OTDM systems, due to the limited speed of electronic components processing can not presently be implemented in the electronic domain, therefore all-optical processing techniques are a requirement.

It has been predicted that the escalating bandwidth requirement is driving a shift from fixed to reconfigurable optical nodes [50]. In the physical layer, wavelength contention management issues will necessitate the implementation of wavelength conversion and regeneration on demand [51,52]. Thus all-optical wavelength converters will lead to an increased flexibility and capacity in the network, the capability of reconfiguration and the provision of decentralised management of wavelengths. Assigning dynamic links between channels allows for network management by a link-to-link process rather than a fixed start-to-end process, resulting in relaxed requirements. If there are link or node failures local reconfigurations can be carried out rather than a full global reconfiguration. Thus dynamic reconfiguration of a network, by applying all-optical wavelength conversion has the capability of creating a more cost-efficient network [53]. As a result the development and research of all-optical processing components and sub-systems are necessary, and to ensure they are effective they will be required to have high-speed capability, low cost, small footprint and efficient power consumption

1.4 Summary

In 2005, typical commercial transport systems offered a maximum capacity per link near 1 Tb/s. Assuming modest traffic growth rates maximum capacities of 10 Tb/s or higher will be reached within 10 years. This link capacity will require optical bandwidths that exceed devices that are available from the market today. Each multiplexing scheme described in this chapter will have a place in future networks, individually or as a combination. The choice of multiplexing scheme to be implemented will depend on the required transmission speeds, cost, performance, power consumption, footprint, and complexity of the network. However larger serial rate channels are preferable to the parallelism of WDM. Until the technology becomes available to implement very high-speed ETDM/OTDM, WDM will continue as the optimum choice for long-haul and metropolitan area networks. Thus there is a requirement to develop all-optical processing components so that OTDM systems can be implemented with a view that they will enable dynamic and regenerative properties of high-speed signals. In this thesis, novel all-optical components/subsystems are presented that meet the demands in reaching the proposals outlined for future high-speed all-optical networks.

REFERENCES

[1] G. Keiser, "Optical Fiber Communications," *McGraw-Hill,* Singapore, 1991.

[2] Organisation for Economic Co-operation and Development URL: www.oecd.org/sti/ict/broadband "OECD Broadband Statistics to June 2006."

[3] B. Whitman, "Fibre Access Deployment Worldwide: Market Drivers, Politics and Technology Choices," *European Conf. Optical Commun. (ECOC'04),* Market Focus, 2004.

[4] S.V. Kartapoulous, "Consumer Communications in the Next Generation Access Network," *Consumer Commun. Network. Conf. (CCNC'04),* pp. 273-278, 2004.

[5] R.-J. Essiambre, G. Raybon, and B. Mikkelsen, "Pseudo-linear Transmission of High-Speed TDM Signals: 40 and 160 Gb/s," in Optical Fiber Telecommunications*,* I. Kaminov, and T. Li, *Academic Press,* New York, vol. V B, 2002.

[6] R. Sabella, and P. Lugli, "High Speed Optical Communications," *Kluwer,* Dordreacht, 1999.

[7] X. Zhang, A. Gutierrez-Aitken, D. Klotzkin, P. Bhattacharya, C. Caneau, and R. Bhat, "0.98-μm Multiple-Quantum-Well Tunneling Injection Laser with 98 GHz Intrinsic Modulation Bandwidth," *IEEE J. Sel. Top. Quantum Electron.,* vol. 3, pp. 309-314, 1997.

[8] J. Strand, "Optical Network Architecture Evolution," in Optical Fiber Telecommunications*,* I. Kaminow, and T. Li, *Academic Press,* New York, vol. IV B, 2002.

[9] E. Lach, and K. Schuh, "Recent Advances in Ultrahigh Bit Rate ETDM Transmission Systems," *J. Lightwave Technol.,* vol. 24, pp. 4455-4467, Dec. 2006.

[10] W.S. Lee, "80+Gbit/s ETDM Systems Implementation: An Overview of Current Technologies," *Optical Fiber Commun. Conf. (OFC'06),* paper OTuB3, 2006.

[11] S. Kawanishi, "High Bit Rate Transmission Over 1 Tbit/s," *IEICE Trans. Commun.,* vol. E84-B, pp. 1135-1141, May 2001.

[12] G. Raybon, P.J. Winzer, and C.R. Doerr, "10 x 107-Gbit/s Electronically Multiplexed and Optically Equalized NRZ Transmission Over 400 km," *Optical Fiber Commun. Conf. (OFC'06),* paper PDP32, 2006.

[13] K. Schuh, B. Junginger, E. Lach, A. Klelamp, and E. Schlag, "85.4 Gb/s ETDM Receiver with Full Rate Electronic Clock Recovery Circuit," *European Conf. Optical Commun. (ECOC'04),* paper Th4.1.1, 2004.

[14] S.V. Kartalopoulos, "DWDM: Networks, Devices, and Technology," *Wiley-IEEE Press,* New Jersey, 2002.

[15] N.S. Bergano, and C.R. Davidson, "Wavelength Division Multiplexing in Long-Haul Transmission Systems," *IEEE J. Lightwave Technol.,* vol. 14, pp. 1299-1307, 2004.

[16] B. Nyman, M. Farries, and C. Si, "Technology Trends in Dense WDM Demultiplexers," *Optical Fiber Technol.,* vol. 7, pp. 255-274, Oct. 2001.

[17] M.K. Smit, and C. van Dam, "PHASAR-Based WDM-Devices: Principles, Design and Applications," *J. Sel. Top. Quantum Electron.,* vol. 2, pp. 236-250, June 1996.

[18] T. Li, "The Impact of Optical Amplifiers on Long-Distance Lightwave Telecommunications," *IEE Proceedings,* vol. 81, pp. 1568-1579, Nov. 1993.

[19] K.-P. Ho, and J.M. Kahn, "Methods for Crosstalk Measurement and Reduction in Dense–WDM Systems," *J. Lightwave Technol.,* vol. 14, pp. 1127-1135, June 1996.

[20] A.M. Hill, and D.B. Payne, "Linear Crosstalk in Wavelength-Division-Multiplexed Optical-Fiber Transmission Systems," *J. Lightwave Technol.,* vol. LT-3, pp. 643-651, June 1985.

[21] K.-P. Ho, "Statistical Properties of Stimulated Raman Crosstalk in WDM Systems," *J. Lightwave Technol.,* vol. 18, pp. 915-921, July 2000.

[22] P.J. Legg, D.K. Hunter, I. Andonovic, and P.E. Barnsley, "Inter-Channel Crosstalk Phenomena in Optical Time Division Multiplexed Switching Networks," *IEEE Photonics Technol. Lett.,* vol. 6, pp. 661-663, May 1994.

[23] E.L. Goldstein, L. Eskildsen, and A.F. Elrefaie, "Performance Implications of Component Crosstalk in Transparent Lightwave Networks," *IEEE Photonics Technol. Lett.,* vol. 6, pp. 657-660, May 1994.

[24] J.-X. Cai, M. Nissov C.R. Davidson, A.N. Pilipetskii, G.Mohs, H. Li, Y. Cai, E.A. Golovchenko, A.J. Lucero, D.G. Foursa, and N.S. Bergano, "Long-Haul 40 Gb/s DWDM Transmission With Aggregate Capacities Exceeding 1 Tb/s," *J. Lightwave Technol.,* vol. 20, pp. 2247-2258, Dec. 2002.

[25] F. Forghieri, R.W. Tkach, A.R. Chraplyvy, and D. Marcuse, "Reduction of Four-Wave Mixing Crosstalk in WDM Systems using Unequally Spaced Channels," *IEEE Photonics Technol. Lett.,* vol. 6, pp. 754-756, 1994.

[26] J. Zyskind, R. Barry, G. Pendock, M. Cahill, and J. Ranka, "High-Capacity, Ultra-Long-Haul Networks," in Optical Fiber Telecommunications, I. Kaminow, and T. Li, *Academic Press,* New York, vol. IV B, 2002.

[27] J. Hecht, "OTDM Promises Higher Communications Speeds Using Optical Processors," *Laser Focus World,* pp. 121-124, Nov. 2003.

[28] S. Kawanishi, H. Takara, T. Morioka, O. Kamatani, K. Takiiguchi, T. Kitoh, and M. Saruwatari, *IEE Electron. Lett.,* vol. 32, pp. 916-917, 1996.

[29] G. Raybon, B. Mikkelsen, R.-J. Essianbre, A.J. Stentz, T.N. Nielsen, D.W. Peckham, L. Hsu, L. Gruner-Nielsen, K. Dreyer, J.E. Johnson, *Optical Fiber Commun. Conf. (OFC'2000),* paper PD29, 2000.

[30] X.-C. Zhang, G.R. Hulse and R.K. Jain, "Two-Dimensional, High-Speed Optical Time Division Multiplexing Processor," *Patent Disclosure,* 1987.

[31] R.S. Tucker, G. Eisenstein, and S.K. Korotky, "Optical Time-Division Multiplexing for very High Bit-Rate Transmission," *J. Lightwave Technol.* vol. 6, pp. 1737-1749, Nov. 1988.

[32] T. Yamamoto, U. Feiste, J. Berger, C. Schubert, C. Schmidt, R. Ludwig, and H.G. Weber, "160 Gbit/s Demultiplexer with Clock Recovery using SOA-based Interferometric Switches and its Application to 120 km Fiber Transmission," *European Conf. Optical Commun. (ECOC'01)*, pp. 192-193, 2001.

[33] S.L. Jansen, M. Heid, S. Spalter, E. Meissner, C.J. Weiste, A. Schopflin, D. Khoe, and H. de Waarth, "Demultiplexing 160 Gb/s OTDM Signal to 40 Gb/s by FWM in SOA," *IEE Electron. Lett.,* vol. 38, pp. 978-979, 2002.

[34] M. Attygalle, and Y.J. Wen, "Injection-Locked Fabry–Pérot Laser with Electronic Feedback for Clock Recovery from High-Speed OTDM Signals," *IEEE Photonics Technol. Lett.,* vol. 18, pp. 478-480, Feb. 2006.

[35] M. Nakazawa, "Tb/s OTDM Technology," *European Conf. Optical Commun. (ECOC'01),* paper Tu.L.2.3, 2001.

[36] E.J.M. Verdurmen, G.D. Khoe, A.M.J. Koonen, and H. de Waardt, "All-Optical Data Format Conversion from WDM to OTDM Based in FWM," *Microwave and Optical Technol. Lett.,* vol. 48, pp. 992-994, May 2006.

[37] E. Lach, "Terabit/s Optical Transmission Systems based on Ultrahigh Channel Bitrate – Photonic Network Research in IST," *IST-OPTIMIST Workshop,* Düsseldorf, Dec. 2001.

[38] R. Leppla, S. Vorbeck, M. Schneiders, W. Weirshausen, M. Schmidt, M. Witte, F. Buchali, E. Lach, E. Le Rouzic, S. Salaun, S.B. Panernvi, and K. Sanapi,

"Field Trials with Channel Bit Rates of 160 Gbit/s," *OSA Optical Fiber Commun. Conf. (OFC'06),* paper OFE5, Mar. 2006.

[39] K. Schuh, M. Schmidt, E. Lach, B. Junginger, A. Klekamp, G. Veith, and P. Sillard, "4x160 Gbit/s DWDM/OTDM Transmission over 3x80 km TeraLight™-Reverse Teralight™ Fibre," *European Optical Commun. Conf. (ECOC'02),* paper 2.1.2, 2002.

[40] A.R. Chraplyvy, "Limitations on Lightwave Communications Imposed by Optical Fiber Nonlinearities," *J. Lightwave Technol.,* vol. 8, pp. 1548-1557, Oct. 1990.

[41] P.J. Corvini, and T.L. Koch, "Computer Simulation of High-Bit-Rate Optical Fiber Transmission Using Single-Frequency Lasers," *J. Lightwave Technol.,* vol. LT-5, pp. 1591-1595, Nov. 1987.

[42] H. Kogelink, R.M. Jopson, and L. Nelson, "Polarization-Mode Dispersion," in Optical Fiber Telecommunications, I. Kaminow, and T. Li, *Academic Press,* New York, vol. IV B, 2002.

[43] D. Marcuse, "Single-Channel Operation in Very Long Nonlinear Fibers with Optical Amplifiers at Zero Dispersion," *J. Lightwave Technol.,* vol. 9, pp. 356-361, Mar. 1991.

[44] Y.J. Wen, J. Mo, Y. Wang, C. Lu, "Advanced Data Modulation Techniques for WDM Transmission," *IEEE Commun. Mag.,* vol. 44, pp. 58-65, Aug. 2006.

[45] M. Daikoku, N. Yoshikane, and I. Morita, "Performance Comparison of Modulation Formats for 40 Gbit/s DWDM transmission systems," *OSA Optical Fiber Commun. Conf. (OFC'05),* paper OFN2, 2005.

[46] L. Boivin, and G.J. Pendock, "Receiver Sensitivity for Optically Amplified RZ Signals with Arbitrary Duty Cycle," *Optical Amplifiers Applications Conf. (OAA '99),* paper ThB4, Japan, 1999.

[47] P.J. Winzer, and A. Kalmár, "Sensitivity Enhancement of Optical Receivers by Impulsive Coding," *IEEE J. Lightwave Technol.,* vol. 17, pp. 171-177, Feb. 1999.

[48] H. Sunnerud, M. Karlsson, and P.A. Anderkson, "A Comparison between NRZ and RZ Data Formats with Respect to PMD-Induced System Degradation," *IEEE Photonics Technol. Lett.,* vol. 13, pp. 448-450, 2001.

[49] S. Gosselin, and M. Joindot, "Key Drivers and Technologies for Future Optical Networks," *European Conf. Optical Commun. (ECOC'06),* Tutorial We2.2.1, 2006.

[50] T. Freeman, “Not Bigger but Better,” *Fibre Systems Europe,* vol. 3, Editorial p. 5, Apr. 2006.

[51] B. Ma, and Y. Nakano, “Realization of All-Optical Wavelength Converter Based on Directionally Coupled Semiconductor Optical Amplifiers,” *IEEE Photonics Technol. Lett.,* vol. 11, pp. 188-190, 1999.

[52] S.J.B. Yoo, “Wavelength conversion technologies for WDM network applications,” *J. Lightwave Technol.,* vol. 14, pp. 955-966, Jun. 1996.

[53] A.A.M. Saleh, “Transparent Optical Networks for the Next Generation Information Infrastructure,” *OSA Optical Fiber Commun. Conf. (OFC’95),* pp. 241, 1995.

CHAPTER 2 – PICOSECOND PULSE GENERATION FOR FUTURE HIGH-SPEED SYSTEMS

2.1 Introduction

Picosecond pulse generation is of paramount importance for the development of high-speed optical communications. Return-to-zero (RZ) modulation is superior to non return-to-zero (NRZ) modulation at data rates greater than 10 Gb/s due to its inherent receiver sensitivity improvement, and reduced sensitivity to polarisation mode dispersion [1,2]. More advanced modulation formats such as differential phase-shift keying are becoming increasingly popular, and research comparing RZ to NRZ coding, when used with these advanced modulation formats, show that RZ coding provides better tolerance to system nonlinearities [3]. Thus it is likely that future systems will employ RZ coding in some particular form, which requires the development of picosecond optical pulse sources. To implement these pulse sources in future high-speed communications systems specific standards must be met. These requirements include high side mode suppression ratio (SMSR), low temporal jitter, wavelength tunability, and small frequency chirp. Most importantly cost-effectiveness is imperative, as well as a simple configuration. In order to establish the quality of the generated pulses, different measurement techniques can be applied, which include an optical spectral analyser (OSA), a high-speed detector and oscilloscope, and an autocorrelator. However, these measurement schemes are limited in that they cannot retrieve the full electric field of an optical pulse. This limitation is overcome by the measurement technique of frequency-resolved optical gating (FROG).

Picosecond pulse generation can be accomplished through various methods such as external modulation of a continuous wave (CW) source, mode locking and gain switching. This chapter presents an overview of these different pulse generation techniques. Of all the available techniques gain switching presents the simplest and most cost-efficient process for pulse generation. Thus the process of gain switching is explored in-depth, in particular how optical injection can greatly enhance the quality of gain-switched pulses. Then, a novel set-up is presented which generates widely wavelength tunable picosecond pulses via self and external seeding of a dual gain-switched source.

2.2 Pulse Requirements

Picosecond optical pulses need to adhere to specific requirements to be suitable for use in high-speed optical systems. These requirements include picosecond pulse width, narrow spectral width, giving Fourier transform limited pulses. Further characteristics of the pulses should include low temporal jitter, high SMSR, and wide wavelength tunability [4,5]. These parameters are now explained in more detail.

2.2.1 Pulse and Spectral Width

In order to increase the overall achievable data rates of future high-speed systems very narrow pulses in the order of picoseconds and femtoseconds need to be generated. Previous research has shown that a duty cycle of less than 0.4 is the optimum for optical time division multiplexed (OTDM) systems to prevent an induced penalty due to incoherent cross talk [6]. Typically, the duty cycle chosen is 0.33 which equates to a pulse width of 8 ps and 4 ps for 40 Gb/s and 80 Gb/s respectively.

The spectral width is also very important. As pulses get narrower, there is a corresponding increase in the spectral width. However, for each pulse width there is a corresponding minimum spectral width for a particular pulse shape. If the spectral width is wider than its minimum value dispersive effects will be much greater causing the pulse to spread out in time, thus reducing the transmission length of the signal. Thus, transform limited pulses are required. The time bandwidth product (TBP) is a measurement of how transform limited pulses are and it is calculated by multiplying the full width half maximum (FWHM) spectral width (Hz) by the FWHM temporal width (s) [7]. The TBP is a function of the actual pulse shape, thus Gaussian and $sech^2$ pulses have TBPs of 0.441 and 0.315 respectively.

2.2.2 Frequency Chirp

Frequency chirp is related to the dynamic broadening of the spectral bandwidth, which results in pulses which are not transform limited. Chirp can be generated in directly modulated lasers due to the modulation induced changes in the carrier density. It can also be generated as pulses propagate due to self phase modulation (SPM) in optical fibre [8]. The generated chirp is deleterious in optical fibre communication systems as it can cause an increased rate in pulse broadening due to dispersion [9].

2.2.3 Extinction Ratio and Temporal Pedestal Suppression Ratio

The extinction ratio (ER) of a pulse is the ratio of on-state power to off-state power. A similar parameter is the temporal pedestal suppression ratio (TPSR), which is the ratio of

power at the peak of the pulse to the power at the peak of the next pedestal. This is an important parameter to investigate as many pulse sources generate satellite pulses or pedestals, which will lead to increased performance penalty due to interferometric noise [10]. The effect of varying TPSR heights is investigated further in Chapter 3. It has been found that a TPSR of at least 30 dB is required in a high-speed system to ensure penalty free transmission [11,12].

2.2.4 Timing Jitter

Jitter is defined as the random fluctuation of the pulse from its starting position. As pulse widths become shorter, pulse-to-pulse timing jitter becomes a more serious factor determining the whole system performance, such as bit error rate (BER) and temporal resolution. Experiments and theory have shown that the timing jitter should be less than 1/12 of the switching window width of the demultiplexer to achieve a BER of less than 10^{-9} for a signal pulse whose width is equal to 1/5 the time slot width [13]. Thus for 80 Gb/s systems the jitter is required to be better than 1 ps rms for an ideal demultiplexing window of 12 ps.

2.2.5 Side Mode Suppression Ratio

The side mode suppression ratio (SMSR) is defined as the ratio of the main mode power to the power carried by the most intense side mode. Previous results have shown that the SMSR of an optical pulse source needs to at least 30 dB. In wavelength division multiplexing (WDM) systems this is a stringent parameter as low SMSR can cause interference between side modes and adjacent wavelength channels, and can also result in mode partition noise (MPN) [14]. The side modes may interfere with adjacent WDM channels of the same wavelength, and this interference generates a beat noise that imposes a power penalty on that channel [15]. MPN is caused by the random pulse-to-pulse power fluctuation among longitudinal modes of laser diodes in conjunction with chromatic dispersion induced by transmission in optical fibre [16]. In a laser random fluctuations between the main mode and side mode can occur but the overall power in the pulse can remain constant. However when this laser light is transmitted through a dispersive fibre, the signals emitted in different modes will be delayed and attenuated with increasing distance. Since the power fluctuations among the dominant modes can be quite large, significant variations in signal levels can occur at the receiver. This will result in timing jitter and pulse broadening at the receiver for high bit rates [17].

2.2.6 Wavelength Tunability

Wavelength tunablity is another parameter that needs to be considered. A wider tuning range translates to a greater number of channels that then can be used in an optical

communications system. This is an especially important feature in next generation hybrid WDM/OTDM systems were dynamic provisioning enabled by wavelength tunability will be employed.

2.3 Pulse Measurement Schemes

To determine the quality of pulses in high-speed optical communication systems a variety of pulse measurement schemes are required. An oscilloscope in conjunction with a photodiode, an OSA, and an autocorrelator can provide indications of the spectral or temporal quality of the pulse under measurement. However, a full electric field characterisation is required to fully understand the effects that pulses undergo in optical components [18] and in fibre transmission [19]. Applications of short pulse characterisation includes optimisation of pulse carving [20], characterisation of pulse source parameters [21], and analysis of optical signals after propagation in optical fibre [19,22]. In this section a brief overview of the measurement techniques used in this thesis is given but a more comprehensive review of high-speed measurement techniques can be found in Ref. [23].

2.3.1 Oscilloscope in Conjunction with a Photodiode

From test and measurement applications, such as performance monitoring in an optical communications network, the signal of interest is repetitive rather than a unique singular event. This allows the use of sequential sampling which uses the concept of equivalent time [24]. In general picosecond optical pulses are detected and characterised using a high-speed photodiode in conjunction with a high-bandwidth oscilloscope. Two types of oscilloscopes which can be used to view high-speed signals are a wide-bandwidth sampling oscilloscope and a real-time sampling oscilloscope. A real-time sampling scope can be regarded as an ultrafast analogue-to-digital converter. The sampling rate can presently detect signals as fast as 5 Gb/s accurately [25]. A wide-bandwidth sampling oscilloscope samples at a much slower rate but can have an 'overall bandwidth' in excess of 80 GHz. This is achieved through the triggering mechanism. The trigger periodically samples the data signal, but after each sweep the pulse is sampled at a very small incremental time delay so that the same point is not sampled again. This process is then repeated, to give the pulse trace on the screen.

The experiments described within this thesis use an Agilent DCA series 86100 (A-C) with a 60 GHz maximum bandwidth in conjunction with a 50 GHz u^2t photodiode to measure the eye diagrams and oscilloscope traces of incident pulses. These bandwidths translate to a pulse width measurement resolution of ~9 ps [26]. In addition to the DCA

measuring the pulse shape, it is also used for jitter measurements in the following chapters. Jitter measurements can be accurately measured down to 1 ps, but values below this are limited by the resolution of the trigger.

Another method to record pulses in the temporal domain is to use streak cameras [27,28], however the highest temporal resolution to date is 200 fs [29]. Thus for a 2 ps pulse only 10 measurement values will be obtained. An alternative to bandwidth limited photodetectors is the application of pulse sampling [30]. The presently available DCAs can be used in conjunction with an optical sampler to achieve optical bandwidths capable of measuring a 320 Gb/s signal [31]. A 100 fs pulsed laser interacts with the input data signal in a nonlinear crystal to generate an optical signal at a new wavelength, which is measured in a fast photodiode. However the main disadvantage of sampling is that the phase information relating to the pulse is lost.

2.3.2 Optical Spectrum Analyser

The measurement of a pulse in the frequency domain is achieved using an optical spectrum analyser (OSA), which can incorporate either spectrometers or interferometers. The most common spectrometer involves diffracting a collimated beam off a diffraction grating and focusing it on a camera [32]. Alternatively, Fourier transform spectrometers operate in the time domain and measure the integrated intensity from a Michelson interferometer, to give the field autocorrelation. The Fourier transform of the field autocorrelation is the spectrum [33]. Spectral measurements taken for experiments within this thesis are measured using an Anritsu diffraction grating spectrum analyser (MS9717A and MS9710B), for the measurement of wavelengths from 0.6 μm to 1.7 μm, with 0.05 nm resolution in the 1.55 μm range [34].

2.3.3 Autocorrelation

Typically, the most common method to measure ultrashort pulses in the temporal domain, which are too narrow for high-speed oscilloscopes and detectors, is to use autocorrelators [35,36]. The basic principle behind an autocorrelator is that the pulse is used to measure itself. The typical configuration of an autocorrelator is displayed in Figure 2-1 [37]. The input pulse to be measured is split in two by a beam splitter. One arm is delayed by a small time delay, τ with respect to the other arm, and the two pulses overlap and combine in a nonlinear medium to generate a second harmonic generated (SHG) signal. SHG is the nonlinear process where an input wave can generate a wave with twice the optical frequency (i.e. half the wavelength) [38,39].

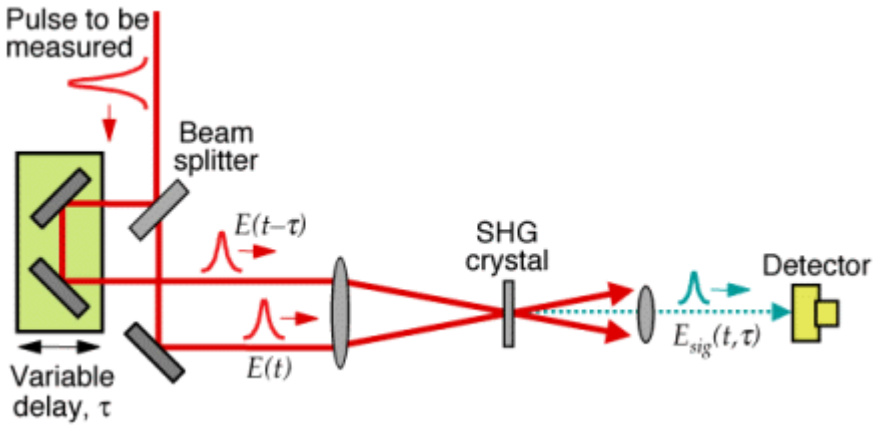

Figure 2-1 The configuration of a typical SHG autocorrelator [37].

The SHG light generated in the nonlinear crystal is directed on to the detector and the resultant electrical signal is integrated over a period that is long compared to the pulse duration. The total optical field incident on the nonlinear crystal is the sum of the direct and retarded fields [33]:

$$\varepsilon(t) = \varepsilon_1(t) + \varepsilon_1(t-\tau)\exp(-i\omega\tau) \qquad \text{Equation 2-1}$$

The second harmonic field has a complex amplitude that is proportional to the square of the complex amplitude $\varepsilon(t)$ of the original incident field and it can be shown that:

$$E_{sig}^{SHG}(t,\tau) \propto E(t)E(t-\tau) \qquad \text{Equation 2-2}$$

This signal is then incident on the optical detector. The detector has a slow response and integrates the signal resulting in an output that is a function of delay, τ only to give:

$$I_{sig}^{SHG}(t,\tau) \propto I(t)I(t-\tau) \qquad \text{Equation 2-3}$$

Detectors are too slow to time resolve $I_{sig}^{SHG}(t,\tau)$, so the measurement produces the intensity autocorrelation $A^{(2)}(\tau)$ which is a time integral:

$$A^{(2)}(\tau) = \int_{-\infty}^{\infty} I(t)I(t-\tau)dt \qquad \text{Equation 2-4}$$

The autocorrelation always has its maximum at $\tau = 0$, and is symmetrical and does not give any phase information regarding the pulse. An interferometric autocorrelation (which is generally based on a Michelson-type interferometer) measures an autocorrelation of collinear beams. Some chirp information regarding the pulse can be extracted using this method [40,41]. However, for both cases certain assumptions have to be made about the pulses in order to ascertain characteristics from the measured

autocorrelation. Thus a very different pulse width and pulse shape can be retrieved from the autocorrelation in comparison to the real/actual pulse structure [37,42].

Other nonlinearities can be used for autocorrelation and would have different mathematical functions to describe their autocorrelation. However the SHG nonlinearity is the most sensitive, such that it is most suitable for use in telecoms as the optical pulses to be characterised are typically low in power.

2.3.4 Second Harmonic Generation Frequency-Resolved Optical Gating

Over the past decade there has been increased interest in using the technique of frequency-resolved optical gating (FROG) for full electric field characterisation [37,45]. The FROG measurement technique involves taking a measurement in the time-frequency domain. It is an extension of the autocorrelator as described above, however it measures the spectrum of the pulses rather than the signal energy at each delay. Many techniques exist which use the FROG technique to measure ultra-short pulses [37,46], but the following description concentrates on SHG FROG, as SHG FROG is the measurement set-up used for pulse characterisation throughout this thesis. The experimental configuration of the FROG is shown in Figure 2-2 [37]. The spectrometer outputs the spectrogram of *E(t)* which in turn can determine *E(t)*. An example of a spectrogram is shown in Figure 2-3.

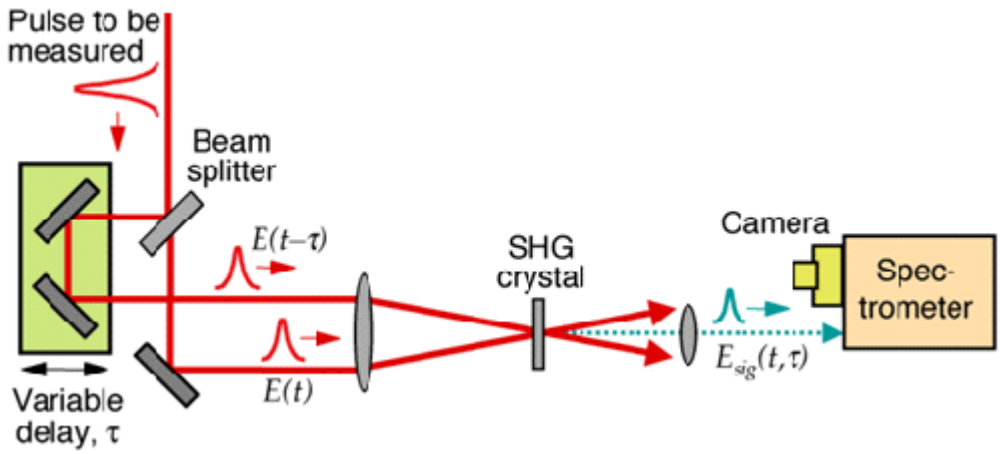

Figure 2-2 Experimental configuration of the SHG FROG [37].

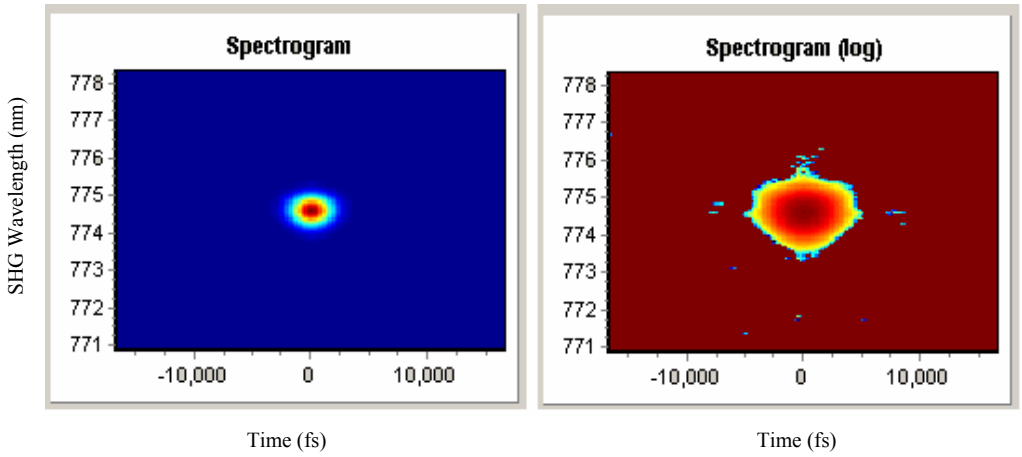

Figure 2-3 (a) A linear and (b) a logarithmic spectrogram of a 2 ps mode-locked source. The spectrogram builds up information about the pulse in the temporal and spectral domain and the colour indicates intensity.

The spectrogram measured by a SHG FROG can be described by the following equation:

$$I_{FROG}^{SHG}(\omega,\tau) = \left|\int_{-\infty}^{\infty} E(t)E(t-\tau)\exp(-i\omega t)dt\right|^2 \qquad \text{Equation 2-5}$$

The pulse is spectrally resolved at each delay point, i.e. the FROG measures the signal spectrum vs. delay rather than the autocorrelator signal energy vs. delay.

The pulse intensity and phase are obtained from this measured spectrogram by applying a 2-D phase retrieval program [47-49]. The basic algorithm starts with an initial guess of the electric field, and applies the signal field to it (i.e. for SHG $E(t)E(t-\tau)$), before Fourier transforming it to find the signal field in the frequency domain. The FROG trace is then used to generate an improved signal field. This improved signal field is inversely Fourier transformed and the new signal field is used to generate a better guess to continue the process again. This is repeated until the estimated signal field has a low error between it and the measured FROG trace.

Thus this retrieval gives the complex amplitude of the optical wave as described in Equation 1 of Appendix I. As a result the temporal profile of the pulse, its spectral amplitude and corresponding spectral phase can all be measured. However there are some ambiguities associated with the SHG FROG (which can be overcome with other FROG techniques). These ambiguities include:

1. The absolute phase remains unknown.
2. There is no absolute time reference because the pulse is used to measure itself, therefore the pulse arrival time or delay is not measured.
3. The signal can be inverted in the temporal domain, i.e. there is a time ambiguity.

4. If the pulse consists of two or more well-separated pulses, then the relative phase of the pulses have an ambiguity. In addition if the well separated pulses are symmetrical, one pulse's phase can be time reversed with respect to the other.

However FROG completely determines the pulse with essentially infinite temporal resolution, even if the temporal delay is of the order of the pulse itself [50]. This is because the time delay measurement gives long time resolution and the frequency domain measurement provides the short time resolution of the pulse structure.

2.3.5 Accurate Picosecond Pulse Measurement using FROG

In taking a FROG measurement it is important that the FROG trace has returned to a reference level so that the pulse is fully measured by the temporal span of the spectrometer, in order for the algorithm to retrieve an accurate pulse. The FROG measurement scheme deals well with noise in the system for example 10% additive or 10% multiplicative noise will lead to only a 1% rms error in the retrieved intensity and phase [37]. If the background noise is too large, this will result in large frequency fluctuations in the retrieved pulses. Thus to avoid background noise, the background noise is initially measured and subtracted before the pulses are measured experimentally. Then following a FROG measurement of a pulse, simple processing can be applied to filter any further noise in the measurement.

The FROG error measures the rms average difference between the experimental FROG trace and the retrieved FROG across the entire trace. Errors less than 0.005 result in an accurate retrieval of low noise data on a 128 x 128 pixel trace. The acceptable error scales by $N^{-1/2}$ with the grid size, thus 0.0035 is the acceptable error for a 256 x 256 grid size.

A 2 mm thick Lithium Niobate ($LiNbO_3$) crystal is employed in the FROG used for the experiments in the following chapters to perform the process of SHG. For low pump intensities, the second harmonic conversion efficiency, γ is small and grows linearly with increasing pump intensity, so that the intensity of the second-harmonic wave, P_2 grows with the square of the pump intensity, P_1.

$$(SHG) \quad P_2 = \gamma P_1^2 \qquad \text{Equation 2-6}$$

An important consideration is to ensure that the nonlinear crystal is phase matched. This is achieved through optimising the polarisation of the input signal and aligning the crystal orientation for different wavelengths. When the polarisation wave and light wave

at the SHG frequency are phase matched (i.e. when the phase velocities of the two waves are equal) there is maximum transfer of energy to the SHG wave from the pump [39]. Phase matching is very sensitive to crystal orientation, therefore the $LiNbO_3$ crystal is rotated to achieve optimum phase matching for different input wavelengths. The phase matching condition can be described as a medium whose refractive index at ω and 2ω are the same [37]. As $LiNbO_3$ crystals have a large phase matching condition, they can be employed in measurements that range over a large wavelength span.

The FROG has a temporal step delay of 26.66 fs, achieved by a high accuracy stepper motor (linear resolution of 4 μm). The spectrometer is a double pass diffraction grating, which has a focal length of 30 cm. The pixel-to-pixel spectral spacing of the linear charge coupled device (CCD) array is 0.023 nm which gives an optical resolution of <0.05 nm at 750 nm.

A typical measurement of a pulse involves a optimising the number of counts measured on the spectrometer by adjusting the polarisation and crystal angle to obtain optimum phase matching of the nonlinear crystal. A 2 ps high-quality pulse at 10 GHz would require 13 dBm input power to obtain maximum sensitivity of the FROG measurement scheme and to minimise the time taken to acquire the results. Thus for the measurement of typical pulses generated by low-power telecommunication pulse sources an amplifier is required in conjunction with the FROG in order to obtain a sufficient power level. Therefore all FROG characterisations carried out in this thesis employed a high power Erbium doped fibre amplifier (EDFA). This EDFA is specifically designed for the amplification of pulses in the order of 2 ps and is operated in the linear gain regime such that it does not alter the phase of the optical pulses being characterised by the FROG.

The number of counts measured by the spectrometer can also be increased by increasing the integration time. Longer integration periods relate to a greater CCD exposure time. An exposure time of 0.1 s is sufficient for most signals, but for weaker signals this time can be increased anywhere up to 10 s. Once the signal viewed on the spectrometer is optimised, the spectrogram is then taken; this is initiated through the pulse analyser user interface as shown in Figure 2-4.

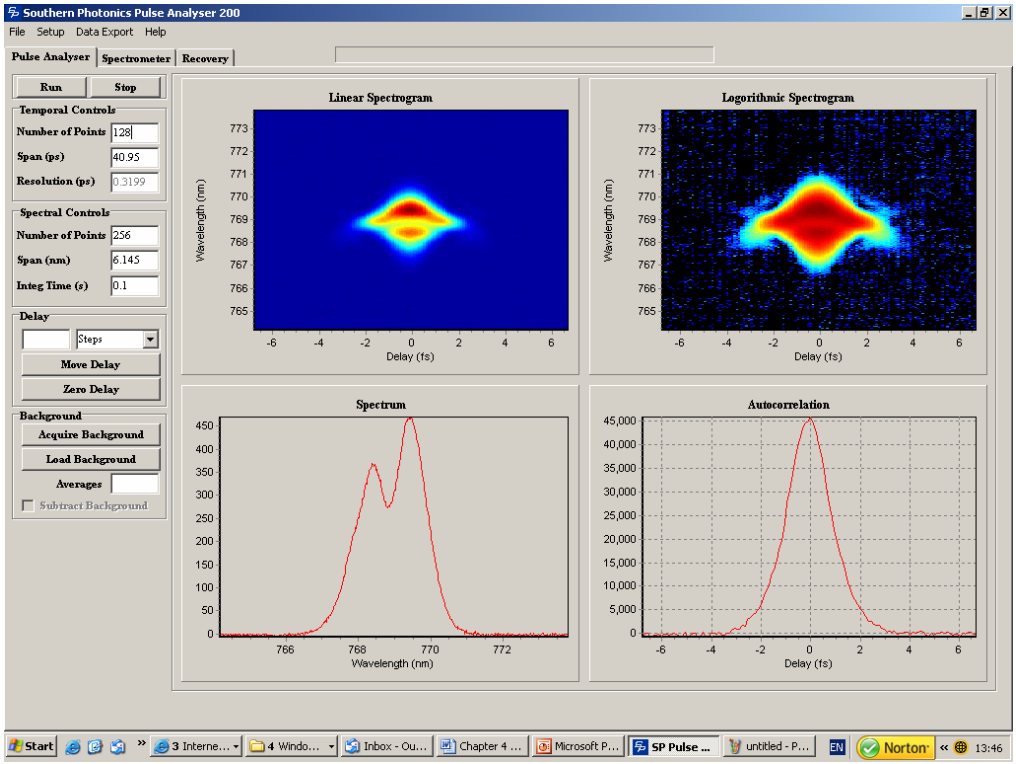

Figure 2-4 The pulse analyser interface of the FROG, which initiates and records the spectrogram and autocorrelation measurement of the pulse.

Post-processing techniques can then be applied to the acquired raw spectrogram to manipulate the data so that it is in an appropriate format for the retrieval. This process involves thresholding and interpolating the data. A 2-D phase retrieval algorithm is then applied to the spectrogram which retrieves the electric field of the pulse. The number of iterations for the algorithm is set in the user interface and typically 50-100 iterations are sufficient to achieve convergence. The algorithm generates a spectrogram and a low error difference between this spectrogram and the measured spectrogram indicates an accurate retrieval. The retrieval user interface is shown in Figure 2-5. In all the experimental work presented within this thesis, the pulse recovery routinely gave retrieval errors <0.005 on a 128 x 128 grid thus indicating the accuracy of all the retrieved pulse measurements.

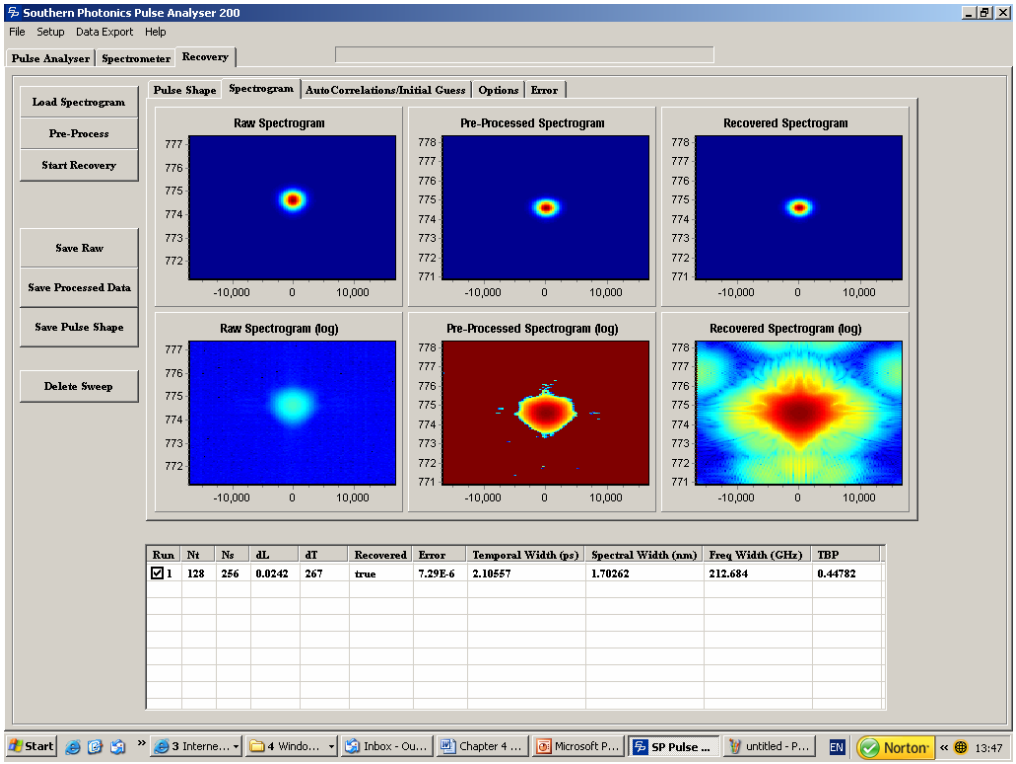

Figure 2-5 The pulse recovery interface which applies the 2-D phase retrieval algorithm to the post processed spectrogram to retrieve the pulse electric field.

2.4 Pulse Generation Techniques

2.4.1 Pulse Carving by an External Modulator

Pulse generation can be achieved by the modulation of a CW light by an external modulator as shown in Figure 2-6. Pulse generation is obtained as a result of the nonlinear response of the modulator as a function of drive voltage. Modulators can have the form of a Mach-Zehnder interferometer (MZI) or an electro-absorption modulator (EAM). The MZI is typically configured using LiNbO3 as it has a strong electro-optic effect. Constructive interference due to phase matching of the two waveguides occurs when no voltage is applied. Upon an applied voltage the refractive index of the waveguides change, causing a phase difference between the waveguides. When the two arms are 180º out of phase with respect to one another there is complete destructive interference. Thus if the propagation delays are equal for the two waveguides chirp free pulse generation can be achieved [51].

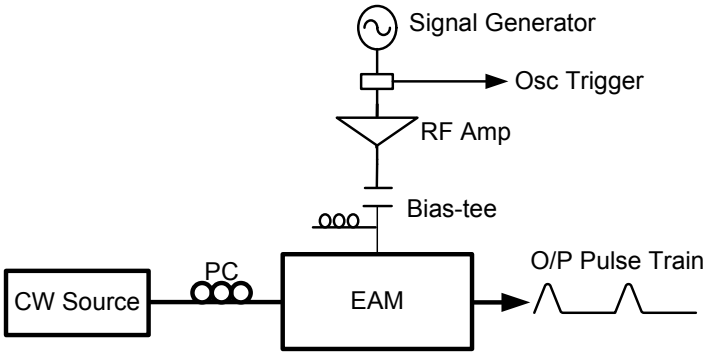

Figure 2-6 An experimental set-up of a modulator pulse carving scheme. Pulse generation is accomplished by applying a sinusoidal RF signal to a modulator (e.g. EAM), which carves optical pulses in the CW signal as a result of the nonlinear transfer function of the modulator.

EAMs in comparison to other modulators can achieve shorter pulse widths due to their larger nonlinear transfer curve [52]. An EAM is a semiconductor device, whereby an applied reverse bias causes the effective bandgap energy to decrease due to the resultant electric field in the depletion region [26]. Thus photons with energy smaller than the bandgap are absorbed. This electro-optic effect is due to the Franz-Keldysh effect in bulk EAMs and due to the quantum confined Stark effect in quantum-well (QW) EAMs [53]. Pulses generated by an EAM in comparison to a Mach Zehnder modulator (MZM) typically have a larger chirp, as an EAM is made from a semiconductor material. Therefore carrier density changes result in a corresponding phase change. However in comparison to directly modulated lasers the chirp is considerably less as there is not the same ringing of carriers due to relaxation oscillations [51].

An example of a DC bias transfer curve of an EAM is presented in Figure 2-7 (a). Using the experimental set-up as shown in Figure 2-6, 5 ps FWHM pulses are generated. The EAM was driven by a 15 dBm sine wave at a repetition rate of 40 GHz, and a CW signal of 3 dBm was optically input. The pulse temporal profile and its corresponding chirp profile as measured by the FROG technique are presented in Figure 2-7 (b). The small chirp (TBP = 0.45) translates to a pulse which is nearly transform limited. This example illustrates the advantages of pulse generation based on external modulation of a CW signal. They include the generation of nearly transform limited pulses with very low jitter and the scheme has a simple configuration with the ability to employ tunable repetition rates. However the major disadvantages are that the modulator is an expensive component, it introduces a substantial insertion loss and further compression techniques are required to generate shorter pulse widths.

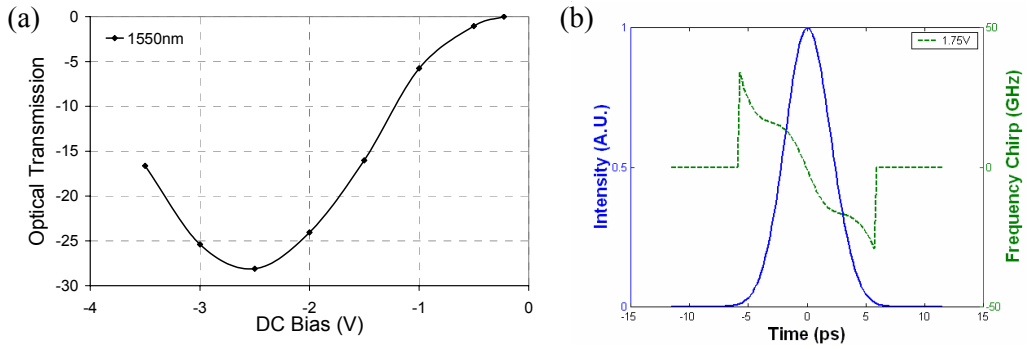

Figure 2-7 (a) DC transfer characteristic of an EAM at 1550 nm and (b) a corresponding generated pulse at 40 GHz with a FWHM of 5ps.

2.4.2 Mode Locking

In general shorter pulse widths can be obtained by mode locking a laser. A full review of mode locking is given in Ref. [54-56]. The output of a laser occurs at a number of discrete wavelengths corresponding to different resonant frequencies (modes) of the resonator. If there is no fixed phase relationship between these modes, the various frequencies will interfere with each other, and the output will fluctuate over time. By fixing the relative phases of these modes, the laser will emit a train of narrow light pulses due to constructive and destructive interference, which is the basic principle of mode locking. The larger the band of frequencies (the gain bandwidth) over which the laser oscillates the shorter the duration of the mode-locked generated pulses. In order to induce the phase modulation of the laser, either passive or active mode locking can be applied.

Passive mode locking is achieved by placing a nonlinear element within the cavity of the laser to switch high intensity light. The cavity structure of a passively mode-locked source is illustrated in Figure 2-8. The nonlinear element typically a saturable absorber (SA) has a nonlinear transfer curve whereby high intensity light is transmitted and low intensity light is absorbed. Initially there will just be CW light in the cavity, but random intensity fluctuations will occur, leading to high intensity spikes oscillating in the cavity. After a number of round-trips these high intensity spikes will result in a train of optical pulses. Passive mode locking can produce a stable pulse train with very short pulse widths. However there can be issues regarding initiation of the mode-locking process as it relies on random noise fluctuations [7].

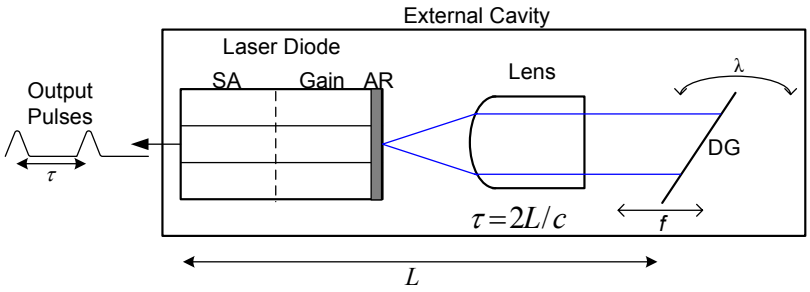

Figure 2-8 An illustration of the process of passive mode locking. SA: saturable absorber, AR: anti-reflection coating, L: the cavity length, c: the speed of light, DG: diffraction grating.

In active mode locking, the switching is typically achieved by a modulator driven by an external power source. The loss modulator that is commonly used may be pictured as a shutter that periodically opens and closes. When the modulation frequency is correctly adjusted the shutter period is then exactly synchronized to the resonator round-trip time. Thus a short pulse travelling back and forth within the laser may pass through the shutter without loss, again and again. Active mode locking generates broader pulses in comparison to pulses generated by passive mode locking, because passive mode locking pulses are generally related to the response time of the SA which is inherently faster than the shutter speeds achievable by active mode locking.

Hybrid mode locking is a mixture of passive and active mode locking. It has the benefit of passive mode locking i.e. narrow pulse widths, and the advantage of active mode locking i.e. the pulse jitter is improved and becomes close to the jitter of the applied electrical source. Figure 2-9 displays the intensity and corresponding chirp profile of a hybrid mode-locked source measured using the FROG technique. The pulses are generated using a commercially available tunable mode-locked laser (TMLL 1550) source available from u^{2}t [57]. The TMLL was driven by a 30 dBm 10 GHz sine wave and generates pulses in the order of 2 ps tunable over a 70 nm wavelength range. The inset of Figure 2-9 shows the oscilloscope trace of the pulse which gives an indication of the low jitter levels achievable by this pulse source.

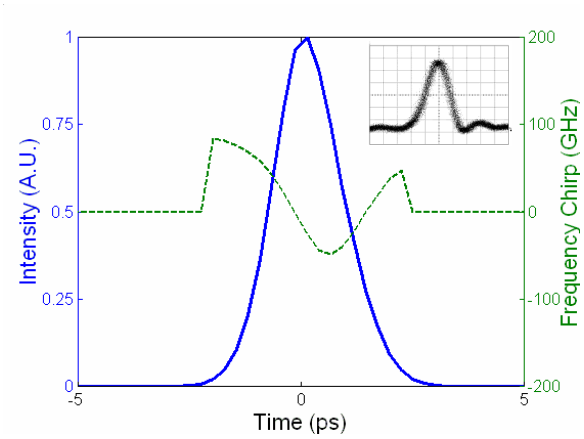

Figure 2-9 The intensity and corresponding chirp profile of a 10 GHz mode-locked source with a 1.5 ps FWHM driven by a 30 dBm RF sine wave. The inset shows an oscilloscope trace of the source to give an indication of the low jitter performance of the pulse.

Although the mode-locking process has many advantages, it has a serious drawback due to the described cavity complexity, which limits mode locking to a harmonic of the cavity frequency [58].

2.4.3 Gain Switching

One of the simplest and most reliable methods to generate picosecond pulses involves gain switching [56,59,60]. The pulses can be wavelength tunable and can be modulated at any arbitrary repetition rate. Gain switching is achieved by applying an electrical pulse or sine wave of high amplitude to a DC biased laser below threshold. The outputted pulse can be up to 10 times shorter than the applied electrical signal. The disadvantages of gain switching, which include low SMSR and large jitter, can be easily overcome by seeding the laser by self or external injection. The next two chapters examines optical processing techniques used to enhance gain-switched pulses in order to generate high quality picosecond pulse sources, because gain switching is a very simple and cost-effective method in comparison to the other pulse generation schemes previously outlined.

2.5 Gain Switching

2.5.1 Principle of Gain Switching

Gain switching is achieved by applying an electrical pulse or sine wave of high amplitude to a DC biased laser, thus switching the optical gain through the modulation of the driving current [56]. The first indications that short optical pulses could be generated by the gain-switching technique came about with the observations of relaxation oscillations when turning on a laser diode from below threshold using electrical pulses with fast leading edges. The generated optical pulses were considerably

shorter than the applied electrical pulses [61]. Gain switching consists of exciting the first relaxation oscillation and terminating the electrical pulse before the onset of the next oscillation. Electrical pulses can be generated using an electrical comb generator typically utilised by a step recovery diode [62]. Alternatively a high-frequency large-amplitude sine wave can be applied to the laser diode.

The principle of gain switching is illustrated in Figure 2-10. The laser is DC biased below threshold at I_0, and a step current is applied (Figure 2-10 (a)). The resultant relaxation oscillations are clearly visible, until the laser reaches steady-state [63]. These periodic oscillations are due to the time delay between the build-up of gain in the active region and the initiation of photon generation. The carrier density population in the active region increases due to the applied step current. The carrier decay due to spontaneous emission is typically of the order of 10's ps. Due to the increasing carrier density, net gain is achieved and initiates stimulated emission. As the photon density rises, the carrier density quickly decreases. When the carrier density is depleted to below the carrier threshold, the optical pulse is terminated, leading to the process repeating again until steady state is reached. At steady-state the carrier density threshold, n_{th} remains clamped, as any increase in applied current leads to an increase in generated photons via stimulated emission. To generate a single optical pulse, the step current is replaced by an electrical pulse or sine wave as illustrated in Figure 2-10 (b). The electrical current switches off just after the first relaxation oscillation, suppressing the generation of further relaxation oscillations. However, if optimum settings are not applied to the RF and DC bias currents, a secondary pulse can be generated on the tail of the gain-switched pulse. It occurs when the electrical sine wave continues to pump carriers into the laser active region, bringing the carrier density above threshold again, reinitiating the lasing process until the carriers are once again depleted to below threshold.

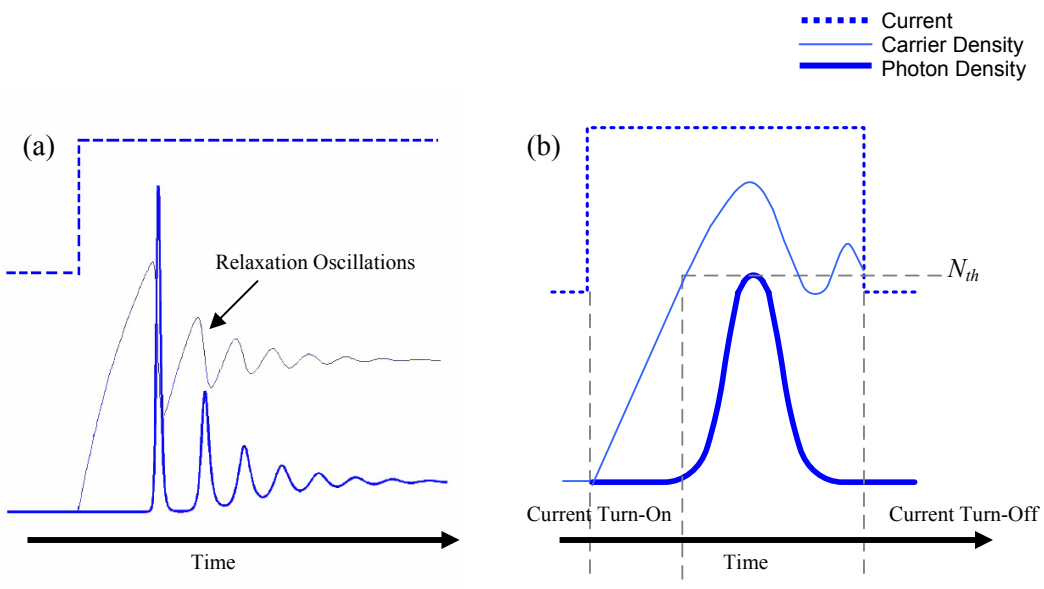

Figure 2-10 An illustration of the current and photon densities for (a) a current step and (b) a current pulse. N_{th}: carrier density threshold.

2.5.2 Laser Diode Parameters which Determine the Gain-Switched Pulse Shape

The pulse shape of a gain-switched diode can be described as a combination of two exponential curves with time constants τ_r (rising edge) and τ_f (falling edge). The pulse rise time is inversely proportional to the net charge transferred by the electrical signal to the active region. The fall time depends on how far below threshold the carrier density is brought. If I_0 remains too high, a pedestal can form on the trailing edge of the gain-switched pulse, which is a consequence of the second relaxation oscillation. These two examples are illustrated in Figure 2-11 which compares a gain-switched Fabry–Pérot (FP) laser DC biased at $I_{th}/2$ and at I_{th}.

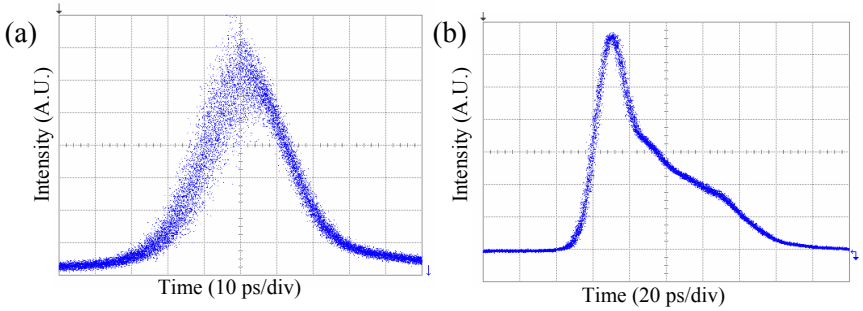

Figure 2-11 A gain-switched laser biased (a) below threshold (14 mA), and (b) at threshold (28 mA) with a large RF amplitude modulation (29 dBm).

The optimum DC drive bias, I_0 is typically half the threshold current, i.e. $I_{th}/2$, in order to achieve the smallest pulse width [56]. By increasing the DC bias current above this

optimum value the pulses are broadened. As I_0 increases above I_{th}, the gain-switched pulse width becomes insensitive to the further increases in I_0. The amplitude and frequency of the applied modulation current, I_{sig} also determines the pulse characteristics. An increase in the amplitude of the modulation signal leads to a decrease in pulse width, while an increase in its frequency results in an increase in the optical pulse width, and a reduction in peak power. The pulse width broadening is due to a reduction of the modulation depth.

One of the main reasons limiting the further reduction of the gain-switched pulse width (10-40 ps) is due to the difficulty of sustaining a large inversion level (i.e. a build up of free carriers in the active region) before the emission of the optical pulse [64]. Thus there is a trade off in optimising the bias for a gain-switched laser. If the laser is unbiased, a large build-up of charge is achieved but it is possible for the laser not to reach positive inversion. On the other hand if the laser is biased above threshold, the existing stimulated emission will clamp the inversion level to just above threshold, thus the generated pulses are wider and have less peak power. The maximum achievable inversion is limited by the fundamental parameters of the laser, such as the differential gain, the photon lifetime and nonlinear gain compression.

The bandwidth of a laser can be improved by increasing the differential gain and reducing the photon lifetime [65]. The differential gain is dependent on the material and structure of the device, in particular the length of the device. The photon lifetime can also be reduced by shortening the device length of the laser diode and by applying an antireflection coating to one of the facets. Thus, a shorter device length results in the generation of narrower pulse widths [66]. Nonlinear gain compression is detrimental in that it limits the peak photon density by damping the large frequency oscillation, thus increasing the pulse width and reducing the peak power. The nonlinear gain compression is dependent particularly on the device structure and its effects can be offset by introducing a destabilising effect (e.g. the introduction of an intracavity SA) [67]. The nonlinear gain coefficient sets the limit on the minimum obtainable pulse width and maximum obtainable peak power.

2.5.3 Laser Diode Multimode Rate Equations

To numerically determine pulse shape generated by the gain-switching process, the rate equations can be used [68]. The carrier density rate equation incorporates all the mechanisms by which the carriers are generated or lost inside the active region. Since

the number of electrons is equal to the number of holes, it is sufficient to consider one rate equation for electrons alone. The multimode carrier density rate equation is:

$$\frac{dN}{dt} = \frac{I}{qV} - \sum_m g_m S_m - \frac{N}{\tau_n} \qquad \text{Equation 2-7}$$

where, N is the carrier density, t is the time, I is the applied current, q is the electronic charge, V is the volume of the active region, τ_n is the carrier lifetime, g_m and S_m are the optical gain and photon density of the m^{th} longitudinal mode respectively. Carrier diffusion is neglected for lasers where the active region width is very small in comparison to the diffusion length. The first term on the right-hand-side (RHS) of this equation governs the rate at which the carriers, electrons or holes are injected into the active region because of external pumping. For a gain-switched pulse, the applied current is described as a sine wave, I_{sig} sitting on a DC bias, I_0. The other terms take into account the carrier loss owing to various radiative and non-radiative recombination processes. The second term describes stimulated emission and leads to a nonlinear coupling between photons and charge carriers. $g_m = dg/dN(N-N_0)$, where dg/dN is the differential gain and N_0 is the carrier density required to achieve transparency. The last term takes monomolecular, spontaneous and Auger recombination into account. Monomolecular recombination is due to mechanisms such as trap or surface defects, and results in electronic levels near the centre of the bandgap. It only affects one carrier-type. Spontaneous emission involves both types of carriers, whereby an electron in the conduction band and a hole in the valence band recombine in a random process and a photon is spontaneously emitted. Auger recombination occurs when two carriers collide. The collision transfers the energy released from the recombining carrier to the surviving carrier, and the surviving carrier goes to a higher energy level.

The photon density rate equation for each longitudinal mode is described by:

$$\frac{dS_m}{dt} = \left(\Gamma g_m - \frac{1}{\tau_s}\right) S_m + \Gamma \beta_{sp} \frac{N}{\tau_{sp}} \qquad \text{Equation 2-8}$$

where, Γ is the optical confinement factor (the fraction of mode energy confined within the active region), τ_s and τ_{sp} is the photon and spontaneous recombination lifetime respectively and β_{sp} is the spontaneous emission factor. The first term on the RHS gives the number of photons that are created due to stimulated emission in the optical gain region. The second term is the photon decay rate which reduces the photon density as it accounts for the photons lost through the cavity facets at each end of the laser and to internal processes. The last term governs the number of photons that add to the lasing

process due to spontaneous emission. A certain fraction of the carriers that spontaneously recombine emit photons that enter the waveguide travelling in the correct direction and a proportion of these have the same wavelength as the stimulated emitted photons.

2.5.4 Frequency Chirping due to Gain Switching

Gain switching is a result of a large variation of the carrier density in the active region of the laser as illustrated in Figure 2-10 (thin blue line). This large change in the carrier density results in a large frequency chirp in pulses generated by the gain-switching process. The pulses can be far from transform limited and thus can cause detrimental effects in the propagation of these pulses in high-speed systems. The origin of this chirp can be accounted for by the Kramers-Kronig equations, which relate a change in the gain (or loss) in a semiconductor to a corresponding change in its refractive index [69]. The linewidth enhancement factor (LEF), α which relates the changes in gain to changes in refractive index is defined by the following expression [70]:

$$\alpha = \frac{-4\pi}{\lambda}\frac{dn/dN}{dg/dN} \qquad \text{Equation 2-9}$$

where n and g are the refractive index and gain of the semiconductor material respectively. This equation shows that a large change in carrier density during the emission of a gain-switched pulse leads to a variation of the refractive index, causing a variation of the frequency distribution across the pulse [71]. The chirp, $\Delta v(t)$ which is the differentiation of the phase, can be expressed in terms of the LEF as shown here [72]:

$$\frac{d\phi}{dt} = \frac{\alpha}{2}\left(\Gamma g - \frac{1}{\tau_p}\right) \qquad \text{Equation 2-10}$$

$$\Delta v(t) = -\frac{1}{2\pi}\frac{d\phi}{dt} = -\frac{\alpha}{4\pi}\left(\Gamma g - \frac{1}{\tau_p}\right) \qquad \text{Equation 2-11}$$

Equation 2.9 shows that a higher differential gain (dg/dN), results in lower chirp. In addition to the benefits listed above with regard to the generated pulse shape a high differential gain (achievable in short devices and quantum-well structures) will also generate pulses with smaller chirp. Chirp reduction can also be achieved by increasing the bias current above threshold as this reduces the magnitude of carrier density variation. However this has the detrimental effect of damping the relaxation oscillations thus increasing the pulse width and reducing the output pulse peak power.

Previous studies have analysed the chirp generated by gain-switched lasers including FROG measurement techniques [73], interferometric two-photon absorption (TPA) autocorrelation [74], and numerical calculations [75]. An example of a gain-switched pulse and its corresponding chirp profile measured by the FROG technique are illustrated in Figure 2-12. The chirp is linear across the central part of the pulse going from high frequency components (blue chirp) to low frequency components (red chirp), which is due to the depletion of carriers during optical pulse emission via stimulated emission. The chirp is nonlinear in the wings of the gain-switched pulse, which is a result of the increased carrier density in the gain medium during the pulse build-up time [76]. Thus dispersion compensating techniques are required to compensate for the chirp and to reduce the pulse width. Generally linear compression techniques are applied, however the nonlinear chirp in the wings of the pulse result in the generation of pedestals due to the insufficient compression of the nonlinear chirp. This is discussed in more detail in Chapter 3, Section 3.4.

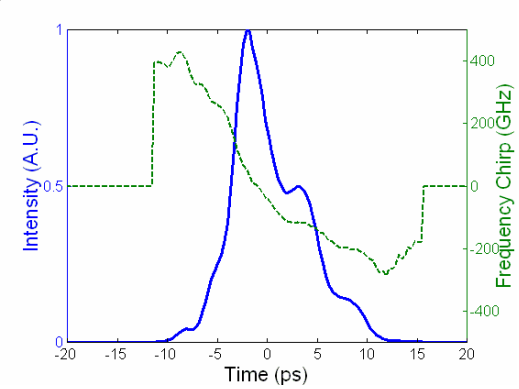

Figure 2-12 The temporal profile and corresponding chirp of a gain-switched DFB laser. A 10 GHz sine wave biased at 2.5 I_{th} with a corresponding power of 30dBm was applied to the laser to generate pulses at a wavelength of 1551.54 nm.

2.5.5 Side Mode Suppression Ratio of a Gain-Switched Laser Diode

The SMSR of a gain-switched source is degraded due to the large fluctuation in the photon density as the laser is pulled below threshold, which strongly excites the side modes. This SMSR degradation is illustrated in Figure 2-13, which compares the spectrum of a laser operating in CW and a gain-switched laser. As can be clearly seen the SMSR reduces dramatically from 40 dB to 6 dB.

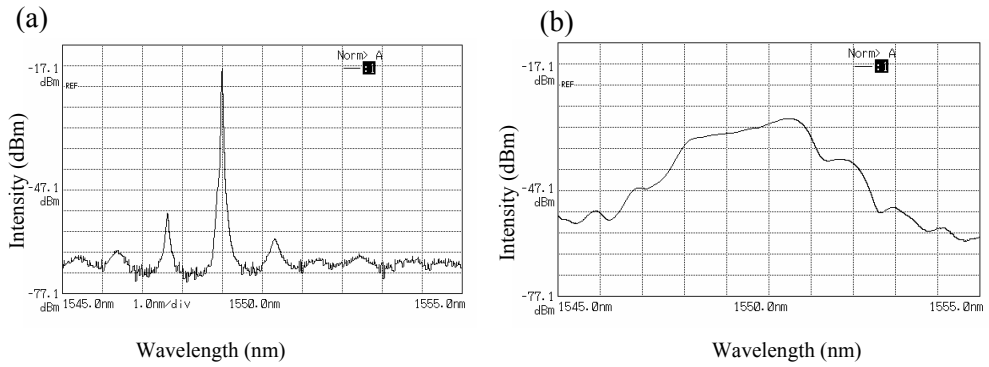

Figure 2-13 SMSR degradation is illustrated here by comparing the spectrum of a laser (a) before gain-switched modulation (i.e. CW operation) and (b) following gain switching.

2.5.6 Extinction Ratio of a Gain-Switched Laser Diode

The ER of a gain-switched laser can be enhanced by increasing the differential gain of the laser [77]. As is expected the ER is highly dependent on the current drive conditions. To achieve the highest ER, the DC drive bias current, I_0 should be operated below threshold. If I_0 is greater than I_{th}, the ER is severely degraded. In addition, the modulation amplitude, I_{sig} will determine the power in the 'one' level.

2.5.7 Jitter of a Gain-Switched Source

The timing jitter of a gain-switched pulse originates from random fluctuations of the photon density in the laser cavity. The start-up phase of each pulse in a gain-switched laser relies on the generation of random spontaneous photons. Thus a lower DC current, I_0 causes a longer turn-on delay of the optical pulse. In gain-switched lasers where the pulse turn-on is dependent on the build-up of spontaneously generated photons the phase is not retained for each subsequent pulse and these phase variations lead to wide-band noise. Timing jitter decreases as the ratio I_0/I_{th} increases. There are two sources of jitter, correlated and uncorrelated [78]. The timing jitter due to the random spontaneous emission is uncorrelated jitter and depends largely on the drive current. If the drive conditions are not optimised uncorrelated rms timing jitter up to 14 ps has been measured [79]. The rms timing jitter is proportional to the ratio of the standard deviation to the mean cavity photon density around t_0, where t_o is the time at which the carrier density reaches threshold [7]. By contrast, mode-locked lasers exhibit a negligible contribution of uncorrelated jitter due to the strong coupling between spectral modes (as was discussed in Section 2.4.2). In both gain-switched and mode-locked sources the correlated jitter is dependent on the laser diode electronics and the driving RF source, thus very low values can be obtained if low phase noise electronics are used. The gain-switched source shown in Figure 2-11 (a) shows the large jitter that can be present on a gain-switched FP laser.

Gain-switched sources are dependent on the random build-up of spontaneous emitted photons. The jitter in a gain-switched single-mode distributed feedback (DFB) laser is larger than in a multimode free running laser. This is because the relative fluctuation of the photon number which as a random process is estimated to scale inversely proportional to the square root of the photon number, which is significantly lower for a multimode laser than for a single mode laser, resulting in a lower jitter [80].

2.6 Gain Switching and Optical Injection

Optical injection of gain-switched sources can provide reduced chirp, linewidth reduction, enhanced SMSR, large reduction in timing jitter and a higher frequency bandwidth [81] at the expense of a small increase in pulse width. There are two methods of providing optical injection, through self seeding or external injection.

2.6.1 Self Seeding of a Gain-Switched Laser Diode

Self seeding was first investigated by Lundquist et al. [82]. Self seeding entails the use of a wavelength selective external cavity to re-inject a small fraction of the output light back into the gain-switched laser at only one longitudinal mode frequency [83,84]. Provided that the optical signal re-injected back into the laser arrives during the build-up of an optical pulse in the cavity, then a single-mode output pulse is obtained. This is achieved by either adjusting the frequency of the RF applied to the laser or by inserting a tunable optical delay (ODL) line in the set-up. Figure 2-14 illustrates the principle of operation of self seeding. Pulses from the gain-switched DFB laser are reflected from the wavelength selective device back into the active region of the laser. A polarisation controller (PC) is used to ensure that the light being fed back is aligned with the optical axis of the laser, thus maximizing the effect of feedback. To achieve single mode steady-state takes approximately 5-10 round-trips of the pulse in the cavity, depending on the feedback wavelength [85]. In comparison it takes approx 100 round-trips for an active mode-locked device to achieve optimum pulse width conditions [7].

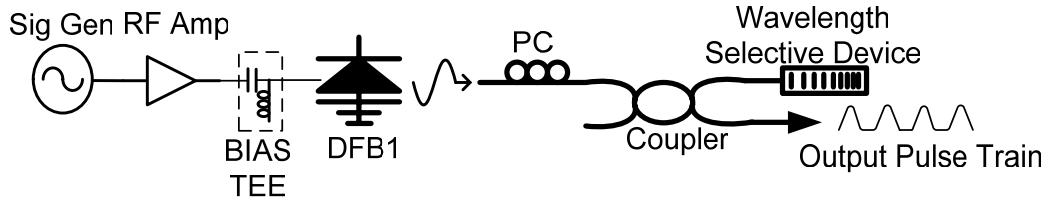

Figure 2-14 Principle of operation of self seeding a gain-switched laser diode.

2.6.2 External Injection of a Gain-Switched Laser Diode

An alternative technique to self seeding entails external light injection from a CW source into a gain-switched laser [86,87]. External injection has an advantage over self seeding because no adjustment of the repetition rate or the external cavity length is required. The effects of the external injection on the gain-switched laser are immediate unlike self seeding and mode locking which take time to stabilise. The wavelength is tuned by changing the injection wavelength to the desired mode. Thus, external injection provides a more stable operation in comparison to self seeding as it has an instantaneous switching time, which is only dependent on the CW laser switching time. This advantage is at the expense of a costly tunable CW source.

2.7 Experimental Investigation of the Effects of Optical Injection on a Gain-Switched Pulse

The initial experiments undertaken investigate the effect of external optical injection on the spectral profile, pulse width, and chirp of a gain-switched source. The experimental set-up is shown in Figure 2-15. The laser which provides the optical injection is a commercially available single mode tunable CW source, with a precision of 1 pm (125 MHz) and delivers up to 6 mW of power. The isolator ensures uni-directional propagation of the light from the CW source to the gain-switched laser. The gain-switched source consists of a commercially available NEL DFB laser (data sheet included in Appendix 2), which is modulated by the 10 GHz sine wave amplified by a high power RF amplifier to 30 dBm. The bias-tee combines the DC bias ($2.5I_{th}$) and the RF signal which is applied to the laser. The laser is characterised by a 3 dB bandwidth of 20 GHz and an output power of 4.7 dBm, both measured at a bias of $3I_{th}$. The output pulses had a wavelength of 1551.54 nm.

The components that make up the pulse source and external injection are polarisation maintaining, so that the polarisation of the injected field is controlled to ensure constant coupling, except for the fibre output of the gain-switched source. Thus a PC is included to align the axis of the polarisation of the injected light to the polarisation of the gain-switched laser. Throughout the experiment the parameters of the gain-switched laser remain fixed. The injected power, P_{inj} can be varied through the variable optical attenuator (VOA) and the detuning (ν_{cw}-ν_{gs}) is set to around 20 GHz (1551.383 nm), to give optimum performance [88].

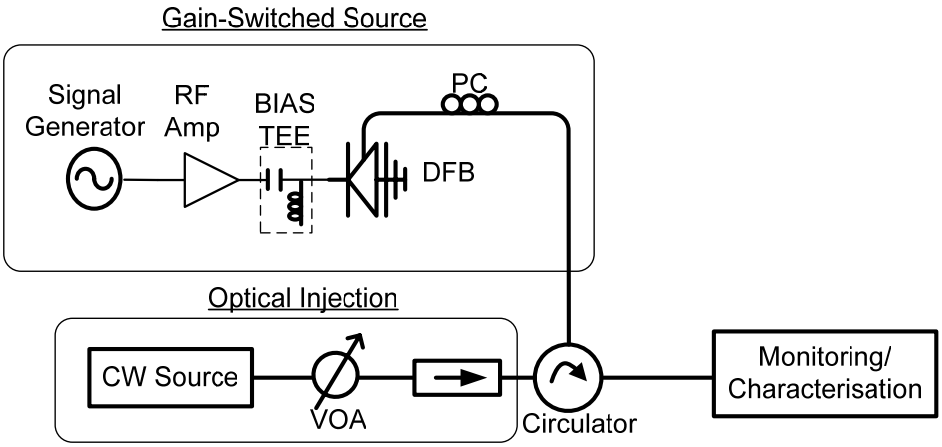

Figure 2-15 The experimental set-up used to investigate the impact of optical injection on a gain-switched laser source.

2.7.1 Spectral and Temporal Width Analysis as a Function of Injected Power

Initially the externally injected gain-switched spectrum is characterised as a function of P_{inj} as shown in Figure 2-16 (a). As previously reported, as the injected power is increased there is a corresponding decrease in the FWHM spectral width and an increase in the SMSR [73,86]. The origin of this reduction of the spectral width can be attributed to the reduced threshold gain induced by the optical injection field. If the power of the optical injection field is greater than the power of the spontaneous emission of the gain-switched source, the injected field acts as a source to initiate gain switching [64]. Thus the peak inversion level is reduced and the gain variation during the emission of a pulse also decreases, leading to a reduced spectral width, and a smaller chirp at the expense of a small increase in temporal width of a pulse. A sufficient SMSR of 30 dB is achieved at -10 dBm injected power. The small increase in pulse width as a function of increasing injected power is illustrated in Figure 2-16 (b). The pulse width increases from 7.7 ps to 8.7 ps when comparing a gain-switched pulse with no optical injection to a pulse with optical injection equal to -10 dBm.

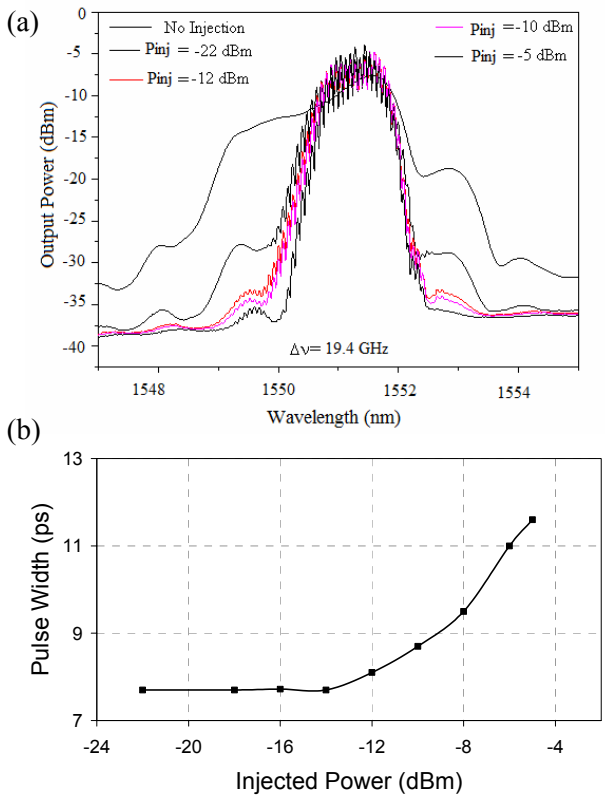

Figure 2-16 (a) Optical spectrum of a gain-switched DFB laser under different levels of optical injection and (b) the variation of pulse width as a function of injected power.

2.7.2 Chirp Reduction due to Optical Injection

Chirp reduction due to optical injection has been demonstrated experimentally by Mohrdiek et al. [89], using eye diagrams obtained with a transmission experiment with and without injection. Here the chirp is measured directly using the FROG technique. As illustrated in Figure 2-17, the chirp is greatly reduced for the gain-switched source with optical injection in comparison with no injection. The gain-switched laser with no injection has an approximate amplitude of 700 GHz and this is reduced to approx 200 GHz under injection for an injection power of -11 dBm at a detuning of 20 GHz. For both cases the chirp is nonlinear in the wings of the pulse.

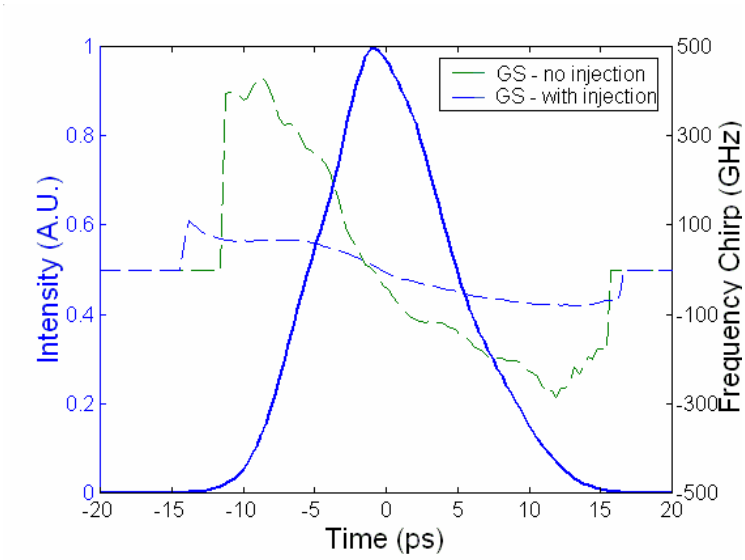

Figure 2-17 A gain-switched temporal profile overlaid by the chirp profile without and with optical injection (P_{inj} = -11 dBm).

2.7.3 Jitter Improvement due to Optical Injection

As was explained the jitter in an unseeded gain-switched laser is dominated by random spontaneous emission. As was discussed in Section 2.5.7, the gain-switched pulses are initiated by spontaneously emitted photons. When optical injection is used the injected photons initiate the pulse generation process a lot sooner in comparison to spontaneously emitted photons [90]. This reduces relative fluctuations in the photon density resulting in a corresponding reduction in timing jitter. Thus as the optical injection increases the timing jitter decreases. For maximized jitter reduction the optical injection wavelength is required to be injected over a small span close to the centre of the gain-switched spectrum [88]. The improvement in jitter of a gain-switched source is clearly visible by applying optical injection as shown in Figure 2-18. The measured jitter was approximately 3 ps for the unseeded gain-switched laser and was <1 ps for the seeded gain-switched laser, corresponding to Figure 2-18 (a) and (b) respectively.

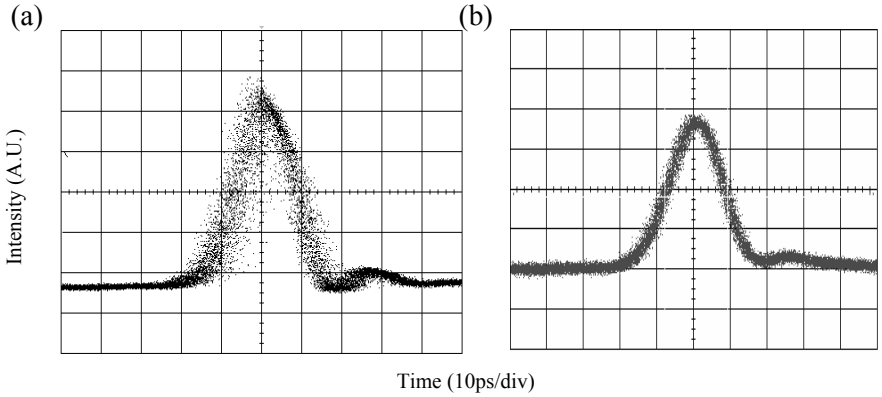

Figure 2-18 (a) A large uncorrelated jitter is identifiable on the gain-switched pulse and (b) indicates the improvement which can be obtained by applying optical injection to the gain-switched source.

2.8 Wavelength Tunable Self-Seeded Gain-Switched Pulse Source

In this section a novel set-up is presented which employs self-seeding in a dual laser source to provide transform limited pulses, with an approximate width of 20 ps at FWHM, which are highly wavelength tunable over 50 nm. This source is an excellent candidate for WDM and hybrid WDM/OTDM systems due to its large wavelength tunability, high SMSR and low pulse width. This work extends research that has been carried out in the development of wavelength tunable self-seeded gain-switched sources that resulted in the generation of 90-130 ps optical pulses with SMSRs of around 32 dB, that are tunable over 19 and 26 nm respectively [91,92].

2.8.1 Experimental Set-up

Figure 2-19 illustrates the experimental configuration of the pulse source. It essentially consists of two gain-switched FP laser diodes that are self seeded using a single external cavity. Two FP lasers were used to expand the tuning range of the source. They were chosen in such a way as to ensure that there was only a very small overlap between their gain profiles as illustrated in Figure 2-20 (a).

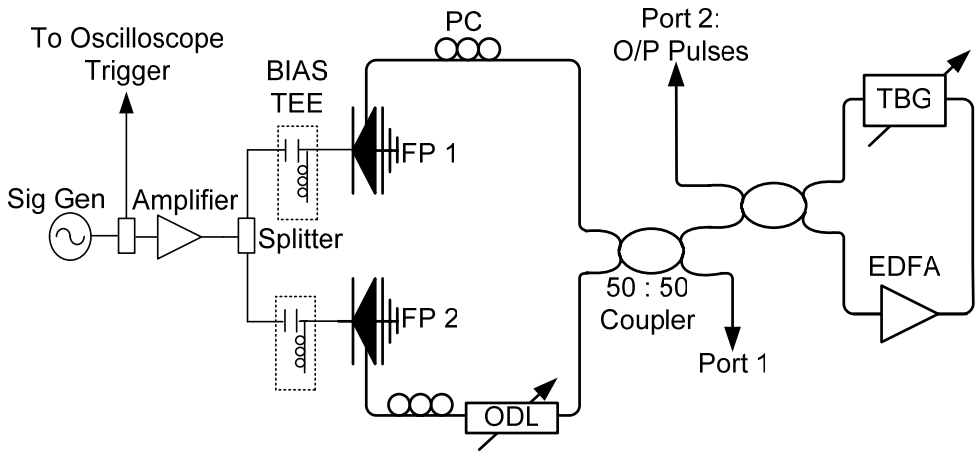

Figure 2-19 Experimental set-up for self-seeded gain-switched pulses.

The FP lasers used were commercial 1.5 μm InGaAsP devices, with threshold currents of about 26 mA and mode spacings of 1.12 nm. Gain switching of both lasers was carried out by applying a DC bias current of 17 mA, and a 2.5 GHz sinusoidal modulation signal with a power of 29 dBm to both devices. The gain-switched output from both lasers was coupled together before being fed into the external cavity configuration, which selects out the wavelength of the mode to be re-injected back into the laser. The external cavity consists of a PC, a 3 dB coupler, a tunable Bragg grating (TBG) and an EDFA. An optical isolator in the EDFA ensures that light only propagates in one direction around the feedback loop. The tunable filter eliminates unwanted amplified spontaneous emission (ASE) from the EDFA in addition to selecting the lasing mode of operation. The TBG has a 3 dB spectral bandwidth of 0.23 nm, a wavelength tuning range of 1460-1575 nm, and an insertion loss of 5 dB. The external cavity for self-seeding FP2 contains a tunable ODL to ensure that self seeding of FP1 and FP2 can be achieved. The EDFA is required to overcome the high losses obtained in the TBG and to ensure that there is sufficient light re-injected into either laser to obtain a suitable SMSR on the output pulses.

To achieve optimum pulse generation, the Bragg grating was initially tuned to one of the longitudinal modes of the gain-switched FP1 laser. The frequency of the modulation was then varied to ensure that the signal re-injected into the laser, from the external cavity, arrives as an optical pulse is building-up in the laser. An operating frequency of 2.498 GHz was found to be suitable. The grating was then tuned to one of the longitudinal modes of FP2, and in this case, the ODL was varied to ensure that the signal fed back into FP2 arrives at the correct instant. The bias currents of FP1 and FP2 were then

slightly changed to obtain the minimum pulse width. By subsequently tuning the grating across the gain curves of the lasers, single mode operation was achieved over a wide range of wavelengths.

2.8.2 Results and Discussion

The optical spectrum of the dual wavelength signal from the gain-switched lasers without self seeding is shown in Figure 2-20 (a). Figure 2-20 (b, c & d) shows in their respective order the shortest, central and longest wavelengths that can be seeded. The seeded spectra shown are the composite output of the two self-seeded gain-switched lasers before passing through the optical filter and amplifier measured at port 1.

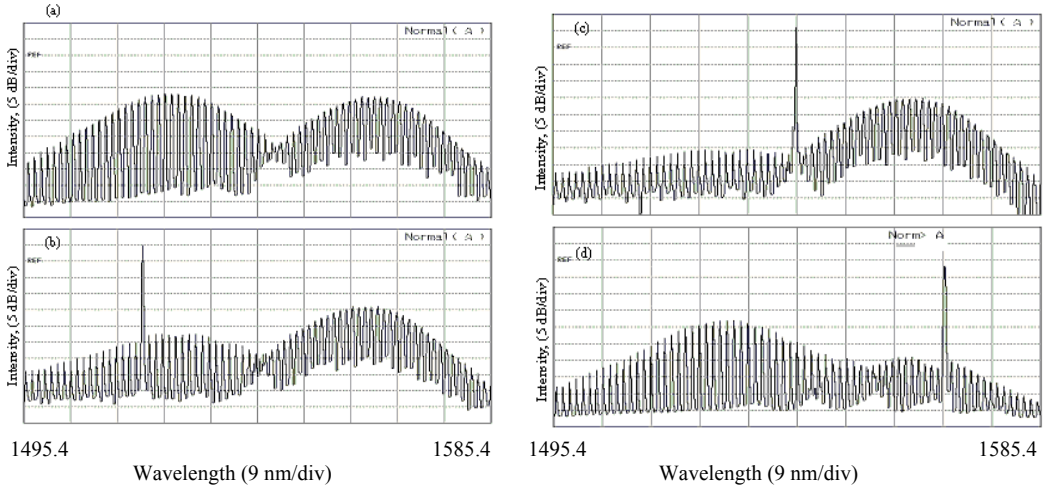

Figure 2-20 Output optical spectra at port 1 of: (a) dual wavelength signal, and an illustration of three wavelengths obtained at the: (b) shortest wavelength (1517.73 nm), (c) central wavelength (1540.4 nm) and longest wavelength (1566.64 nm).

The composite signal from the self-seeded gain-switched lasers is then passed through the external cavity before being outputted at port 2. The effect of this is to eliminate the signal from the unseeded laser, and greatly improve the SMSR of the generated optical pulses from the seeded laser (as shown below in Figure 2-21 (b) and (d)). The output pulses and their associated spectra, generated at two specific wavelengths (1524 and 1560 nm), are shown in Figure 2-21. The deconvolved pulse width for the 1524 nm signal was 16 ps while that of the 1560 nm was 18.5 ps. The associated spectral widths of these two signals were 27 GHz and 26 GHz respectively, while the SMSR of the generated pulses were 54 and 56 dB respectively. The measured pulse width remained reasonably constant (16 – 20 ps) as the output pulses were tuned across the tuning range, with slight increases at the limits of tunability, and the TBP of the generated pulse varied slightly from 0.43 to 0.49 over the wavelength tuning range. The average output power is around 1.8 mW. The main limitation on the wavelength tuning of the generated pulses

was imposed by the gain bandwidth of the EDFA used in the experimental set-up. The tuning range could be enhanced by using an EDFA with a wider gain bandwidth or eliminating the need for an EDFA. The latter is demonstrated in the next experiment and shows a tuning range increase from 50 nm to 65 nm.

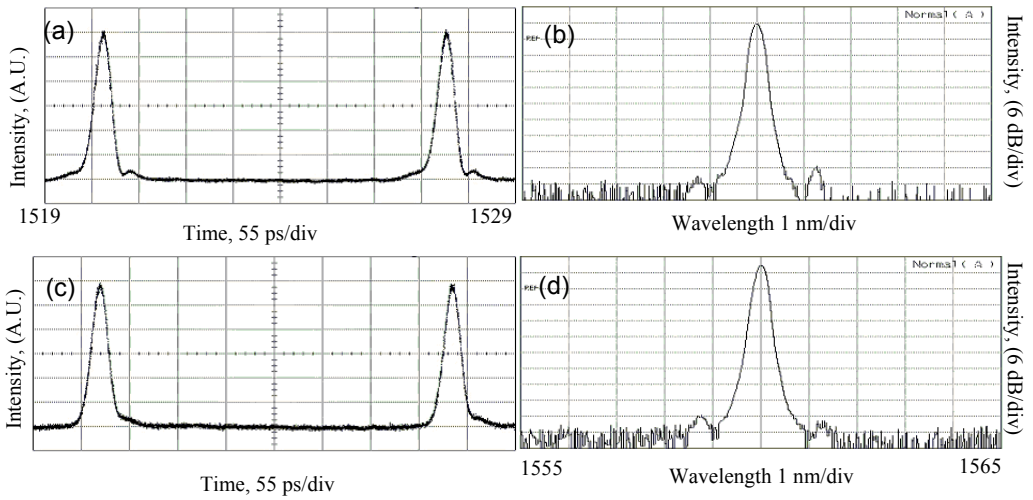

Figure 2-21 Output optical pulses (a) & (c) and their corresponding spectra (b) & (d) at wavelengths 1524 and 1560 nm respectively.

The dependence of the SMSR on the seeding wavelength is plotted and shown in Figure 2-22. It can be clearly seen that an SMSR of 50 dB and above is obtainable within the range of 48.91 nm (1517 .73 to 1566.64 nm). Figure 2-22 also shows the pulse width variation as the wavelength is tuned. The point where the pulse width exhibits a sudden increase is the juncture when the seeded wavelength is moved from FP1 to FP2.

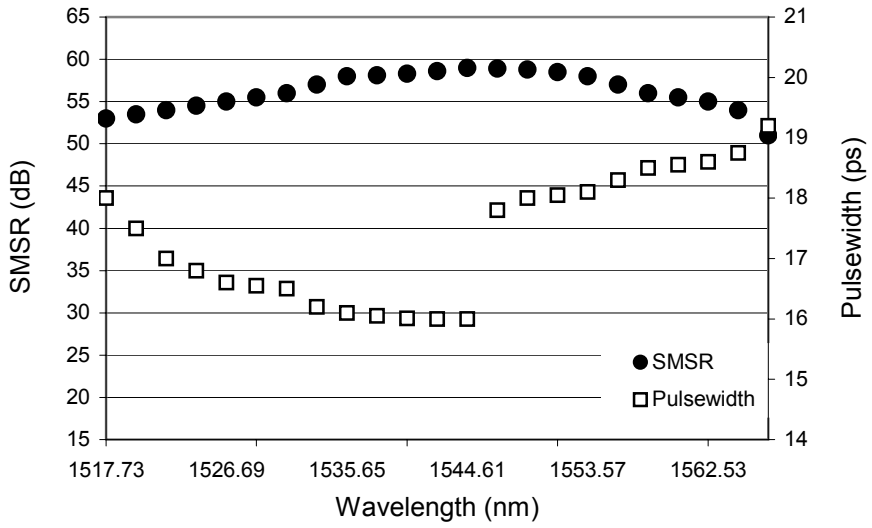

Figure 2-22 SMSR (left-hand-side (LHS) axis) and deconvolved pulse width (RHS axis) against tunable wavelength range.

2.9 Widely Tunable Picosecond Pulse Source using External Injection

The results obtained in the experiment above (Section 2.8) are improved on further by replacing the self-seeding feedback loop by an external injection source. Thus the generation of pulses over a larger tuning range (>65 nm) with SMSRs in excess of 60 dB over the entire tuning range [93,94] is achieved. This complete pulse source offers the largest tuning range and SMSR that has been based on gain-switching laser diodes to date.

2.9.1 Experimental Set-up

The experimental set-up is shown in Figure 2-23. The gain switching of the two laser diodes is the same as the previous experiment. The seeding is now provided by external injection from a tunable CW source, via an isolator to prevent any re-injection of the light into the CW source. Without the need of an EDFA (that had previously limited the wavelength span due to its gain curve) the wavelength tuning range has been increased. In addition there is no need for the ODL because a CW source is used rather than pulses to provide injection. Therefore the set-up is very stable and has a repetition rate that can be easily tuned without the need to adjust the feedback cavity length.

The output power of the CW source is set at -3 dBm, however, taking into account various losses, we estimate the injection level into the gain-switched sources to be about -13 dBm. The resulting single-mode output obtained after external injection into one of the FP lasers, together with the signal from the unseeded FP laser is passed through the TBG filter. The filter is used to eliminate the optical output from the gain-switched FP laser that is not influenced by the external injection, and to enhance the SMSR of the generated pulses.

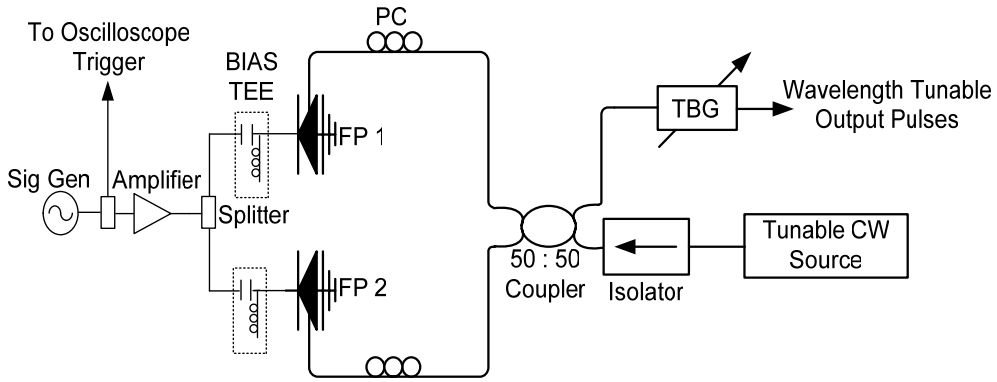

Figure 2-23 The experimental set-up used for external injection seeding of a gain-switched dual laser source.

2.9.2 Results and Discussion

Similar to the first set-up, the use of two FP lasers enables injection over a large wavelength span. Different longitudinal modes of each FP laser were selectively excited when the seeding wavelength from the external cavity laser (ECL) was tuned near the centre of any desired mode. Figure 2-24 (a) and (c) displays the resulting spectral and temporal (non-averaged) output before the optical filter showing good SMSR for the seeded gain-switched diode and a clean optical pulse with a good ER at a wavelength of 1520 nm. With the addition of the filter, the optical output from the unseeded FP laser is eliminated and the SMSR of the output pulses is improved such that it becomes almost impossible to detect the sidemodes above the noise floor of the OSA. The resulting SMSR is around 60 dB for the entire wavelength tuning range that can be achieved with this set-up. The spectral and temporal profile of the pulse following the filter are shown in Figure 2-24 (b) and (d), which clearly illustrates the excellent temporal and spectral purity of the pulse source. The pulse width FWHM is 28 ps while the spectral width is approximately 20 GHz, resulting in a TBP of 0.56 (slightly larger than that of a transform limited Gaussian pulses). The ER was measured to be 25 dB, and the timing jitter was estimated to be less than 1 ps.

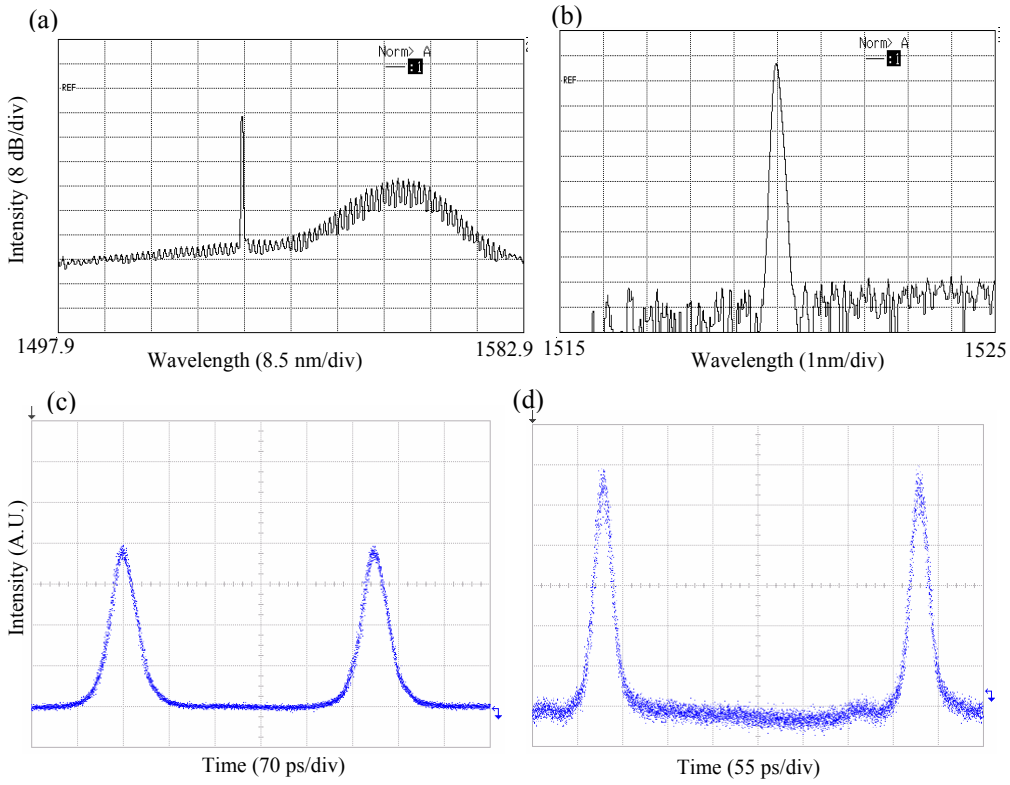

Figure 2-24 Output results taken at a wavelength at 1519.9 nm showing (a) the spectrum before the filter, (b) the spectrum following the filter, (c) the optical pulse before the filter and (d) the optical pulse after the filter.

Figure 2-25 (a) illustrates the SMSR before and after the filter as a function of wavelength across the tuning range of the pulse source. It is important to note that the use of the filter in this set-up is dependent on achieving a suitably high SMSR from the gain-switched externally injected laser before the filter, which is clearly shown to be greater than 30 dB. If this was not the case then MPN could seriously affect the temporal quality of the pulse (from Figure 2-25 (a) this is clearly not the case). Figure 2-25 (b) shows the variation in pulse width over the tuning range. The pulse width increase of FP2 in comparison to the pulse width obtained for FP2 in the self-seeding experiment is due to the use of a different FP laser. The electrical bandwidth of the laser will determine the obtainable pulse width. The variation in pulse width around 1545 nm is due to the external injection from the ECL changing from seeding FP1 to seeding FP2. Differences in various physical parameters (e.g. gain) of the two lasers are responsible for the variation in output pulse width. This set-up exhibited very stable operation even at the crossover section when the injection seeding changes from FP1 and FP2. This is achieved because there is no overlap between the modes from the two different FP lasers, and thus, light is never injected into the modes of the same wavelength of both FP lasers at the same time. This source could play a vital part in ensuring optimal performance of high-speed hybrid WDM/OTDM optical communication networks. It should also be noted that the tuning range could be expanded further by introducing a third FP laser with an appropriate spectral profile (e.g. 1470 –1510 nm), which would provide a source that covers the S, C and L bands [95]. In addition, by simultaneously injecting another light source into the FP lasers used, it could be possible to develop a multiwavelength pulse source.

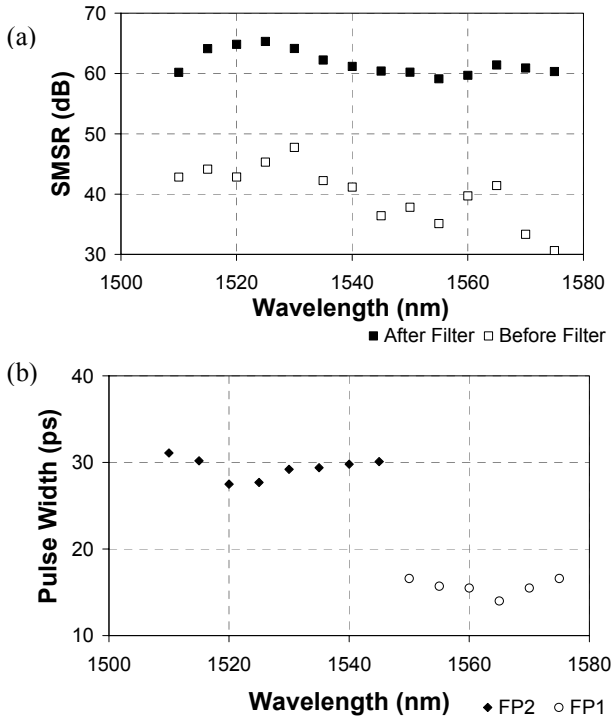

Figure 2-25 (a) SMSR of output pulses as a function of wavelength before and after the filter, and (b) the measured pulse width as a function of wavelength tuning range of FP1 and FP2.

2.10 Summary

This chapter has provided an overview of the different parameters required by pulse sources which will be utilised in future OTDM and hybrid WDM/OTDM optical systems. In order to measure the quality of pulses, different measurement and characterisation equipment is required. In addition to typical spectral and temporal measurements as carried out using OSA and a high-speed detector with a DCA, the FROG technique provides full electric field characterisation. Different pulse generation techniques exist which include external modulation of a CW source, mode locking and gain switching. Gain-switched semiconductor diodes provide short pulse width generation in a simple and stable configuration. The undesirable quality of the gain-switched pulse can be overcome by the use of optical injection through self or external seeding. Two novel techniques to generate high quality optical pulses were presented, which could be implemented in 20 Gb/s OTDM or hybrid OTDM/WDM systems. With the advancement of laser device fabrication technology, higher repetition rates could be applied and the generation of shorter pulses could be achieved at increased line rates. The first experiment employing self seeding generated <20 ps pulses over a 50 nm range. By employing a tunable CW source to provide external injection, the tuning range was extended to 65 nm as there was no EDFA incorporated in the source which was the

limiting factor in the first set-up. In both cases for the self-seeded and external injection sources, closely transform limited pulses were generated with large SMSR values (<60 dB) and very low timing jitter (<1 ps). The next chapter develops this work further by using optical processing techniques to improve the characteristics of gain-switched pulse sources, and present bit error rate (BER) measurements which demonstrate that these sources can achieve the same high quality as other commercially available sources.

REFERENCES

[1] P.J. Winzer, and A. Kalmár, "Sensitivity Enhancement of Optical Receivers by Impulsive Coding," *IEEE J. Lightwave Technol.,* vol. 17, pp. 171-177, Feb. 1999.

[2] H. Sunnerud, M. Karlsson, and P.A. Anderkson, "A Comparison Between NRZ and RZ Data Formats with Respect to PMD-Induced System Degradation," *IEEE Photonics Technol. Lett.*, vol. 13, pp. 448-450, 2001.

[3] M. Daikoku, N. Yoshikane, and I. Morita, "Performance Comparison of Modulation Formats for 40 Gbit/s DWDM Transmission Systems," *OSA Optical Fiber Commun. Conf. (OFC'05),* paper OFN2, 2005.

[4] S. Kawanishi, "Ultrahigh-Speed Optical Time Division Multiplexed Transmission Technology Based on Optical Signal Processing," *IEEE J. Quantum Electron.,* vol. 34, pp. 2064-2079, 1998.

[5] L.A. Jiang, E.P. Ippen, and H. Yokoyama, "Semiconductor Mode-locked Lasers as Pulse Sources for High Bit Rate Data Transmission," *J. Optical Fiber Commun.,* vol. 2, pp. 1-31, May 1995.

[6] A.T. Clausen, H.N. Poulsen, L.K. Oxenlowe, A.I. Siahlo, J. Seoane, and P. Jeppesen, "Pulse Source Requirements for OTDM Systems," *IEEE Lasers and Electro-Optics Society 16th Annual Meeting (LEOS),* vol. 1, pp. 382-383, 2003.

[7] A.E. Siegman, "Lasers," *University Science Books,* Sausalito, California, 1986.

[8] G.P. Agrawal, "Nonlinear Fiber Optics – 2nd Edition," *Academic Press,* New York, 1995.

[9] D.A. Fishman, "Design and Performance of Externally Modulated 1.5-μm Laser Transmitter in the Presence of Chromatic Dispersion," *IEEE J. Lightwave Technol.,* vol. 11, pp. 624-632, Apr. 1993.

[10] M.C. Gross, M. Hanna, K.M. Patel, S.E. Ralph, "Reduction of Power Fluctuations in Ultrafast Optically Time-Division-Multiplexed Pulse Trains by Use of a Nonlinear Amplifying Loop Mirror," *IEEE Photonics Technol. Lett.,* vol. 14, pp. 690-692, May 2002.

[11] P.L. Mason, A. Wonfor, D.D. Marcenac, D.G. Moodie, M.C. Brierley, R.V. Penty, I.H. White, and S. Bouchoule, "The Effects of Pedestal Suppression on Gain Switched Laser Sources for 40 Gbit/s OTDM Transmission," *IEEE Lasers and Electro-Optics Society 10th Annual Meeting (LEOS),* vol. 1, pp. 289-290, 1997.

[12] A.M. Clarke, P.M. Anandarajah, L. Bramerie, C. Guignard, D. Massoubre, A. Shen, J.L. Oudar, L.P. Barry, and J.C. Simon, "Enhancement of System Performance in 80Gb/s OTDM Systems by using a Vertical Microcavity based Saturable Absorber," *European Conf. Optical Commun.(ECOC'06),* paper Th1.4.6, 2006.

[13] J. Zhang, M. Yao, X. Chen, L. Xu, M. Chen, and Y. Gao, "Bit Error Rate Analysis of OTDM System Based on Moment Generation Function," *J. Lightwave Technol.,* vol. 18, pp. 1513-1518, Nov. 2003.

[14] P. Anandarajah, L.P. Barry, and A. Kaszubowska, "Performance Issues Associated with WDM Optical Systems using Self-Seeded Gain Switched Pulse Sources due to Mode Partition Noise Effects," *IEEE Photonics Technol. Lett.,* vol. 14, pp. 1202-1204, 2002.

[15] S. Rubin, E. Buimovitz, and D. Sadot, "The Dependence of Side Modes on Modulation Index in Directly Modulated GCSR Laser," *IEEE Electrical and Electronic Eng. in Israel 21st Convention,* pp. 83-86, 2000.

[16] K. Ogawa, and R.S. Vodhanel, "Measurements of Mode Partition Noise of Laser Diodes," *IEEE J. Quantum Electron.,* vol. QE-18, pp. 1090-1093, July 1982.

[17] N.H. Jensen, H. Olesen, and K.E. Stubkjaer, "Partition Noise Semiconductor Lasers under CW and Pulsed Operation," *IEEE J. Quantum Electron.,* vol. 23, pp. 71-80, Jan. 1987.

[18] A.M. Clarke, M.J. Connelly, P. Anandarajah, L.P. Barry, and D. Reid, "Investigation of Pulse Pedestal and Dynamic Chirp Formation on Picosecond Pulses After Propagation Through an SOA," *IEEE Photonics Technol. Lett.,* vol. 17, pp. 1800-1802, Sept. 2005.

[19] L.P. Barry, J.M. Dudley, P.G. Bolland, J.D. Harvey, and R. Leonhardt, "Complete Characterisation of Pulse Propagation in Optical Fibres using Frequency-Resolved Optical Gating," *IEE Electron. Lett.,* vol. 32, pp. 2339-2340, Dec. 1996.

[20] C. Dorrer, and I. Kang, "Real-time Implementation of Linear Spectrograms for the Characterisation of High-bit Rate Optical Pulse Trains," *IEEE Photonics Technol. Lett.,* vol. 16, pp. 858-860, Mar. 2004.

[21] L.P. Barry, B.C. Thomsen, J.M. Dudley, and J.D. Harvey, "Characterisation of 1.55-μm Pulses from a Self-seeded Gain-switched Fabry-Perot Laser Diode using Frequency-resolved Optical Gating," *IEEE Photonics Technol. Lett.,* vol. 10, pp. 935-937, Jul. 1998.

[22] C. Dorrer, "Investigation of the Spectrogram Technique for the Characterization of Picosecond Optical Pulses," *OSA Optical Fiber Commun. Conf. (OFC'05),* paper OTuB3, 2005.

[23] C. Dorrer, "High-Speed Measurements for Optical Telecommunications Systems," *IEEE J. Quantum Electron.,* vol. 12, pp. 843-858, Jul/Aug. 2006.

[24] P. Andrekson, "Tutorial: Ultra High Bandwidth Optical Sampling Oscilloscopes," *OSA Optical Fiber Commun. Conf. (OFC'04),* paper TuO1, 2004.

[25] Agilent, URL: http://cp.literature.agilent.com/litweb/pdf/5989-2603EN.pdf, "Triggering Wide-Bandwidth Sampling Oscilloscopes For Accurate Displays of High-Speed Digital Comunications Waveforms".

[26] J.C. Palais, "Fiber Optic Communications," *Pearson Prentice Hall,* London, UK, 2005.

[27] M. Ya. Schelev, M.C. Richardson, and A.J. Alcock, "Image Converter Streak Camera with Picosecond Resolution," *Appl. Phys. Lett.,* vol. 18, pp. 354-356, 1971.

[28] M.C. Richardson, "Investigation of the Characteristics of a Mode-Locked Nd:Glass Laser with the Aid of a Picosecond Streak Camera," *IEEE Quantum Electron.,* vol. QE-9, pp. 768-772, Jul. 1973.

[29] Hamamatsu, URL: http://sales.hamamatsu.com/assets/pdf/hpspdf/Femtosecond.pdf, "Femtosecond Streak Camera Data Sheets".

[30] G.C. Vogel, A. Savage, M.A. Duguay, "Picosecond Optical Sampling," *J. Quantum Electron.,* vol. QE-10, pp. 642-646, Sept., 1974.

[31] Agilent, URL: http://cp.literature.agilent.com/litweb/pdf/5988-6017EN.pdf, "Designing 40 Gb/s and beyond?"

[32] E. Hecht, and A. Zajac, "Optics," *Addison-Wesley,* Reading, 1974.

[33] A. Yariv, "Optical Electronics in Modern Communications," *Oxford University Press,* Oxford, 1997.

[34] Anritsu, URL: http://www.eu.anritsu.com/files/MS9710B_E1600.pdf, "Anritsu MS9710B, Optical Spectrum Analyser Data Sheet."

[35] E.P. Ippen, and C.V. Shank, "Ultrashort Light Pulses – Picosecond Techniques and Applications," *Springer-Verlag,* Berlin, 1977.

[36] K.A. Dala, G.A. Kenny-Wallace, and G.E. Hall, "CW Autocorrelation Measurements of Picosecond Laser Pulses," *J. Quantum Electron.,* vol. QE-16, pp. 990-996, Sept. 1980.

[37] R. Trebino, "Frequency-Resolved Optical Gating: The Measurement of Ultrashort Laser Pulses," *Kluwer,* Norwell, MA, 2000.

[38] P.A. Franken, et al, "Generation of Optical Harmonics," *Phys. Rev. Lett.,* vol. 7, p. 118, 1961.

[39] P.N. Butcher, and D. Cotter, "The Elements of Nonlinear Optics," *Cambridge University Press,* Cambridge, UK, 1991.

[40] J.C. Diels, J.J. Fontaine, and F. Simoni, "Phase Sensitive Measurements of Femtosecond Laser Pulses from a Ring Cavity," *International Conf. on Lasers,* pp. 348-355, 1983.

[41] A. Watanbe, and H. Saito, Y. Isida, and T. Yajima, "A Rapid Scanning Interferometric Autocorrelator for Monitoring Femtosecond Pulses," *Optics Commun.,* vol. 69, pp. 405-408, Jan. 1989.

[42] Z.E. Penman, T. Schittkowski, W. Sleat, D.T. Reid, and W. Sibbett, "Experimental Comparison of Conventional Pulse Characterisation Techniques and Second-Harmonic Generation Frequency-Resolved Optical Gating," *Optics Commun.,* vol. 155, pp. 297-300, 1998.

[43] R. Trebino, K.W. DeLong, D.N. Fittinghoff, J.N. Sweetser, M.A. Krumbugel, and B.A. Richman, "Measuring Ultrafast Laser Pulses in the Time-Frequency Domain Using Frequency-Resolved Optical Gating," *Rev. Sci. Instrum.,* vol. 68, pp. 3277-3295, May 1997.

[44] C.W. Siders, A.J. Taylor, and M.C. Downer, "Multipulse Interometric Frequency-Resolved Optical Gating: Real-time Phase-sensitive Imaging of Ultrafast Dynamics," *OSA Optics Lett.,* vol. 22, pp. 624-326, May 1997.

[45] D.J. Kane, G. Rodriguez, A.J. Taylor, and T.S. Clement, "Simultaneous Measurement of Two Ultrashort Pulses from a Single Spectrogram in a Single Shot," *J. Opt. Soc. Amer. B,* vol. 14, pp. 935-943, 1997.

[46] C. Dorrer, and I. Kang, "Real-Time Implementation of Linear Spectrograms for the Characterisation of High Bit-Rate Optical Pulse Trains," *IEEE Photonics Technol. Lett.,* vol. 16, pp. 858-860, Mar. 2004.

[47] H. Stark, "Image Recovery: Theory and Application," *Academic Press,* Orlando, 1987.

[48] K.W. DeLong, D.N. Fittinghoff, R. Trebino, B. Kohler, and K. Wilson, "Pulse Retrieval in Frequency-Resolved Optical Gating Based on the Method of Generalized Projections," *OSA Optics Lett.,* vol. 19, pp. 2152-2154, 1994.

[49] V. Wong, and I.A. Walmsley, "Ultrashort-pulse Characterization from Dynamic Spectrograms by Iterative Phase Retrieval," *J. Opt. Soc. Amer., B,* vol. 14, pp. 944-949, 1997.

[50] K.W. DeLong, D.N. Fittinghoff, and R. Trebino, "Practical Issues in Ultrashort-Laser-Pulse Measurement Using Frequency-Resolved Optical Gating," *IEEE J. Quantum Electron.,* vol. 32, pp. 1253-1264, 1996.

[51] F. Koyama, and K. Iga, "Frequency Chirping in External Modulators," *J. Lightwave Technol.,* vol. 6, pp. 87-93, Jan, 1988.

[52] H.F. Chou, Y.J. Chiu, and J.E. Bowers, "Standing-Wave Enhanced Electroabsorption Modulator for 40-GHz Optical Pulse Generation," *IEEE Photonics Technol. Lett.,* vol. 15, pp. 215-218, 2003.

[53] T.H. Wood, "Multiple Quantum Well (MQW) Waveguide Modulators," *J.Lightwave Technol.,* vol. 6, pp. 743-757, June 1998.

[54] E.A. Avrutin, J.H. Marsh, and E.L. Portnoi, "Monolithic and Multi-Gigahertz Mode-Locked Semiconductor Lasers: Constructions, Experiments, Models and Applications," *IEE Proc. Optoelectronics,* vol. 147, pp. 251-278, Aug. 2000.

[55] P.W. Smith, "Mode-locking of Lasers," *Proc. of the IEEE,* vol. 58, pp. 1342-1363, Sept. 1970.

[56] P. Vasil'eV, "Ultrafast Diode Lasers; Fundamentals and Applications," *Artech House*, Boston**,** pp. 95-149, 1995.

[57] R. Ludwig, and A. Ehrhardt, "Turn-Key-Ready Wavelength-, Repetition Rate- and Pulsewidth-Tunable Femtosecond Hybrid Modelocked Semiconductor Laser," *IEE Electron. Lett.,* vol. 31, pp. 1165-1166, July 1995.

[58] J.E. Bowers, P.A. Morton, A. Mar, and S.W. Corzine, "Actively Mode-Locked Semiconductor Lasers,**"** *J. Quantum Electron.*, vol. 25, pp. 1426-1439, June 1989.

[59] K.Y. Lau, "Short-Pulse and High-Frequency Signal Generation on Semiconductor Lasers," *J. Lightwave Technol.,* vol. 7, pp. 400-419, Feb. 1989.

[60] P.-L. Liu, C. Lin, I.P. Kaminow, and J.J. Hsieh, "Picosecond Pulse Generation from InGaAsP Lasers at 1.25 and 1.3 μm Optical Pulse by Electrical Pulse Pumping," *IEEE J. Quantum Electron.,* vol. QE-17, pp. 671-674, 1981.

[61] N.G. Basov, V.N. Morozov, V.V. Nikitin, and A.S. Semenov, "Investigation of GaAs Laser Radiation Pulsation," *Soviet Physics-Semiconductors,* vol. 1, pp. 1305-1308, 1968.

[62] S. Hamilton, and R. Hall, "Shunt Mode Harmonic Generation Using Step Recovery Diodes," *Microwave Journal,* pp. 69-78, Apr. 1967.

[63] C. Rullière, "Femtosecond Laser Pulses: Principles and Experiments, 2nd Edition," *Springer,* New York, 2003.

[64] K.Y. Lau, "Gain-Switching of a Semiconductor Injection Lasers," *Appl. Phys. Lett.,* vol. 52, pp. 257-259, Jan. 1988.

[65] H.-F. Liu, M. Fukazawa, Y. Kawai, and T. Kamiya, "Gain-Switched Picosecond Pulse (<10 ps) Generation from 1.3 μm InGAAsP Laser Diodes," *IEEE J. Quantum Electron.,* vol. 25, pp. 1417-1425, 1989.

[66] G.J. Aspin, J.E. Carroll, and R.G. Plumb, "The Effect of Cavity Length on Picosecond Pulse Generation with Highly RF Modulated AlGaAs Double Heterostructure Lasers," A*ppl. Phys. Lett.,* vol. 39, pp. 859-861, Dec. 1981.

[67] K.Y. Lau, and N. Bar-Chaim, "High-Speed Operation of Single-Quantum-Well Lasers with Large Gain Compression," *IEEE Photonics Technol. Lett.,* vol. 4, pp. 118-120, 1992.

[68] K.Y. lau, and A. Yariv, "Ultra-High Speed Semiconductor Laser," *IEEE J. Quantum Electron.,* vol. QE-21, pp. 121-137, Feb. 1985.

[69] G.P. Agrawal, and N.K. Dutta, "Semiconductor Lasers," *Van Nostrand Reinhold,* New York, 1993.

[70] C.H. Henry, "Theory of the Linewidth of Semiconductor Lasers," *J. Quantum Electron.*, vol. 18, pp. 259-264, Feb 1982.

[71] R. Sabella, and P. Lugli, "High Speed Optical Communications," *Kluwer Academic Publishers,* Dordrecht, Chap. 2, 1999.

[72] T.L. Koch, "Nature of Wavelength Chirping in Directly Modulated Semiconductor Lasers," *IEE Electron. Lett.,* vol. 25, pp. 203-204, 1974.

[73] L.P. Barry, B.C. Thomsen, J.M. Dudley, and J.D. Harvey, "Characterization of 1.55 μm Pulses from a Self-Seeded Gain-Switched Fabry–Perot Laser Diode Using Frequency-Resolved Optical Gating," *IEEE Photonics Technol. Lett*., vol. 10, pp. 935-937, Jul. 1998.

[74] S.H. Chin, Y.J. Kim, H.S. Song, and D.Y. Kim, "Complete Chirp Analysis of a Gain-Switched Pulse using an Interferometric Two-Photon Absorption Autocorrelation," *OSA J. Optical Networking,* vol. 45, pp. 7718-7722, Oct. 2006.

[75] M. Osinski, and M.J. Adams, "Picosecond Pulse Analysis of Gain-Switched 1.55 μm InGaAsP Lasers," *IEEE J. Quantum Electron.,* vol. QE-21, pp. 1929-1936, Dec. 1985.

[76] C. Lin, T.P. Lee, and C.A. Burrus, "Picosecond frequency chirping and dynamic line broadening in InGaAsP injection lasers under fast excitation," *Appl. Phys. Lett.,* vol. 42, pp. 141-143, Jan. 1983.

[77] S. Bouchale, E. Lach, G. Lemestreallan, S. Slempkes, D. Mathoorasing, C. Kazierski, and A. Ougazzaden, "High speed gain-switched laser as very simple 4x10Gbit/s and up to 8x10Gbit/s OTDM source," *European Conf. Optical Commun. (ECOC'98),* vol. 1, pp. 215-216, 1998.

[78] M. Jinno, "Correlated and Uncorrelated Timing Jitter in Gain-Switched Laser Diodes," *IEEE Photonics Technol. Lett.,* vol. 5, pp. 1140-1143, 1993.

[79] E.H. Bottcher, K. Ketterer, and D. Bimberg, "Turn-on Delay Time Fluctuations in Gain-Switched AlGaAs/GaAs Multiple-Quantum-Well Lasers," *Appl. Phys. Lett.,* vol. 63, pp. 2470-2472, Apr. 1988.

[80] A.G. Weber, W. Ronghan, E.H. Bottcher, M. Schell, and D. Bimberg, "Measurements and Simulation of the Turn-on Delay Time Jitter in Gain-Switched Semiconductor Lasers," *IEEE J. Quantum. Electron.,* vol. 28, pp. 441-446, 1992.

[81] L.P. Barry, P. Anandarajah, and A. Kaszubowska, "Optical Pulse Generation at Frequencies up to 20 GHz Using External-Injection Seeding of a Gain-Switched Commercial Fabry–Pérot Laser," *IEEE Photonics Technol. Lett.,* vol. 13, pp. 1014-1016, Sept. 2001.

[82] S. Lundquist, T. Anderson, and S.T. Eng, "Generation of Tunable Single-Mode Picosecond Pulses from an AlGaAs Semiconductor Laser with Grating Feedback," *Appl. Phys. Lett.,* vol. 43, pp. 715-717, 1983.

[83] L.P. Barry, R.F. O' Dowd, J. Debeau, and R. Boittin, "Tunable Transform Limited Pulse Generation Using Self-Injection Locking of a FP Laser," *IEEE Photonics Technol. Lett.*, vol. 5, pp. 1132-1134, 1993.

[84] D. Huhse, M. Schell, W. Utz, J. Kassner, and D. Bimberg, "Dynamics of Single-Mode Formation in Self-Seeded Fabry-Perot Laser Diodes," *IEEE Photonics Technol. Lett.,* vol. 7, pp. 351-353, 1995.

[85] M. Schell, D. Huhse, W. Utz, J. Kaessner, D. Bimberg, and I.S. Tarasov, "Jitter and Dynamics of Self-Seeded Fabry–Perot Laser Diodes,"*IEEE J. Quantum Electron.,* vol. 1, pp. 528-534, June 1995.

[86] Y. Matsui, S. Kutsuzawa, S. Arahira, and Y. Ogawa, "Generation of Wavelength Tunable Gain Switched Pulses from FP MQW Lasers with External Injection Seeding," *IEEE Photonics Technol. Lett*., vol. 9, pp. 1087-1089, Aug. 1997.

[87] M. Zhang, D.N. Wang, H. Li, W. Jin and M.S. Demokan**, "**Tunable Dual Wavelength Picosecond Pulse Generation by the Use of Two Fabry-Perot Laser Diodes in an External Injection Seeding Scheme," *IEEE Photonics Technol. Lett.*, vol. 14, pp. 92-94, Jan. 2002.

[88] D.-S. Seo, H.-F. Liu, D.Y. Kim, and D.D. Sampson, "Injection Power and Wavelength Dependence of an External-Seeded Gain-Switched Fabry–Perot Laser," *Appl. Phys. Lett.,* vol. 67, pp. 1503-1505, Sept. 1995.

[89] S. Mohrdiek, H. Burkhard, and H. Walter, "Chirp Reduction of Directly Modulated Semiconductor Lasers at 10 Gb/s with strong CW Light Injection Seeding," *IEEE Photonics Technol. Lett*., vol. 12, pp. 418-424, Mar. 1994.

[90] D.S. Seo, D.Y. Kim, and H.F. Liu, "Timing Jitter Reduction of Gain-Switched DFB Laser by External Injection-seeding," *IEE Electron. Lett.,* vol. 32, pp. 44-45, Jan. 1996.

[91] J.W. Chen, and D.N. Wang, "Self-seeded Gain Switched Optical Short Pulse Generation with High Side Mode Suppression Ratio and Extended Wavelength Tuning Range," *IEE Electron. Lett*., vol. 39, pp. 679-681, 2003.

[92] X. Fang and D.N. Wang, "Mutual Pulse Injection Seeding by the Use of Two Fabry Perot Laser Diodes to Produce Wavelength Tunable Optical Short Pulses," *IEEE Photonics Technol. Lett*., vol. 15, pp. 855-857, 2003.

[93] A.M. Clarke, P. Anandarajah, P.J. Maguire, and L.P. Barry, "External Injection of a Gain Switched Integrated Dual Laser for the Generation of Widely Tunable Picosecond Pulses with Large SMSR," *Conf. Lasers and Electro-Optics (CLEO'04),* vol. 1, pp. 591-592, 2004.

[94] A.M. Clarke, P.M. Anandarajah, and L.P. Barry, "Generation of Widely Tunable Picosecond Pulses with Large SMSR by Externally Injecting a Gain Switched Dual Laser Source," *IEEE Photonics Technol. Lett.,* vol. 16, pp. 2344-2346, 2004.

[95] A.K. Srivastava and Y. Sun,, "Advances in Erbium-Doped Fiber Amplifiers," in Optical Fiber Telecommunications*,* I. Kaminow, and T. Li, *Academic Press,* New York, vol. IV A, 2002.

CHAPTER 3 – ALL-OPTICAL PROCESSING TECHNIQUES FOR PULSE GENERATION

3.1 Introduction

An optical pulse source is a key determining factor in optimising the overall performance of a high-speed optical system. Thus the design of a high-quality pulse sources is vital (as was discussed in detail in Chapter 2). In this chapter novel techniques are introduced which enhance optical pulse generation methods, generating high quality optical pulses which are transform limited, with high side mode suppression ratio (SMSR) and large temporal pedestal suppression ratio (TPSR). To understand the extent of the detrimental effect of insufficient TPSR, varying levels of pulse TPSR on the performance of an optical time division multiplexed (OTDM) system is examined. Generated pulses, when multiplexed to higher data rates, should not overlap in order to avoid interference between adjacent channels. One method to overcome these large pedestal levels is to introduce a saturable absorber (SA) to the pulse source. Large TPSR improvement is demonstrated through the use of a vertical microcavity SA. System results show that the use of the SA with the pulse source not only eliminates the penalty introduced by large TPSR levels but it also improves the receiver sensitivity as it enhances the overall pulse quality. For gain-switched diode lasers, the generation of temporal pedestals are problematic due to the incomplete compensation of nonlinear chirp by linear pulse compression schemes. A novel technique is introduced to obtain the design criteria for the fabrication of a custom-made nonlinear fibre Bragg gratings (FBG). These FBGs when used in conjunction with gain-switched sources result in pedestal free pulse trains. The grating has a nonlinear chirp profile which is opposite to the chirp profile of the gain-switched pulse. The precise nonlinear chirp profile is determined by using the measurement technique of frequency-resolved optical gating (FROG). It is shown that the gain-switched source in conjunction with the nonlinear grating overcomes the serious penalty in the transmission system in comparison to when a linear compression technique is implemented.

3.2 OTDM System Performance Investigation due to Varying TPSR Levels of a Pulse Source

Considering the main pulse generation techniques available, namely; mode locking, gain switching, and the use of electro-absorption modulators (EAM), it is extremely difficult

to achieve a TPSR or extinction ratio (ER) in excess of 30 dB. This can have a serious detrimental effect in high-speed communications systems as it can result in a large interferometric noise which degrades system performance [1]. The actual ER or TPSR required to prevent degradation of system performance will depend on the number of return-to-zero (RZ) channels multiplexed together to obtain the overall OTDM signal, which in turn will be determined by the pulse width and repetition rate of the optical pulse source employed at the transmitter. Thus, an experimental verification of the effect of varying levels of TPSR has on the power penalty in an 80 Gb/s system is presented. Other research studies have given indications about the required TPSR level for a pulse source [2,3], however a full experimental analysis has not yet been published.

3.2.1 Introduction and Verification of Varying TPSR Levels of a Pulse Source

The experimental set-up used to introduce the pulse pedestal of varying levels is shown in Figure 3-1. The main element of the set-up is a hybrid mode-locked semiconductor laser that generates 2.1 ps pulses with a time-bandwidth-product (TBP) of 0.35 at 10 GHz. The outputted pulse train was split into two paths by a 3 dB coupler. The top path (pedestal generation arm) was delayed by around 8 ps with respect to the pulses in the lower path by a variable optical delay line (ODL), and attenuated via a variable optical attenuator (VOA). The main pulse and pedestal arms were then recombined via a second coupler. A polarisation controller (PC) and a polarizer were used to match the polarisation of the main pulse with the pedestal so that an accurate measurement of the TPSR could be taken by using the FROG technique.

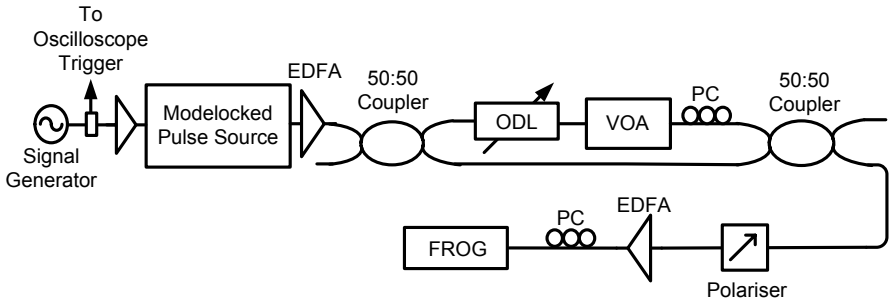

Figure 3-1 Experimental set-up used to introduce varying TPSR levels.

By adjusting the attenuation of the VOA the height of the pedestal was set to different values, and was then measured using the FROG. The resulting pulses with varying TPSR levels are shown in Figure 3-2. This plot verifies that the FROG technique can measure TPSR up to levels of approximately 30 dB, given that pulses portray a high signal-to-noise ratio (SNR).

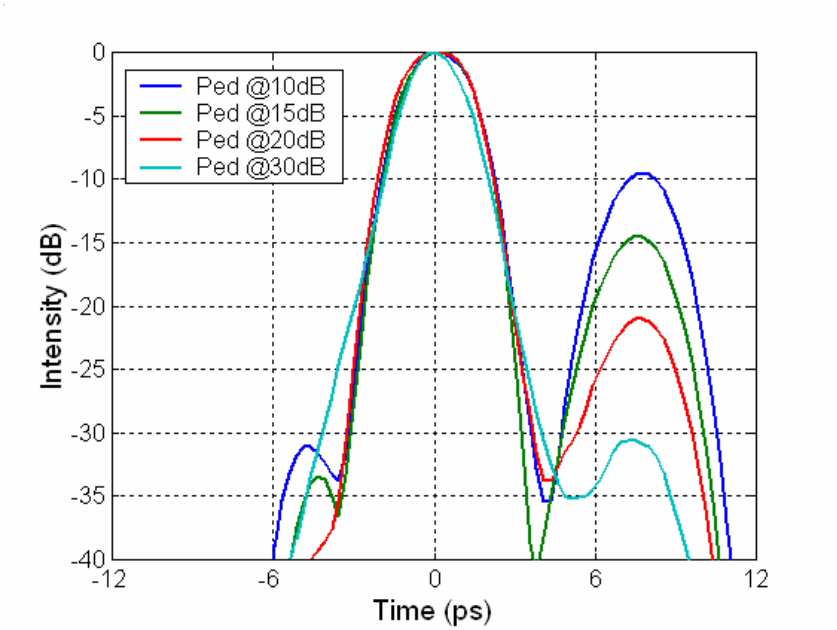

Figure 3-2 FROG measurement of varying TPSR levels determined by increasing the VOA to generate TPSR levels of 10, 15, 20, and 30 dB.

3.2.2 80 Gb/s OTDM System Test-bed

To test the back-to-back (B2B) performance of the optical pulse source with varying TPSR levels, in an 80 Gb/s OTDM system, we used the experimental test-bed presented in Figure 3-3. The pulses generated in Figure 3-1, were modulated with a pseudo random bit sequence (PRBS) of length 2^7-1 from a pulse pattern generator (PPG) with the aid of a Mach-Zehnder modulator (MZM). The resultant STM 64 RZ optical signal is then passed into a passive fibre based interleaver and multiplexed up to 80 Gb/s. A PC at the input and a polarizer at the output of the multiplexer ensure that the same state of polarisation is maintained in each of the tributaries. In order to take bit error rate (BER) measurements, the 80 Gb/s signal is initially demultiplexed down to 40 Gb/s using an EAM and then to 20 Gb/s using a MZM. The EAM is driven with a 40 GHz sine wave to yield a 6 ps switching window, and the MZM is driven with a 20 GHz sine wave to give a 10 ps switching window. The signal is then optically pre-amplified prior to being received by a photodetector after which it is demultiplexed back down to the base rate (10 Gb/s) using an electrical demultiplxer. BER measurements are performed for a range of received optical powers, (indicated by P_{rec} in Figure 3-3).

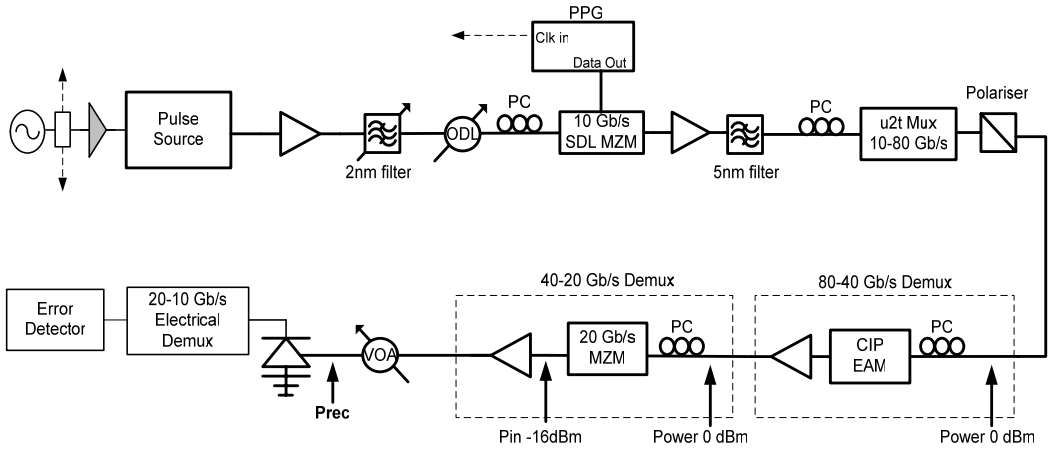

Figure 3-3 An 80 Gb/s OTDM test-bed to characterise the performance of picosecond pulses with varying TPSR levels.

3.2.3 Varying TPSR Levels of a Pulse Source in an 80 Gb/s OTDM System

The effect of pulses with varying input TPSR values was examined by measuring the power penalties introduced, as displayed in Figure 3-4. This plot clearly displays the effect of TPSR on the performance of an 80 Gb/s OTDM system. TPSR values of 15 and 20 dB exhibit power penalties of 3 and 1 dB respectively at a BER $1e^{-9}$, compared to a TPSR of 30 dB (which results in negligible system degradation). The pedestal delay of 8 ps was chosen, as this delay corresponded to the point where the penalty due to the introduced pedestal level becomes significant. As the delay is increased the penalty correspondingly increases for the same TPSR as the power overlap between the next pulse and pedestal increases until it reaches the bit slot duration (12.5 ps). The increase in pulse and pedestal overlap leads to a larger generation of interferometric noise.

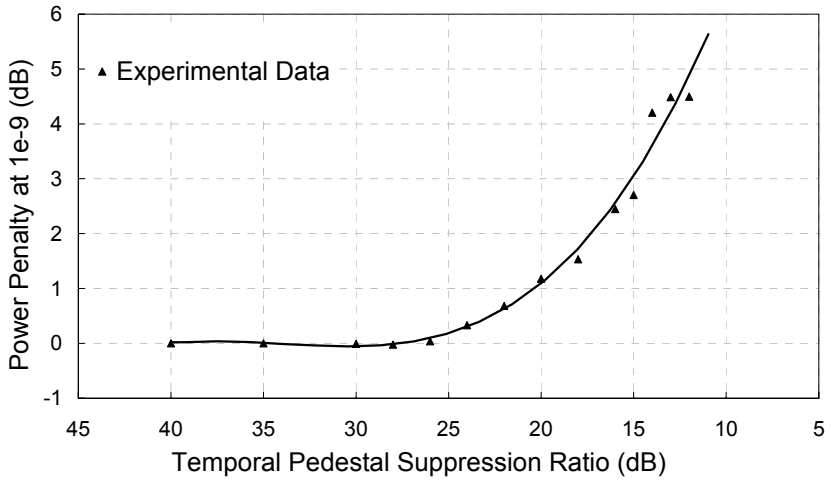

Figure 3-4 Induced power penalty as a function of varying pulse TPSR levels in an 80 Gb/s OTDM system.

3.3 TPSR Enhancement Using a Vertical Microcavity based Saturable Absorber

In order to overcome the limitation that poor TPSR and ER levels of pulse sources have in high-speed communications systems, a number of techniques have been developed to improve the generated optical pulses. These techniques include the use of an EAM [4], a nonlinear amplifying loop mirror (NALM) [2], or self phase modulation (SPM) in a semiconductor optical amplifier (SOA) in conjunction with shifted filtering [5]. The EAM can provide a large increase in TPSR values however it is an active and expensive component, which may significantly increase the cost of the pulse source. The NALM is fibre-based, which makes it bulky, and suffers from instability problems, and the SOA scheme exhibits limited TPSR improvement (~7 dB). The limitation of these ER enhancement techniques maybe overcome through the use of a vertical microcavity based SA. An experimental demonstration is presented to show how the use of a SA following a pulse source with insufficient TPSR can overcome the large power penalty introduced by poor TPSR and in addition provide a small negative power penalty.

A SA is an optical device which introduces an increased loss for reducing optical intensities [6]. Below, a threshold value, the photonic absorption of the SA is high and the device is opaque to the signal (low transmittance). Above the threshold level, the SA transmittance rapidly increases and saturates at a level to give near unity output (excluding the insertion loss). The nonlinear transfer curve of the SA makes it ideal for use in mode-locking lasers to aid the start-up process of pulse formation [7,8] and for optical pulse regeneration [9]. The SA which is used here to enhance the TPSR of an optical pulse source is a passive device that can be monolithically integrated with semiconductor lasers. It has already been shown that this SA is very efficient for ER enhancement and 'space' noise attenuation [9,10].

The SA is a 7 quantum-well (QW) structure (InGaAs/InAlAs) placed in a resonant microcavity with a dielectric mirror (2x[TiO2/SiO2]) as the front mirror, and a broadband high-reflectivity metallic based mirror (Ag + SiO2) as the back mirror [11]. A heavy-ion-irradiation shortens the absorption recovery time to 1.5 ps, which is short enough for the SA to be employed in 160 Gb/s systems [10]. The SA is placed on a high precision mount and free space coupling of the light to and from the fibre is optimised by analysing the reflection spectrum of the SA on an OSA. Figure 3-5 shows the optimised reflection profile of the SA characterised with amplified spontaneous emission (ASE)

from an EDFA incident on the device. The average power from the EDFA ASE was approximately 9 dBm, measured at the fibre output before the SA mount.

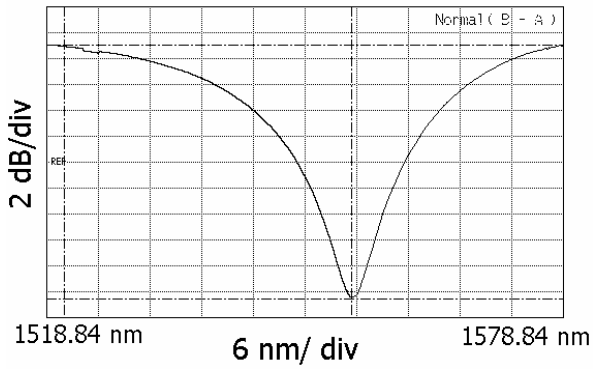

Figure 3-5 The reflection profile of the SA, measured using ~9 dBm (average power) from an EDFA ASE incident on the SA.

3.3.1 Experimental Characterisation of the TSPR Enhancement due to the SA

The SA was introduced after the pulse source with varying TPSR levels (as used in the previous experiment) via a circulator as shown in Figure 3-6. The average power at the input of the circulator (point A) was approximately 9 dBm and the output power following light incident on the SA was approximately -9 dBm (point B). With the introduction of the SA the TPSR is improved by around 10 dB (to 20 dB) when its input value to the SA is 10 dB as shown in Figure 3-7. As the input pedestal level decreases, the improvement in TPSR following the SA (measured at point B) increases due to the nonlinear transmission curve of the SA. Due to the limitation of the FROG the TPSR values greater than 30 dB were extrapolated and are represented by the dashed line in the figure.

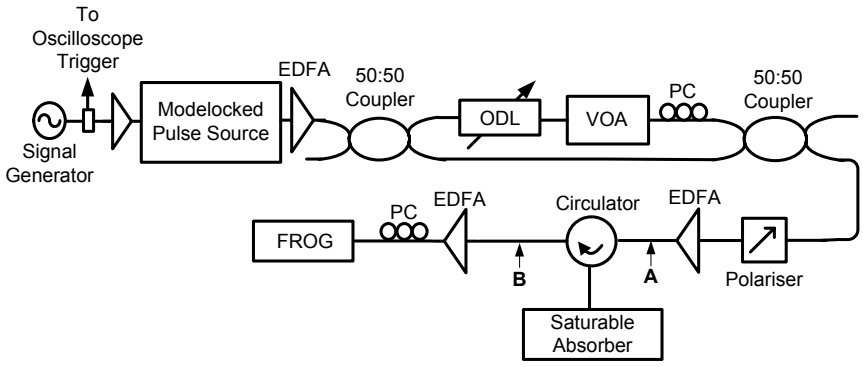

Figure 3-6 Experimental set-up to verify the TPSR improvement obtainable through the use of a SA.

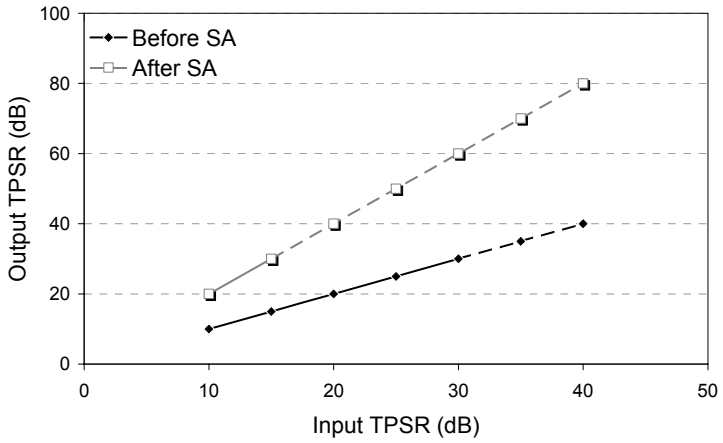

Figure 3-7 Graph of input and output TPSR to the SA measured at point A and B respectively by the FROG. The TPSR values are extrapolated at values greater than 30 dB (represented by a dashed line) as the FROG is limited by the noise floor of the system.

Figure 3-8 displays the intensity and chirp profile of the pulse before and after the SA, with an input TPSR of 20 dB. This figure demonstrates that the SA reduces the pedestal level to greater than 40 dB from the peak of the pulse, and also has very little effect on the frequency chirp of the pulse, an additional benefit of the device. Furthermore, it can be seen that the nonlinear response of the SA slightly compresses the pulse to 1.8 ps, and has a corresponding TBP of 0.33.

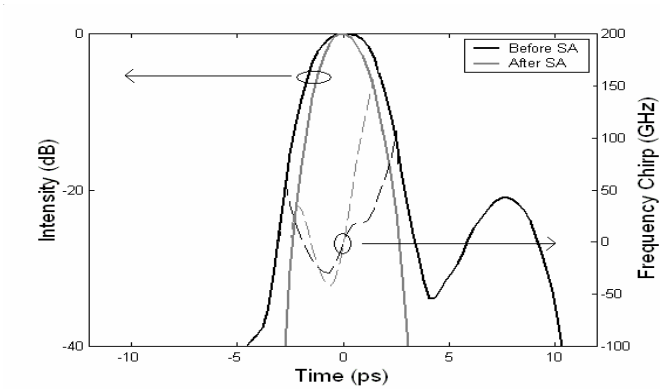

Figure 3-8 A temporal profile of a pulse and its corresponding chirp profile with a TPSR of 20 dB measured before and after the SA.

3.3.2 System Performance Enhancement due to SA

The introduction of the SA to the pulse source with poor TPSR was investigated to demonstrate the power penalty performance improvement obtained when used in an 80 Gb/s OTDM system. The 80 Gb/s OTDM system was the same as used in Figure 3-3. For this work we used a pulse source with an initial TPSR of 15 dB, (which is improved to 30 dB after the SA). Figure 3-9 displays the BER vs. received power when using (i) the pulse source with a TPSR of 15 dB, (ii) this pulse source followed by the SA, which

improves the TPSR to 30 dB, and (iii) a mode-locked pulse source with a TPSR set to 30 dB. The results show that the SA improves the system performance by 3.3. dB. It is also important to note that the introduction of the SA improves the performance by 0.3 dB greater than what would be expected due to the increase in TPSR alone. This additional improvement is due to the narrowing of the main pulse which improves the main pulse which improves the overall sensitivity of the OTDM system. The demultiplexed eye diagram measured at the receiver in Figure 3-10 shows the nose improvement due to the inclusion of the SA in the pulse source without a SA with TPSR levels of 15 dB.

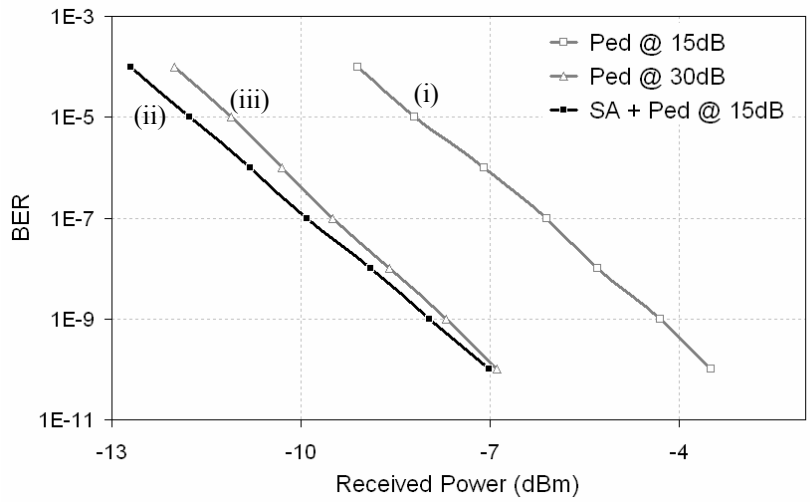

Figure 3-9 BER vs. received power for (i) pulse source with15 dB TPSR, (ii) this pulse source after the SA, showing TPSR improvement to 30 dB, and (iii) a mode-locked pulse source with a TPSR of 30 dB.

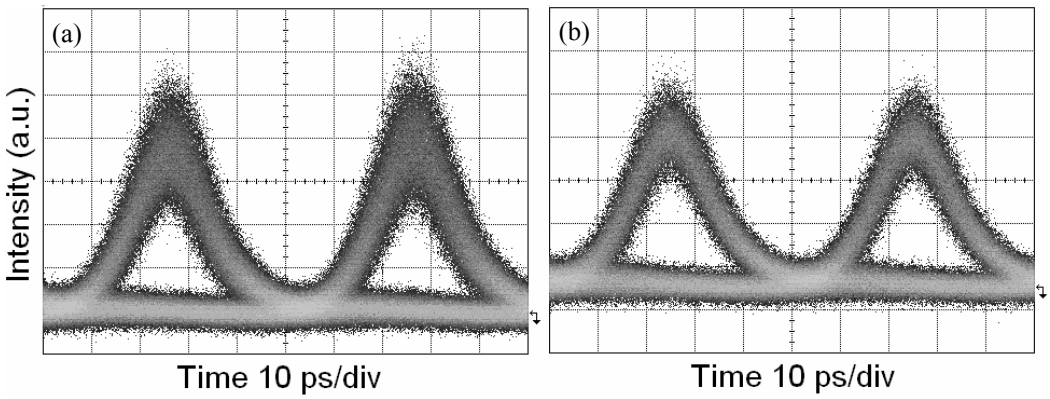

Figure 3-10 The demultiplexed 20 Gb/s eye diagram for a) a pulse source with 15 dB TPSR and b) this pulse source including the SA.

3.4 Optimised Gain-Switched Pulse Source to achieve Transform Limited Pulses for 80 Gb/s OTDM

In this section, further development and enhancement of the gain-switched pulse sources described in Chapter 2 is presented. The generated gain-switched pulses undergo spectral shaping, temporal compression and chirp compensation, resulting in transform limited short optical pulses. This optical processing is achieved by a nonlinearly chirped grating. The novel technology is the method used to measure the design criteria of these nonlinearly chirped gratings. The specially designed grating in conjunction with an externally injected gain-switched source generates 3.5 ps pulses exhibiting a TBP of 0.45. This technique overcomes the poor pulse TPSR resultant from the commonly used linear compression techniques, thus ensuring optimum system performance at high bit rates of 80 Gb/s.

3.4.1 Chirp Compensation and Pulse Compression of Gain-Switched Sources

To implement gain-switched sources in high-speed communications systems, pulse compression techniques are required to achieve short pulse widths and compensation of the large chirp present on the pulses. Many studies have examined pulse compression techniques following gain-switched sources by applying dispersion compensating fibre (DCF) [12-14] and linearly-chirped fibre Bragg gratings (L FBG) [15-18]. Typically these methods compensate for the linear chirp across the centre of the pulse, but do not eliminate the nonlinear chirp in the wings of the pulse. Thus the compression techniques can result in the generation of pedestals on either side of the pulse, rendering them unsuitable in high-speed communications systems. Thus nonlinearly-chirped FBGs (NL FBG) are required to compensate fully for the nonlinearly chirp profile of the gain-switched pulses.

To date applications of NL FBGs have had interest in dynamic dispersion compensation of higher order dispersion [19-21], and polarisation mode dispersion (PMD) using a high birefringence photosensitive fibre [22]. However to the best of our knowledge, the concept of applying a NL FBG to a gain-switched source to obtain transform limited pulses with negligible pedestals suitable for 80 Gb/s OTDM transmission is first presented here.

One method to compensate nonlinear chirp of a quadratic profile in mode-locked sources has been proposed in [23], in which a four-pass grating compressor is used with S-band

profiles. The disadvantages of this technique are that the grating is an active device which requires a large applied voltage, and the set-up is sensitive to accurate positioning and is bulky. Due to the quadratic chirp profile of the grating compressor the exact chirp profile is unable to be fully compensated for. Other examples try to eliminate the pedestals using more complex arrangements involving nonlinear loop mirrors or external modulators after the linearly compressed pulse to reduce the pedestals [4,21]. A simple technique to reduce pedestals can be carried out by eliminating the spectral edges where the group delay profile becomes nonlinear. However spectral-filtering results in a large pulse width increase [24]. Another technique investigated includes specifically designing a multi-quantum well (MQW) laser (which is gain-switched) so that it has a large differential gain and small damping factor to overcome the nonlinearity of the chirp. However an ER of only 24 dB was achieved following linear compression for this technique [25].

3.4.2 Fibre Bragg Gratings

A fibre Bragg grating (FBG) is a piece of fibre with a periodic perturbation in its refractive index along the fibre core [26]. The periodic index perturbation is formed by exposing the fibre to an intense optical interference pattern in ultra-violet (UV) light [27]. The advantages of a FBG are its low loss, low cost and polarisation insensitivity and overall its inherent fibre compatibility and flexibility to achieve desired spectral characteristics [28]. A chirped reflective grating provides a wavelength dependent delay of the reflected optical signal, as is illustrated in Figure 3-11. The first report of linearly chirped FBGs was made by Ouellette et al. [29]. If a FBG has a periodicity that varies nonlinearly along the length of the fibre it will produce a time delay that varies nonlinearly with wavelength [30]. Chirp in gratings may take many different forms, such that the period may vary symmetrically, linearly [31], quadratically [32] or with random variations along its length [33].

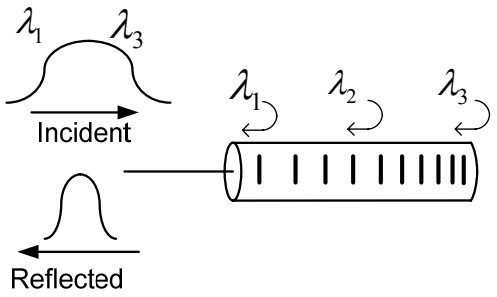

Figure 3-11 Conceptual Diagram of a chirped FBG.

3.4.3 FBG Design

A review of the design techniques for FBGs is given by Erdogen [34]. The gratings used in our optimised pulse source below were manufactured by Redfern Optical Components [35]. The design parameters of the gratings was accomplished by applying the group delay measured by the FROG technique to an inverse scattering algorithm, which converts the group delay into a chirped term of the FBG [36-38]. The algorithm calculates the FBG design (i.e. refractive index modulation amplitude and the phase of the index modulation versus the fibre position) from a given complex reflection spectrum. The complex reflection spectrum can be constructed from the given reflectivity amplitude and a given group delay (or optical phase) profile. The FBGs are fabricated using a holographic writing method [39], where a computer electronically controls the FBG phase and amplitude and does not require a custom-made phase mask. Hence it possible to fabricate NL FBGs for each individual laser in large volumes at low cost, if the chirp profile is different from one laser to the next.

3.4.4 Experimental Method to Retrieve the NL FBG Complex Reflection Spectrum

The characterisation of the externally injected gain-switched source using the measurement scheme of FROG yields the parameters that are required for the design of a NL FBG with a group delay which is opposite to the measured pulse. The experimental set-up is shown in Figure 3-12. A 10 GHz sine wave is amplified with the aid of a high-power RF amplifier. A bias tee is then used to combine the electrical RF signal with a DC bias ($2.5I_{th}$) to enable gain switching of a commercially available distributed feedback (DFB) laser contained within a hermetically sealed high-speed package. The laser used has a 3-dB bandwidth of 20 GHz and an output power of 4.7 dBm measured at $3I_{th}$. The resulting pulses generated were at a wavelength of 1549.35 nm. Wavelength tunability of a laser mode over a range of 2 nm could be achieved by temperature controlling the diode. To overcome the poor SMSR (~5 dB) and timing jitter (~2 ps) of the gain-switched pulses, CW light (via an optical circulator), from a second DFB laser (DFB 2) biased at ($\sim 1.2I_{th}$) was injected into DFB1. A PC was used to ensure that the injected light was aligned to the axis of polarisation of the gain-switched laser. The injected power incident on the modulated laser was measured to be about -20 dBm after considering the losses incurred in the optical injection path. External injection improves the SMSR to around 30 dB and reduces the timing jitter to less than 1 ps. The actual jitter is expected to be in the order of 200 fs or less as demonstrated in previous work by Nogiwa et al. [40].

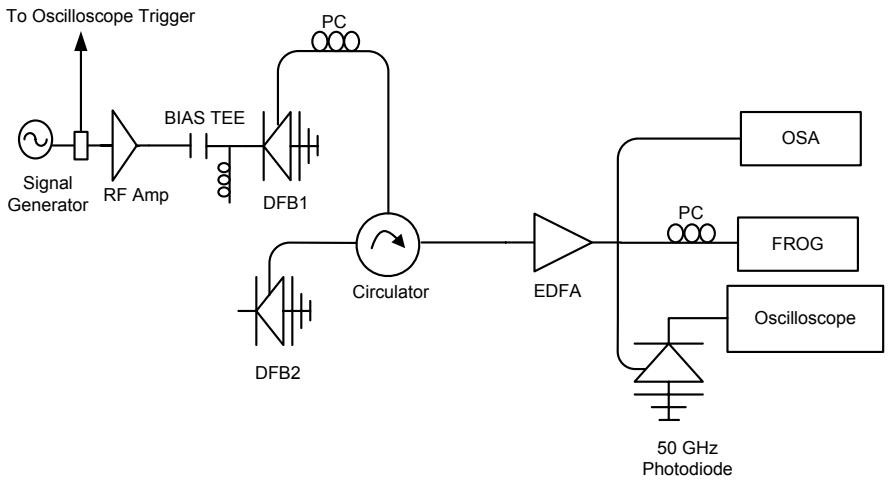

Figure 3-12 The experimental set-up to retrieve the group delay profile for the NL FBG.

Figure 3-13 (a) and (b) displays the optical spectra of the gain-switched laser both without and with external injection respectively. Degradation of the SMSR and a relatively large temporal jitter are inherent problems associated with the technique of gain switching. However by externally injecting a gain-switched laser, the above mentioned short comings can be overcome [4,41]. It is clearly visible that the external injection improves the degraded SMSR from 5 dB to an acceptable level of 30 dB. The overlapping of the broadened modes in prevents the side mode being distinguished from the main mode in Figure 3-13 (a). The spectral width of the externally injected gain-switched laser is measured as approximately 140 GHz. Figure 3-13 (c) shows the non-averaged oscilloscope trace of the detected pulse. This figure gives an indication of the low jitter and high ER as a result of applying optical injection. To accurately characterise the pulse, it is necessary to use the FROG technique.

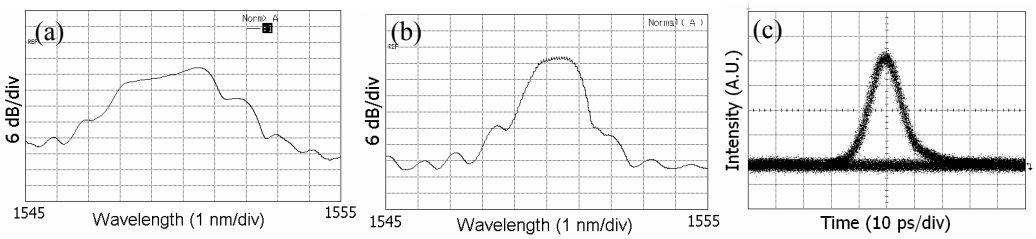

Figure 3-13 Spectra of gain-switched laser (a) without and (b) with optical injection and (c) an oscilloscope trace of the pulse following injection.

Using the FROG measurement scheme we can accurately characterise the intensity and chirp profile across the optical pulses from the gain-switched laser with external injection. Figure 3-14 (a) indicates that the pulses have a duration of 10.5 ps FWHM and the frequency chirp becomes nonlinear in the wings of the pulse due to the gain-

switching mechanism, resulting in a TBP of 1.5. The group-delay profile of this gain-switched laser diode source was measured and this was used to fabricate a NL FBG. The process involves the initial creation of the group-delay response for the FBG based on the group-delay data derived from the FROG measurements. The FBG target group-delay response is simply selected as the inverse of the pulse group delay, which should result in a constant group-delay profile of the reflected pulse from the FBG. In addition to a constant group-delay profile over the pulse bandwidth, for an optimised pulse source, a Gaussian spectrum is also required. The Fourier transform of a rectangular spectrum, which results in a Sinc temporal pulse [42], can result in the presence of pedestals. Gain-switched spectra are generally more rectangular in comparison to Gaussian spectra. Thus the reflection profile of the NL FBG is constructed as the difference between the spectral amplitude of the gain-switched output and of a Gaussian profile. This spectrally shapes the output pulse so that it will portray a Gaussian spectrum. Once the FBG target spectrum and group-delay profile are obtained as shown in Figure 3-14 (b), the FBG can be designed by implementing an inverse scattering algorithm as outlined in Section 3.4.3.

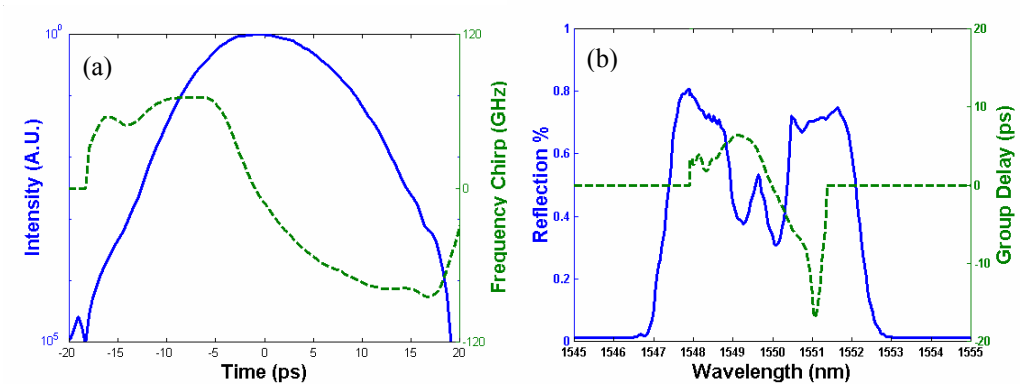

Figure 3-14 (a) Log intensity and chirp profiles of the generated pulses from the externally injected gain-switched laser and (b) target reflection spectrum and group-delay profile of the NL FBG.

The FWHM bandwidth of the grating is 5 nm and has 71 % reflectivity at the maximum point of reflectivity. The grating length is 20 mm. The reflective and group-delay profiles of the fabricated NL FBG are shown in Appendix II. A L FBG that has a chirp profile opposite to a linear approximation of the chirp across the gain-switched pulse was fabricated also. In both the cases, the agreement between the measured and the target group-delay profile was very good, with a standard deviation of the measurement error <2 ps, which is quite close to the estimated noise level of ± 1 ps for the group-delay measurements. It is also important to note that a large group delay ripple (GDR) in the compressing FBG could cause low-intensity temporal pedestals [43,44]. However, in

this set-up no such pedestals were observed due to the low level of GDR which was mentioned earlier, with a standard deviation of less than half the compressed pulse width.

3.4.5 Characterisation of the Generated Pulses following the NL FBG

By placing the nonlinear and linear fibre gratings after the externally injected gain-switched laser, as shown schematically in Figure 3-15 the subsequent pulse compression was characterised using the FROG technique.

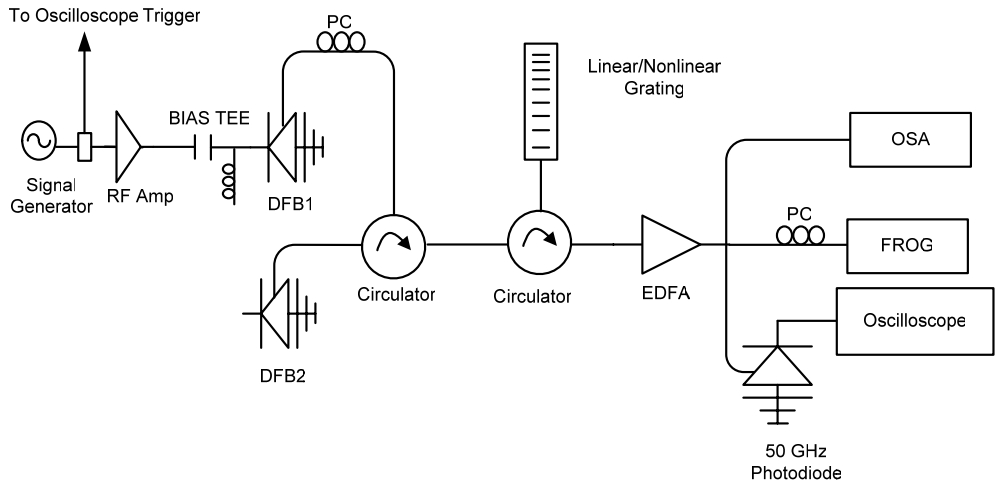

Figure 3-15 The experimental set-up for optimised pulse generation by applying a L/NL FBG to an externally injected gain-switched source.

Figure 3-16 (a) and (b) shows the measured intensity and chirp profile of the gain-switched optical pulses after compression with the linearly and nonlinearly chirped gratings, respectively. In both cases the gratings have eliminated any frequency chirp across the centre of the pulses. However when the linearly chirped grating is used, it can be seen how the nonlinearity of the chirp directly from the gain-switched laser results in significant pedestals on the leading and trailing edges of the pulse. Such pedestals, which are around 23 dB from the peak of the pulse, would clearly pose significant problems (through interferometric noise), for the use of these pulses in high-speed OTDM systems (which has been previously established).

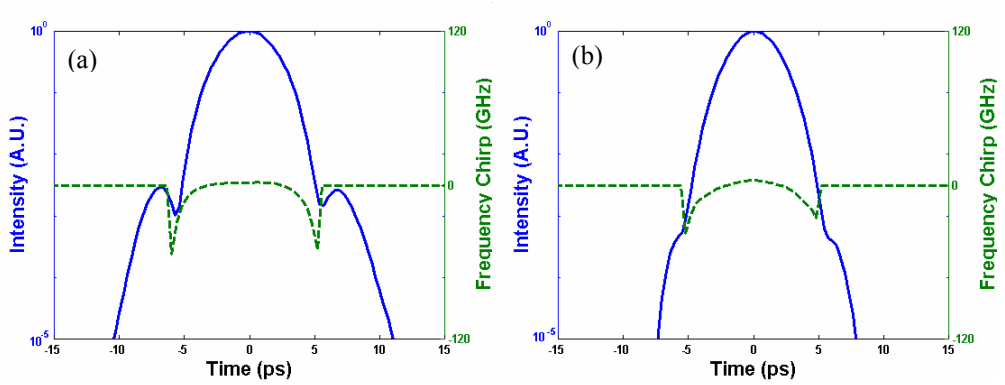

Figure 3-16 Intensity and chirp profiles of externally-injected gain-switched pulses following (a) linearly chirped and (b) nonlinearly chirped gratings.

The compression in the nonlinear fibre grating results in a 3.5 ps pulse at FWHM. The resultant chirp is flat and has a very small value across the pulse. In addition the pedestals have been virtually eliminated (TPSR >35 dB). The elimination of the pedestals is due to the compensation of the chirp and also the spectral shaping of the compressed pulse, as well as the small GDR. To confirm the effect of a non-Gaussian output spectrum, simulations were carried out which showed the generation of pedestals at approximately 20 dB below the peak of the pulse [24].

The spectra and group delay of the input and output pulses to and from the NL FBG are shown in Figure 3-17. It is clear that the group delay has been compensated for entirely by the tailor-made NL FBG. The output spectrum is more Gaussian shaped and symmetric in comparison to the input, which is due to the nonlinear reflection profile of the NL FBG. The spectral width is 130 GHz which results in a TBP of 0.45.

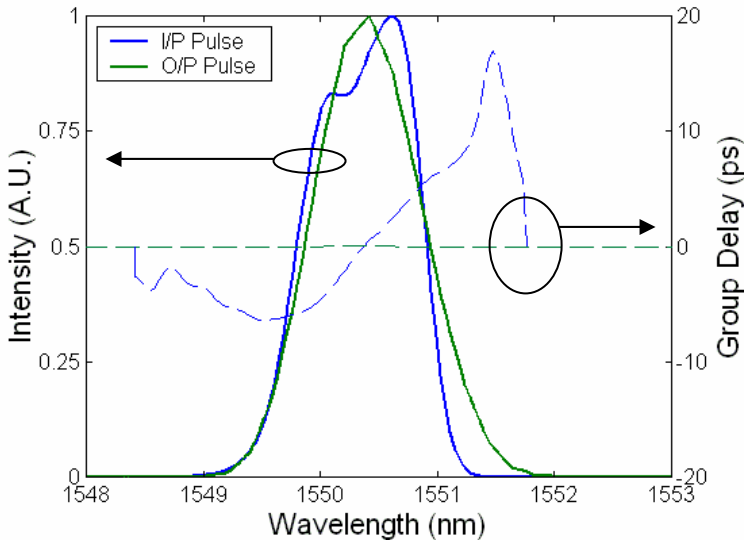

Figure 3-17 The input and output spectra to the NL FBG and their corresponding group-delay profiles.

The pulse generation/compression technique portrays excellent repeatability. Within laboratory conditions, the scheme exhibited stable operation over a 5 day period as shown in Figure 3-18. This could be mainly attributed to the fact that the two DFB lasers (modulated and seeding) were temperature and current controlled by precision Profile controllers. Hence, drifts in wavelength of the lasers, due to current or temperature variations were negligible. Furthermore, the wavelength variation with temperature of the fabricated FBGs being relatively small (~0.009 nm/°C) also leads to the stable generation of optimised pulses over very long periods of time.

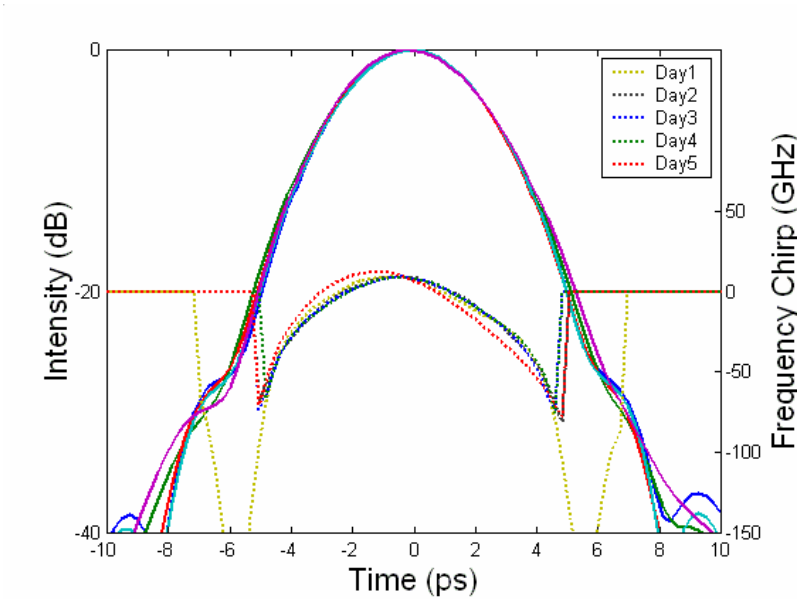

Figure 3-18 Pulse and chirp profiles as measured by the FROG over a 5 day period which demonstrates the excellent stability of the NL FBG gain-switched source.

3.4.6 80 Gb/s System Performance of the Optimised Pulse Source

To verify the system performance improvement the gain-switched pulse sources, one employing the NL FBG (TPSR ~ 35 dB), and the other using the L FBG (TPSR ~20 dB), were employed in a 40 Gb/s and 80 Gb/s OTDM system. Further performance confirmation of the optimised pulse source is carried out by comparing it to a commercially available tunable mode-locked laser (TMLL) pulse source in the same 80 Gb/s test-bed. The TMLL generates 2 ps pulses at a repetition rate of 10 GHz. This result acts as a reference when encompassed with the overall evaluation.

The test-bed used in this work to characterize the performance of the three different pulses sources employed in-turn as the transmitter is demonstrated in Figure 3-3. In the first instance of system performance characterisation, the externally injected gain-switched laser diode was followed by the NL FBG. Secondly, the NL FBG was replaced

by the L FBG. The final transmitter consisted of the commercially available TMLL. The pulses generated by the three different techniques are compared in Figure 3-19. The generated pulses after the NL FBG (bold line), the L FBG (faint line), and the TMLL (dotted line) have FWHM pulse widths of 3.5 ps, 3.6 ps and 1.6 ps respectively. The associated TBPs of the three pulse sources were 0.45, 0.47 and 0.33 respectively. As can be seen, the pulses compressed by the L FBG portray a TPSR of about 20 dB while that compressed by the NL FBG and the TMLL exhibit a TPSR >35 dB.

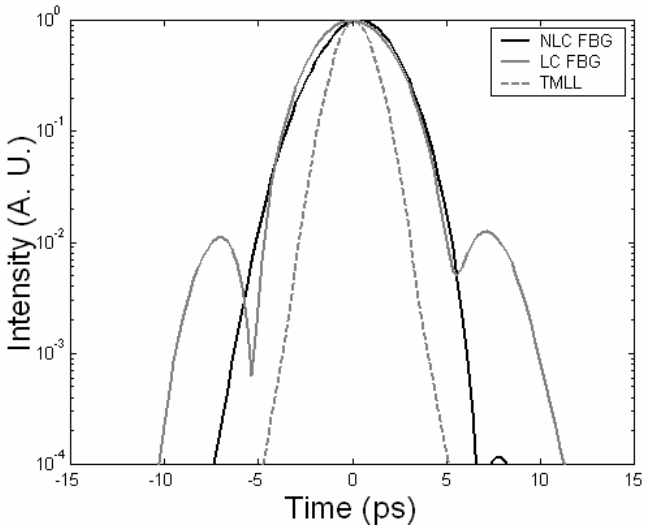

Figure 3-19 Intensity profiles of NL FBG gain-switched pulses (bold), L FBG gain-switched pulses (faint) and TMLL pulses (dotted).

Figure 3-20 displays the BER versus received power curves for one of the demultiplexed channels at 40 Gb/s and 80 Gb/s. It can be observed that to achieve a BER of 10^{-9}, power penalties of 1.2 dB and 3.5 dB are incurred in the case of the L FBG when compared to the NL FBG, when operated at 40 and 80 Gb/s respectively. This degraded performance is due to the presence of the pedestals about 20 dB below the peak of the pulse. These pedestals deteriorate the extinction between the adjacent timeslots of the temporally multiplexed signal thereby leading to intensity fluctuations that causes the BER degradation. At 80 Gb/s a difference of 0.4 dB was noticed in the case of the commercial TMLL and the optimised gain-switched pulse source employing the NL FBG. This variation could be attributed to the difference in pulse width, with the narrower pulse width leading to a slightly better sensitivity at the receiver. The degraded performance (3.5 dB power penalty) in the case of the L FBG, even though both sources generate Gaussian pulses that are transform-limited and have durations < 30% of the 80 Gb/s bit slot, is attributed to the presence of pulse pedestals. Thus, it has been demonstrated that the externally injected gain-switched source employing a NL FBG exhibits excellent performance when employed in an 80 Gb/s OTDM system.

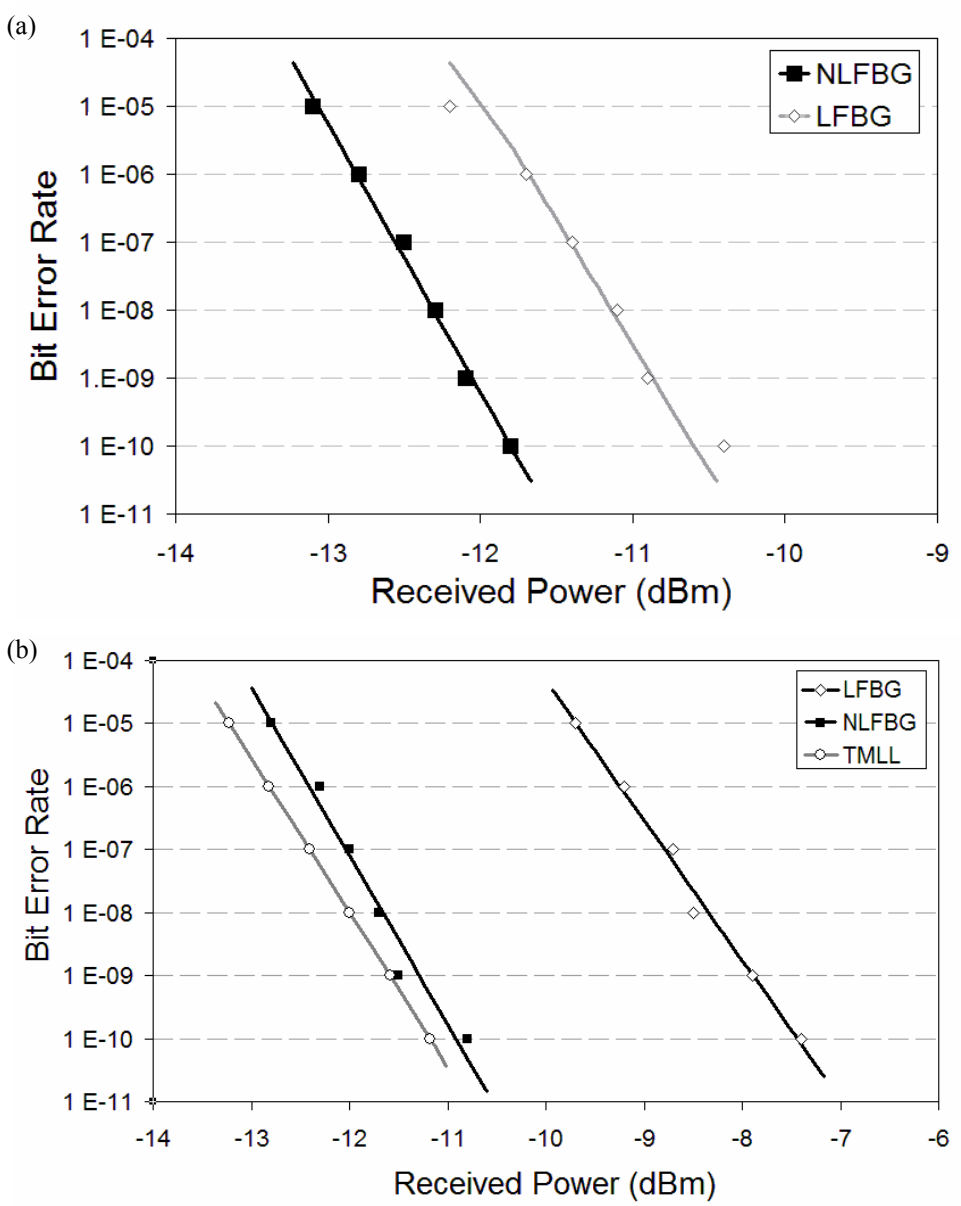

Figure 3-20 (a) BER vs. received power for NL FBG, L FBG at 40 Gb/s and (b) for both sources and the 2ps TMLL source at 80 Gb/s.

3.5 Summary

This chapter has experimentally investigated the importance for pulse sources to have a high TPSR when used in high-speed OTDM systems. A 3 dB improvement in performance was obtained when the TPSR values were improved from 15 to 30 dB. In doing so the accuracy of the FROG measurement scheme in the measurement of low intensity temporal artefacts was confirmed. For pulse sources that display poor pedestal suppression, the detrimental effects of poor TPSR values can be overcome, by the introduction of a vertical microcavity-based SA, which has the potential to be integrated

with a semiconductor-based pulse source. It was demonstrated that a SA can improve a pulse source with an initial TPSR of 15 dB, to a TPSR of 30 dB, and improve the overall system performance by 3.3 dB when implemented in an 80 Gb/s OTDM system.

In the case of a gain-switched source, instead of applying linear compression and an extra component to reduce high pedestal levels generated due to insufficient chirp compensation, a grating can be designed that can compensate fully for the nonlinear chirp. Thus pedestal free pulse generation can be achieved (TPSR >35 dB). The measurement technique of FROG enabled the extraction of the exact group-delay profile of the filter as it is the inverse of that across the gain-switched pulse directly from the laser. In addition the fibre grating required a specially adapted transfer characteristic to yield an output Gaussian profile. Thus a very simple and reliable pulse source is proposed, generating picosecond pulses with low jitter and high SMSR by externally injecting a gain-switched laser and applying a tailor-made NL FBG. A major improvement in system sensitivity (3.5 dB) achieved by the increased suppression of the temporal pedestals was recorded when compared with a gain-switched source employing a L FBG in an 80 Gb/s OTDM system. A commercially available mode-locked pulse source, used as a benchmark, further stressed the excellent performance of the proposed pulse source.

REFERENCES

[1] J. Zhang, M. Yao, Q. Xu, H. Zhang, C. Peng, and Y. Gao, "Interferometric Noise in Optical Time Division Multiplexing Transmission System," *J. Lightwave Technol.,* vol. 20, pp. 1329-1334, Aug. 2002.

[2] M.C. Gross, M. Hanna, K.M. Patel, and S.E. Ralph, "Reduction of Power Fluctuations in Ultrafast Optically Time-Division-Multiplexed Pulse Trains by Use of a Nonlinear Amplifying Loop Mirror," *IEEE Photonics Technol. Lett.,* vol. 14, pp. 690- 692, May 2002.

[3] P.L. Mason, A. Wonfor, D.D. Marcenac, D.G. Moodie, M.C. Brierley, R.V. Penty, I.H. White, and S. Bouchale, "The Effects of Pedestal Suppression on Gain-switched Laser Sources for 40 Gb/s OTDM Transmission," *IEEE Lasers and Electro-Optics Society 10th Annual Meeting (LEOS),* vol. 1, pp. 289-290, Nov. 1997.

[4] P. Gunning, J.K. Lucek, D.G. Moodie, K. Smith, R.P. Davey, S.V. Chernikov, M.J. Guy, J.R. Taylor, and A.S. Siddiqui, "Gainswitched DFB Laser Diode Pulse Source using Continuous Wave Light Injection for Jitter Suppression and an Electroabsorption Modulator for Pedestal Suppression," *IEE Electron. Lett.,* vol. 32, pp. 1010-1011, 1996.

[5] Z. Hu, M. Davanco, and D.J. Blumenthal, "Extinction Ratio Improvement by Strong External Injection and SPM in an SOA for OTDM Pulse Using a DBR Laser Diode," *IEEE Photonics Technol. Lett.,* vol. 15, pp. 1419-1421, Oct. 2003.

[6] O. Leclerc, B. Lavigne, D. Chiaroni, and E. Desurvire, "All-Optical Regeneration: Principles and WDM Implementation," in Optical Fiber Telecommunications, I. Kaminow, and T. Li, *Academic Press,* New York, vol. IV A, 2002.

[7] F.X. Kartner, I.D. Jung, and U. Keller, "Soliton Mode-Locking with Saturable Absorbers," *IEEE J. Sel. Top. Quantum Electron.,* vol. 2, pp. 540-556, Sept. 1996.

[8] H.A. Haus, Y. Silberberg, "Theory of Mode-locking of a Laser Diode with a Multiple-Quantum-well Structure," *J. Opt. Soc. Am. B,* vol. 2, pp. 1237-1243, July 1985.

[9] M. Gay, L. Bramerie, J.C. Simon, A. O'Hare, D. Massoubre, J.L. Oudar, A. Shen, "Cascadability and Wavelength Tunablility Assessment of a 2R Regeneration Device based on a Saturable Absorber and a Semiconductor

Optical Amplifier," *OSA Optical Fiber Commun. Conf.*, paper OThB1, Annaheim, March 2006.

[10] D. Massoubre, J.L. Oudar, J. Fatome, S. Pitios, G. Millot, J. Decobert, and J. Landreau, "All-optical Extinction-ratio Enhancement of a 160 GHz Pulse Train by a Saturable absorber Vertical Microcavity," *European Conf. Optical Commun. (ECOC'05),* paper We4.P.018, Scotland, 2005.

[11] D. Massoubre, J.L. Oudar, J. Dion, and J.C. Harmand, "Scaling of the Saturation Energy in the Microcavity Saturable Devices," *Appl. Phys. Lett.,* vol. 88, no. 153513, Apr. 2006.

[12] K.A. Ahmed, H.F. Liu, N. Onderra, P. Lee, R.S. Tucker, and Y. Ogawa, "Nearly Transform Limited Pulse (3.6 ps) Generation from Gain-switched 1.55 μm Distributed Feedback Laser by using Fibre Compression Technique," *IEE Electron. Lett.,* vol. 29, pp. 54-56, Jan. 1993.

[13] H.-F. Liu, Y. Ogawa, and S. Oshiba, "Generation of an Extremely Short Single Mode Pulse (~2 ps) by Fiber Compression of a Gain-switched Pulse from a 1.3 μm Distributed-feedback Laser Diode," *Appl. Phys. Lett.,* vol. 59, pp. 1284-1286, Sept. 1991.

[14] J.M. Dudley, L.P. Barry, J.D. Harvey, M.D. Thomson, B.C. Thomsen, P.G. Bolland, and R. Leonhardt, "Complete Characterization of Ultrashort Pulse Sources at 1550 nm," *IEEE J. Quantum Electron.,* vol. 35, pp. 441-450, Apr. 1999.

[15] S. Li, K.S. Chiang, W.A. Gambling, Y. Liu, L. Zhang, and I. Bennion, "Self-Seeding of Fabry–Perot Laser Diode for Generating Wavelength-Tunable Chirp Compensated Single-Mode Pulses with High-Sidemode Suppression Ratio," *IEEE Photonics Technol. Lett.,* vol. 12, pp. 1441-1443, Nov. 2000.

[16] B.J. Eggleton, P.A. Krug, L. Poladian, K.A. Achmed, and H.-F. Liu, "Experimental Demonstration of Compression of Dispersed Optical Pulses by Reflection from Self-Chirped Optical Fiber Bragg Gratings," *Optics Lett.,* vol. 19, pp. 877-879, June 1994.

[17] K.A. Ahmed, B.J. Eggleton, H.-F. Liu, P.A. Krug, and F. Ouellette, "Simultaneous Mode Selection and Pulse Compression of Gain-Switched Pulses from a Fabry–Perot Laser Using a 40-mm Chirped Optical Fiber Grating," *IEEE Photonics Technol. Lett.,* vol. 7, pp. 158-160, Feb. 1995.

[18] P. Gunning, R. Kashyap, A.S. Siddiqui, and K. Smith, "Picosecond Pulse generation < 5 ps from Gain-switched DFB Semiconductor Laser Diode using a

Linearly Step-chirped Grating," *IEE Electron. Lett.,* vol. 31, pp. 1066-1067, 1995.

[19] K.-M. Feng, V. Grubsky, D.S. Starodubov, J.-X. Cai, A.E. Willner, J. Feinberg, "Tunable Nonlinearly-chirped Fiber Bragg Grating for use as a Dispersion Compensator with a Voltage-controlled Dispersion," *OSA Optical Fiber Commun. Conf. (OFC'98)*, paper TuM3, 1998.

[20] T. Komukai, T. Inui, and M. Nanazawa, "The Design of Dispersion Equalizers Using Chirped Fiber Bragg Graings," *IEEE J. Quantum Electron.,* vol. 36, pp. 409-417, Apr. 2000.

[21] T. Inui, T. Komukai, and M. Nakazawa, "A Wavelength-Tunable Dispersion Equalizer Using a Nonlinearly Chirped Fiber Bragg Grating Pair Mounted on Multilayer Piezoelectric Transducers," *IEEE Photonics Technol. Lett.,* vol. 12, pp. 1668-1670, Dec. 2000.

[22] S. Lee, R. Khosravani, J. Peng, V. Grubsky, D.S. Starodubov, A.E. Willner, and J. Feinberg, "Adjustable Compensation of Polarization Mode Dispersion using a High-birefringence, Nonlinearly Chirped Fiber Bragg grating," *IEEE Photonics Technol. Lett.,*vol.11, pp. 1277-1279, Oct. 1999.

[23] A. Azouz, N. Stelmakh, P. Langlois, J.M. Lourtioz, and P. Gavrilovic, "Nonlinear Chirp Compensation in High-Power Broad-Spectrum Pulses from Single-Stripe Mode-Locked Laser Diodes," *IEEE J. Sel. Top. Quantum Electron.,* vol. 1, pp. 577-582, June 1995.

[24] P.M. Anandarajah, C. Guignard, A. Clarke, D. Reid, M. Rensing, L.P. Barry, G. Edvell, and J.D. Harvey, "Optimized Pulse Source Employing an Externally Injected Gain-Switched Laser Diode in Conjunction With a Nonlinearly Chirped Grating," *IEEE J. Sel. Top. Quantum Electron.,* vol. 12, pp. 255-264, Mar/Apr. 2006.

[25] S. Bouchoule, E. Lach, G. Lemestreallan, S. Slempkes, D. Mathoorasing, C. Kazmierski, and A. Ougazzaden, "High Speed Gain-Switched Laser as Very Simple 4x10Gbit/s and up to 8x10Gbit/s OTDM Source," *European Conf. Optical Commun, (ECOC'98),* vol. 1, pp. 215-216, Sept. 1998.

[26] R. Kashyap, "Fiber Bragg Gratings," *Academic Press,* London, 1999.

[27] K. Hill, B, Malo, K.A. Vineberg, F. Bilodeau, D.C. Johnson, and I. Skinner, "Efficient Mode Conversion in Telecommunication Fibre using Externally Written Gratings," *IEE Electron. Lett.,* vol. 26, pp. 1270-1271, 1990.

[28] A.E. Willner, K.-M. Feng, S. Lee, J. Peng, H. Sun, "Tunable Compensation of Channel Degrading Effects Using Nonlinearly Chirped Passive Fiber Bragg

Gratings," *IEEE J. Sel. Top. Quantum Electron.,* vol. 5, pp. 1298-1311, Sept/Oct. 1999.

[29] F. Ouellette, "Dispersion Cancellation using Linearly Chirped Bragg Grating Filters in Optical Waveguides," *Optics Lett.,* vol. 12, pp. 847-849, Oct. 1987.

[30] J. Williams, I. Bennion, and N. Doran, "The Design of In-fiber Bragg Grating Systems for Cubic and Quadratic Dispersion Compensation," *Optical Commun.,* vol. 116, pp. 62-66, 1995.

[31] K.C. Byron, K. Sugden, T. Bircheno, and I. Bennion, "Fabrication of Chirped Bragg Gratings in Photosensitive Fibre," *IEE Electron. Lett.,* vol. 29, pp. 1659-1660, 1993.

[32] B. Eggleton, P.A. Krug, and L. Poladin, "Dispersion Compensation by using Bragg Grating Filters with Self Induced Chirp," *OSA Optical Fiber Commun. Conf. (OFC'94),* p. 227, 1994.

[33] H. Ghafouri-Shiraz, and M. Tang, "Interaction between Ultrashort Optical Pulse and Fibre Gratings with Random Profile Noise," *IEE Proc.-Optoelectron.,* vol. 151, pp. 16-26, Feb.2004.

[34] T. Erdogan, "Fiber Grating Spectra," *J. Lightwave Technol.,* vol. 15, pp. 1277-1294, Aug. 1997.

[35] Redfern Optical Components, URL: http://www.redferncomponents.com /003Poducts/_Custom/ROC_FBG_Foundry_Service_2pg_.pdf "Custom Made FBG Data Sheet".

[36] R. Feced, M.N. Zervas, and M.A. Muriel, "An Efficient Inverse Scattering Algorithm for the Design of Nonuniform Fiber Bragg Gratings," *IEEE J. Quantum Electron.,* vol. 35, pp. 1105-1115, Aug. 1999.

[37] A. Rosenthal, and M. Horowitz, "Inverse Scattering Algorithm for Reconstructing Strongly Reflecting Fiber Bragg Gratings," *IEEE J. Quantum Electron.,* vol. 39, pp. 1018-1026, Aug. 2003.

[38] J. Skaar, and O.H. Waagaard, "Design and Characterization of Finite-Length Fiber Gratings," *IEEE J. Quantum Electron.,* vol. 39, pp. 1238-1245, Oct. 2003.

[39] C. Knothe, and E. Brinkmeyer, "Reset-free Phase Shifter in a Sagnac-type Interferometer for Control of Chirp and Apodization of Bragg Gratings," *OSA Bragg Gratings, Photosensitivity and Poling in Glass Waveguides (BGPP'03),* paper TuB3, Monterey, CA, 2003.

[40] S. Nogiwa, Y. Kawaguchi, H. Ohta, and Y. Endo, "Generation of Gain-switched Optical Pulses with very Low Timing Jitter by using External CW-light Injection Seeding," *IEE Electron. Lett.,* vol. 36, pp. 235-236, Feb. 2000.

[41] D.-S. Seo, D.Y. Kim, and H.F. Liu, “Timing Jitter Reduction of Gain-switched DFB Laser by External Injection Seeding,” *IEE Electron. Lett.,* vol. 32, pp. 44-45, Jan. 1996.

[42] R.A. Gabel, and R.A. Roberts, “Signals and Linear Systems,” *Wiley,* New York, 1987.

[43] N. Litchinitser, Y. Li, M. Sumetsky, P. Westbrook, and B. Eggleton, “Tunable Dispersion Compensation Devices: Group Delay Ripple and System Performance,” *OSA Optical Fiber Commun. (OFC’03),* vol. 1, pp. 163-164, 2003.

[44] B.J. Eggleton, A. Ahuja, P.S. Westbrook, J.A. Rogers, P. Kuo, T.N. Nieksen, and B. Mikkelsen, “Integrated Tunable Fiber Gratings for Dispersion Management in High-Bit Rate Systems,” *J. Lightwave Technol.,* vol. 18, pp. 1418-1432, Oct. 2000.

CHAPTER 4 – PULSE PROPAGATION CHARACTERISATION FOLLOWING AMPLIFICATION IN A SEMICONDUCTOR OPTICAL AMPLIFIER

4.1 Introduction

Semiconductor optical amplifiers (SOAs) are attracting a lot of interest in the field of telecommunications due to their high gain, small size, low noise figure and opportunities for integration and low cost [1]. The development of SOAs followed soon after the invention of the semiconductor laser and the progression of the SOA device design went hand in hand with the advancement in design of the laser diode. During the 1990's due to the development of the erbium doped optical amplifier (EDFA) the popularity of the SOA as a linear amplifier declined as the EDFA provided more gain without the detrimental nonlinearities associated with an SOA [2]. However, there was renewed interest in SOAs in the late 1990's as SOA design techniques developed, and thus its possibilities for integration and cost effectiveness led the SOA to become a competitive component in comparison to the EDFA. The design of SOAs developed in two directions, one to reduce the detrimental nonlinearities so that it could be used as an amplifier and second to take advantage of these nonlinear effects and exploit them for use in all-optical signal processing. Therefore, it is an essential study to examine the operation of SOAs in high bit rate communications systems both as gain amplifiers and optical data processing [3].

In this chapter, a brief overview of the various optical amplifiers that are available is conducted. A basic introduction of the SOA design is then given followed by a description of its carrier dynamics which affect propagation of a picosecond pulse through it. The main contribution of pulse and spectral distortion is caused respectively by gain saturation and corresponding self phase modulation (SPM) due to interband filling. As pulse widths reduce and approach 2 ps effects such as carrier heating (CH) and spectral hole burning (SHB) become much more dominant and cause greater nonlinearities to occur. The main contribution of this chapter is the accurate and full characterisation of pulses following propagation through an SOA. This is an important result in order to understand how SOA dynamics affect its application as an amplifier and as an all-optical processing device. The pulses are analysed as a function of input power, pulse duration and wavelength. High input pulse power to the SOA results in temporal

pedestal suppression ratio (TPSR) deterioration and generation of large chirp due to gain saturation which can render the pulses unsatisfactory for use in high-speed optical time division multiplexed (OTDM) systems.

4.2 Optical Amplifiers

Optical amplifiers can be categorised into three major classes; rare earth doped amplifiers (e.g. EDFA), semiconductor-based amplifiers (e.g. InGaAsP SOA), and amplification based on stimulated Raman scattering (SRS) in silica fibre (e.g. distributed Raman amplifier (DRA)) [4]. The gain in EDFAs and similar doped fibre amplifiers is provided by the fibre, doped by a rare earth element e.g. erbium. The input signal and pump laser are coupled together into the doped fibre. The pump excites electrons of the doped fibre to a higher energy level and the signal is amplified via stimulated emission as the input photon results in the decay of the electrons to a lower energy level. Thus the EDFA is optically pumped. The gain bandwidth in an EDFA is limited to the C and L band windows. New rare earth dopants are being developed so that amplification can be provided in other telecommunications windows of the wavelength spectrum. An SOA is an optoelectronic device where the gain is provided by an active semiconductor material, typically a III-V compound which can provide gain for wavelengths between 1200 and 1700 nm. In contrast to the EDFA, the SOA is electrically pumped by the injected bias current. Raman amplification is generally used in long haul systems in conjunction with EDFAs to improve the transmission performance of the signal. It is generally a distributed amplification technique although some discrete units are available [5]. Raman amplifiers use the physical property of SRS to provide gain. A pump laser at a certain power and wavelength is launched into the fibre together with the propagating signal and amplification occurs when the pump photon gives up energy to create a new photon at the signal wavelength. In addition some residual energy is absorbed as phonons. The available gain is highly dependent on the wavelength offset and power of the pump. Typically optimum amplification for signals propagating at 1550 nm is achieved when the pump is offset by 100 nm to lower wavelengths.

There are three different areas where amplification is deployed, as a power booster (to boost signal power of a source), as an inline amplifier (to compensate signal due to attenuation in the transmission line) and as a preamplifier (to improve receiver sensitivity). EDFAs are the dominant amplifiers in long-haul systems as they have lower noise levels and much better crosstalk properties for multi-channel amplification in comparison to SOAs. However the SOA offers a cost competitive alternative to the

EDFA when used as an inline amplifier in metro networks, as a power booster and as a preamplifier. Additional benefits of the SOA include the possibility of monolithic integration with other semiconductor components, a small footprint and low energy consumption.

One important property of the SOA is that it has varying recombination times, associated with different carrier dynamics. This can cause large gain compression and nonlinear effects to the applied signals. In contrast to SOAs, EDFAs have a much longer recombination time for excited states in erbium and thus cause minimal nonlinearities in high-speed systems. Although these nonlinear effects are detrimental to the SOA for use as an amplifier, this nonlinearity can be exploited for all-optical signal processing in high-speed systems.

4.3 Semiconductor Optical Amplifiers

An SOA is based on very similar technology to the semiconductor laser diode. There are two types of SOA, the Fabry–Pérot amplifier (FPA) and the travelling wave amplifier (TWA), both of which have the same basic structure but differ in their reflectivities of the mirrors. FPAs have reflectivities in the order of 0.01-0.3, thus creating resonant devices. However, this reflectivity limits the amplifier bandwidth and the transmission characteristics are highly dependent on fluctuations in bias current, temperature and input signal polarisation. In order to amplify only, it is necessary to protect the device against self oscillations generating a lasing effect. This is accomplished by TWAs which block cavity reflections using both an antireflection coating and the technique of angle cleaving the chip facets. Thus there is only a single pass of the signal through the cavity [6]. Telecom applications require a TWA design, which allows amplification over a larger bandwidth (e.g. up to 40 nm in the 1550 nm window) and is the type of SOA which is discussed from now on.

4.3.1 Device Structure of a Bulk SOA

A bulk SOA is a simple forward biased p-n junction as shown in Figure 4-1 [7]. By doping the semiconductor material with donor and acceptor impurities, the Fermi level can be raised above or below the centre of the bandgap to create n-type and p-type semiconductors respectively [8]. The dominant carrier is electrons in the n-type material and holes in the p-type material. When the two materials are brought together, as the majority, holes in the p-type material tend to diffuse towards the n-type material (which has a majority of electrons), and forms a thin depletion layer. The thin depletion layer is

free of mobile carriers, and a built in potential is created. By applying a forward bias electric field (in the opposite direction of the built-in potential), the width of the depletion layer shrinks and the potential barrier is reduced. Electrons and holes can flow more easily across the active region. As a result both free electrons and holes are present in the depletion region leading to a high inversion level. A high population inversion translates to the population of the higher energy level exceeding the population of the lower energy level so that photonic emission can exceed photonic absorption. This is achieved through applied electrical bias.

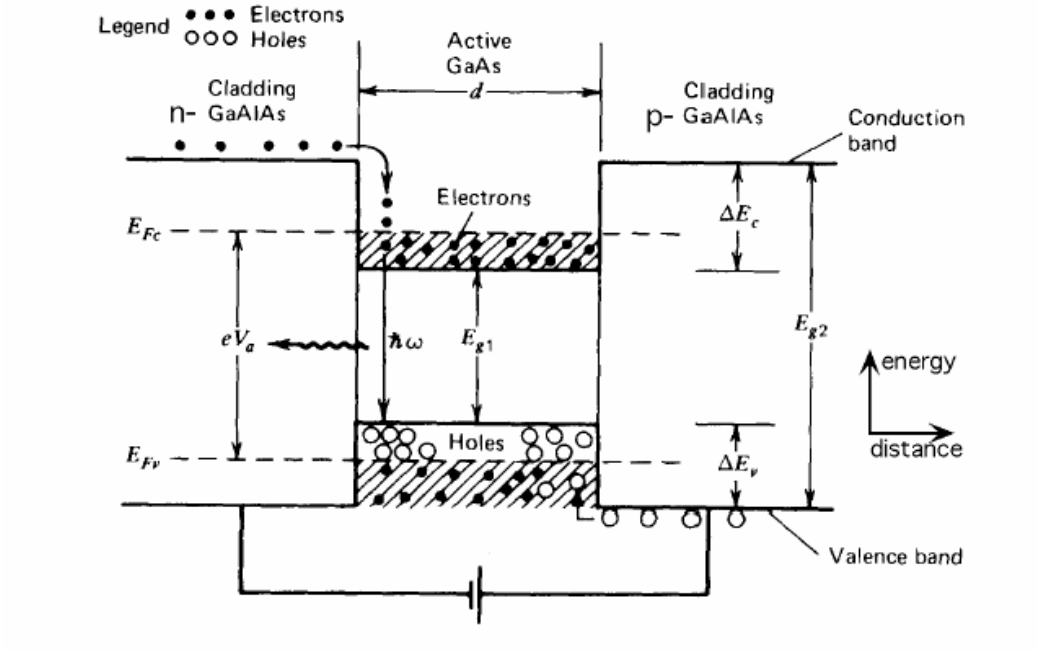

Figure 4-1 A schematic of a p-n junction diode illustrating the process of radiative emission [7].

Electrical and optical confinement in the SOA can be improved by using a double-hetero structure. In this configuration materials which have a higher bandgap are placed on either side of the p-n junction. These cause potential barriers to improve electrical confinement to the active region. These materials with a higher bandgap also have a smaller refractive index and thus due to total internal reflection improve the optical confinement area. A typical structure of a chip SOA is displayed in Figure 4-2.

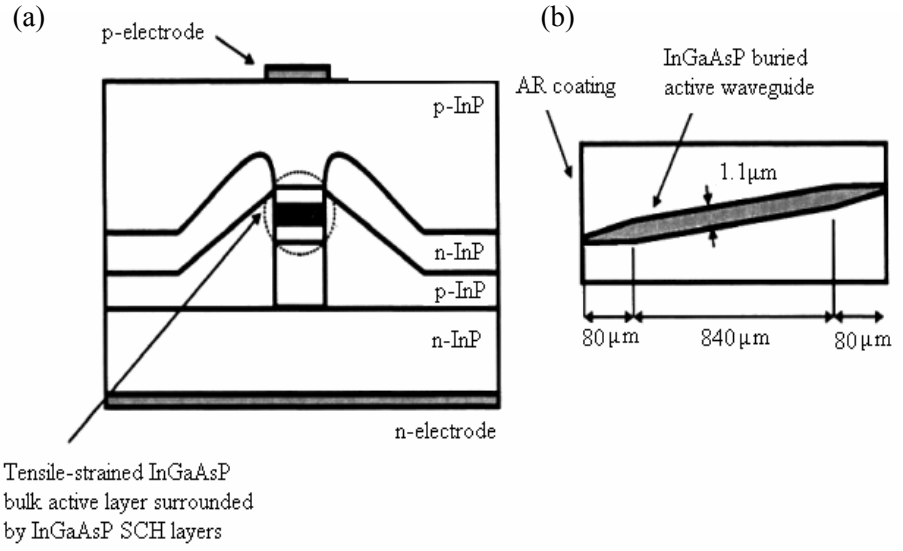

Figure 4-2 Diagram of structure of an SOA from (a) a cross section view, and (b) a top view of the active waveguide.

Technological advancement in the design of a bulk SOA can give enhanced performance in terms of reduced threshold current, higher gain efficiency lower noise and higher saturation power [9,10]. These devices can be categorised as quantum well (QW) and quantum dot (QD) SOAs.

4.3.2 Quantum Well SOAs

A quantum well (QW) device is very similar in structure to a bulk SOA except for the thickness of the active layer. When the thickness of a semiconductor active layer is reduced to the order of a 100 Angstroms (10 nm), effects not typical of the bulk material called quantum size effects occur [11]. When a thin layer is sandwiched between wider band gap materials, electrons or holes in the middle layer are restricted (confined) to a finite potential well and the usual band-to-band recombination process is then modified in a fundamental manner. Quantum confinement in the well causes the conduction and valence bands to break up into a series of subbands with a step-like density of states function, thus stimulated emission only occurs at discrete energy levels. Thus it is the difference between QW energy levels, rather than the bandgap energy, which is responsible for the stimulated emission process.

4.3.3 Quantum Dot Amplifiers

Quantum dot (QD) lasers and SOAs have active regions in which the gain material is confined in all three spatial dimensions [12]. If the density of states for a conventional diode-laser hetero structure is regarded as three-dimensional (i.e. continuous) and a QW structure is regarded as two dimensional, a QD structure is zero-dimensional. A QD is a very small piece of semiconductor material on the nanometre dimension scale and thus

has quantum-like properties. QDs are defined by a size limit whose volume is smaller than the volume defined by the Bohr radius of that particular semiconductor (e.g. 0.053 nm) [13]. QD SOAs are even more attractive devices for future signal amplification and all-optical signal processing, due to their high material gain, low threshold current and small chirp. However, these devices are currently only in research stages with the promise of becoming commercially available in the next four years [14]. Research carried out so far has measured gain responses on the order of a few picoseconds [15,16].

4.4 Radiative Processes of an SOA

An SOA undergoes three different radiative processes. Photon emission can be achieved by spontaneous and stimulated emission and the third process is absorption of input photons. These processes can be described by simple rate equations [17].

4.4.1 Stimulated Emission

Stimulated emission is the process where an input photon to the SOA interacts with an electron in the conduction band, thus causing it to recombine with a hole, thereby emitting a photon. The incident photon must have an energy equal to the recombination energy of the electron-hole pair. Due to stimulated emission, an input optical wave (of the correct wavelength) to the active region undergoes gain. The gain available to the input signal increases as the number of electrons and holes injected across the junction increases. This process is illustrated in Figure 4-3. The emitted signal has the same frequency, phase, direction and polarisation of the incident photon, thus, outputting a highly coherent amplified signal.

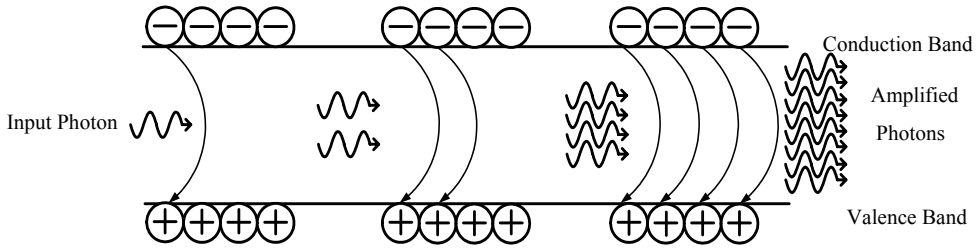

Figure 4-3 An illustrative view of stimulated emission within an SOA

4.4.2 Spontaneous Emission

When an electron and a hole are present in the same region, they may recombine by spontaneous emission, i.e. the electron may re-occupy the energy state of the hole, emitting a photon with energy equal to the difference between the electron and hole states

involved. Spontaneous emission is a random radiative process whereby the resultant emitted photons have no corresponding phase and can be emitted in any random direction [18]. As spontaneously emitted photons travel along the active region, they can also be amplified generating amplified spontaneous emission (ASE). ASE is considered as noise, which degrades the SOA performance. If the spontaneous emission photons happen to be emitted close to the direction of travel of the signal photons, they will interact with the signal photons, causing both amplitude and phase fluctuations. Thus, the measured power of the amplifier output consists of both amplified signal power and the ASE power.

4.4.3 Absorption

An electron in a lower energy state is raised to an excited energy state after having absorbed a photon with energy equivalent to bandgap energy. Without population inversion the probability of stimulated emission and absorption taking place are equal. Thus for an SOA to provide gain, population inversion must be achieved such that the population of the higher energy level exceeds the population of the lower energy level.

4.4.4 SOA Rate Equations

The SOA rate equations are very similar for the rate equations described in Chapter 2, Section 2.5.3, however they also need to account for the changes due to an input light signal. Generally, single mode evaluation is sufficient to describe the carrier dynamics in an SOA. The carrier density rate equation can be described as [17]:

$$\frac{dN}{dt} = \frac{I}{qV} - \frac{N}{\tau_n} - \Gamma g S \qquad \text{Equation 4-1}$$

where N is the carrier density, t is the time, I is the injected bias current, q is the electronic charge, V is the volume of the active region, τ_n is the carrier lifetime, Γ is the optical confinement factor g is the material gain and S is the photon density. The first term describes the generation of carriers due to the applied bias current, the second term describes the carriers lost due to recombination processes such as spontaneous emission, monomolecular and Auger recombination. The last term describes the carriers depleted due to stimulated emission. The gain is defined as $g = a(N-N_0)$, where, a is the differential gain (dg/dN) and N_o is the carrier density at transparency.

The photon density rate equation of an SOA is:

$$\frac{dS}{dt} = -\frac{S}{\tau_s} + \Gamma g S + \Gamma \beta_{sp} \frac{N}{\tau_{sp}} + S_{in} \qquad \text{Equation 4-2}$$

where τ_s is the photon cavity lifetime, β_{sp} is the spontaneous emission factor, τ_{sp} is the spontaneous emission lifetime, and S_{in} is the photon density injected by the incident optical signal per second. The first term describes the decrease in photon density due to losses in the cavity. For a TWA the mirror losses are nearly 100% due to the very low facet reflectivities now achievable. The next two terms describe the generation of photons due to stimulated emission, and the generation of photons due to spontaneous emission which are confined to the active region respectively. Finally the last term takes onto account the increase in photon density due to the input optical signal.

When an optical pulse is injected into an amplifier the majority of the electrons in the excited state are depleted due to stimulated emission. The reduction in the density of excited electrons has two consequences. First, amplifier gain is reduced, and consequently the refractive index as seen by the waveguide changes [19] as described by Kramers-Kronig relations [8]. This causes a change in wavelength of the output pulse as a function of time i.e. chirp. The gain recovery processes following depletion by an injected optical pulse are described below.

4.5 Carrier Dynamics of an SOA

When an optical beam is injected into an SOA, electrons in the excited states are depleted due to the electron-hole recombination. This depletion in carriers due to interband effects leads to a reduction in available gain. In addition ultrafast phenomena such as SHB and CH also lead to gain suppression for amplification of further optical signals. The gain recovers on different timescales for these afore mentioned interband and ultrafast processes. Figure 4-4 shows the gain recovery of an SOA following each of the gain saturation effects. In addition there is an associated change in the phase for each change in gain. In the following section a more detailed description of these effects will be given and it will be shown how they are important for applications of the SOA.

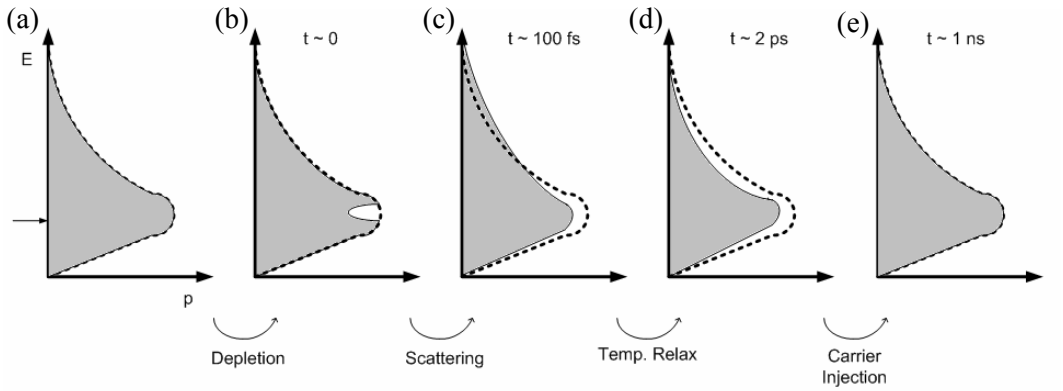

Figure 4-4 Carrier evolution of the electron density (p) versus electron energy (E) in the active region of an SOA.

4.5.1 Spectral Hole Burning

Spectral hole burning (SHB) is a localised reduction in gain (or carriers) around the spectral region of the lasing wavelength [20] as shown in Figure 4-4 (b). At the amplifying wavelength, intense stimulated emission depletes carriers in this spectral area faster than the rate at which the carriers can 'fill in' the 'hole'. The magnitude of gain compression produced by this effect depends critically on the intraband relaxation times of the carriers. There is a subsequent redistribution of carrier energies due to carrier-carrier scattering as shown in Figure 4-4 (c). The scattering process due to SHB is more prominent in InGAsAsP optical amplifiers in comparison to GaAs-AlGaAs amplifiers as they have time scales of the order of 50-100 fs and <20 fs respectively [21]. SHB affects gain as seen by the incident pulse as the gain reduction is localised at the incident pulse wavelength. For some optical signal processes such as wavelength conversion, the probe signal is not affected by SHB as the CW signal is located at a different wavelength which does not see the localised gain reduction.

4.5.2 Carrier Heating

Carrier heating (CH) is a transient heating of electron and hole temperatures [22]. Thus carriers are excited into the high momentum states. When a pulse at the wavelength corresponding to the gain curve of the SOA is transmitted through an SOA, it reduces the carrier population but heats the plasma (by removing cool carriers). As a result, the gain reduces, since the active layer gain is a sensitive function of the carrier temperature. The carrier temperatures relax towards the lattice temperature by electron-phonon scattering on the time scale of 0.5-2 ps as shown (c-d) of Figure 4-4. The main mechanism of CH within the lattice structure is stimulated emission however there are other contributions such as free-carrier absorption (FCA) and two-photon absorption (TPA). FCA is an effect where a free carrier (arising from lattice vibrations) can absorb a photon and move to a

higher energy state within the band, thus increasing the temperature of the lattice [23]. TPA becomes an important parameter to consider upon the input of high power pulses to the SOA [24]. The strong injection pulse causes the generation of free carriers of very high energy, which results in heating of the conduction band electrons (and to a lesser extent, heating of the valence band holes). TPA is a process where two photons are absorbed in the generation of a single electron-hole carrier pair [25]. It occurs when a photon of energy E_s is incident on an active area of a semiconductor device with a bandgap exceeding E_s but less than $2E_s$, and thus the probability of TPA increases with an increase in input signal [51].

4.5.3 Interband Recovery

The interband carrier recovery time is the time it takes for the carriers depleted from the conduction band to be replenished by the applied bias current. The interband relaxation time is the step illustrated from (d-e) in Figure 4-4. It has an intrinsic timescale of approximately 40-200 ps. This large time range which the interband gain recovery time occurs is highly dependent on many parameters such as the length of the SOA, the bias current and the injected optical power [26,27].

4.5.4 Phase Dynamics

The changes in gain lead to a variation of the refractive index. This relationship between the gain and refractive index is related by the linewidth enhancement factor (LEF), or alpha factor [28] and can be described by Kramers-Kronig relations. There is an LEF associated with each of the SOAs individual gain recovery processes [29]. A reduction in carrier density or gain results in an increase in refractive index and thus an increase in phase shift. Small changes in carrier density in an SOA can lead to a large change in its refractive index and thus large phase-shift changes.

4.5.5 Self Phase Modulation

The large refractive index change in the SOA leads to a modulation of the phase of the input signal. This nonlinear change which is a result of gain saturation is described as self phase modulation (SPM) and is the physical mechanism which leads to spectral distortion of the input signal [19]. Relatively low input powers can result in considerable distortion in the spectral domain. SPM due to gain depletion leads to an asymmetric spectral broadening biased towards longer wavelengths i.e. red chirp. Gain recovery results in a negative phase shift and thus spectrally there is a corresponding shift to lower wavelengths i.e. blue chirp. Additionally the spectrum develops a multi-peak structure after propagation through the SOA, due to interference effects. The same value of instantaneous frequency can exist at two points within the profile of the pulse, and this

leads to constructive and destructive interference occurring resulting in an oscillatory nature of the spectra [19].

For pulse widths greater than 10 ps, the time resolved gain is just the integral of the pulse intensity, which leads to an instantaneous frequency shift which is directly proportional to the intensity envelope of the input optical pulse. The instantaneous frequency therefore has its maximum deviation at the peak of the optical pulse. As the pulse width reduces, in a similar fashion to the ultrafast gain recovery of the SOA, there is a corresponding ultrafast phase change [30]. There is a SPM contribution due to the thermalisation or cooling of hot carriers [31]. The time varying gain of the SOA leads to a temporally varying refractive index due to carrier depletion, however the LEF relating these changes is much smaller in magnitude in comparison to carrier induced refractive index change. Thus the ultrafast phase change has a much smaller contribution to the overall phase recovery of the SOA.

The LEF, α describes the amplitude-phase coupling of an SOA. There is an associated LEF for each carrier dynamic relating to band filling, CH and SHB. Typical LEFs for SOAs are reported to be 3.1 and 1.9 for carrier density gain saturation and the nonlinear gain reduction caused by CH respectively [38]. The LEF, α_N for interband effects is defined as the change of the real and imaginary parts of susceptibility, i.e. the change in refractive index, n and in the gain, g with respect to changes in the carrier density, dN as described by the following expression [28]:

$$\alpha_N = \frac{-4\pi}{\lambda} \frac{dn/dN}{dg/dN} \qquad \text{Equation 4-3}$$

The alpha factor dependence on wavelength and current in a SOA is described by Storkfelt et al. [32]. The large differential gain at lower wavelengths corresponds to a small alpha factor and thus a small chirp. With increasing applied bias current the gain peak wavelength decreases linearly. The alpha factor and thus the chirp increases with increasing wavelength as the differential gain reduces.

The ultrafast gain dynamics of an SOA cannot be measured using an oscilloscope due to its limited bandwidth resolution. Therefore the ultrafast gain and phase dynamics of an SOA can be measured using time and spectrally resolved pump-probe experiments [23]. The gain and phase dynamics of a typical Kamelian SOA are shown in Figure 4-5 [33]. The input pulses were 2 ps FWHM. The gain recovery time due to CH is 1 ps and the associated gain recovery is 3 dB. The magnitude of the ultrafast gain recovery of the CIP

SOA is only approximately a half of the ultrafast gain recovery of the Kamelian SOA [34]. The ultrafast phase recovery is typically an order of magnitude smaller than the associated ultrafast gain recovery [35].

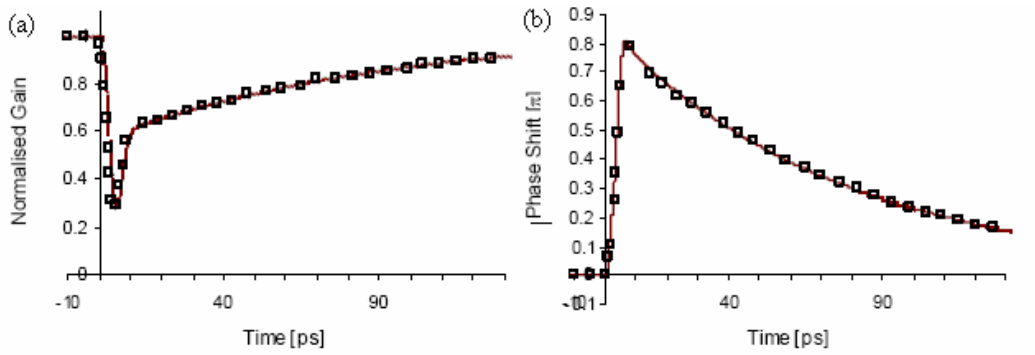

Figure 4-5 Measured (a) gain and (b) phase dynamics of a Kamelian SOA displaying a large ultrafast gain recovery, and a small ultrafast phase recovery [33].

4.5.6 Gain Saturation

High energy input pulses induce gain saturation of the SOA which in turn results in pulse deformation. Amplification of an optical signal consumes carriers, thereby transiently saturating (i.e. reducing) the gain. Gain saturation induced nonlinearities lead to pulse distortion in all amplifiers because the leading edge saturates the amplifier and reduces the gain available for the trailing edge. If the input pulse energy is only a small fraction of that required for gain saturation then there is little distortion to the pulse. However, large input pulse energies could prove detrimental to communications system performance. If the amplifier does not provide approximately the same gain for all data bits, it results in the generation of patterning effects and the quality of the optical data signal is significantly degraded [18]. To avoid distortion of the signal, the magnitude of gain saturation must be sufficiently small, or the amplifier dynamics must be such that transient gain changes do not affect the neighbouring bits.

Gain saturation is dependent not only on the energy of the input pulses but is also dependent on the width of the input pulses. Therefore the saturation energy for pulse widths of 150 fs is much less than for pulse widths of 15 ps [36]. This pulse width dependence is due to the nonlinear gain saturation effects of CH and SHB. Bori et al. have shown that a critical pulse width of 10-12 ps is the point where saturation of the carrier density and nonlinear effects contribute equally [37]. Therefore data streams output from an SOA undergo linear and nonlinear patterning effects at high bit rates. The maximum line rate of an SOA for use as an amplifier to date is 40 Gb/s, due to the effects of patterning which leads to eye closure.

4.6 Experimental Characterisation of Amplified Pulse following Propagation through an SOA

There has been a proliferation of publications concerning the ultrafast gain and phase dynamics of SOAs measured and explained through pump-probe experiments [20,33,38,39], autocorrelation techniques [40], cross-correlation analysis [41], spectral characterisation [19,42] and spectrogram measurements [43,44]. Delfyett et al. [45,46] analysed the pulse intensity and its corresponding temporal shift of 2 ps pulses propagating through an SOA to retrieve some chirp information. Other methods used the measurement technique of frequency-resolved optical gating (FROG) to characterise pulses and their phase for pulse widths around 175 fs in the absorption, transparency and gain regimes following propagation in an SOA [47,48].

However there is no single complete study of short picosecond pulses suitable for high-speed systems (2 ps and 8 ps FWHM suitable for 160 Gb/s and 40 Gb/s OTDM respectively) following propagation in an SOA to date. The following experimental characterisation fills this void by characterising the temporal, spectral and chirp profiles of the outputted pulses as a function of varying SOA and input pulse parameters (input power, wavelength, and polarisation for two different SOA devices). The changes in pulse shape and the amplitude of the SOA induced chirp is important in determining the propagation distance of the amplified pulses. In addition the induced nonlinear chirp shape is measured. Thus this characterisation is important in examining the effects of these amplified pulses in a high-speed network but also how these effects will impact nonlinear processing capabilities of the SOA. A significant result of the characterisation which has not been previously published is the large TPSR deterioration of the input pulse due to SOA gain saturation [49].

4.6.1 Kamelian and CIP SOA Device Characterisation

Two commercially available SOAs were used in the experiment available from Kamelian and CIP. (See Appendix II for basic device characterisation for both SOAs). The Kamelian SOA as illustrated in Figure 4-2 is a 1 mm long device including tapers for the improvement of chip-fibre coupling (detailed device information is reported in [50]). The material gain curve of the Kamelian SOA is shown in Figure 4-6, modelled for a carrier density of 2.9×10^{24} m^{-3} [50]. The CIP SOA is a multiple QW (MQW) device 1.5 mm long [34]. Both devices have an active region which is tilted 7º from the normal axis to prevent the gain from having a resonant peak due to the formation of an optical cavity. The CIP device is nonlinear in that it has a low saturation output power of 9 dBm, while

the Kamelian device does not reach the same level of saturation until 13 dBm. The Kamelian and CIP SOA have an unsaturated fibre-to-fibre gain of 21 dB and 26 dB at an operating current of 200 mA at a wavelength of 1550nm respectively.

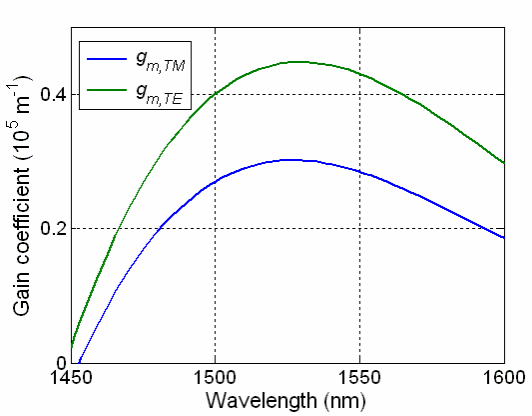

Figure 4-6 Material gain curve of the Kamelian SOA for a carrier density of 2.9×10^{24} m^{-3} [50].

The gain recovery of each SOA was measured as shown in Figure 4-7 (a). A 2 ps pulse train and a CW signal (also known as probe signal) are coupled together and are input to the SOA. The CW signal is modulated by the gain of the SOA. The input pulse train is filtered from the output of the SOA and the probe signal measured by the digital communications analyser (DCA) represents the gain recovery of the SOA. The normalised gain recovery of the Kamelian and CIP SOAs are shown for an input probe power of -12.8 dBm in Figure 4-7 (b). The interband gain recovery time of the Kamelian and CIP SOAs are 68.1 ps and 58.2 ps respectively. The ultrafast gain recovery is also visible but an accurate measurement of its time frame cannot be measured due to the limited temporal resolution of the DCA. However this figure shows that the magnitude of intraband gain recovery is larger (~3 dB) for the Kamelian SOA in comparison to the CIP SOA for hese operating conditions.

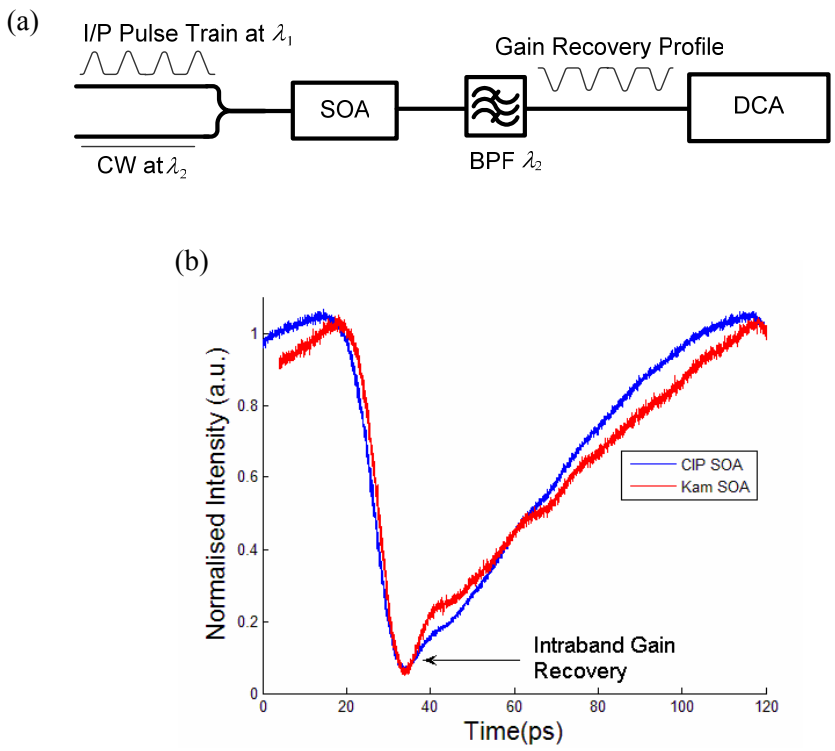

Figure 4-7 (a) Experimental set-up to measure the interband gain recovery time of an SOA and (b) the gain recovery response of the Kamelian and CIP SOAs (68.1 ps and 58.2 ps respectively).

4.6.2 Experimental Set-up

The experimental set-up used to characterise the SOA amplified pulses using the FROG measurement technique is shown in Figure 4-8. Two different pulse sources were used to generate the 8 ps and 2 ps pulses. The generation of the 8 ps pulse train was accomplished through gain switching in conjunction with a nonlinearly-chirped fibre Bragg grating (NL FBG) as shown in Figure 4-8 (a). The generated Gaussian pulses have a time bandwidth product (TBP) of 0.44 (transform limited), a wavelength of 1549.5 nm and a repetition rate of 2.5 GHz. The pulse generation method is described in detail in Chapter 3 Section 5.4. The second pulse source comprised of a 10 GHz hybrid mode-locked semiconductor laser, which generates pulses with an approximate FWHM of 2 ps, tunable from 1530 – 1565 nm as shown in Figure 4-8 (b). In each set-up the pulse train was amplified and then selectively attenuated via a variable optical attenuator (VOA) and then injected into the SOA. In the case of the 2 ps pulses the experiment was carried out by setting the input pulses to match the either the transverse electric (TE) and transverse magnetic (TM) polarisation of the SOA. The SOA TE and TM axis of polarisation was found by respectively maximising or minimising its ASE following a polarizer. The input signal was then matched to the TE/TM axis of the SOA by adjusting the polarisation controller (PC) to give maximum output power following the SOA and polarizer. Isolators were placed before and after the SOA to ensure no lasing action could take

place due to reflections from other components in the set-up, (due to the very high gain of both SOAs a small reflection can initiate lasing action in the SOAs). The output pulses were characterised using the FROG via an EDFA and PC.

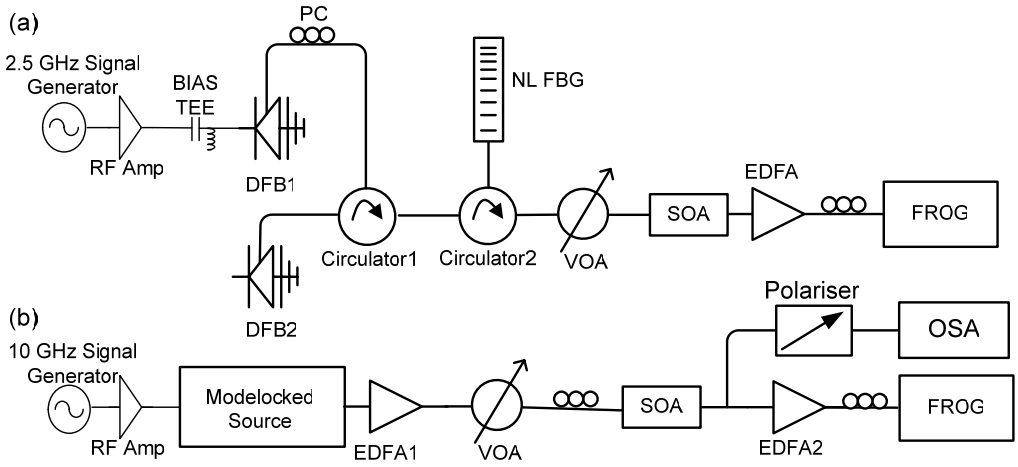

Figure 4-8 Experimental set-up of pulse characterisation following propagation through an SOA for (a) 8 ps pulses generated by a gain-switched laser in conjunction with a NL FBG and (b) 2 ps pulses generated by a mode-locked source.

4.6.3 Characterisation of 8 ps and 2 ps Pulse Widths as a Function of Input Peak Power

The first important characterisation is to investigate different pulse widths to determine how they affect the intensity and phase of pulses following propagation in an SOA. Pulse widths of 8 ps and 2 ps were chosen as they are the typical pulse widths used in 40 Gb/s and 160 Gb/s OTDM systems respectively. Figure 4-9 displays the intensity profile and corresponding chirp of the 8 ps input and output pulses at different input powers. The input peak power is varied from 1.5 mW to 150 mW, the SOA bias current is 150 mA and the input wavelength is 1550 nm. For low input peak powers (<1.5 mW) the output pulses only show a small degree of distortion in comparison to the input pulses. With an increase in input peak power the pulse width increases from 8.8 ps to 12.4 ps. The reason for pulse broadening is as follows: the leading edge sees a large gain, and is linearly amplified. However the gain of the SOA begins to saturate with increased power, resulting in less gain available for the rest of the pulse causing pulse broadening. The TBP deteriorates from 0.44 to 0.63, and the formation of a large amount of nonlinear chirp due to the SOA SPM is clearly visible. The chirp becomes more nonlinear as the input power to the SOA is increased. Carrier density depletion induced SPM is the main mechanism contributing to the nonlinear chirp for these 8 ps pulses [19]. The chirp profile is shaped closely to the shape of the pulse. The chirp minimum corresponds to the pulse maximum as this point corresponds to the point of maximum red-shift of the pulse.

From this point onwards the pulse is in less saturation and thus the chirp returns to its initial level.

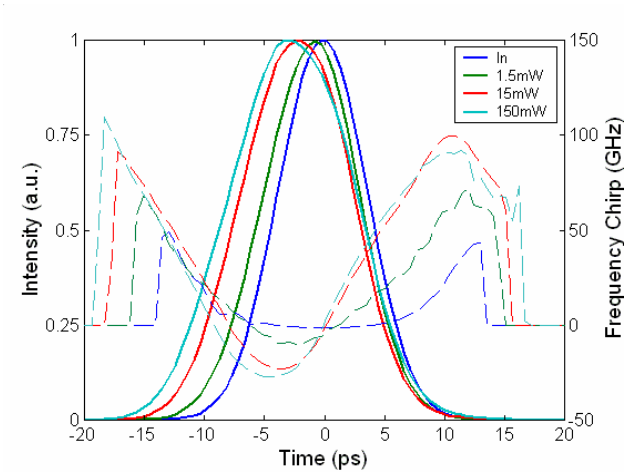

Figure 4-9 The intensity profile and corresponding chirp of an 8 ps gain-switched pulse input to and output of the SOA as the input peak power is varied from 1.5 to 150 mW.

Previous studies have shown that as pulse widths become narrower the ultrafast gain and phase recovery effects become more prominent [37]. Thus we repeated the above experiment with a 1.5 ps pulse to examine how the narrower input pulse width and the contribution of the ultrafast gain and phase recovery affect the pulse intensity and chirp profile. The intensity profile and the chirp before and after propagation through the SOA as a function of input peak power varied from 2 mW to 125 mW are shown Figure 4-10. The wavelength of the input pulse is 1550 nm, the bias current to the SOA is 200 mA and the input polarisation of the pulse is set to match the TE mode of the SOA. This figure shows the pulse width increases from 1.5 ps at the input to 1.8 ps, 2.4 ps, and 2.7 ps as the input power increases. This pulse width increase is due to the interband gain saturation effects (similar to 8 ps pulse widths) but there is also a further gain compression due to the ultrafast effects. Thus the pulse width increase factor is 1.5 for the 8 ps pulses and 1.8 for the 2 ps pulses at the maximum input peak power. The magnitude of the chirp for the 1.5 ps pulse is much greater than the 8 ps pulse for the same input peak powers. Taking the maximum input power to the SOA for both pulse widths the chirp magnitude increases from 125 GHz to 300 GHz. This is due to the pulse width dependence on the energy saturation level of the SOA as was described in section 4.5.6 and the corresponding refractive index dependence outlined in section 4.5.4. For 2 ps pulses, the contribution of CH due to effects of stimulated emission, FCA and in particular TPA [51] is much greater in comparison to the case of pulse widths of 8 ps. An additional contribution to SPM originates from the instantaneous non-linear index [52].

Together all these effects result in gain suppression and a corresponding change in phase through the process of SPM.

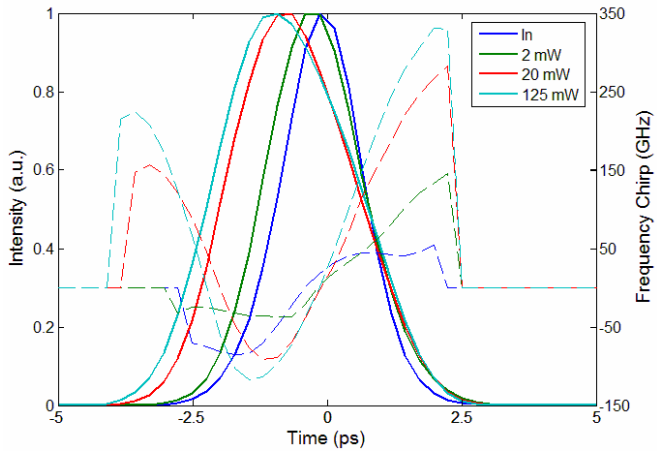

Figure 4-10 Input and output pulse profiles and corresponding chirp as a function of input peak power (2, 20, 125 mW) to the Kamelian SOA. (Set-up parameters include I_B = 200 mA, λ = 1550 nm, and TE polarisation).

The Kamelian SOA has a fast intraband gain recovery of at least 1 dB as shown in Figure 4-7 (b) (This will increase as the input pump power increases). This introduces a corresponding ultrafast phase recovery response, i.e. a blue chirp. Figure 4-11 shows some blue chirp on the trailing edge corresponding to the intraband gain recovery. When the magnitude of the chirp is greater on the trailing edge in comparison to the magnitude of the chirp on the leading edge of the pulse, the excess chirp corresponds to blue chirp. There was no blue chirp visible for the 8 ps pulses, thus confirming that as pulse widths reduce the contribution of intraband effects to shaping the intensity and chirp profiles increase.

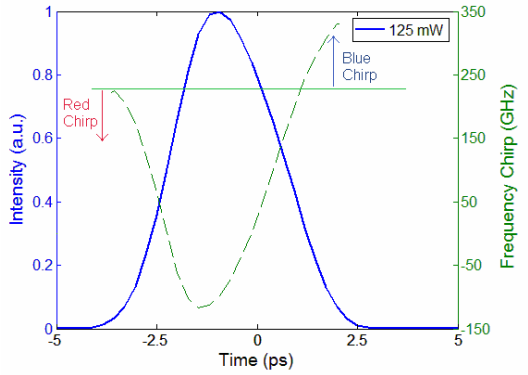

Figure 4-11 Diagram to show red and blue chirp of amplified pulse. (Set-up parameters: P_{in}= 125 mW, I_B = 200 mA, λ = 1550 nm, and TE polarisation).

An important finding from this characterisation is the large TPSR degradation associated with gain suppression. A detailed study has not been previously published [49]. Figure 4-12 shows the dramatic increase in pedestals on the pulse leading and trailing edges as the input power is increased. The pedestals on the input pulses to the SOA cannot be seen

as they are below the noise level of our measurement system. We estimate that they are 40 dB down from the peak of the pulse[i]. At the output of the SOA the pulse TPSR reduces from 40 dB to 22 dB. The leading pedestal in the unsaturated regime sees a 25 dB gain and partially saturates the gain available for the main pulse. The high intensity main pulse fully saturates the gain of the SOA and sees only 8 dB gain. Thus the resulting output TPSR is 23 dB between the peak of the leading pedestal and the peak of the main pulse. Upon the onset of the trailing edge pedestal (7.7 ps from peak of input pulse) the gain in the Kamelian SOA has recovered by a few decibels due to the ultrafast gain recovery dynamics of the SOA. Thus the trailing pedestal sees an approximate gain of 15 dB, reducing the TPSR to 35 dB on the trailing edge of the pulse. The large increase in these pedestals would clearly pose significant problems for the use of these pulses in high-speed OTDM systems as described in detail in Chapter 3 Section 5.2. In most cases the SOAs when used as amplifiers would not have such large input peak powers, however for all-optical processing SOAs are most generally used in saturation and these large pedestals could cause considerable detrimental effects to the processes pulses.

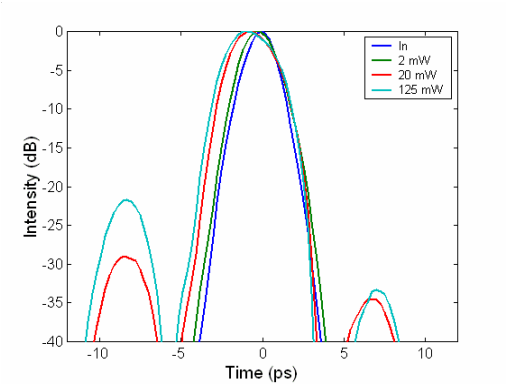

Figure 4-12 Input and output pulse profiles (log scale) as a function of input peak power (2, 20, 125 mW) to the Kamelian SOA to illustrate the large TPSR degradation introduced by SOA gain suppression.

4.6.4 Characterisation of Different SOAs as a Function of Input Peak Power

To compare the performance and effects of different SOAs, the same 1.5 ps mode-locked pulses were characterised following propagation in the CIP SOA. The operating conditions were the same as the Kamelian SOA, except the bias current to the CIP SOA was set to 300 mA. The output pulses and their corresponding chirp profiles are shown in Figure 4-13. The pulse width broadened from an input pulse width of 1.5 ps to 2.1 ps, 2.9 ps and 3.4 ps as the input power was increased and the magnitude in chirp increased from

[i] Pedestals can be formed in mode-locked lasers due to a small residual reflectivity as small as 10^{-5} from the antireflection coatings of the cavity. These pulses are separated by the round trip time of the diode cavity (7.7 ps).

100 GHz to 380 GHz (80 GHz greater than Kamelian SOA). No blue shift of the CIP SOA is visible in the output chirp for the high input power pulses. The magnitude of the ultrafast gain recovery is less in the CIP SOA in comparison to the Kamelian SOA, thus the corresponding blue chirp is not visible for these pulses. Due to the lower saturation power (P_{sat}) value of the CIP SOA the pedestals on the leading edge see a large gain, however the main pulse sees a much smaller gain and thus the TPSR is reduced to 12 dB. The trailing pedestals see negligible gain as the CIP SOA does not have a large ultrafast gain recovery component.

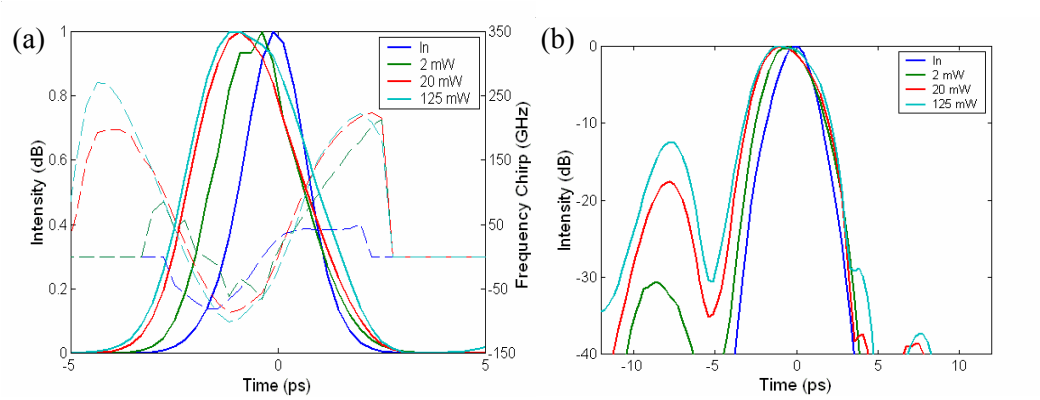

Figure 4-13 (a) Input and CIP SOA output pulse profiles and corresponding chirp and (b) logarithmic pulse profiles as a function of input peak power (2, 20, 125 mW). Other pulse parameters included I_B = 200 mA, λ = 1550 nm, and TE Polarisation.

Figure 4-14 shows the spectra of the input pulse and output pulses for different input peak powers of 2-125 mW for the Kamelian and CIP SOA respectively measured using an optical spectrum analyser (OSA). The overall red-shift of the signal following propagation through the SOAs is clearly visible. The oscillatory nature of the spectra is due to the interference effect common to nonlinear media, whereby the same value of instantaneous frequency existing at two points within the profile of the pulse can lead to constructive and destructive interference occurring causing a multi-peak structure [19].

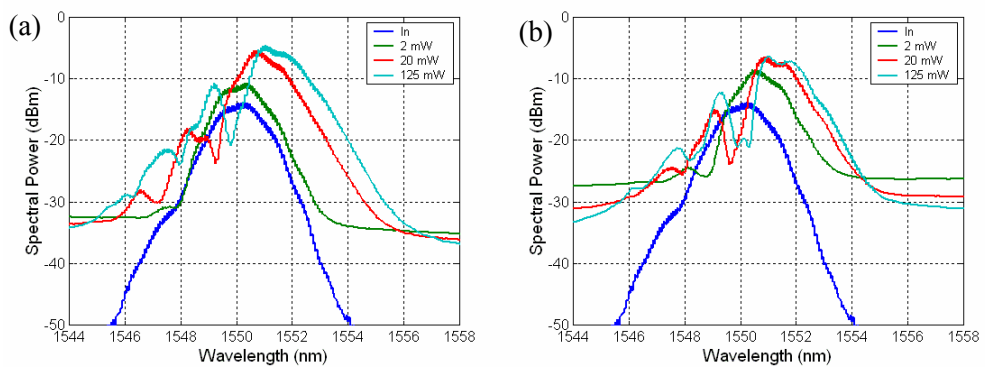

Figure 4-14 Input (125 mW) and output OSA spectra as a function of input peak power (2, 20, 125 mW) for (a) the Kamelian and (b) the CIP SOA.

The CIP SOA would most likely have superior performance to the Kamelian SOA when used as linear amplifier as its total gain recovery time is less than the Kamelian SOA, thus reducing patterning effects at higher bit rates. In contrast the Kamelian SOA has a larger intraband gain recovery and this would contribute to reducing a small portion of interband patterning [53]. We will look in more detail in the next chapter at the performance difference of these two SOAs used as all-optical wavelength converters.

4.6.5 Characterisation as a Function of Input TE and TM Polarisations

Following on from this the SOA amplified pulses were characterised as a function of TE and TM polarisation to examine the sensitivity of the SOAs to the different polarisations [54]. Figure 4-15 (a) shows the output pulse intensity and chirp for TE and TM polarisations for the Kamelian SOA with a small signal input of 2 mW. The wavelength is 1550 nm, the bias current is 200 mA. For a small signal input there is negligible polarisation dependence on the characteristics of the output pulses. In Figure 4-15 (b) and (c) a large input signal of 125 mW is injected into the SOA. Here the differences due to TE and TM polarisations are more visible. The chirp of the pulses aligned to TE polarisation is greater due to the larger gain available for TE polarisation, and thus the larger carrier density variation. Input pulses aligned to TM polarisation see less gain and have a lower P_{sat} in comparison to pulses aligned to the TE polarisation of the SOA. Thus effects of gain saturation are more visible on the pulses aligned to the TM polarisation of the SOA. Hence, the pulse leading edge is sharper with a longer trailing edge and the TPSR is less. The results show that the Kamelian SOA shows some polarisation dependence but it is not significant enough to have a large impact on the amplified pulses.

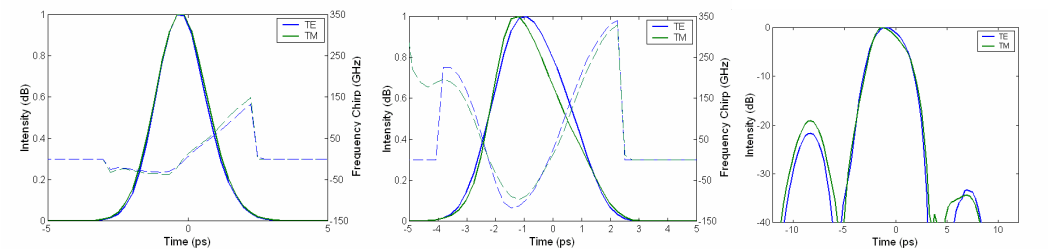

Figure 4-15 Comparison of how TE and TM polarisation signals affect the linear temporal and chirp profiles following propagation through the Kamelian SOA at input powers of (a) 2 mW (b) 125 mW and (c) the logarithmic temporal profile for the high input power of 125 mW.

4.6.6 Characterisation of Pulses following an SOA as a Function of Wavelength

To further characterise the effects on the pulses output from the SOA, the pulses were examined as a function of wavelength. The Kamelian SOA was investigated and the bias current was set at 200 mA, at an input peak power of 125 mW. The respective input pulse

widths for wavelengths of 1540 nm, 1550 nm, and 1560 nm are 1.3 ps, 1.5 ps, and 2.1 ps. The temporal and chirp characterisation of the pulses at 1540 nm, 1550 nm, and 1560 nm are displayed in Figure 4-16. As can be seen from the gain curve of the Kamelian SOA shown in Figure 4-6 the gain peak is situated at 1530 nm. As the wavelength of the input pulses move further from the gain peak of the SOA, the gain available for the input pulses is reduced. The output pulse widths are 2.1 ps, 2.9 ps, and 3.1 ps, indicating an approximate 50% increase in pulse width, showing that there is negligible dependence of the pulse-width increase on wavelength. The TPSR reduces as the input wavelength moves further from the gain peak of the SOA, as there is a corresponding increase in the effective carrier lifetime. The chirp profile does not show a large dependence on wavelength. The reduction in chirp at longer wavelengths is more likely due to the larger input pulse width rather than related to the wavelength dependence. A larger chirp is expected at longer wavelengths, because the differential gain is smaller which results in a larger alpha factor [32].

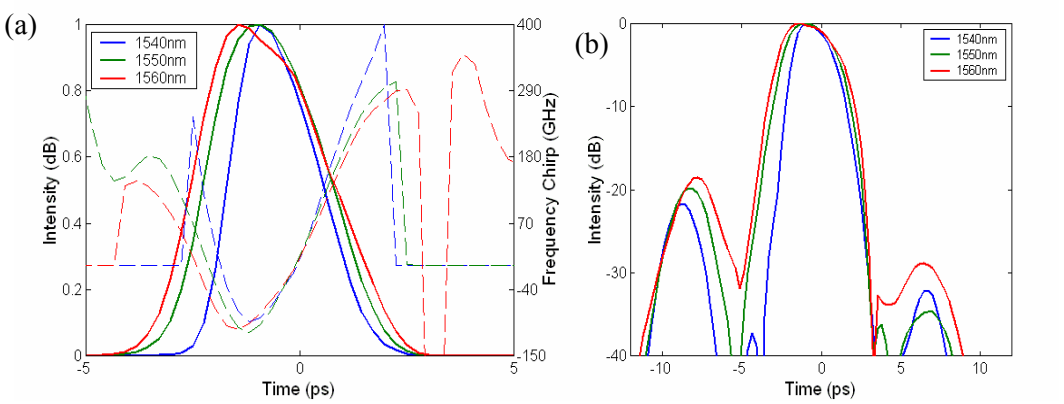

Figure 4-16 (a) Kamelian SOA output pulse profiles and corresponding chirp and (b) logarithmic pulse profiles as a function of different input wavelengths (1540 nm, 1550 nm, 1560 nm).

4.7 Summary

This chapter introduces SOAs and their basic device structure. A brief analysis was given to explain the different gain and phase dynamics that the SOA undergoes upon the input of a signal. When a pulse of high intensity is input to the SOA, carriers in the SOA are instantaneously reduced via stimulated emission. In addition, the carrier dynamics are affected by intraband effects such as SHB and CH. Sources of CH include stimulated emission, FCA and TPA (for high power input pulses). Inter and intraband effects introduce gain compression and a phase shift via the change in refractive index, inducing a large nonlinear chirp. Recovery following gain compression occurs over different

timescales. Intraband effects recover on a timescale of ~2 ps and generally the intrinsic gain recovery time of the SOA due to carrier injection is of the order of 10-100's ps.

Experimentally, this chapter characterised typical pulses used in Gb/s high-speed systems following propagation in an SOA. The intensity and corresponding phase of the amplified pulses were characterised by the FROG measurement scheme. Amplified pulses with input powers varying from 2 mW to 150 mW were analysed for input pulse widths of 2 ps and 8 ps. These results show that shorter pulses undergo a higher degree of gain saturation effects due to the larger contribution of intraband effects, and thus a partial fast gain recovery in comparison to the longer pulses. There is also a corresponding increase in chirp magnitude. An important result of these characterisations is the large deterioration in TPSR as the input peak power to the SOA is increased. As the wavelength of the input pulses moves further from the gain peak of the SOA the TPSR deteriorates due to lower power saturation levels. It was shown how the TPSR on the trailing edge of the pulse is dependent on the ultrafast gain recovery of the SOA. The different ultrafast gain recovery of each of the SOAs also affected the magnitude of blue chirp measured across the pulse. The generation of blue-chirped components agreed with the gain recovery measurements which show that the Kamelian SOA has a larger ultrafast component in comparison to the CIP SOA. The nonlinear shape of the chirp was confirmed as outlined by previous studies and the overall wavelength shift to longer wavelengths and the multi-peak structure of the spectrum was measured. The accurate characterisation of the effects of SOA amplification on picosecond pulses is vital for the design of high-speed systems that may employ SOAs as amplifiers and as optical processing elements. In an amplification system nonlinear chirp and gain saturation are detrimental to the performance of the system, however these characteristics are desirable when SOAs are used as an all-optical processor. The above detailed analysis of the picosecond pulses following propagation through an SOA, will aid in the optimisation and development a wavelength conversion scheme, which is introduced in the next chapter.

REFERENCES

[1] M.J. Connelly, "Semiconductor Optical Amplifiers," *Kluwer Academic Press,* Dordreacht, 2002.

[2] M.C. Farries, P.R. Morkel, R.I. Laming, T.A. Birls, D.N. Payne, and E.J. Tarbox, "Operation of Erbium-Doped Fiber Amplifiers and Lasers Pumped with Frequency-Doubled Nd:YAG Lasers," *J. Lightwave Technol.,* vol. 7, pp. 1473-1477, Oct. 1989.

[3] M.J. O'Mahony, "Semiconductor Optical Amplifiers for use in Future Fiber Systems," *J. Lightwave Technol.,* vol. 6, pp. 531-543, Apr. 1988.

[4] G. van den Hoven, "Alternative Amplifiers," *OSA Optical Fiber Commun. Conf. (OFC'04),* paper ThJ3, 2004.

[5] M.N. Islam, "Raman Amplifiers for Telecommunications," *J. Quantum Electron.*, vol. 8, pp. 548-559, May/June 2002.

[6] T. Saitoh, and T. Mukai, "Travelling-Wave Semiconductor Laser Amplifiers for Optical Communications Systems," *Global Telecommun. Conf.,(Globecom'90),* vol. 2, pp. 1274-1280, 1990.

[7] A. Yariv, "Quantum Electronics" *Wiley,* New York, 1989.

[8] B.A. Saleh, and M.C. Teich, "Fundamentals of Photonics," *Wiley,* New York, 1991.

[9] P.J.A. Thijs, L.F. Tiemeijer, P.I. Kuindersma, J.J. M. Binsma, and T. Van Dongen, "High-Performance 1.5 μm Wavelength InGaAs-InGaAsP Strained Quantum Well Lasers and Amplifiers," *IEEE J. Quantum Electron.,* vol. 27, pp. 1426-1439, 1991.

[10] D. Tauber, R. Nager, A. Livne, G. Eisenstein, U. Koren, and G. Raybon, "A Low-Noise-Figure 1.5 μm Multiple-Quantum-Well Optical Amplifier," *IEEE Photonics Technol. Lett.,* vol. 4, pp. 238-241, 1992.

[11] N. Holonyak, R.M. Kolbas, R.D. Dupuis, and P.D. Dapkus, "Quantum-Well Heterostructure Lasers," *IEEE J. Quantum Electron.,* vol. 16, pp. 170-186, 1980.

[12] D. Bimberg, and N. Ledentsov, "Quantum Dots: lasers and amplifiers," *J. Phys. Condens. Matter,* vol. 15, pp. R1063-R1076, 2003.

[13] Dept. of Chmeistry – Florida State University URL: http://www.chem.fsu.edu/editors/strouse/learning.html, "The Basics of Quantum Dots".

[14] Compound Semiconductor, URL: http://compoundsemiconductor.net/articles/news/9/3/6, "Quantum Dot Amplifier Restores 40Gb/s Signals".

[15] P. Borri, W. Langbein, J.M. Hvam, F. Heinrichsdorff, M.-H. Mao, and D. Bimberg, "Spectral Hole-Burning and Carrier-Heating Dynamics in InGaAs Quantum-Dot Amplifiers," *J. Sel. Top. Quantum Electron.*, vol. 6, pp. 544-551, May/June 2000.

[16] T. Akiyama, H. Kuwatsuka, T. Simoyama, Y. Nakata, K. Mukai, M. Sugawara, O. Wada, and H. Ishikawa, "Nonlinear Gain Dynamics in Quantum-Dot Optical Amplifiers and Its Application to Optical Communications Devices," *IEEE J. Quantum Electron.,* vol. 37, pp. 1059-1065, 2001.

[17] H. Ghafouri-Shiraz, "The Principles of Semiconductor Laser Diodes and Amplifiers – Analysis and Transmission Line Laser Modeling," *Imperial College Press,* London, 2004.

[18] J. Mork, M.L. Nielsen, and T.W. Berg, "The Dynamics of Semiconductor Optical Amplifiers, Modelling and Applications," *Optics and Photonics News,* pp. 42-48, July 2003.

[19] G.P. Agrawal, and N.A. Olsson, "Self-Phase Modulation and Spectral Broadening of Optical Pulses in Semiconductor Laser Amplifiers," *J. Quantum Electron.*, vol. 25, pp. 2297-2306, Nov. 1989.

[20] B.N. Gomatam, and A.P. DeFonzo, "Theory of Hot Carrier Effects on Nonlinear Gain in GaAs-GaAlAs Lasers and Amplifiers," *J. Quantum Electron.*, vol. 26, pp. 1689-1703, Oct. 1990.

[21] K.L. Hall, J. Mark, E.P. Ippen, and G. Eisenstein, "Femtosecond Gain Dynamics in InGaAsP Optical Amplifiers," *Appl. Phys. Lett.,* vol. 56, pp. 1740-1742, 1990.

[22] M. Willatzen, A. Uskov, J. Mork, H. Olesen, B. Tromborg, and A.-P. Jauho, "Nonlinear Gain Suppression in Semiconductor Lasers due to Carrier Heating," *IEEE Photonics Technol. Lett.*, vol. 3, pp. 606-609, July 1991.

[23] M.S. Stix, M.P. Keslar, and E.P. Ippen, "Observations of Subpicosecond Dynamics in GaAlAs Laser Diodes," *Appl. Phys. Lett.,* vol. 48 pp. 1722-1724, June 1986.

[24] J. Mork, and J. Mark, "Carrier Heating in InGaAsP Laser Amplifiers due to Two Photon Absorption," *Appl. Phys. Lett.* vol. 64, pp. 2206-2208, Apr. 1994.

[25] B.C. Thomsen, L.P. Barry, J.M. Dudley, and J.D. Harvey, "Ultrahigh Speed All-Optical Demultiplexing on Two-Photon Absorption in a Laser Diode," *IEE Electron. Lett.*, vol. 34, pp. 1871-1872, Sep. 1998.

[26] R.J. Manning, D.A.O. Davies, and J.K. Lucek, "Recovery Rates in Semiconductor Laser Amplifiers: Optical and Electrical Bias Dependencies," *IEE Electron. Lett.*, vol. 30, pp. 1233-1234, July 1994.

[27] F. Girardin, G. Guekos, and H. Houbavlis, "Gain Recovery in Bulk Semiconductor Optical Amplifiers," *IEEE Photonics Technol. Lett.,* vol. 10, pp. 784-786, June 1998.

[28] C.H. Henry, "Theory of the Linewidth of Semiconductor Lasers," *J. Quantum Electron.*, vol. 18, pp. 259-264, Feb 1982.

[29] A. Dienes, J.P. Heritage, M.Y. Hong, and Y.H. Chang, "Time- and Spectral-Domain Evolution of Subpicosecond Pulses in Semiconductor Optical Amplifiers," *Optics Lett.* vol. 17, pp. 1602-1604, Nov. 1992.

[30] C.T. Hultgren, and E.P. Ippen, "Ultrafast Refractive Index Dynamics in AlGaAs Diode Laser Amplifiers," *Appl. Phys. Lett.* vol. 59, pp. 635-637, Aug. 1991.

[31] P.J. Delfytt, Y. Silberberg, and G.A. Alphonse, "Hot-Carrier Thermalization Induced Self-Phase Modulation in Semiconductor Travelling Wave Amplifiers," *Appl. Phys. Lett.,* vol. 59, pp. 10-12, 1991.

[32] N. Storkfelt, B. Mikkelsen, D.S. Olesen, M. Yamaguchi, and K.E Stubkjaer, "Measurement of Carrier Lifetime and Linewidth Enhancement Factor for 1.5-μm Ridge-Waveguide Laser Amplifier," *IEEE Photonics Technol. Lett.,* vol. 3, pp. 632-634, Jul. 1991.

[33] R. Giller, R.J. Manning, and D. Cotter, "Gain and Phase Recovery of Optically Excited Semiconductor Optical Amplifiers," *IEEE Photonics Technol. Lett.*, vol. 18, pp. 1061-1063, May 2006.

[34] A. Poustie, "Semiconductor Devices for All-Optical Signal Processing," *European Conf. Optical Commun. (ECOC'05),* paper We 3.5.1, 2005.

[35] R. Giller, and R.J. Manning, "Recovery Dynamics of Optically Excited Semiconductor Optical Amplifiers," *OSA Optical Fiber Commun. Conf. (OFC'06),* paper OWI74, 2006.

[36] A. Uskov, J. Mork, and J. Mark, "Theory of Short-Pulse Gain Saturation in Semiconductor Laser Amplifiers," *IEEE Photonics Technol. Lett.*, vol. 4, pp. 443-446, May 1992.

[37] P. Borri, S. Scaffetti, J. Mork, W. Langbein, J.M. Hvam, A. Mecozzi, and F. Martelli, "Measurement and Calculation of the Critical Pulsewidth for Gain Saturation in Semiconductor Optical Amplifiers," *Optics Comms.* vol. 164, pp. 51-55, June 1999.

[38] M.Y. Hong, Y.H. Chang, A. Dienes, J.P. Heritage, P.J. Delfyett, S. Dijaili, and F.G. Patterson, "Femtosecond and Self- and Cross-Phase Modulation in Semiconductor Laser Amplifiers," *J. Sel Top Quantum Electron.*, vol. 2, pp. 523-539, Sep. 1996.

[39] Y. Lai, K.L. Hall, E.P. Ippen, and G. Eisenstein, "Short Pulse Gain Saturation in InGaAsP Diode Laser Amplifiers," *IEEE Photonics Technol. Lett.*, vol. 2, pp. 711-713, Oct. 1990.

[40] T. Saitoh, T. Mukai, "Gain Saturation Characteristics of Travelling-Wave Semiconductor Laser Amplifiers in Short Optical Pulse Amplification," *J. Quantum Electron.,* vol. 26, pp. 2086-2094, Dec. 1990.

[41] H. Kawaguchi, and Y. Ito, "Precise Measurement of Nonlinear Propagation Characteristic of Sub-Picosecond Optical Pulses in SOAs," *Conf. Lasers and Electro-Optics Europe (CLEO Europe'00),* paper CTuP6, 2000.

[42] J.H. Kim, K.-R. Oh, K.-M. Cho, "Spectral Characteristics of Optical Pulse Amplification with a Holding Light in Semiconductor Optical Amplifiers," *Optics Commun.,* vol. 170, pp. 99-109, Oct. 1999.

[43] J.M. Dailey, and T.L. Koch, "Impact of Carrier Heating on SOA Dynamics for Wavelength Conversion," *IEEE Lasers and Electro-Optics Society 19th Annual Meeting (LEOS),* paper MP4, 2006.

[44] I. Kang, and C. Dorrer, "Measurements of Gain and Phase Dynamics of a Semiconductor Optical Amplifier using Spectrograms," *OSA Optical Fiber Commun. Conf. (OFC'04)*, paper MF43, 2004.

[45] P.J. Delfyett, H. Shi, S. Gee, I. Nitta, J.C. Connolly, and G.A. Alphonse, "Joint Time-Frequency Measurements of Mode-locked Semiconductor Diode Lasers and Dynamics using Frequency-Resolved Optical Gating," *IEEE J. Quantum Electron.,* vol. 35, pp. 487-500, 1999.

[46] K. Sutkus, K. Shum, R.R. Alfano, and P.J. Delfyett, "Effect of Carrier Heating on the Wavelength Chirp of Ultrashort Laser Pulses in Semiconductor Optical Amplifiers," *IEEE Photonics Technol. Lett.,* vol. 6, pp. 372-374, 1994.

[47] F. Romstad, P. Borri, W. Langbein, J. Mork, and J.M. Hvam, "Measurement of Pulse Amplitude and Phase Distortion in a Semiconductor Optical Amplifier," *IEEE Photonics Technol. Lett.,* vol. 12, pp. 1674-1676, 2000.

[48] S. Hughes, P. Borri, A. Knorr, F. Romstad, and J.M. Hvam, "Ultrashort Pulse-Propagation Effects in a Semiconductor Optical Amplifier: Microscopic Theory and Experiment," *J. Sel. Top. Quantum Electron.*, vol. 7, pp. 694-702, Jul/Aug. 2001.

[49] A.M. Clarke, M.J. Connelly, P. Anandarajah, L.P. Barry, D. Reid, "Investigation of Pulse Pedestal and Dynamic Chirp Formation on Picosecond Pulses after Propagation Through an SOA," *IEEE Photonics Technol. Lett.,* vol. 17, pp. 1800-1802, 2005.

[50] M.J. Connelly, "Wideband Steady-State Numerical Model and Parameter Extraction of a Tensile-Strained Bulk Semiconductor Optical Amplifier," *IEEE J. Quantum Electron.,* to be published.

[51] J.M. Tang, and K.A. Shore, "Amplification of Strong Picosecond Optical Pulses in Semiconductor Optical Amplifiers," *IEE Proc.-Optoelectron.*, vol. 146, pp. 45-50, 1999.

[52] M.Y. Hong, Y.H. Chang, A. Dienes, J.P. Heritage, and P.J. Delfyett, "Subpicosecond Pulse Amplification in Semiconductor Laser Amplifiers: Theory and Experiment," *IEEE J. Quantum Electron.,* vol. 25, pp. 2297-2306, 1989.

[53] M.L. Nielsen, J, Mork, R. Suzuki, J. Sakaguchi, and Y. Ueno, "Experimental and Theoretical Investigation of the Impact of Ultra-fast Carrier Dynamics on High-speed SOA-based All-optical Switches," *OSA Optics Express,* vol. 14, pp. 331-347, Jan. 2006.

[54] B. Kennedy "A study of the Origin and Applications of Nonlinear Polarization Rotation in Semiconductor Optical Amplifiers," *PhD Thesis,* pp. 136-146, Dublin City University, Mar. 2007.

CHAPTER 5 – ALL-OPTICAL WAVELENGTH CONVERSION USING SEMICONDUCTOR OPTICAL AMPLIFIERS

5.1 Introduction

In order to implement high-speed networks and to make full use of the bandwidth potential of optical fibre, networks must be fully transparent. Thus to realise these transparent optical networks it is imperative to develop photonic devices that can undertake basic processing at ultrahigh data rates. One specific processing element that is of particular importance is a wavelength converter, as it is required to avoid wavelength conflict at nodes and generally to render wavelength division multiplexed (WDM) systems more flexible [1]. Although optical transmission is a mature technology, optical switching functionalities are not. Presently, optical switching platforms are primarily based on optical-electronic-optical (OEO) approaches, limiting processing speeds to maximum line rates of 40 Gb/s. The COST 290 report [2] strongly advises that investment should continue in the area of wavelength conversion (and other all-optical processing techniques) because of the various advantages (e.g. transparency) that it brings. In the long term, increases in individual line rates will demand processing speeds approaching terabits per second, but for the short term, the next step is likely to be 160 Gb/s for each individual line rate. In particular, wavelength conversion has the potential to increase the capacity of WDM networks by using dynamic provisioning (by assigning dynamic channels between links). This allows for network management by a link-to-link process thus network requirements become more relaxed. For example if there is a link or node failure a local reconfiguration can be carried out rather than implementing a global reconfiguration, thus creating a more cost-efficient WDM network [3].

An ideal candidate for the functional application of wavelength conversion is the semiconductor optical amplifier (SOA) [1,4-7]. It is a highly nonlinear device, with a refractive index dependence related to the gain saturation of the SOA itself as was discussed in the previous chapter. The wide gain bandwidth of the SOA provides a large span to realise wavelength conversion and the tens of picoseconds carrier lifetime provides the speed necessary for gigabit per second bit-rate conversion. SOA nonlinearities which can be used for wavelength conversion include cross gain modulation (XGM), cross phase modulation (XPM) and four wave mixing (FWM) [4,5].

By operating the SOA under these nonlinear settings, the SOA can be used in applications in addition to wavelength conversion, which include clock recovery [8,9], time-domain demultiplexing [10-12], and 3R (reamplify, reshape, and retime) regeneration [13-15]. To date wavelength conversion implemented using SOAs can perform at data rates of 160 Gb/s [16-18] and 320 Gb/s [19]. To enhance the switching speeds further for processing of femtosecond pulses ultrafast carrier dynamics such as carrier heating (CH), spectral hole burning (SHB), free carrier absorption (FCA) and two photon absorption (TPA) can be exploited [20,21]. The very short gain recovery time for these processes provides the potential for terabit per second wavelength conversion.

This chapter provides an overview of the different techniques available to implement wavelength conversion. From this overview it will be clear why SOA-based switches are ideal candidates for future all-optical network wavelength converters. An explanation of the nonlinearities which occur in an SOA which can provide wavelength conversion via XGM, XPM and FWM is given. In particular we examine a popular wavelength conversion scheme, which uses shifted filtering in conjunction with XPM in an SOA to overcome the interband patterning effects of the SOA. The placement of the filter to the red or blue-wavelength side of the converted signal is analysed using the bit error rate (BER) measurements and frequency-resolved optical gating (FROG) characterisation. The main contribution of this work is the achievement of an 80 Gb/s error-free wavelength conversion scheme using XPM and blue-shifted filtering (BSF). This scheme provides many advantages in that it is a very simple technique, it is polarisation insensitive, and it preserves the polarity of the input signal. This chapter also provides an in-depth analysis of the converted pulse shape and output chirp which to date has not yet been carried out. This aids in the understanding of the SOA gain and phase dynamics effects and also the effects of the filtering on this type of wavelength conversion scheme.

5.2 All-Optical Wavelength Conversion Overview

There are a wide range of schemes which enable wavelength conversion which are now briefly examined. To ensure negligible performance penalty in a system and to provide large dynamic functionality, all-optical wavelength converters must meet the following parameters so that they can be implemented in real high-speed network [4]:

- gigahertz switching speeds (>40 GHz)
- bit-rate transparency
- high extinction ratio (ER)
- large signal-to-noise ratio (SNR) at output (to ensure cascadability)
- moderate input power levels (~0 dBm)

- high conversion efficiency (CE)
- large wavelength span for both input and output signals
- possibility for same input and output wavelength (i.e. no conversion)
- low chirp
- insensitivity to input signal polarisation and
- simple implementation.

5.2.1 Fibre-Based All-Optical Wavelength Conversion Schemes

Fibre-based switches have an inherent potential to provide terahertz processing speeds due to the nearly instantaneous nonlinearities that occur on a timescale in the order of a few femtoseconds. However, due to the very small nonlinear coefficient of silica fibre, very large input powers and long lengths of fibre are required. This can introduce instabilities in these systems. Thus, all-optical fibre-based switches are not commercially viable devices. For example, 1 W peak power is typically required for a 1 km long fibre to operate as an efficiently controlled optical switch [22].

All-optical switching can be performed by fibre-based switches by exploiting nonlinearities such as the Kerr effect, FWM and XPM. These switches may use polarisation, the newly generated wavelength and/or the induced π phase shift as the discriminating factor [23]. The latter two methods have demonstrated wavelength conversion at 160 Gb/s [24] and 640 Gb/s [25]. Generally these nonlinearities are exploited through the use of interferometric set-ups. For fibre-based systems typical Mach-Zehnder interferometer (MZI) configurations are highly susceptible to instabilities due to arm length mismatching. This can be overcome by joining the two arms of the coupler to form a nonlinear optical loop mirror (NOLM) [22,26], or by passing both signals through the same fibre for example a Symmetric MZI (SMZI).

5.2.2 Difference-Frequency Generation Wavelength Conversion

Wavelength conversion can be carried out using difference-frequency generation (DFG). DFG is a consequence of a nonlinear interaction of a material with two optical waves: a pump wave and a signal wave [1]. DFG has been demonstrated in $LiNbO_3$ and AlGaAs waveguides [27,28]. In passive waveguides it is anticipated that DFG can offer transparent wavelength conversion with quantum noise limited operation. It is also capable of chirp reversal and multi-wavelength conversions with extremely low cross-talk [28]. The CE remains low, but research in fabrication techniques continues to improve phase-matching of the waveguide materials.

5.2.3 Other All-Optical Wavelength Conversion Techniques

Wavelength conversion can also be achieved by using single-mode semiconductor lasers [29]. This can typically be achieved by using a distributed Bragg reflector (DBR) laser [30], which has a saturable absorber (SA) region. When no input light is injected into the cavity the SA absorbs the light from the laser. Upon the injection of light into the cavity the absorption loss decreases so that the wavelength converted light is emitted. The response speed of the device is limited to the response of the SA. Alternatively, wavelength conversion can be achieved using single-mode semiconductor lasers below threshold [31]. The lasing mode at one wavelength can be modulated by injecting an intensity-modulated light signal at a different wavelength. The response of this wavelength conversion scheme is dependent on the bandwidth of the laser [32]. Additionally, all-optical wavelength conversion devices can be implemented using optical micro-electro-mechanical systems (MEMS)-based switches, thermal optical switches, additional electro-optical switches (rather than the SOA), and acoustic-optic switches. A full review and comparison is given in Ref. [33]. However to enable future bit-level time division multiplexing applications, switching speeds on the order of a few picoseconds will be required. Thus to date SOA-based switches and fibre-based switches are so far the only technologies that can operate at these picosecond switching speeds, and the SOA-based switches are most efficient due to their low switching energy requirements and their small footprint.

5.3 SOA Wavelength Conversion

5.3.1 Hybrid Fibre and SOA-Based Wavelength Conversion

In order to overcome the bulky footprint, large input powers, and instability of the fibre-based designs some research has moved towards implementing hybrid fibre and SOA-based techniques. In this hybrid set-up the SOA provides a large nonlinearity, thus only a small input signal power is required and the overall footprint of the switch is reduced. However the elimination of the inherent terahertz switching capability of the fibre is a drawback, as the switching speed is now determined by the longer carrier recovery time of the SOA. The switches mentioned in the previous section can be implemented using an SOA as the nonlinear element. An SOA in a NOLM set-up, known as a semiconductor laser amplifier in a loop mirror (SLALOM) [34], has shown operation up to 40 GHz [35] and an SOA-based SMZI has exhibited 160 Gb/s performance [17].

5.3.2 Monolithically Integrated Waveguide Devices

Although the above mentioned hybrid fibre and SOA-based devices display many benefits, they still exhibit some of the disadvantages of the complete fibre switches. Their footprint remains quite large and they are difficult to mass produce. Therefore the direction of commercial application development is to integrate active and passive waveguides [36]. SOAs are ideal devices to incorporate monolithically on a single integrated chip [37]. The nonlinearities which are exploited in order to achieve wavelength conversion are now discussed.

5.3.3 Cross Gain Modulation

Cross gain modulation (XGM) requires inputting a high power signal (pump) coupled with a continuous wave (CW) signal (probe) into the SOA [38-40] as illustrated in Figure 5-1 (a). The pump signal modulates the gain of the SOA. The probe signal at the desired output wavelength is then modulated by the gain variation of the SOA [4,41]. Thus a signal which is an inverted replica of the pump is output from the SOA at a new wavelength as shown in Figure 5-1 (b) and (c). The filter following the SOA is centred at the wavelength of the probe to remove the input pump signal.

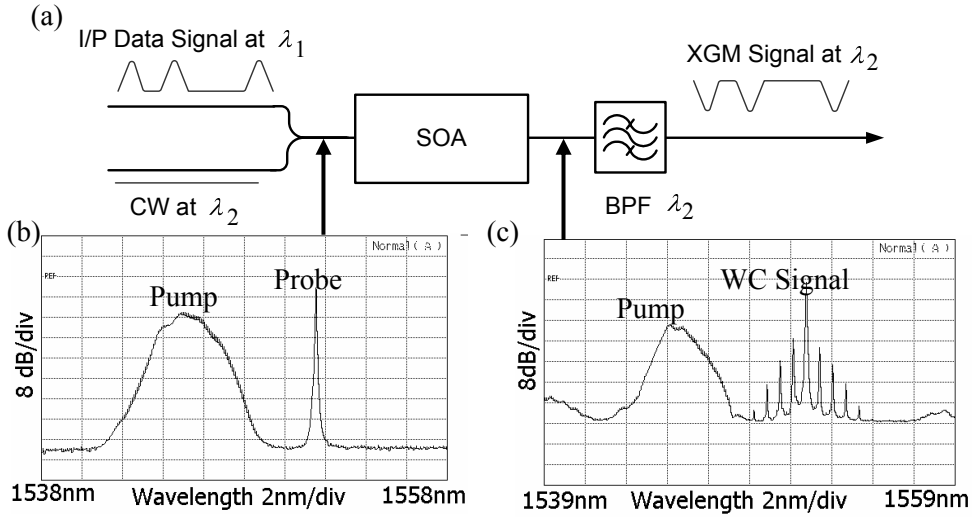

Figure 5-1 (a) An illustration of simple XGM in an SOA, (b) the pump and probe spectra at the input to the SOA and (c) the pump and modulated probe spectra following XGM in an SOA.

The use of a filter can be avoided by implementing the scheme in counter-propagation, i.e. when the probe signal is input in the opposite direction to the pump signal. A circulator will then be required to further transmit the signal. This technique becomes problematic as pulses get shorter as the transit time of the pulse through the SOA must be less than the pulse width, which will require very short waveguides [7]. In counter

propagation schemes the wavelength-conversion response is therefore limited to the input-pulse's transit time through the SOA (e.g. 4 ps for 400 μm long SOA).

The technique of XGM in an SOA is desirable for the implementation of wavelength conversion due to its very simple configuration, polarisation insensitivity, and relatively low input powers. However, the disadvantages of this technique are that the converted signal is inverted with respect to the input, it has a relatively large chirp, and the ER can be significantly degraded when the signal is up converted to a higher wavelength. Simple XGM is limited by the interband gain recovery time of SOAs. Typical SOAs which are presently available and which were discussed in the previous chapter have gain recovery times ranging from 30-55 ps. For 20 Gb/s and 40 Gb/s systems the period is 50 and 25 ps respectively. Therefore XGM in these SOAs is limited to 40 Gb/s, as increased bit rates would lead to patterning effects and closure of the eye.

5.3.4 Cross Phase Modulation

In addition to the modulation of the SOA gain, the phase of the probe signal is also modulated upon the input of an optical signal and this is known as cross phase modulation (XPM). As was explained in Chapter 4 Section 4.5.4, the refractive index of an SOA is dependent on the amplifier gain and thus there is a gain-phase coupling via the alpha factors. This phase modulation causes a shift of the probe signal first to longer wavelengths (red shift) and then to shorter wavelengths (blue shift). Wavelength conversion employing XPM is a method that improves the shortcomings of XGM in that it generates a converted signal with a small chirp (due to the reduced gain modulation) and can be up-converted or down-converted without degradation of the ER [42-44]. This phase modulation can be converted to an intensity modulation by using interferometers or shifted filtering for further propagation of the signal. XPM in conjunction with shifted filtering is the technique chosen in this chapter to provide high bit rate wavelength conversion.

5.3.5 Four Wave Mixing

Four wave mixing (FWM) in an SOA is an attractive mechanism for wavelength conversion in WDM systems since it provides modulation format and bit rate transparency over wide tuning ranges [45,46]. FWM is an inherently fast process in comparison to XGM and XPM and in addition many wavelength channels can be handled simultaneously. A schematic of a typical FWM set-up is shown in Figure 5-2. An input data signal (probe) at a frequency of ω_0-Ω and a CW pump at a frequency of ω_0 are coupled in the SOA. To achieve optimum efficiency the pump and probe are required

to be at the same polarisation. The input probe signal is a much weaker signal in comparison to the strong CW pump. Inside the SOA, the two electric fields cause the amplifier gain to be modulated at the beat frequency, Ω. The generated signal is the phase conjugate replica as the original input signal. This is shown in the spectrum of Figure 5-2 (a) where the conjugate is a shifted spectrally inverted replica of the input data signal.

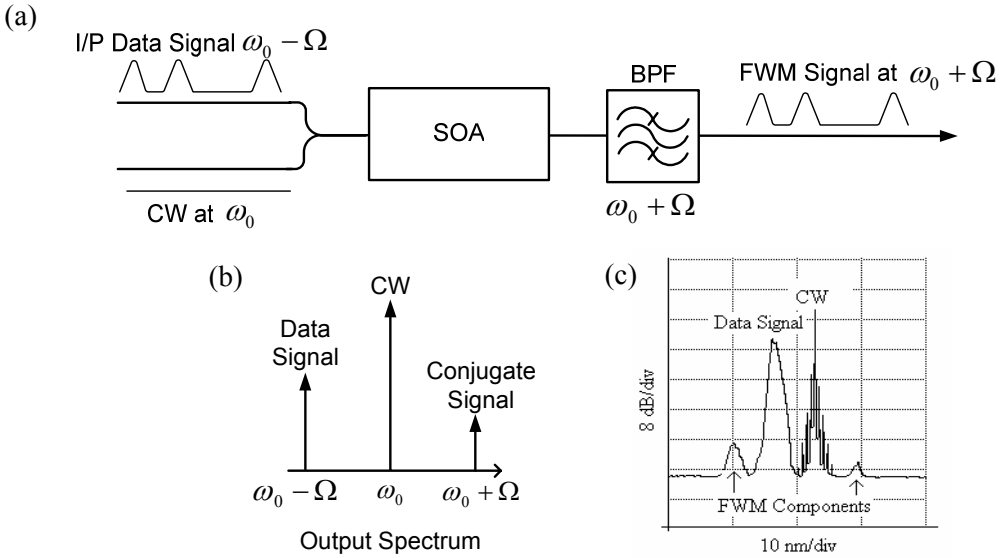

Figure 5-2 (a) Wavelength conversion using FWM in an SOA, (b) the new FWM frequency generated signals at the output of the SOA, and (c) an example of FWM components measured on an OSA.

FWM in an SOA is a third order nonlinear effect, thus the carrier density modulation and nonlinear gain effects in the SOA contribute to the generation of FWM. The gain of the SOA is modulated at the beat frequency between the pump and the probe signals. Therefore as the detuning is increased the gain of the SOA is modulated at increasingly smaller timeframes. At low Ω i.e. small detunings**,** the dominant mechanism is the modulation of the carrier density. This implies that this particular mechanism will only manifest itself for detuning frequencies of the order of gigahertz. With increasing detunings CH and then SHB become the dominant mechanism respectively as they relate to smaller gain recovery time frames. FWM is one method used to measure the contribution of each of the gain processes as a function of time as they each occur on a separate timescale as a function of frequency detuning, Ω [47].

The major disadvantage of FWM is the input to output signal efficiency decreases with the bandwidth separation of the pump and the input signal. Consequently, it is difficult to retain a large SNR for the converted signal at $\omega_0+\Omega$, and thus to cascade more converters. Although the resultant CE and SNR have been considered a weakness of

FWM, acceptable efficiency has been demonstrated using two amplifiers in cascade [48]. Another consideration is that the output signal wavelength depends on both the pump and the input signal wavelengths, so the pump must be tunable even for converters with fixed output wavelength. In addition FWM is polarisation sensitive. To remove its polarisation sensitivity an extra pump signal is required [49,50].

5.4 The Effects of Various SOA Operating Parameters on XGM/XPM Wavelength Converted Pulses

For optimised wavelength conversion, the SOA must have a reduced effective carrier lifetime to avoid patterning, and the output pulses must have a high ER and a large CE. The carrier recovery time expresses the speed with which the SOA carrier number recovers to its steady state value after removal of the switching light. An SOA has an intrinsic carrier lifetime which is on the order of a few hundred picoseconds but it can have a shorter effective carrier lifetime by increasing the stimulated emission contribution. This can be achieved by improving the waveguide confinement factor, increasing the number of photons into the active layer, and by enhancing the differential gain [51]. Maximising the SOA bias current optimises the stimulated recombination factor [52] and placing the pump signal to a wavelength shorter than the wavelength of the gain peak of the SOA, increases the differential gain. A high power probe signal or the addition of a CW assist light adds to the number of photons in the active region [53]. Figure 5-3 shows the improvement of the effective gain recovery as a function of increasing input probe power. As the probe power is increased (-12.8 dBm, -5.8 dBm, 1.2 dBm) the gain recovery time of the Kamelian (68.1 ps, 63.6ps, 54.25 ps) and CIP SOAs (58.15 ps, 49.24 ps, 37.70 ps) respectively decrease. The probe signal rapidly replenishes the carrier density after the propagation of a pulse through the SOA and reduces the gain saturation output power.

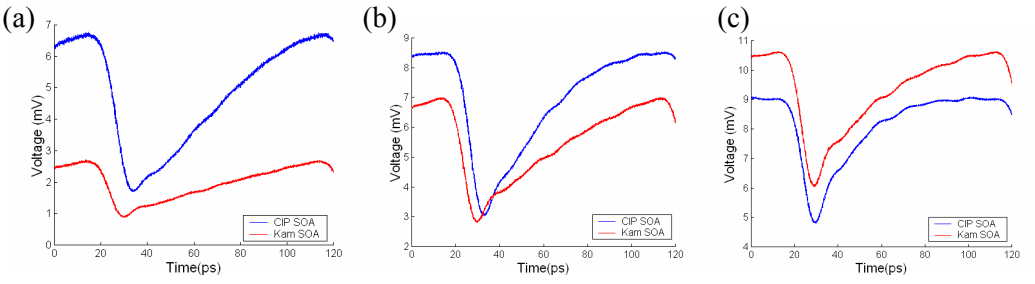

Figure 5-3 Comparison of gain recovery for the Kamelian and CIP SOAs as a function of input probe power of (a) -12.8 dBm, (b) -5.8 dBm, and (c) 1.2 dBm.

The extinction ratio (ER) is the ratio of power in the optical signal when there is a '1' to the power in the optical signal when there is a '0'. An important feature for wavelength

conversion is equal performance for the up and down-converted signals. In XGM, the ER increases as the CW wavelength decreases with respect to the gain peak, and when the pump is situated at the gain peak. Thus down-conversion (translation from long wavelengths to short wavelengths) results in an output signal with high ER. On the other hand, up-conversion gives rise to a poorer performance. The change in ER is due to the variation of the differential gain with respect to the CW and signal wavelengths [4]. As the gain is saturated, the gain peak of the amplifier shifts to longer wavelengths, resulting in a higher slope on the shorter wavelength side of the gain peak. Therefore, the probe channels at the shorter wavelengths will experience larger gain variations. This effect is enhanced by increasing the wavelength separation between the input pump and probe [54]. The ER can also be improved by increasing the input signal power, as further saturation of the SOA induces a larger gain modulation of the CW probe signal.

The conversion efficiency (CE) is the ratio of the input optical signal to the output optical signal measured at the input and output device facets respectively by the optical spectrum analyser (OSA). Maximum CE is obtained when both pump and probe are close to the gain peak of the SOA and when they are reasonably close to each other. A low CE results in the output signal requiring further amplification and thus a reduction in optical signal-to-noise (OSNR) due to addition of amplified spontaneous emission (ASE) to the signal. Thus there is a trade-off between optimum ER and highest achievable CE. The CE can be improved by increasing the length of the SOA or by reducing the input pump average power [55]. Reducing the average pump power is the better option so that a sufficient ER can be maintained.

5.5 Wavelength Conversion in Conjunction with Shifted Filtering

One of the most detrimental aspects in employing SOAs as wavelength converters is the patterning effects associated with the SOA carrier recovery time which limits the overall bit rate achievable. It has been shown that simple XGM/XPM in an SOA in conjunction with shifted filtering can overcome this carrier recovery limitation [56-58]. Depending on the offset of the shifted filter XGM or XPM is the primary nonlinearity being exploited. Ellis et al. were the first to demonstrate high bit rate operation using the XGM and shifted filtering technique at 100 Gb/s [59]. Similarly Liu et al. have improved on this performance and have shown error-free wavelength conversion up to 320 Gb/s [19,60]. Alternatively Nielsen et al. have achieved error-free operation at 40 Gb/s primarily exploiting XPM by extending the offset of the shifted filter [61]. Although the bit rates achievable for XPM and shifted filtering are limited in comparison to the schemes that utilise XGM, this scheme offers many advantages which include preserving

the polarity of the wavelength converted signal, a higher ER, and the elimination of a complicated interferometric configuration (used to invert the XGM wavelength converted signal). In this chapter an experiment is presented, which builds on the work of Nielsen et al. [61] and achieves 80 Gb/s error-free performance using XPM in an SOA in conjunction with shifted filtering. B2B BER measurements are taken for a variety of filter offsets and two different SOAs are compared to establish the impact of their different gain recoveries on the wavelength conversion performance.

Due to the popularity of this technique many studies have been carried out to achieve further understanding and improved results. Leuthold et al. proposed a pulse reformatting optical filter (PROF), which was designed to keep both the red and blue-chirped components of the wavelength converted signal enabling 40 Gb/s error-free performance [62]. The impact of ultrafast carrier dynamics for XGM and XPM shifted filtering schemes is analysed experimentally and theoretically by Nielsen et al. [21]. This work is further enhanced by the FROG characterisation carried out for different filter spectral offsets. The analysis reveals important results as the FROG characterisation shows the contribution of the different carrier dynamics of the SOA and the filter have on influencing the shape and chirp of the wavelength converted pulses.

5.5.1 Principle of Shifted Filtering in Conjunction with XGM/XPM

An optical signal input to an SOA results in both gain and phase changes of the SOA related via Kramers-Kroning equations. In the case of XGM and XPM the gain and phase changes modulate the probe signal respectively. An illustrative example of the gain and chirp SOA dynamics following propagation of a ~2 ps pulse is illustrated in Figure 5-4. The probe signal undergoes a positive phase shift corresponding to the generation of red-chirped components as a consequence of gain depletion and has a time frame corresponding to the input pulse width. The SOA gain then begins to recover resulting in a negative phase shift and the generation of blue-chirped components. The gain and phase recovery occurs in accordance to different recovery processes, SHB (~100 fs), CH (~ 2 ps) and interband carrier recovery (~55 ps).

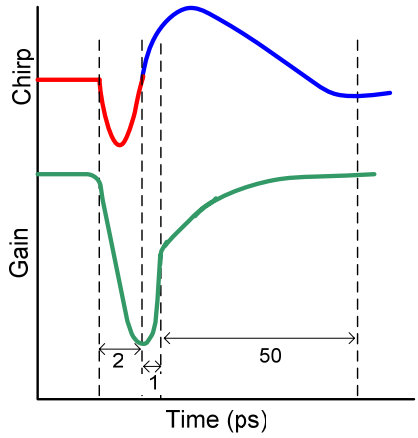

Figure 5-4 An illustrative example of the gain and corresponding chirp dynamics in an SOA upon the input of a short picosecond pulse.

The principle of red-shifted filtering (RSF) and blue-shifted filtering (BSF) is illustrated in Figure 5-5 (a) and (b) respectively. By placing a filter to retain only the red chirp (or longer wavelength components) of the probe signal, is known as RSF, and correspondingly if a filter is placed to keep only the blue-shifted spectral probe components, it is called BSF. The high bit-rate performance of the BSF scheme is due to the large blue chirp generated by ultrafast carrier effects and thus short picosecond pump pulses are required to achieve optimum performance [63].

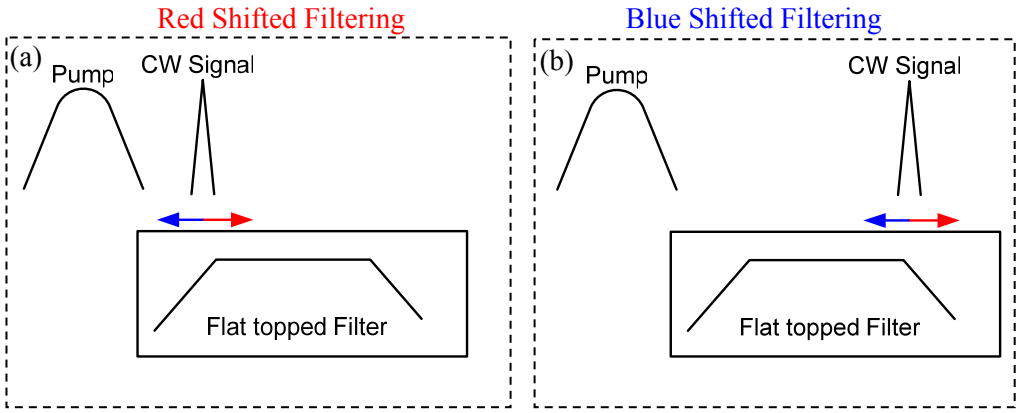

Figure 5-5 Schematic illustrating the principle of (a) red and (b) blue-shifted filtering.

If the filter is shifted such that the original CW potion of the probe and either the red/blue shifted components are kept this process primarily exploits XGM. The output signal remains inverted in comparison to the input signal as displayed in Figure 5-6 (a) and (c) and displays a poor ER. In the case where the CW portion of the probe is suppressed and the only either the red or blue-chirped components of the probe are kept the process of XPM is primarily exploited. This results in polarity preserved pulses with

an enhanced ER in comparison to the previous case. This is illustrated in Figure 5-6 (b) and (d).

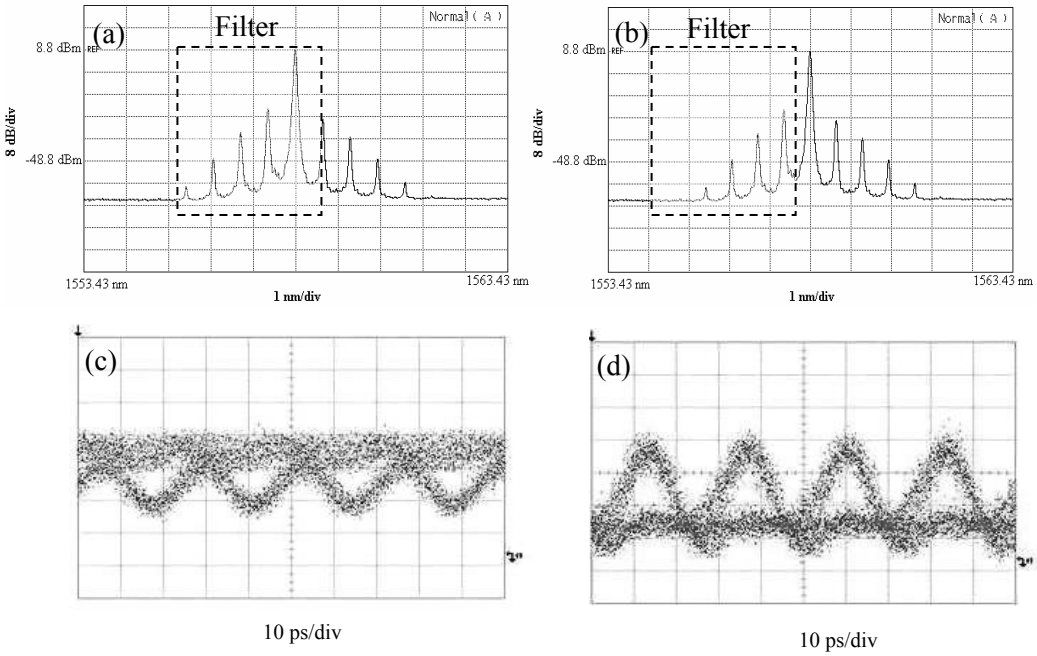

Figure 5-6 Diagram to explain the principle of shifted filtering which either primarily exploits XGM (a) and (c) (the CW component of the probe is conserved) or XPM (b) and (d) (the CW component of the probe is rejected). Both examples undertake BSF, i.e. the blue-chirped spectral components are retained.

The oscilloscope traces clearly show that the long gain recovery time is overcome as the eyes diagrams in Figure 5-6 (c) and (d) show clear eye openings at 40 Gb/s. One can see that the disadvantage of both these wavelength conversion schemes is the large spectral power which is lost due to the filtering. However the scheme can continue to operate at such high data rates due to noise suppression function of the filter that is otherwise a large detrimental effect for SOAs due to their inherent ASE [63].

5.5.2 Experimental Set-up for 10 GHz Characterisation of Shifted Filtering Scheme

An initial characterisation was carried out at 10 GHz to investigate the dependence of pump and probe parameters on the performance of the converted pulses. The experimental set-up is displayed in Figure 5-7. The pulses were generated by a 2 ps hybrid mode-locked pulse source operating at a repetition rate of 10 GHz. The pulses were amplified and coupled with a CW signal and injected into the SOA. The pump power was kept constant at 1.75 dBm, and the input probe power measured at the fibre input to the SOA was 1.2 dBm and -5.8 dBm. The Kamelian SOA was kept fixed at 250 mA. Following the SOA there was a fixed flat top bandpass filter with a 5 nm width at the full width half maximum (FWHM). The CW laser was tuned to the short and long wavelength sides of the filter to achieve RSF and BSF respectively. The wavelength

converted pulses were then characterised using the high-speed digital communications analyser (DCA) and the FROG measurement scheme.

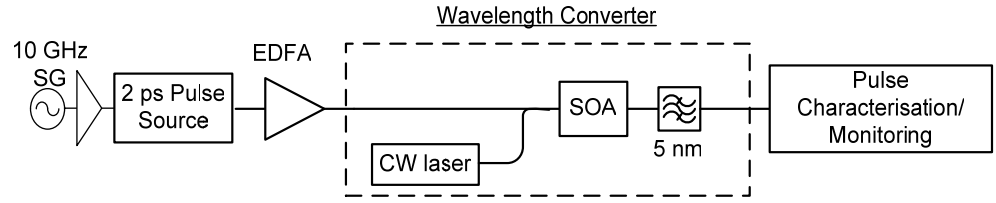

Figure 5-7 The experimental set-up for the 10 GHz characterisation of the shifted filtering wavelength conversion scheme.

5.5.3 Comparison of RSF and BSF in XGM Configuration

The CE for the shifted filtering scheme is quite poor as a lot of power is rejected by the filter and can lead to a reduced OSNR. However the filter also removes a large portion of ASE and so a relatively high OSNR can still be maintained [63]. The probe power, wavelength position and wavelength separation is investigated to determine their effect on the effective carrier lifetime and ER of the converted pulses. The effective carrier lifetime, τ is measured as the 10-90% rise time. The measurement for the ER and τ are measured from the DCA.

The results for the case of XGM and shifted filtering are outlined in Table 5-1. The first result clearly shows how the filtering technique clearly improves the ER of the converted pulses for both RSF and BSF in comparison to the case when no filtering is employed. For XGM and shifted filtering wavelength conversion, BSF is optimum. The operating conditions of the pump and probe follow the same trends as they do for the general XGM case as described in Section 5.4.

	Type of Filtering	Pump λ (nm)	Probe λ (nm)	λ Separation (nm)	Probe Power (dBm)**	τ (ps)	ER (dB)
Input	No Filtering	1556	1543.03	-13	1.2	54.25	2.39
(1)	RSF	1556	1543.03	-13	1.2	53.63	4.65
(2)	RSF	1556	1543.03	-13	-5.8	63.65	5.72
(3)	RSF	1533	1543.05	+10	1.2	51.09	3.94
(4)	RSF	1545	1552.81	+8	1.2	51.5	3.86
(5)	BSF	1556	1548.30	-8	1.2	38.32	4.48
(6)	BSF	1556	1548.30	-8	-5.8	52.00	2.93
(7)	**BSF**	**1533**	**1548.26**	**+15**	**1.2**	**21.01**	**3.57**
(8)	BSF	1545	1558.3	+13	1.2	22.01	3.12

Table 5-1 Investigation of the dependence of τ and ER on the wavelength position of the input pump and probe, their separation and power for RSF and BSF, for the XGM (polarity unpreserved) wavelength conversion scheme. (** measured at the input to the SOA, the pump power was kept constant at 1.75 dBm).

A large probe power results in a reduced recovery time (compare (1) to (2) and (5) to (6)). The ER is optimum when the probe is at a shorter wavelength than the pump i.e. down-conversion. However this results in an increased τ (compare (1) to (3) and (5) and (7)), and therefore a compromise is required. When the scheme (both pump and probe) is operated at shorter wavelengths, there is a small improvement in τ and ER (compare (3) to (4) and (7) to (8)). The slight enhancement of τ may be due to the larger differential gain when the pump and probe are operated at lower wavelengths. Therefore, optimum performance for this type of wavelength conversion scheme is found when the wavelength converted signal is down-converted, when both the pump and probe are placed at lower wavelengths, and when BSF is used (as highlighted in (7)). The wavelength converted pulses are illustrated in Figure 5-8. Although the output power from the BSF pulses is less in comparison to the RSF, the overall improvement in effective carrier lifetime is clearly seen.

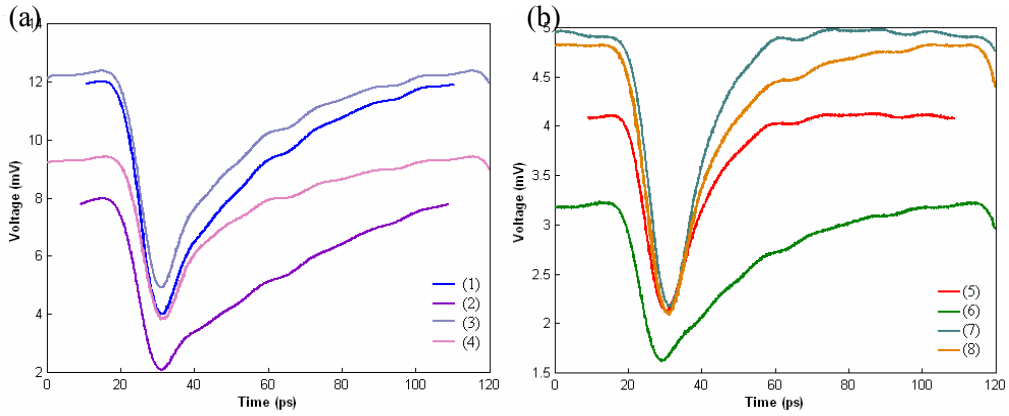

Figure 5-8 Wavelength converted pulses of (a) RSF and (b) BSF polarity unpreserved pulses (labels correspond to parameters outlined in Table 5-1).

5.5.4 Comparison of RSF and BSF in XPM Configuration

The nonlinear process of XPM is primarily exploited when the filter is offset further from the centre of the probe so that the CW portion of the probe signal is suppressed. The optimum parameters for this scheme outlined in Table 5-2 differ significantly from the XGM case. The most significant differences are that both the ER and τ have considerably improved for RSF and BSF configurations.

	Type of Filtering	**Pump λ (nm)**	**Probe λ (nm)**	**λ Separation (nm)**	**Probe Power (dBm)****	**Tau (ps)**	**ER (dB)**
Input	No Filtering	1556	1543.03	-13	1.2	54.25	2.39
(1)	RSF	1556	1542.01	-14	1.2	5.55	11.49
(2)	RSF	1556	1542.01	-14	-5.8	5.93	22.93
(3)	RSF	1533	1542.01	+9	1.2	6.3	15.99
(4)	**RSF**	**1545**	**1551.88**	**+7**	**1.2**	**5.93**	**16.43**
(5)	BSF	1556	1548.69	-7	1.2	7.24	7.23
(6)	BSF	1556	1548.69	-7	-5.8	-	-
(7)	BSF	1533	1548.69	+16	1.2	8.03	7.51
(8)	**BSF**	**1545**	**1558.64**	**+14**	**1.2**	**6.70**	**19.96**

Table 5-2 Investigation of the dependence of τ and ER on the wavelength position of the input pump and probe, their separation and power for RSF and BSF, for the XPM (polarity preserved) wavelength conversion scheme. (** measured at the input to the SOA, the pump power was kept constant at 1.75 dBm).

In this scheme the ER is optimum when the wavelength converted signal is up-converted to longer wavelengths i.e. the probe is placed at longer wavelengths to the pump wavelength (compare (1) to (3) and (5) to (6)). Thus the probe sees a lower differential

gain but a higher linewidth enhancement factor (LEF), thus the probe has a larger chirp component which improves the ER [35]. For RSF, the ER is optimum for a reduced probe power (compare (1) to (2)), however with the consequence of reduced output power, and an increased τ. In the case of the BSF, the output power was so low that a measurement could not be taken. For both red and blue-shifted filtering schemes the ER is improved when pump and probe wavelengths are at longer wavelengths (greater than the SOA gain peak) due to the increase in generated chirp components due to a smaller differential gain. This improvement is more evident in BSF (compare (3) to (4) and (6) to (7)). The optimum operating parameters are highlighted for both types of filtering RSF (4) and BSF (8).

The wavelength converted pulses for both RSF and BSF are shown in Figure 5-9 measured using the DCA. The CE (and thus the output power) is significantly degraded for XPM and shifted filtering. This is due to the high filtering of the CW component. This becomes a major limitation for this wavelength conversion scheme when operating at higher bit rates.

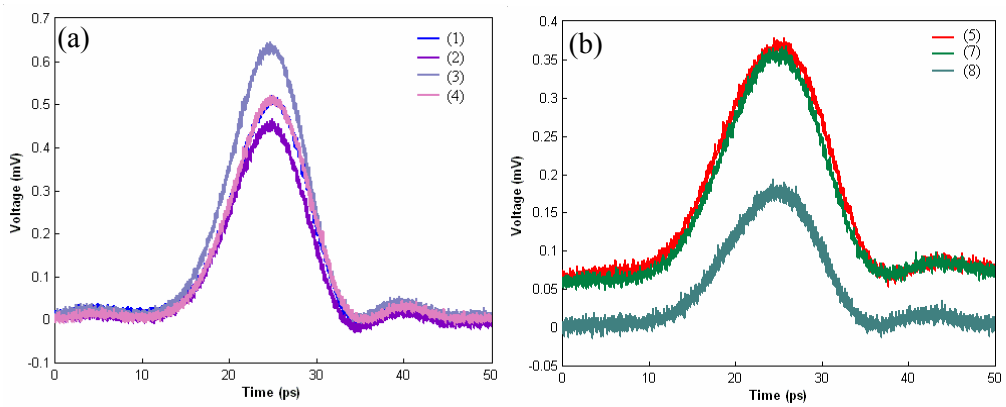

Figure 5-9 Wavelength converted pulses of (a) RSF and (b) BSF polarity preserved pulses (labels correspond to parameters outlined in Table 5-2).

Due to the limited resolution of the DCA, the accurate pulse profile of the wavelength converted pulses cannot be measured. The optimum converted signals for the RSF (4) and BSF (8) were measured using the FROG technique and are shown in Figure 5-10. The FWHM pulse width for RSF and BSF are 2.4 ps and 7.2 ps respectively. The RSF scheme appears to give overall better performance in comparison to the BSF scheme. The ER is larger, and the pulse width is narrower, however BER measurements in the next section show that BSF gives superior system performance. The large signal both pulses are sitting on is eliminated by further filtering, which suppresses the CW component to an even greater extent.

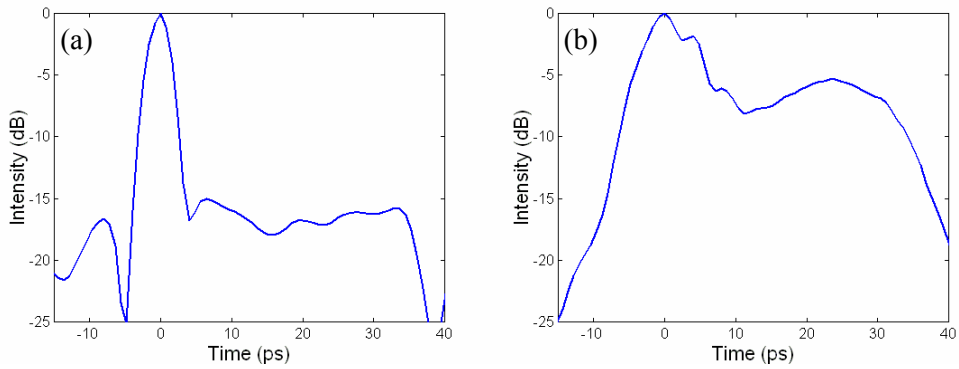

Figure 5-10 A FROG intensity characterisation of (a) the RSF and (b) the BSF schemes corresponding to (4) and (8) in Table 5-2 respectively.

5.6 System Performance and FROG Analysis of an SOA-based XPM and Shifted Filtering Scheme

5.6.1 BER Measurement Experimental Set-up

In Figure 5-11 a schematic of the experimental set-up used to perform BER measurements on the XPM and shifted filtering schemes is shown. A hybrid mode-locked pulse source is used to generate 2 ps pulses at a wavelength of 1545 nm (the pump wavelength). These pulses are amplified and filtered (removes unwanted ASE) and the signal is then modulated by a 10 Gb/s Mach Zehnder modulator (MZM) with a pseudo random bit sequence (PRBS) of 2^7-1. This data signal has a SNR of 12 and displays very little jitter (<1 ps rms) as can be seen in Figure 5-12 (a). The signal was amplified before a passive fibre interleaved multiplexer to overcome its 10 dB insertion loss. A polarizer is included following the multiplexer to ensure equal polarisation on all temporal channels. The 80 Gb/s signal is displayed in Figure 5-12 (b). A 6 dB SNR was measured at 80 Gb/s using the DCA at an input power of 0 dBm.

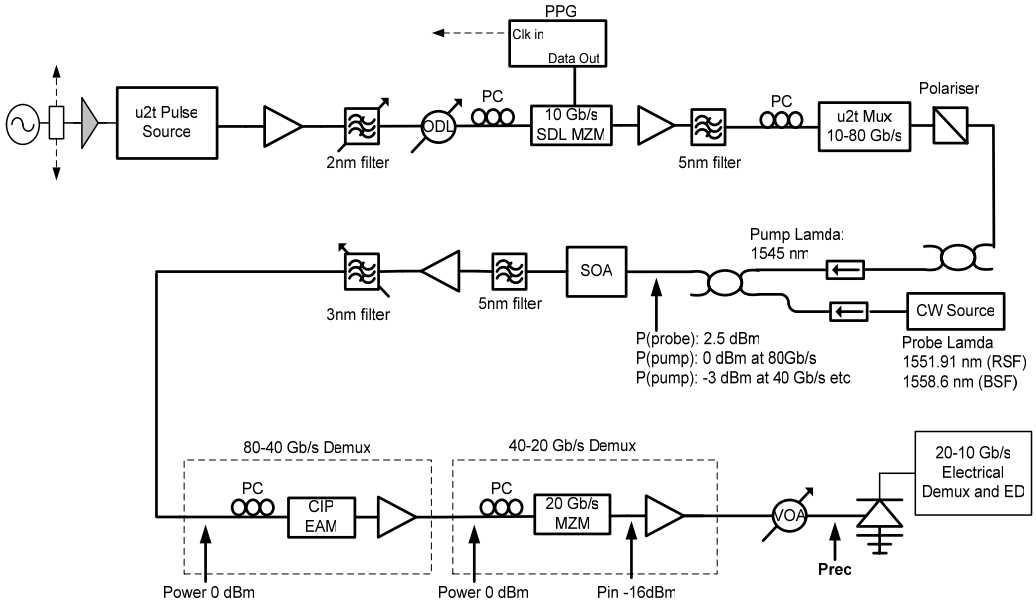

Figure 5-11 Experimental set-up used to examine the BER performance of RSF and BSF polarity preserving wavelength conversion as a function of received power.

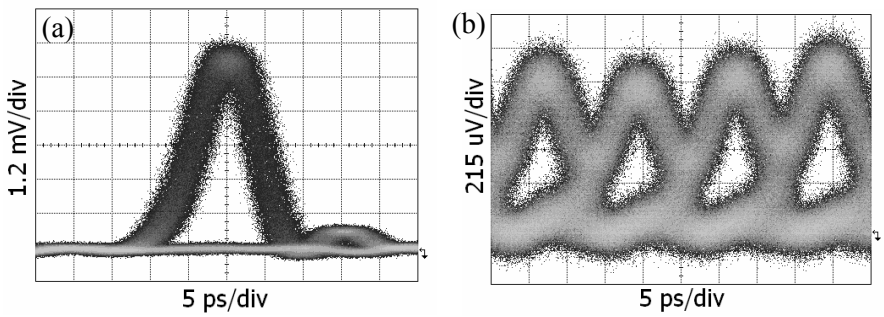

Figure 5-12 (a) The modulated data signal at 10 Gb/s and (b) the 80Gb/s multiplexed data signal before the coupler to the wavelength conversion scheme.

The wavelength converter consisted of a CW probe signal, an SOA (Kamelian and CIP SOAs were compared), a 5 nm fixed filter followed by an EDFA and a second 3 nm tunable filter. The EDFA was required to overcome the loss of the filters. Due to the first filter bandwidth the probe wavelength was tuned to 1551.91 nm and 1558.6 nm to implement RSF and BSF respectively. The probe power was kept constant at 2.5 dBm, measured at the input to the SOA. The pump and probe signals before and after the Kamelian SOA are shown in Figure 5-13. The fixed filter and tunable filter transmission profiles are shown in Figure 5-14. The tunable filter was tuned to a centre wavelength of 1555 nm and 1553 nm for RSF and BSF respectively. Figure 5-15 shows the ER improvement obtained by the addition of the second filter to the wavelength conversion scheme. The pump average power was 0 dBm at 80 Gb/s, translating to a pulse energy of 12.5 fJ. To maintain constant pulse energy entering the SOA the average power was decreased by 3 dB when the bit rate was decreased to 40 Gb/s. The Kamelian and CIP

SOAs were biased at 250 mA and 300 mA respectively. The pump and probe signals were then injected into the SOA where the probe signal is modulated via XGM and XPM. The values for the pump and probe were optimized to give the best SNR measurements just after the wavelength conversion scheme.

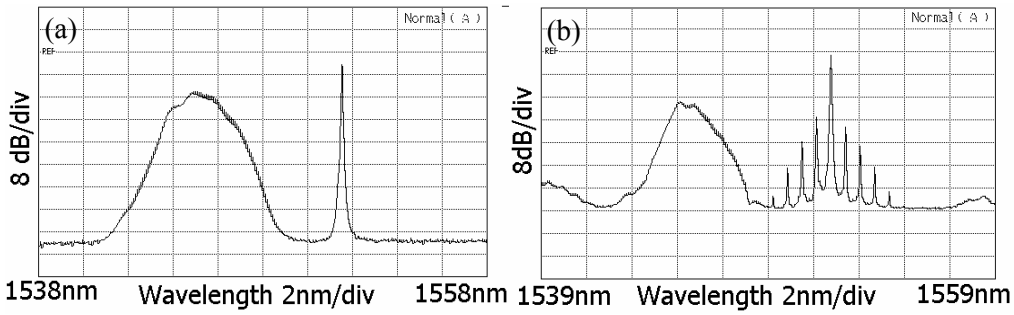

Figure 5-13 Pump and probe spectra (a) at the input to the SOA and (b) following XGM/XPM in the SOA at 80 GHz.

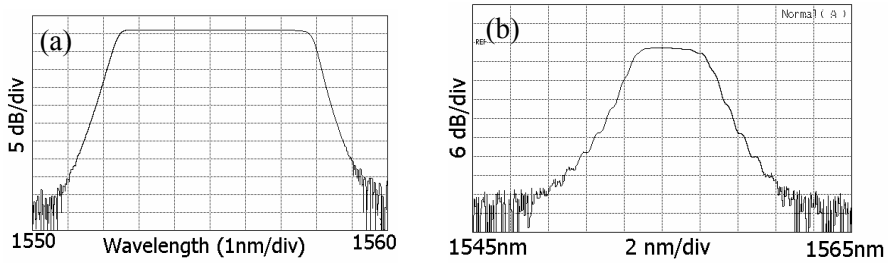

Figure 5-14 Transmission profiles of (a) the fixed filter and (b) the tunable filter.

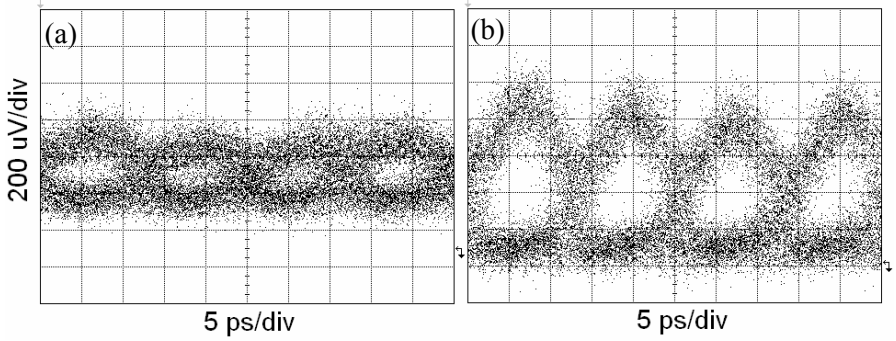

Figure 5-15 ER improvement of the wavelength converted signal for an 80 Gb/s BSF signal after (a) the fixed filter and after (b) the fixed and tunable filters.

The demultiplexing of the signals was achieved using two modulators in series. The first modulator was an electro-absorption modulator (EAM), which had a sharp transfer function generating a narrow gate, to demultiplex signals from 80 Gb/s to 40 Gb/s. A MZM was used to demultiplex from 40 Gb/s to 20 Gb/s. The power received to take BER measurements was recorded before the photodetector. The 20 Gb/s signal was electrically demultiplexed to 10 Gb/s, before being directed to the error detector (ED).

5.6.2 SNR Evaluation and BER Measurements at 40 Gb/s and 80 Gb/s

The initial characterisation for the XPM and shifted filtering schemes would lead one to expect that RSF filtering would give enhanced system performance in comparison to BSF because the output pulses were much shorter with greater output power as shown in Section 5.5.4. However BER measurements will show that BSF gives enhanced system performance and higher achievable bit rates in comparison to RSF. The SNR for the RSF wavelength conversion scheme for the Kamelian and CIP SOA are 5.2 and 5 at 40 Gb/s and 3.1 and 3.5 at 80 Gb/s respectively. The SNR for the BSF wavelength conversion scheme for the Kamelian and CIP SOAs at 80 Gb/s are 4.8 and 5.1 respectively. These values were measured at 0 dBm average power input to the DCA. The wavelength converted eyes for RSF and BSF at 80 Gb/s for the CIP SOA is displayed in Figure 5-16, which clearly show the enhanced eye opening for the BSF case.

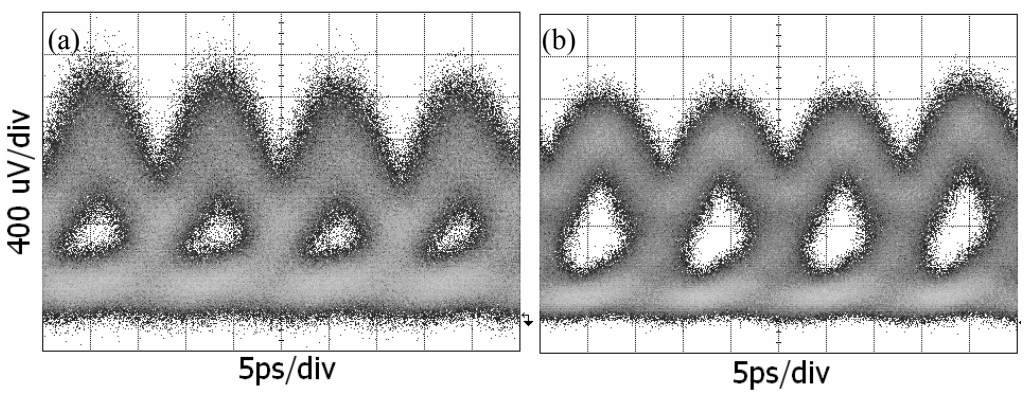

Figure 5-16 80 Gb/s CIP SOA wavelength converted eye following (a) RSF and (b) BSF.

BER measurements of the different wavelength conversion schemes were undertaken. The power received, P_{rec} was measured before the electrical photodiode (shown in Figure 5-11). BER measurements as a function of received power for RSF wavelength conversion at 40 Gb/s and 80 Gb/s for the Kamelian SOA are presented in Figure 5-17. Error-free performance can be achieved for 40 Gb/s RSF (considering $1e^{-9}$ as error free). However a large penalty of 5 dB is introduced in comparison to the 80 Gb/s B2B case (i.e. no wavelength conversion).

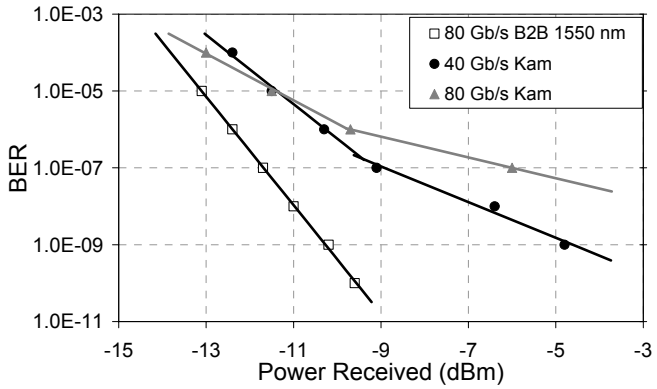

Figure 5-17 Comparison of B2B, 40 Gb/s and 80 Gb/s RSF wavelength conversion for the Kamelian SOA.

BER measurements were then taken to compare the Kamelian and CIP SOAs at 80 Gb/s for RSF and BSF are displayed in Figure 5-18 (a) and (b) respectively. The different SOAs show similar performance characteristics for both RSF and BSF. Although the SOAs have different gain recovery profiles for low probe power, at high input probe power the gain recovery and thus the phase recovery of the two SOAs are similar as shown in Figure 5-3 (c). Thus the penalty introduced by the Kamelian is approximately equal to the penalty induced by the CIP SOA.

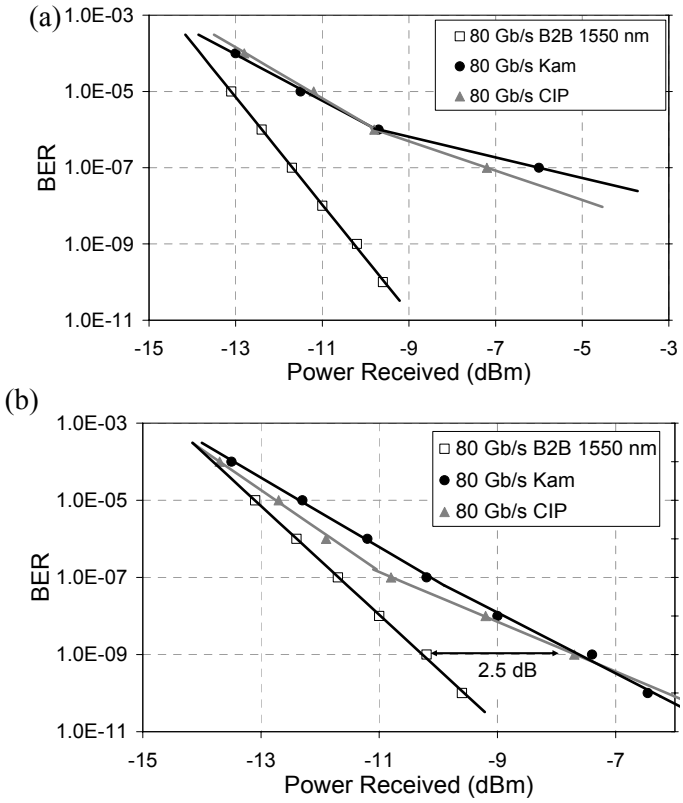

Figure 5-18 BER measurements at 80 Gb/s for both the Kamelian and CIP SOAs for (a) RSF and (b) BSF.

An error floor is introduced by the RSF due to the patterning of the '1' level due to gain saturation of the SOA. However by implementing BSF we show 80 Gb/s error-free performance in spite of the long interband gain recovery which typically limits the SOA performance to 20 Gb/s. A small penalty of 2.5 dB is introduced (measured at $1e^{-9}$) by the BSF wavelength conversion scheme in comparison to the B2B case.

Error-free performance can be achieved at these high bit rates because the BSF overcomes the patterning effects introduced by the slow interband gain recovery. Figure 5-19 displays the patterning dependence when comparing the RSF technique to the BSF technique. An input 40 Gb/s pattern was fixed to '00001010'. The input pump power was -3 dBm. Patterning effects are more prevalent in RSF because the magnitude of chirp generated is directly proportional to the rate of change of phase. Red chirp in an SOA is generated as a result of gain depletion which occurs over a small time scale (i.e. equal to the input pulse width). Thus following a long string of '0's there is high gain depletion which translates into the generation of a large magnitude of red-chirped components. However upon the input of another signal before the gain has time to recover sufficiently the amount of gain depletion is reduced and thus the amount of generated red chirp is reduced. Thus there is a reduction in power of the wavelength converted signal as shown in Figure 5-19 (a). In contrast a smaller magnitude of blue chirped components is generated because the negative phase shift associated with gain recovery occurs over a longer timescale. Therefore the wavelength converted pulses have less power but the generation of blue chirp remains approximately constant for increasing bit rates, irrelevant of the previous data pattern. Thus placement of the filter to implement BSF is optimum to achieve high bit rate performance.

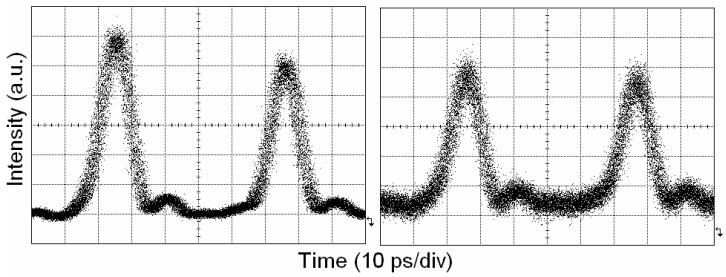

Figure 5-19 Pump power dependence of a 40 Gb/s wavelength converted signal following a fixed pattern '00001010' for (a) RSF and (b) BSF at an input pump power of -3 dBm.

5.6.3 Alternative BER Measurement to Assess BSF Wavelength Conversion

It is important to analyse the BER as a function of OSNR as this gives a more realistic performance estimation of the wavelength conversion scheme due to the influence of

noise in a system. Thus the same BSF wavelength conversion scheme was experimentally tested using the Kamelian SOA but in a different test-bed as illustrated in Figure 5-20 [64]. This test-bed consisted of a 40 GHz mode-locked fibre laser source (generates 2 ps pulses) and the signal was modulated using a $LiNBO_3$ electro-optic modulator and an increased PRBS of 2^{15}-1 was applied (in comparison to 2^7-1). The 40 Gb/s pulse train was multiplexed to 80 Gb/s using a fibre-based multiplexer. The CW probe signal was generated by a distributed feedback (DFB) laser at 1545 nm. The pump and probe signal were coupled and injected into the SOA with an average power of 3 dBm and 5 dBm respectively. The optical demultiplexing from 80-40 Gb/s was achieved through the use of one EAM and error detection was carried out at the 40 Gb/s receiver. The Kamelian SOA was biased at 250 mA. To enable the measurement of the BER evolution as a function of the OSNR signal an ASE source was added to the system to degrade the 80 Gb/s OSNR signal.

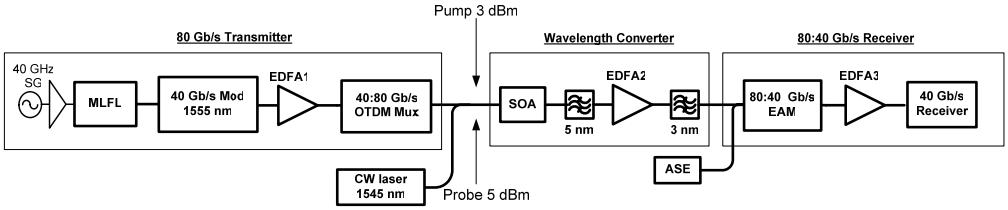

Figure 5-20 Experimental set-up to examine the BER performance of the BSF polarity preserving wavelength conversion scheme as a function of OSNR.

5.6.4 SOA ASE Limited BER Penalty

The generated blue-chirped spectral components due to the phase-amplitude coupling of the SOA are clearly seen in Figure 5-21 (a). The 3 nm filter was shifted by 2.4 nm to the lower wavelength side of the CW probe. Figure 5-21 (b) shows the spectrum before the 3 nm filter and from this we can clearly see that the OSNR of the wavelength converted signal is essentially limited by the ASE of the SOA. In addition, the 3 nm filter selects only a small portion of probe spectrum which reduces the power and thus it also adds to the large reduction in the OSNR. The OSNR of the converted signal was measured as 23 dB over a 2 nm span. The low level of OSNR explains in part the 5 dB penalties measured on the wavelength converted signal as presented in Figure 5-22. The reference signal was measured using the pump data which exhibited an OSNR of 33 dB over a 2 nm span.

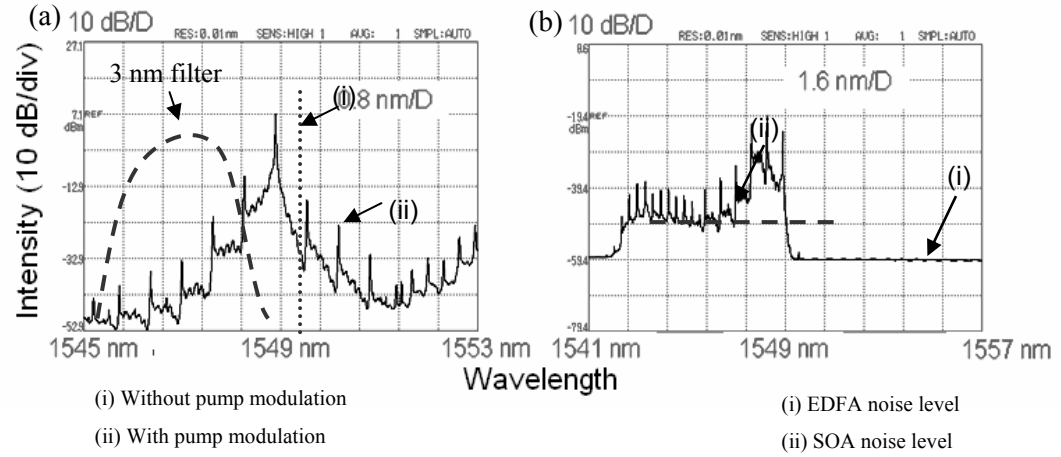

Figure 5-21 (a) Probe spectrum at the SOA output and (b) probe spectrum before 3 nm filter.

At 40 Gb/s we measured a penalty of 1.5 dB similar to [61], but this increases to 5 dB at 80 Gb/s. As explained previously, the penalties are due to the low OSNR of probe signal at the SOA output and are not primarily due to the noise of the EDFA as suggested in [61]. The poor OSNR at the SOA output will place a limitation on the use of this scheme at 160 Gb/s (as when the reference signal is multiplexed up to 160 Gb/s, an OSNR of 23dB corresponds to a BER of $1e^{-8}$). Thus the ASE of the SOA would result in an error floor if this technique were used at 160 Gb/s. The large penalty difference of 5 dB measured here in comparison to 2.5 dB measured in Section 5.6.2, can be attributed to a number of factors. The first is because this system is a function of OSNR, showing that this wavelength conversion scheme is very sensitive to an increase in noise. Additionally although BSF is not affected by the same patterning affects as RSF, it undergoes some patterning dependence. Therefore the increased pattern length of 2^{15}-1 increases the penalty measured for the BSF scheme in comparison to the previous BER measurement of 2^{7}-1.

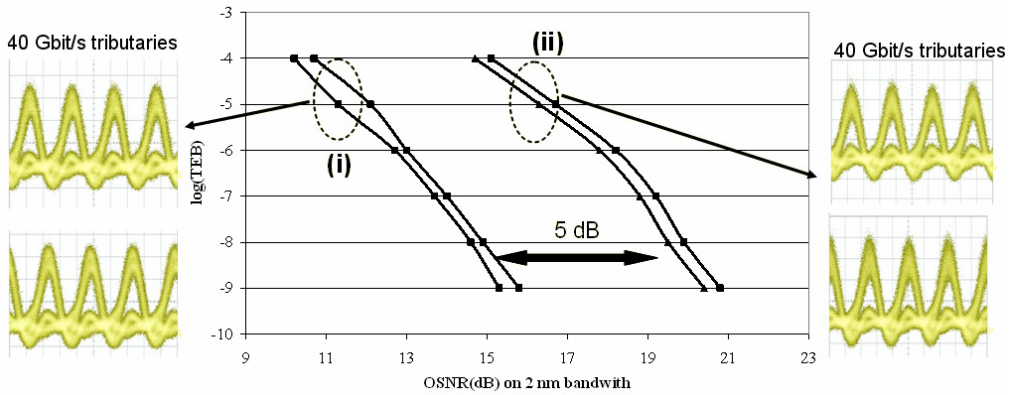

Figure 5-22 BER evolution as a function of OSNR measured over a 2 nm span of the BSF wavelength conversion scheme exploiting XPM in an SOA at 80 Gb/s. (i) represents two tributaries of the B2B signal and (ii) represents two tributaries of the wavelength converted tributaries.

5.6.5 *FROG Characterisation of RSF and BSF Wavelength Conversion at Repetition Rates of 10-80 GHz*

In this section we present a detailed characterisation of red and blue-shifted wavelength conversion schemes using the FROG measurement technique. This characterisation is important as it measures the exact temporal profile of the wavelength converted pulses and its corresponding output chirp as a function of input line rate from 10-80 GHz. Thus temporal patterning effects and the gain dynamics resulting from RSF and BSF can be examined in detail.

The experimental set-up is shown in Figure 5-23. The initial set-up remained the same as described in Figure 5-11 but no data was applied to the MZM to ensure the best accuracy in taking FROG measurements. The pulse train was passively multiplexed to rates ranging from 10-80 GHz and the wavelength converted pulses were analysed directly after the conversion scheme at each output line rate.

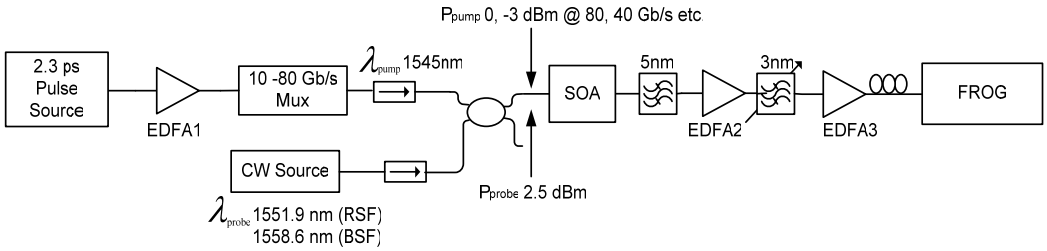

Figure 5-23 Experimental set-up to characterise the pulse temporal and chirp dependence on the applied repetition rate to the SOA for RSF and BSF polarity preserving wavelength conversion schemes.

The intensity profiles of the wavelength converted pulses for RSF and BSF are shown in Figure 5-24. By placing the filter on the red shifted side of the original probe spectrum we obtain very short pulses as shown in Figure 5-24 (a). This is due to the very fast response caused by the depletion of carriers which induces an equally fast red chirp, which corresponds to the input pump pulse width. The shape of the RSF wavelength conversion signals are defined by the shape of the chirp. Furthermore one can note a double slope in the trailing edge of the RSF pulses. This is a consequence of two factors which determine the output pulse intensity; firstly the proportion of the probe transmitted through the shifted filter which is a function of the chirp imparted on probe by the SOA and secondly the level of gain saturation in the SOA. From Figure 5-4 it can be seen that at the point of greatest red chirp the gain has only been depleted by half. After this point the output pulse intensity falls because the decreasing red chirp reduces filter transmission and also due to the gain saturating further. This corresponds to the initial

fast fall of the trailing edge. When the gain saturates to its greatest extent and starts to recover the frequency chirp is still shifting towards the blue wavelengths. At this point the filter transmission is still decreasing but the gain is recovering. This leads to the second slower fall-off in the trailing edge of the pulse. It can also be noted that the change of slope appears earlier as the bit rate increases. This can be explained because generation of red-chirped components is reduced as the bit rate increases, therefore the probe component returns earlier to its original wavelength which reduces the first part of the trailing edge of the pulses. There is the possibility that this double sloping could be removed by using an optimised filter, especially designed for this application.

In the case of BSF, illustrated in Figure 5-24 (b) the wavelength converted pulses are much broader, however the impact of patterning effects is far less evident as shown by the pulses being more independent of repetition rate. The dominant parameters in determining the pulse shape are, as for the RSF case, the gain recovery slope and, in this BSF case, the filter shape instead of the SOA chirp profile. The leading edge of the pulse has a sharp edge due to the initial fast intraband gain recovery and associated increase in the filter transmission (occurs over ~ 2 ps). The probe wavelength returns much more slowly to its original wavelength as the gain recovers, resulting in a pulse with a long trailing edge. The structure at the top of the pulses is due to a combination between the filter transmission and ultrafast gain phenomena such as intraband effects.

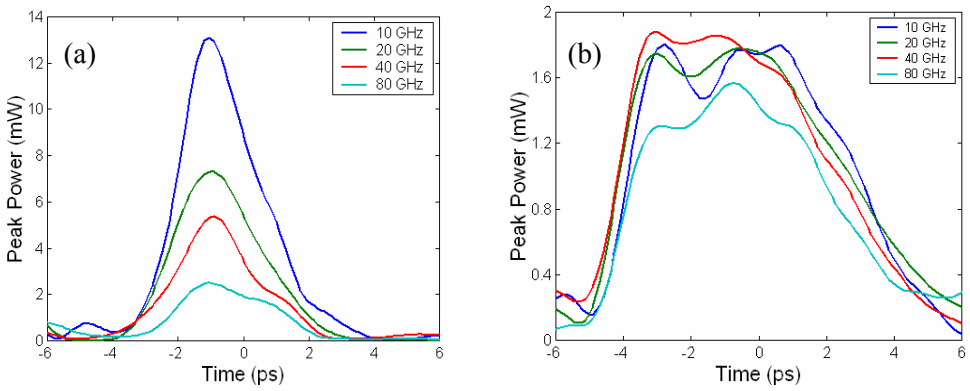

Figure 5-24 Intensity profiles of the wavelength converted pulses which primarily use XPM in conjunction with (a) RSF and (b) BSF in an SOA at line rates of 10, 20, 40 and 80 GHz.

In Figure 5-25 we show the wavelength converted pulses normalised and their corresponding output chirp. The output pulses have pulse widths of 2.5-3.6 ps and 7-6.3 ps for respective red and blue-shifted converted pulses as the repetition rate increases from 10-80 GHz. The large pulse width around 7 ps after BSF may limit this type of wavelength conversion. Shorter pulses could be achieved by using a filter with a

narrower bandwidth, however this would significantly deteriorate the OSNR, and would become the limiting factor in achieving increased bit rates. The chirp in particular for the BSF pulses is approximately linear across the pulse. This is to be expected as the induced phase by the SOA is converted into amplitude modulation by the shifted filter. This linear chirp with an approximate magnitude of 200 GHz could be used to compress the blue-shifted converted pulses to approximately 3.5 ps. The small ripple on the output chirp is due to an uneven filter profile. Enhanced performance could be achieved by using a filter with a smoother profile and pulse compression could be obtained with a filter that has a linear chirp opposite to the wavelength converted pulses.

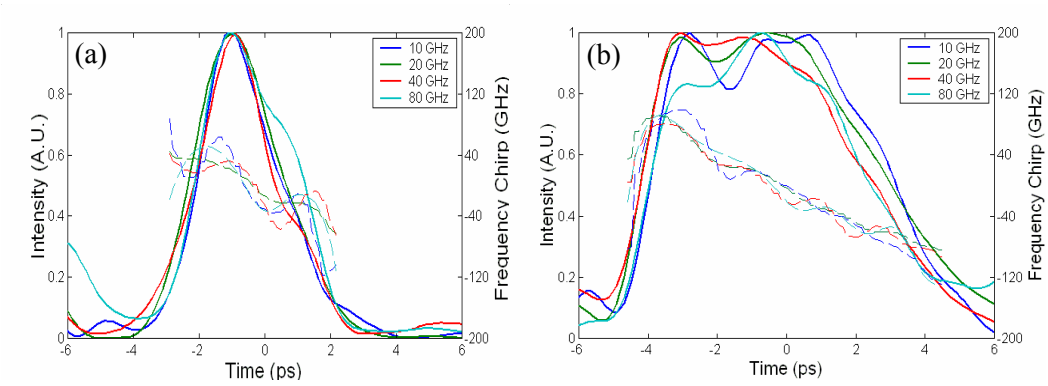

Figure 5-25 Intensity and corresponding chirp profiles of the wavelength converted pulses which primarily use XPM in the Kamelian SOA in conjunction with (a) RSF and (b) BSF at line rates of 10, 20, 40 and 80 GHz.

A comparative analysis was subsequently made with the CIP SOA and is illustrated in Figure 5-26. Similarly to the system performance results in Section 5.6.2 the wavelength converted temporal profile and chirp magnitude of the CIP SOA follow the same trends as the Kamelian SOA. However, the double slope on the trailing edge of the RSF results appears sooner and the dip in BSF pulses is larger, because the gain at these points is less in comparison to the Kamelian SOA (as shown in Figure 5-3 (c)). These differences do not introduce any penalties for the B2B BER measurements but they could lead to greater problems if the pulses are further propagated in fibre that do not undergo full dispersion compensation or are affected by nonlinearities in the fibre.

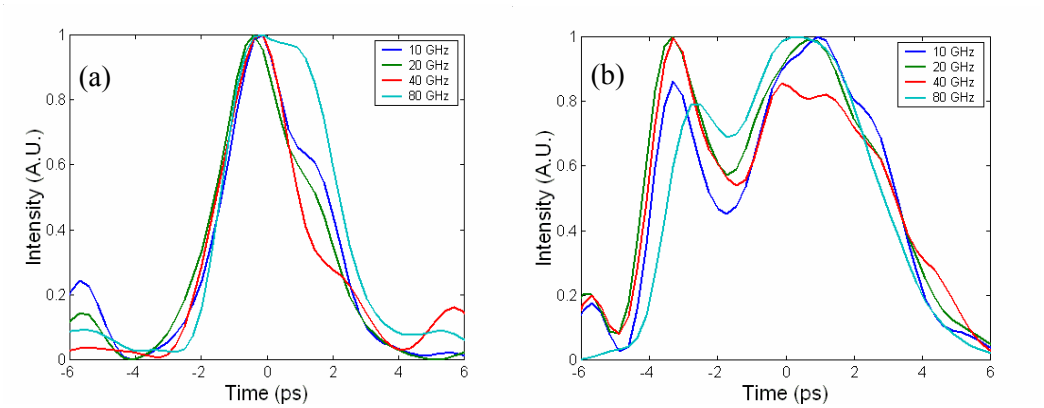

Figure 5-26 Intensity profiles for (a) red and (b) blue shifted filtering wavelength converted pulses implemented using a CIP SOA at line rates of 10, 20, 40 and 80 GHz.

The FROG characterisation gives us an improved understanding of this type of wavelength conversion scheme. In addition, these results have the potential to aid in enhancing the design of a filter to achieve an improved wavelength conversion performance. CW suppression could be improved by utilising a filter with a sharper band edge, the pulses could be optimally shaped by an asymmetric spectral transmission profile and a group delay profile opposite to the group delay of the pulses measured above. Thus, possibilities exist to enhance this wavelength conversion scheme further to provide short wavelength converted transform limited signals.

5.7 Summary

This chapter has presented an overview of the different all-optical wavelength conversion techniques presently being researched, including a detailed description of the three nonlinear processes (XGM, XPM and FWM) which enable wavelength conversion in an SOA. Currently there is a large interest in achieving wavelength conversion at high bit rates. One popular method uses a shifted filter to exploit primarily either XGM or XPM in an SOA. The focus of this chapter is the technique which primarily exploits the nonlinear process of XPM as this allows the polarity of the input pulses to be maintained. Large differences in the shape and performance of the wavelength conversion scheme can be achieved by placing the filter to retain either the red or blue-shifted spectral components. Unlike RSF, error-free performance can be achieved using BSF at 80 Gb/s, due to the phase recovery which is less dependent on the gain saturation that has preceded it. Error-free performance using this scheme has not been achieved at this high bit rate previously. A 5 dB penalty for the wavelength conversion scheme was measured in comparison to the B2B case. The full temporal characterisation of the wavelength conversion scheme presented is an important analysis to achieve a full understanding of the SOA gain and phase dynamics which are exploited using the two

different filtering schemes. The wavelength converted signals were characterised using the FROG technique as a function of repetition rate. This type of characterisation has not been yet been provided before to the best of our knowledge. In general the output pulse shapes for both RSF and RSF are determined by a combination of the generated chirp and filter profile. A combination of intraband gain and chirp effects lead to some structure on the converted pulses. In addition the group delay and chirp information obtained from this FROG analysis would enable the design of an enhanced filter shape so that improved pulse quality in the temporal domain could be obtained giving a reduced system penalty. By achieving this, this wavelength conversion scheme could be presented as an ideal candidate for use in future high-speed photonic systems.

REFERENCES

[1] S.J.B. Yoo, "Wavelength Conversion Technologies for WDM Network Applications," *J. Lightwave Technol.,* vol. 14, pp. 955-966, June 1996.

[2] COST 290, "Report of "US/EU Workshop on Key Issues and Grand Challenges in Optical Networking," US: National Science Foundation/ EU: ePHOTON/One, COST, Belgium, June 2005.

[3] A.A.M. Saleh, "Transparent Optical Networks for the Next Generation Information Infrastructure," *OSA Optical Fiber Commun.(OFC'95),* pp. 241, 1995

[4] T. Durhuus, B. Mikkelsen, C. Joergensen, S.L. Danielsen, and K. Stubkjaer, "All-optical Wavelength Conversion by Semiconductor Optical Amplifiers," *J. Lightwave Technol.,* vol. 14, pp. 942-954, June 1996.

[5] S.-C. Cao, and J.C. Cartledge, "Characterisation of the Chirp and Intensity Modulation Properties of an SOA-MZI Wavelength Converter," *J. Lightwave Technol.,* vol. 20, pp. 689-694, Apr. 2002.

[6] M. Asghari, I.H. White, and R.V. Penty, "Wavelength Conversion Using Semiconductor Optical Amplifiers," *J. Lightwave Technol.,* vol. 15, pp. 1181-1190, July 1997.

[7] D. Nesset, T. Kelly, and D. Marcenac, "All-optical Wavelength Conversion Using SOA Nonlinearities," *IEEE Commun. Mag.,* vol. 36, pp. 56-61, Dec. 1998.

[8] H.J. Lee and H.G. Kim, "Polarization-Independent All-Optical Clock Division using a Semiconductor Optical Amplifier/Grating Filter Switch," *IEEE Photonics Technol. Lett.,* vol. 11, pp. 469-471, 1999.

[9] T. Yamamoto, L.K. Oxenlowe, C. Schmidt, C. Schubert, E. Hilliger, U. Feiste, J. Berger, R. Ludwig and H.G. Weber, "Clock Recovery From 160 Gbit/s Data Signals using Phase-locked Loop with Interferometric Optical Switch Based on Semiconductor Optical Amplifier," *IEE Electron. Lett.*, vol. 37, pp. 509-510, 2001.

[10] K. Uchiyama, S. Kawanishi, and M. Saruwatari, "100-Gb/s Multiple-channel Output All-optical OTDM Demultiplexing using Multichannel Four-wave Mixing in a Semiconductor Optical Amplifier," *IEEE Photonics Technol. Lett*., vol. 10, pp. 890-892, 1998.

[11] S. Fischer, M. Dulk, E. Gamper, W. Vogt, W. Hunziker, E. Gini, H. Melchior, A. Buxens, H.N. Poulsen and A.T. Clausen, "All-optical Regenerative OTDM Add-Drop Multiplexing at 40 Gb/s using Monolithic InP Mach-Zehnder Interferometer," *IEEE Photonics Technol. Lett.*, vol. 12, pp. 335-337, 2000.

[12] S. Nakumura, Y. Ueno, K. Tajima, J. Sasaki, et al, "Demultiplexing of 168 Gb/s Data Pulses with a Hybrid-Integrated Symmetric Mach-Zehnder All-Optical Switch, *IEEE Photonics Technol. Lett.,* vol. 12, pp. 425-427, 2000.

[13] I.D. Phillips, A. Gloag, P.N. Kean, N.J. Doran, I. Bennion, and A.D. Ellis, "Simultaneous Demultiplexing, Data Regeneration, and Clock Recovery with a Single Semiconductor Amplifier-based Nonlinear-optical Loop Mirror," *OSA Optics Lett.,* vol. 22, pp. 1326-1328, Sep. 1997.

[14] G. Raybon, B. Mikkelsen, U. Koren, B.I. Miller, K. Dreyer, L. Bovin, S. Chandrasekhar, and C.A. Burns, "20 Gbit/s All-Optical Wavelength Regeneration and Wavelength Conversion using SOA Based Interferometers," *OSA Optical Fiber Commun. Conf. (OFC'99),* paper FB2, Mar. 1999.

[15] Y. Ueno, S. Nakamura, and K. Tajima, "Penalty-Free Error-Free All-Optical Data Pulse Regeneration at 84 Gb/s by using a Symmetric-Mach-Zehnder-Type Semiconductor Regenerator," *IEEE Photonics Technol. Lett.,* vol. 13, pp. 469-471, May 2001.

[16] J. Leuthold, L. Moller, J. Jaques, S. Cabot, L. Zhang, P. Bernasconi, M. Cappuzzo, L. Gomez, E. Laskowski, E. Chen, A. Wong-Foy, and A. Griffen, "160 Gb/s SOA All-Optical Wavelength Converter and Assessment of its Regenerative Properties," *IEE Electron. Letts.,* vol. 40, no. 9, Apr. 2004.

[17] R.J. Manning, X. Yang, R.P. Webb, R. Giller, F.C. Gunning, and A.D. Ellis, "The 'Turbo-Switch' – a Novel Technique to Increase the High Speed Response of SOAs for Wavelength Conversion," *OSA Optical Fiber Commun. Conf. (OFC'06),* paper OWS8, 2006.

[18] S. Nakamura, Y. Ueno, and K. Tajima, "168-Gb/s All-Optical Wavelength Conversion with a Symmetric-Mach-Zehnder-Type Switch," *IEEE Photonics Technol. Lett.*, vol. 13, pp. 1091-1093, Oct. 2001.

[19] Y. Liu, E. Tangdiongga, Z. Li, H. de Waardt, A.M.J. Koonen, G.D. Khoe, H.J.S. Dorren, X. Shu, and I. Bennion, "Error-free 320 Gb/s SOA-based Wavelength Conversion using Optical Filtering," *Optical Fiber Commun. Conf. (OFC'06),* paper PDP28, 2006.

[20] H.J.S. Dorren, X. Yang, D. Lenstra, H. de Waardt, G.D. Khoe, T. Simoyama, H. Ishikawa, H. Kawashima, and T. Hasama, "All-Optical Processing based on

Ultrafast Carrier Dynamics in Semiconductor Optical Amplifiers," *9th Microoptics Conf. (MOC'03),* paper L1, Oct. 2003.

[21] M.L. Nielsen, J, Mork, R. Suzuki, J. Sakaguchi, and Y. Ueno, "Experimental and Theoretical Investigation of the Impact of Ultra-fast Carrier Dynamics on High-speed SOA-based All-optical Switches," *OSA Optics Express,* vol. 14, pp. 331-347, Jan. 2006.

[22] B.P. Nelson, K.J. Blow, P.D. Constantine, N.J. Doran, J.K. Lucek, L.W. Marshall, and K. Smith, "All-optical Gbit/s Switching Using Nonlinear Optical Loop Mirror," *EE Electron. Letts.,* vol. 27, no. 9, Apr. 1991.

[23] M.N. Islam, "Ultrafast Fiber Switching Devices and Systems," *Cambridge University Press,* Cambridge, New York, 1992.

[24] C. Schubert, R. Ludwig, S. Watanabe, F. Futami, C. Schmidt, J. Berger, C. Boerner, S. Ferber, and H.G. Weber, "160 Gbit/s Wavelength Converter with 3R-Regenerating Capability," *IEE Electron. Letts.,* vol. 38, pp. 903-904, Aug. 2002.

[25] H. Sotobayashi, and W. Chujo, "Inter-Wavelength-Band Conversions and Demultiplexings of 640 Gbit/s OTDM Signals," *OSA Optical Fiber Commun. Conf. (OFC'02),* paper WM2, Mar. 2002.

[26] T. Sakamoto, F. Futami, K. Kikuchi, S. Takeda, Y. Sugaya, and S. Watanabe, "All-Optical Wavelength Conversion of 500-fs Pulse Trains by Using a Nonlinear-Optical Loop Mirror Composed of a Highly Nonlinear DSF," *IEEE Photonics Technol. Lett.*, vol. 13, pp. 502-504, May 2001.

[27] C.Q. Xu, H. Okayama, and M. Kawahara, "1.5 μm Band Efficient Broadband Wavelength Conversion by Difference Frequency Generation in a Periodically Domain-Inverted $LiNbO_3$ Channel Waveguide," *Appl. Phys. Lett.,* vol. 63, pp. 3559-3561, 1993.

[28] S.J.B. Yoo, "Polarisation Independent Multi-channel, Multi-format Wavelength Conversion by Difference-Frequency Generation in AlGaAs Waveguides," *European Conf. Optical Commun. (ECOC'98)*, pp. 653-654, 1998.

[29] H. Yasaka, H. Ishii, K. Takahata, K. Oe, Y. Yoshikuni, and H. Tsuchiya, "Broad-Range Tunable Wavelength Conversion of High-Bit Rate Signals Using Super Structure Grating Distributed Bragg Reflector Lasers," *IEEE J. Quantum Electron.,* vol. 32, pp. 463-470, Mar. 1996.

[30] E.P. Burr, M. Pantouvaki, and A.J. Seeds, "Wavelength Conversion of a 1.53 Micron Picosecond Pulses in an Ion-implanted Multiple Quantum Well All-

Optical Switch," *IEEE Lasers and Electro-Optics Society 15th Annual Meeting (LEOS),* paper CFJ2, 2002.

[31] T. Durhuus, R.J.S. Pedersen, B. Mikkelsen, K.E. Stubkjaer, M. Oberg, and S. Nilsson, "Optical Wavelength Conversion Over 18 nm at 2.5 Gb/s by DBR-Laser," *IEEE Photonics Technol. Lett.*, vol. 5, pp. 86-88, Jan. 1993.

[32] J. Horer, K. Weich, M. Mohrle, and B. Sartorius, "Optimization of the Optical Switching Characteristics of Two-Section Fabry-Perot Lasers," *IEEE Photonics Technol. Lett.*, vol. 5, pp. 1273-1275, Nov. 1993.

[33] X. Ma, and G.S. Kuo, "Optical Switching Technology Comparison: optical MEMS vs. Other Technologies," *IEEE Commun. Mag.,* vol. 41, pp. S16-S23, Nov. 2003.

[34] M. Eiselt, W. Pieper, and H.G. Weber, "SLALOM: Semiconductor Laser Amplifier in a Loop Mirror," *J. Lightwave Technol.,* vol. 13, pp. 2099-2112, Oct. 1995.

[35] L. Schares, C. Schubert, C. Schmidt, H.G. Weber, L. Occhi, and G. Gueko, "Phase Dynamics of Semiconductor Optical Amplifiers at 10–40 GHz," *IEEE J. Quantum Electronics,* vol. 39, pp. 1394-1408, Nov. 2003.

[36] R. Nagarajan, C.H. Joyner, R.P. Schneider, J.S. Bostak, et al, "Large-Scale Photonic Integrated Circuits," *IEEE J. Sel. Top. Quantum Electron.,* vol. 11, pp. 50-65, Jan/Feb. 2005.

[37] A. Poustie, "Semiconductor Devices for All-optical Signal Processing," *European Conf. Optical Commun. (ECOC'05),* paper We 3.5.1, 2005.

[38] J.M. Wiesenfeld, B. Glance, J.S. Perino, and A.H. Gnauck, "Wavelength Conversion at 10 Gb/s using a Semiconductor Optical Amplifier," *IEEE Photonics Technol. Lett.*, vol. 5, pp. 1300-1303, Nov. 1993.

[39] D. Marcenac, and A. Mecozzi, "Switches and Frequency Converters Based on Cross-Gain Modulation in Semiconductor Optical Amplifiers," *IEEE Photonics Technol. Lett.*, vol. 9, pp. 749-751, Jun. 1997.

[40] K. Obermann, S. Kindt, D. Breuer, and K. Petermann, "Performance Analysis of Wavelength Converters Based on Cross-Gain Modulation in Semiconductor-Optical Amplifiers," *J. Lightwave Technol.,* vol. 16, pp. 78-85, Jan. 1998.

[41] K.E. Stubkjaer, "Semiconductor Optical Amplifier-Based All-Optical Gates for High-Speed Optical Processing," *IEEE J. Sel. Top. Quantum Electron.,* vol. 6, pp. 1428-1434, 2000.

[42] R.S. Grant, G.T. Kennedy, and W. Sibbett, "Cross Phase Modulation in Semiconductor Optical Amplifier," *IEE Electron. Letts.,* vol. 27, pp. 800-802, May 1991.

[43] R. Schreieck, M. Kwakernaak, H. Jackel, E. Gamper, E. Gini, W. Vogt, and H. Melchoir, "Ultrafast Switching Dynamics of Mach-Zehnder Interferometer Switches," *IEEE Photonics Technol. Lett.*, vol. 13, pp. 603-605, Jun. 2001.

[44] A. Matsumoto, K. Nishimura, K. Utaka, and M. Usami, "Operational Design on High-Speed Semiconductor Optical Amplifier With Assist Light for Application to Wavelength Converters Using Cross Phase Modulation," *IEEE J. Quantum Electron.,* vol. 42, pp. 313-323, Mar. 2006.

[45] D.F. Geraghty, R.B. Lee, M. Verdiell, M. Ziari, et al, "Wavelength Conversion for WDM Communication Systems Using Four-Wave Mixing in Semiconductor Optical Amplifiers," *IEEE J. Sel. Topics Quantum Electron.,* vol. 3, pp. 1146-1155, 1997.

[46] A. Mecozzi, S. Scotti, A. D'Ottavi, E. Iannone, and P. Spano, "Four-Wave Mixing in Traveling-Wave Semiconductor Amplifiers," *IEEE J. Quantum Electron.,* vol. 31, pp. 689-699, Apr. 1995.

[47] H. Soto, and D. Erasme, "An Experimental Method for Identifying Nonlinear Phenomena Intervening in a FWM Process Developed in a Semiconductor Optical Amplifier," *IEEE J. Quantum Electron.,* vol. 34, pp. 2211-2216, Nov. 1998.

[48] J. Zhou, N. Park, J. Vahala, M.A. Newkirk, and B.I. Miller, "Four-Wave Mixing Wavelength Conversion Efficiency in Semiconductor Traveling-Wave Amplifiers Measured to 65nm of Wavelength Shift," *IEEE Photonics Technol. Lett.*, vol. 8, pp. 984-986, Aug. 1994.

[49] M.J. Connelly, "Semiconductor Optical Amplifiers," *Kluwer Academic Press,* Boston, 2002.

[50] J.P.R. Lacey, M.A. Summerfield, and S.J. Madden, "Tunability of Polarisation-Insensitive Wavelength Converters Based on Four-wave Mixing in Semiconductor Optical Amplifiers," *J. Lightwave Technol.,* vol. 16, pp. 2419-2427, 1998.

[51] L. Zhang, I. Kang, A. Bhardwaj, N. Sauer, C. Cabot, J. Jaques, and D.T. Neilson, "Reduced Recovery Time Semiconductor Optical Amplifier Using p-Type-Doped Multiple Quantum Wells," *IEEE Photonics Technol. Lett.,* vol. 18, pp. 2323-2325, Nov. 2006.

[52] N. Storkfelt, B. Mikkelsen, D.S. Olesen, M. Yamaguchi, and K.E Stubkjaer, "Measurement of Carrier Lifetime and Linewidth Enhancement Factor for 1.5-μm Ridge-Waveguide Laser Amplifier," *IEEE Photonics Technol. Lett.,* vol. 3, pp. 632-634, Jul. 1991.

[53] R.J. Manning, and D.A.O. Davies, "Three-wavelength Device for All-Optical Signal Processing," *Optics Lett.,* vol. 19, pp. 889-891, June 1994.

[54] H. Ghafouri-Shiraz, "The Principles of Semiconductor Laser Diodes and Amplifiers – Analysis and Transmission Line Laser Modeling," *Imperial College Press,* London, 2004.

[55] K. Obermann, S. Kindt, D. Breuer, and K. Petermann, "Performance Analysis of Wavelength Converters Based on Cross-Gain Modulation in Semiconductor-Optical Amplifiers," *J. Lightwave Technol.,* vol. 16, pp. 78-85, Jan 1998.

[56] M.L. Nielsen, and J. Mork, "Increasing the Modulation Bandwidth of Semiconductor Optical-Amplifier-based Switches by using Optical Filtering," *J. Opt. Soc. Am. B,* vol. 21, pp. 1606-1619, Sept.2004.

[57] H.Y. Yu, D. Mahgerefteh, P.S. Cho, and J. Goldhar, "Optimisation of the Frequency Response of a Semiconductor Optical Amplifier Wavelength Converter Using a Fiber Bragg Grating," *J. Lightwave Technol.,* vol. 17, pp. 308-315, Feb. 1999.

[58] D. Mahgerefteh, P.S. Cho, H.-Y. Yu, G.M. Carter, and J. Goldhar, "Improving the Performance of All-Optical Wavelength Converters Using Fiber Gratings," *Taylor and Francis Group, Fiber and Integrated Optics*, vol. 18, pp. 155-166, May, 1999.

[59] A.D. Ellis, A.E. Kelly, D. Nesset, D. Pitcher, D.G. Moodie, and R. Kashyap, "Error free 100Gbit/s Wavelength Conversion using Grating Assisted Cross-Gain Modulation in 2mm Long Semiconductor Amplifier," *IEE Electron. Lett.,* vol. 34, pp. 1958-1559, Oct. 1998.

[60] Y. Liu, E. Tangdiongga, Z. Li, S. Zhang, H. de Waardt, G.D. Khoe, and H.J.S. Dorren, "Error-Free All-Optical Wavelength Conversion at 160 Gb/s Using a Semiconductor Optical Amplifier and an Optical Bandpass Filter," *J. Lightwave Technol.,*vol. 24, pp. 230-236, Jan. 2006.

[61] M.L. Nielsen, B. Lavigne, and B. Dagens, "Polarity-preserving SOA-based Wavelength Conversion at 40 Gbit/s using Bandpass Filtering," *IEE Electron. Lett.,* vol. 39, no. 18, Sept. 2003.

[62] J. Leuthold, D.M. Marom, S. Cabot, J.J. Jaques, R. Ryf, and C.R. Giles, "All-Optical Wavelength Conversion Using a Pulse Reformatting Optical Filter," *J. Lightwave Technol.,* vol. 22, pp. 186-192, Jan. 2004.

[63] M.L. Nielsen, J. Mork, R. Suzuki, J. Sakaguchi, and Y. Ueno, "Theoretical and Experimental Study of Fundamental Differences in the Noise Suppression of High-Speed SOA-based All-optical switches," *OSA Optics Express,* vol. 13, pp. 5080-5086, June 2005.

[64] L. Bramerie, A. Clarke, G. Girault, S. Lobo, M. Gay, C. Guignard, V. Roncin, B. Kennedy, P. Maguire, S. Feve, B. Clouet, F. Ginovert, L. P. Barry, and J.C. Simon, "Investigation of SOA-based Wavelength Conversion at 80 Gb/s using Bandpass Filtering," *Conf. Lasers and Electro-Optics (CLEO'06)*, paper CMT7, May 2006.

CHAPTER 6 – CONCLUSION AND FUTURE OUTLOOK

Optical fibre communications systems will continue to be the physical transmission system to deliver high-bandwidth voice and data information because it has the capability to provide terahertz of bandwidth, and can offer many advantages over other communications systems. As high-bandwidth consumer products unfold (e.g. high-definition television (HDTV) and video sharing), the demand for fibre-to-the-home (FTTH) will increase rapidly. An overall increase in demand for bandwidth in the access and metro networks will in turn result in increased data capacity in the transport/core network. Therefore, it is imperative for network providers to better utilise their installed fibre networks. Due to the limited speeds of electronics it will be necessary to develop transparent networks, whereby the simple processing requirements of the networks will be carried out in the optical domain. This thesis meets these demands by developing all-optical processing techniques for the generation and wavelength routing of optical pulses.

As was discussed in Chapter 1, one way to exploit the large-bandwidth capabilities of optical fibre is to use different multiplexing techniques, where multiple data channels are transmitted simultaneously over a single optical fibre. Electrical time division multiplexing (ETDM) will be the multiplexing technique of choice in the future but due to limited operating speeds of present-day electronics, optical multiplexing techniques will also be required. Wavelength division multiplexing (WDM) is presently in operation globally due to its simple implementation and the ability of the Erbium doped fibre amplifier (EDFA) to amplify many wavelength channels simultaneously (with little distortion). The push for higher data rates on single wavelength channels, which has historically left the development of high-speed electronics behind, necessitates the use of optical time division multiplexing (OTDM) transmitters and receivers until their economically more attractive ETDM equivalents become available. In order to implement OTDM networks, transmitters capable of generating picosecond pulses are required.

In addition to the limited speeds of electronics necessitating the need for all-optical networks, the ability of optics and not electronics as being the most cost effective way to tap the multi-terabit per second capacity of the optical fibre is also motivating the need for the development of all-optical processing components. In doing so the growing demand for bandwidth per user, higher path reliability, and simplified operation and

management is fulfilled. One of the most important components for future networks will be wavelength converters in order to provide dynamic provisioning at each node to avoid wavelength contention, resulting in more flexible networks with the ability to provide more bandwidth at reduced costs.

In order to measure the quality of pulses, different measurement and characterisation equipment is required. The technique of frequency-resolved optical gating (FROG) can provide full electric field characterisation, and is advantageous as it overcomes the limited resolution of opto-electronic measurements and gives phase information corresponding to the pulse. The FROG technique is used throughout this thesis in order to provide full characterisation of the pulses output from developed sub-systems, and results in a greater understanding of the physical processes the components used induce on these optical signals.

High quality pulse sources are required for the implementation of next generation networks and the requirements these pulse sources must meet are introduced in Chapter 2. Different pulse generation techniques exist which include external modulation of a continuous wave (CW) source, mode locking and gain switching. Gain switching has many advantages in comparison to other pulse generation techniques because it is simple to implement, and is very cost efficient and is thus the pulse generation scheme examined in particular. The major disadvantage of gain switching is the poor output pulse quality, which places limits on its use in high-speed networks. However results presented show that by simply applying external or self seeding to the gain-switched laser large temporal and spectral improvements are achieved. These include large improvements in side mode suppression ratio (SMSR), a substantial reduction of temporal jitter to sub-picosecond levels and a considerable decrease in chirp across the pulse. These findings have been known for quite some time but the optical light injection was used in a novel way to develop a widely tunable picosecond pulse source (~ 65 nm) suitable for use in 20 Gb/s systems. Wavelength tunable pulse sources will be of great importance in future optical systems to facilitate dynamic provisioning in the network. The pulse sources presented employs two gain-switched Fabry–Pérot (FP) lasers which provided the large wavelength tuning range (largest span achievable to date by gain switching). With the advancement of laser device fabrication technology, improved performance will be achieved. Enhanced laser bandwidths will provide the generation of shorter pulses at increased bit rates. In addition, this source has the potential to be used as a multi-wavelength source, by simultaneous light injection at two or more wavelengths.

Pulse sources used in high-speed systems will require a high temporal suppression ratio (TPSR) as low TPSR can result in the generation of interferometric noise between OTDM channels. In Chapter 3 we quantifiably investigated the effect varying levels of TPSR have on a pulse source when used in a high-speed OTDM system. A 3 dB power penalty is introduced when TPSR levels are degraded from 30 dB to 15 dB in an 80 Gb/s back-to-back (B2B) system. An increase in pulse and pedestal overlap leads to a larger power penalty. Therefore TPSR is a very important parameter to optimise, however it is typically difficult for pulse generation techniques to achieve TPSR levels greater than 30 dB. A simple and effective method is to employ a vertical microcavity based saturable absorber (SA) as part of the pulse source. We demonstrated that this SA has the ability to improve a pulse source with an initial TPSR of 15 dB, to a TPSR of 30 dB, and improve the overall system performance by 3.3 dB (provides additional regenerative properties to the TPSR enhancement). This SA also displays extra benefits, it can be monolithically integrated with a semiconductor-based pulse source and can operate at even greater bit rates due to its fast recovery time of <1.5 ps.

To achieve short picosecond pulse widths (<10 ps) gain-switched sources require pulse compression. However linear compression of gain-switched pulses results in the generation of pedestals due to insufficient compensation of its nonlinear chirp. Therefore a specifically designed nonlinearly chirped grating is required to achieve full chirp compensation of the gain-switched pulses. We proposed a novel design method to extract the parameters required to fabricate a tailor-made nonlinearly chirped fibre Bragg grating (NL FBG). The FROG measurement technique enabled the extraction of the exact group-delay profile of the grating as it is the inverse of that across the gain-switched pulse measured directly from the laser. In addition the grating design had a specially adapted transfer characteristic to give a symmetric output Gaussian spectral profile. Thus by applying this tailor-made NL FBG to a gain-switched laser a very simple and reliable pulse source is presented. This pulse source generates 3.5 ps picosecond transform limited (0.45) Gaussian pulses, with a negligible TPSR (>35 dB), low jitter (<1 ps) and high SMSR (>30 dB). The NL FBG gain-switched source demonstrates major improvement in system sensitivity (3.5 dB) when compared to the same source employing a liner grating in an 80 Gb/s OTDM system. To examine the quality of the proposed pulse source, B2B BER measurements of a commercially available mode-locked pulse source were carried out also and the NL FBG gain-switched source compared well to this commercial benchmark. In order to further extend the commercial benefits of this source (cost and simplicity), an investigation could be

carried out to determine if one grating design would suffice for a large group of lasers manufactured on a single wafer.

In Chapters 2 and 3 we investigated in detail the applicability of gain switching as a pulse source candidate for future high-speed networks. A variety of optical pulse processing techniques were introduced which enhanced the pulse quality so short picosecond pulses were generated suitable for use in 80 Gb/s OTDM systems. To further develop high-speed networks, processing data at each node (e.g. wavelength conversion) requires optical processing to overcome the optical-electronic-optical (OEO) conversion bottleneck. It is shown that a semiconductor optical amplifier (SOA) is an ideal candidate as an all-optical processing device, due to its large gain and phase nonlinearities. Both the interband and intraband gain and phase dynamics of an SOA dictate the performance of the SOA both as an amplifier and as an all-optical processing device. Two SOAs (a Kamelian and CIP SOA) show different gain and phase recoveries when used as an amplifier. The Kamelian SOA has a longer interband gain recovery time scale but a larger intraband gain recovery magnitude in comparison to the CIP SOA. This intraband gain recovery results in the generation of some blue-chirped components and in the degradation of TPSR on both the leading and trailing edges of the amplified pulse. In contrast blue-chirped components were not visible on the CIP SOA amplified pulses and only the TPSR on the leading edge of the pulse was degraded due to the small intraband gain magnitude. Characterisations also showed that shorter pulses (2 ps in comparison to 8 ps pulses) displayed a higher degree of gain saturation due to the larger contribution of intraband effects and thus an increase in generated chirp components. This in-depth characterisation of the effects of SOA amplification on picosecond pulses is vital in the design of high-speed systems that employ SOAs as amplifiers and as optical processing elements. In particular these results are significant as they are the first detailed report of the dependence of TPSR on ultrafast gain recovery.

Chapter 5 examines the benefits of an SOA as an all-optical wavelength converter, and introduces the three nonlinear processes which enable the process of wavelength conversion (cross gain modulation (XGM), cross phase modulation (XPM), and four wave missing (FWM)). The most significant limiting factor of SOA wavelength conversion at high bit rates is its interband gain recovery time (55 ps for the Kamelian SOA) which introduces detrimental patterning effects. One popular method to overcome the patterning effects induced by the long interband gain recovery time is to use XGM/XPM in conjunction with shifted filtering. We focus in detail on XPM and shifted filtering because this scheme has the benefits of simple configuration, high extinction

ratio (ER), polarity preserved operation and polarisation independence (unlike the XGM shifted filtering scheme no complicated interferometric set-up is required). Large differences in the shape and performance of the wavelength conversion scheme can be achieved by placing the filter to retain either the red or blue-shifted spectral components of the wavelength converted probe. We presented for the first time 80 Gb/s error-free performance for XPM in conjunction with blue-shifted filtering (BSF). We also show that error-free performance for red-shifted filtering (RSF) is limited to 40 Gb/s. Although initial characterisation presented RSF wavelength conversion as the optimum process (high output power and short wavelength converted pulse width), RSF has a large gain-saturation dependence resulting in patterning effects. High bit rate operation is achievable by BSF because the blue-shifted spectral components relate to gain recovery rather than gain depletion. The related magnitude and time frame of phase recovery remains approximately constant (therefore so does the generated blue-chirped components) as it does not have a large dependence on the previous input data signal. A relatively modest 5 dB power penalty is introduced by this wavelength conversion scheme.

A full temporal characterisation of the RSF and BSF wavelength converted pulses is an important analysis to characterise the effect and contribution the gain and phase dynamics and the filter shape have on the shape and chirp. This type of characterisation has not yet been provided to the best of our knowledge. The wavelength converted pulses are characterised using the FROG technique as a function of repetition rate. In general the output pulse shapes for both RSF and RSF are determined by a combination of the generated chirp and filter profile. A combination of intraband gain and chirp effects lead to some structure on the converted pulses. Although the filter converts the phase modulation of the probe into intensity modulation, some linear chirp remains on the wavelength converted pulses. The power penalty introduced by the BSF wavelength converter can be reduced by using the FROG results to design an enhanced filter. The measured chirp can be compensated for to compress the converted pulse and a designed spectral transmission profile can provide spectral optimisation. Enhancement of the filter would make this BSF XPM wavelength converter an ideal candidate for use in future high-speed photonic systems.

As outlined in the first chapter, research and development of components and sub-systems suitable for high-speed transparent networks are required so that the bandwidth capabilities of optical fibre can be fully exploited in a cost-efficient manner. This thesis presents novel and original research on optical pulse processing techniques towards

enabling terabit per second photonic systems. Particular focus is given to optimising pulse generation schemes and realising a high-speed SOA-based wavelength converter. 80 Gb/s operation is achieved and simple and cost-effective methods are proposed with high commercial potential.

APPENDIX I – MATHEMATICAL DESCRIPTION OF A PULSE

The temporal dependence of the pulse electric field (ignoring the spatial portion of the field) can be described as [i]:

$$\varepsilon(t) = \tfrac{1}{2}\sqrt{I(t)}\exp\{i[\omega_0 t - \phi(t)]\} \qquad \text{Equation I-1}$$

Where t is the time in the reference frame of the pulse, ω_0 is a carrier angular frequency, $I(t)$ and $\phi(t)$ are the time dependent intensity and phase of the pulse. The rapidly varying carrier wave and the complex conjugate are not included to simplify the equation. The complex amplitude, $E(t)$ of this wave is:

$$E(t) = \sqrt{I(t)}\exp[-i\phi(t)] \qquad \text{Equation I-2}$$

The temporal intensity of the pulse is found by:

$$I(t) = \left|E(t)\right|^2 \qquad \text{Equation I-3}$$

When the electric field is given in Cartesian Coordinates, the phase, $\phi(t)$ is found by:

$$\phi(t) = -\arctan\left\{\frac{\mathrm{Im}\,E(t)}{\mathrm{Re}\,E(t)}\right\} \qquad \text{Equation I-4}$$

The instantaneous frequency, or chirp, ν_{inst} is given by:

$$\nu_{inst}(t) = \nu_0 - [d\phi/dt]/2\pi \qquad \text{Equation I-5}$$

Generally, the instantaneous frequency is measured in Hertz (Hz) rather than radians/sec, thus the phase which is measured in angular coordinates is divided by 2π. Figure I-1 (a) and (b) illustrates the fast varying component of the electric field i.e. the carrier wave, the real amplitude of the electric field and the temporal intensity of the pulse for a non-chirped and chirped pulse respectively. Figure I-1 (c) and (d) show the resultant phase and chirp of the pulses displayed in (a) and (b).

---

[i] R. Trebino, "Frequency Resolved Optical Gating: The Measurement of Ultrashort Laser Pulses," *Kluwer,* Norwell, MA, 2000.

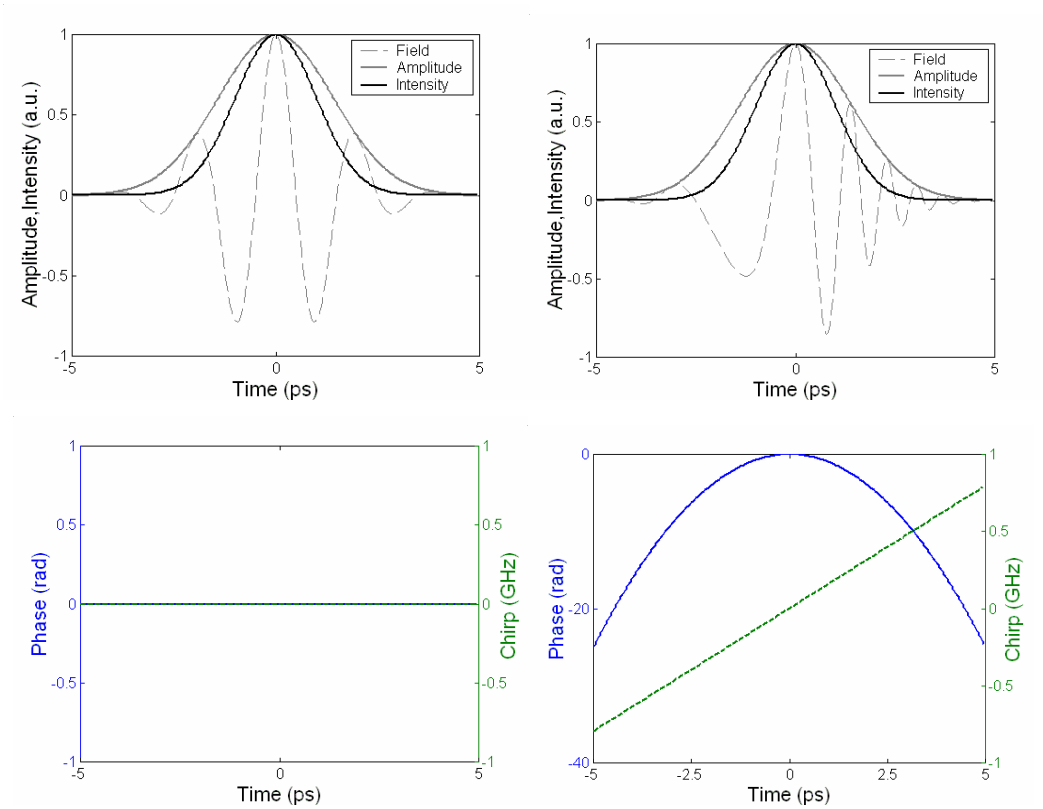

Figure I-1 The electric field intensity, (real) amplitude, and intensity of a Gaussian Pulse. The intensity distribution of a Gaussian Pulse is $\sqrt{2}$ narrower than its real amplitude. The phase of (a) is zero and (b) is quadratic ($-1t^2$), as shown in corresponding graphs of (c) and (d) displaying the phase and chirp.

The pulse field in the frequency domain is the Fourier transform of the time-domain field. To convert the spectrum measured in the frequency domain into the wavelength domain the following relation is used:

$$\varphi_{\lambda}(\lambda) = \varphi_{\omega}(2\pi c / \lambda) \qquad \text{Equation I-6}$$

Since,

$$\omega = \frac{2\pi c}{\lambda} \qquad \text{Equation I-7}$$

Where φ is the spectral phase measured in radians, c is the speed of light, and λ is the centre wavelength of the field, and ω is the angular frequency measured in radians/sec. The subscripts indicate the phase represented in the wavelength and frequency domains.

While the temporal phase contains frequency vs. time information, the spectral phase contains time vs. frequency information. Thus the group delay vs. frequency as $t_{group}(\omega)$ is:

$$t_{group}(\omega) = d\varphi / d\omega \qquad \text{Equation I-8}$$

APPENDIX II – DATA SHEETS

The following pages contain data sheets for the following devices:

- DFB NEL Laser – 108998
- Redfern Nonlinearly Chirped FBG
- Kamelian Bulk SOA – 39-03-020377
- CIP Nonlinear Quantum Well SOA – 02895

【 10Gb/s 1500 nm DFB-LD Module Test Data 】

Product Type	KELD1552SSC-L
Module No.	108998

ELECTRICAL/OPTICAL CHARACTERISTICS $T_{CASE}=T_{LASER}=25°C$

No.	Parameter	Symbol	Condition	Specifications			Test Results	Units
				Min	Typ	Max		
1	Forward Voltage	V_F	CW, I_F=30mA		1.2		1.04	V
2	Threshold Current	$I_{(TH)}$	CW		15		20.2	mA
3	Fiber Output Power	Φ_e	CW, ΔI_F=40mA		4		2.8	mW
4	Peak Wavelength	λ_p	CW, Φ_e=4mW	1540.00	1550.00	1560.00	1550.74	nm
5	Side Mode Suppression Ratio	SMS	CW, Φ_e=4mW		30		43	dB
6	Monitoring Current (PD)	$I_{R(E)}$	CW, Φ_e=4mW		0.1		0.738	mA
7	Dark Current (PD)	$I_{r(0)}$	CW, V_{DR}=5V		100		1.0	nA
8	Tracking Error	E_R	$I_{R(E)}$=Constant		±0.5		-0.16	dB
9								
10								
11								
12								
13								
14								
15								
16								
17								
18								
19								
20								

$\Delta I_F=I_F-I_{(TH)}$, $\Delta T=|Tcase-Tsub|$
Put DC into the Choke coil only

LD Characteristics

Module No.	108998	T-Case[℃]	25.0
		T-Sub[℃]	25.0

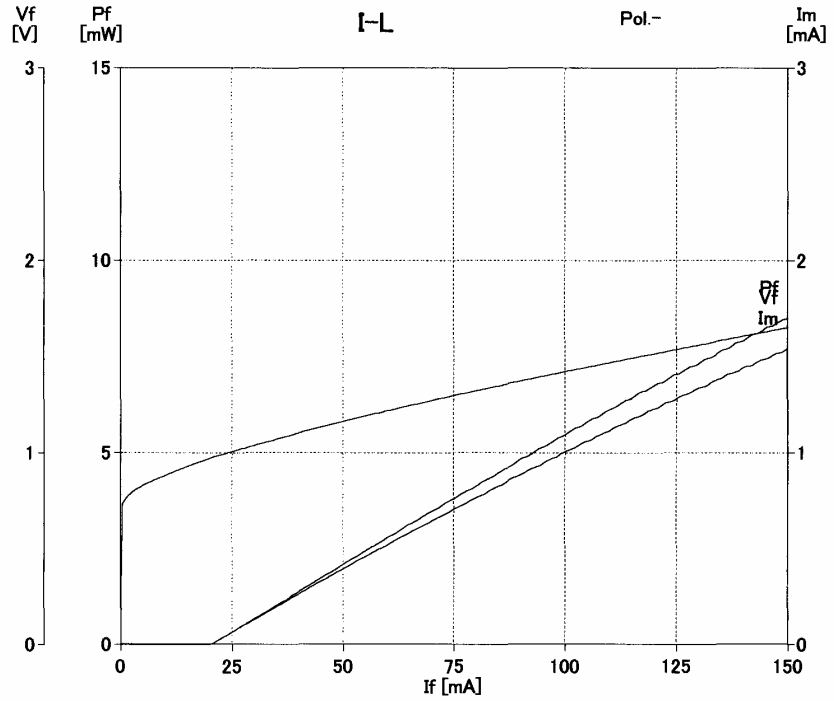

SPECTRUM

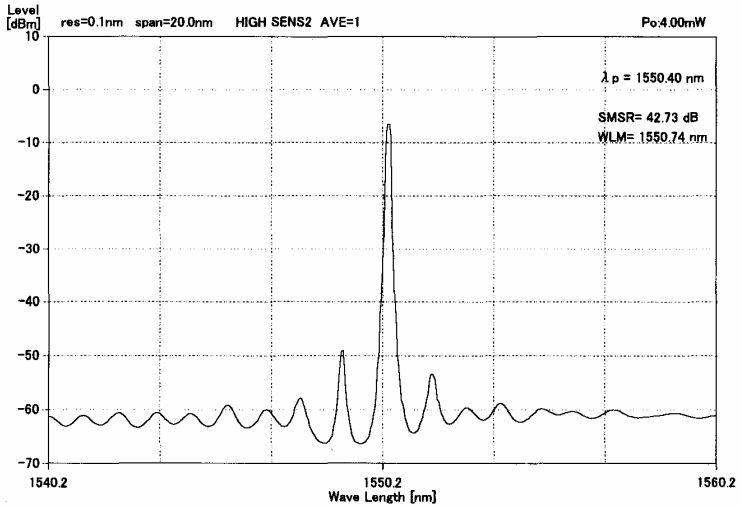

Grating type:	Non-Linear Chirp
Center Wavelength at 25degC, 10g (nm):	1550.065
Reflection bandwidth @ -3dB (nm):	5
Peak Reflectivity (%):	71
Fibre Type:	Photosensitive
Storage and operating temperature:	-40 to +85 degC

Reflection and Transmission Spectrum

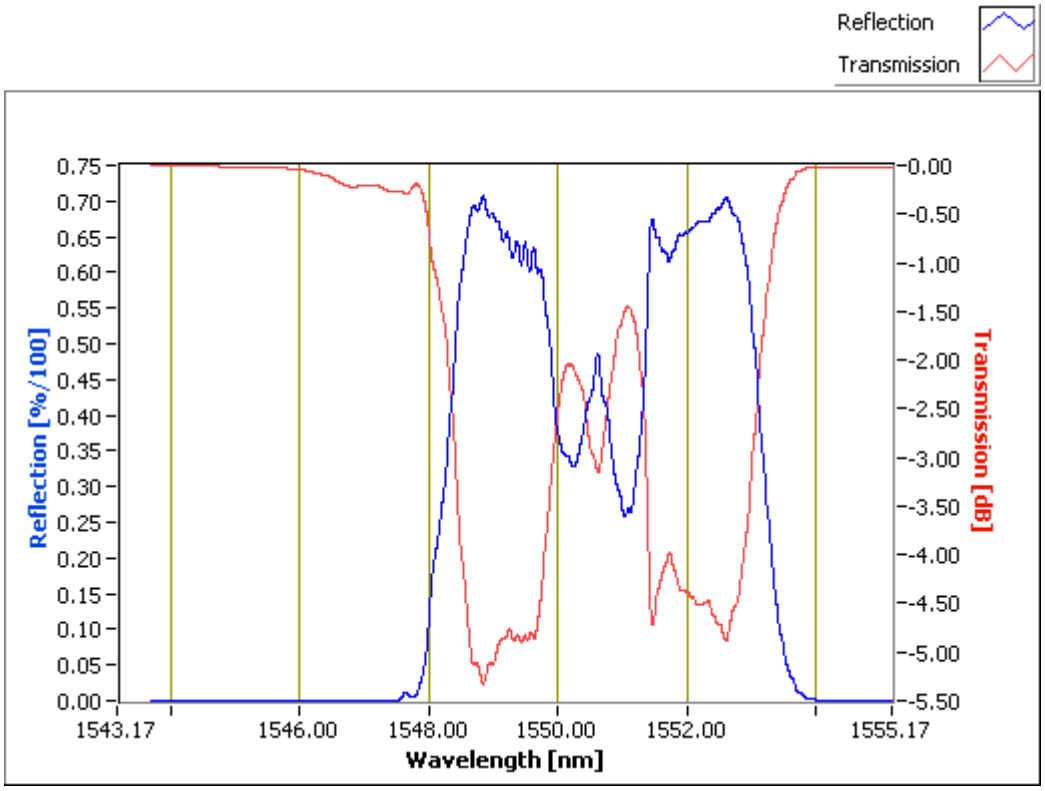

FBG position in relation to color marks on fiber

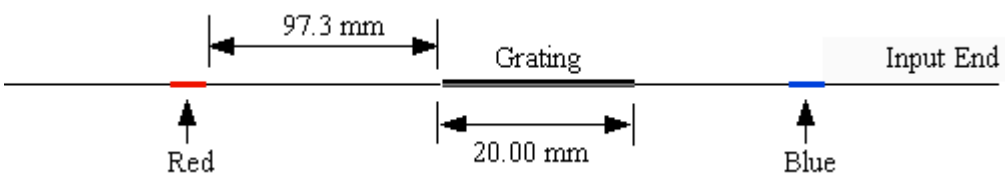

The measurement data has been shifted -0.65nm in order to maximize the fit between the Target GD profile and the Measured GD profile

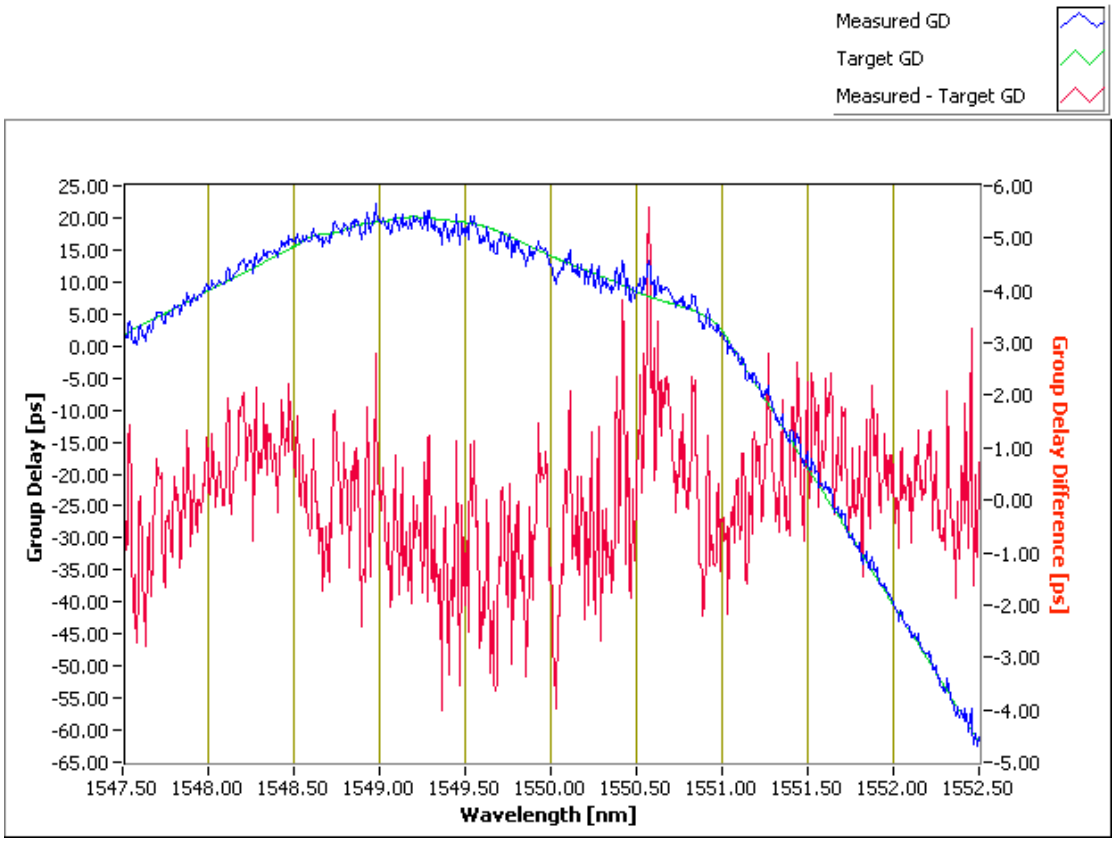

Device Performance

Part # **OPA-20-N-C-FA**
Device Serial # **39-03-020377**

Pin Allocation & Package Dimensions

pin	Description
1	TEC +
2	Thermistor
3	NC
4	NC
5	Thermistor
6	NC
7	NC
8	NC
9	NC
10	SOA Anode (+)
11	SOA Cathode (–)
12	NC
13	Case GND
14	TEC -

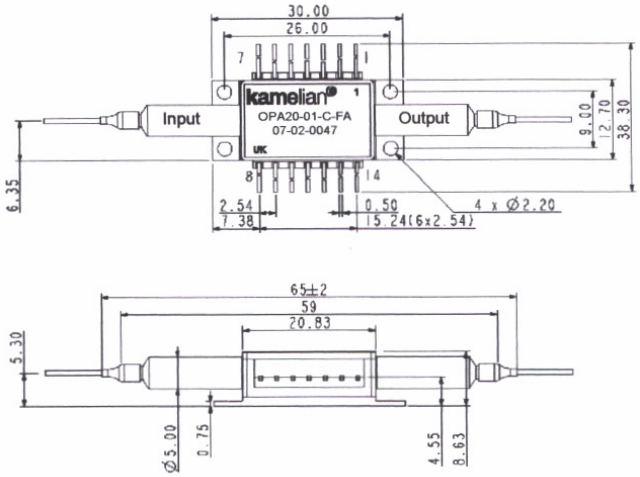

Maximum Ratings

Operating case temperature	-5 to +70 °C
Reverse voltage	< 3 V
Forward current	< 250 mA
TEC cooler current	< 2.0 A

LVI Characterisation

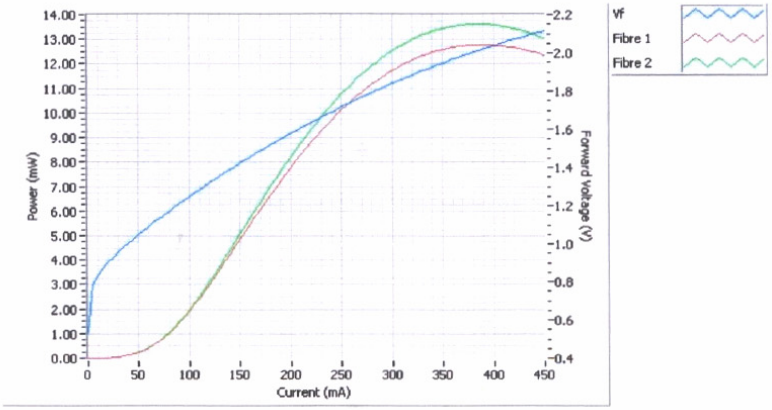

Gain vs Forward Current

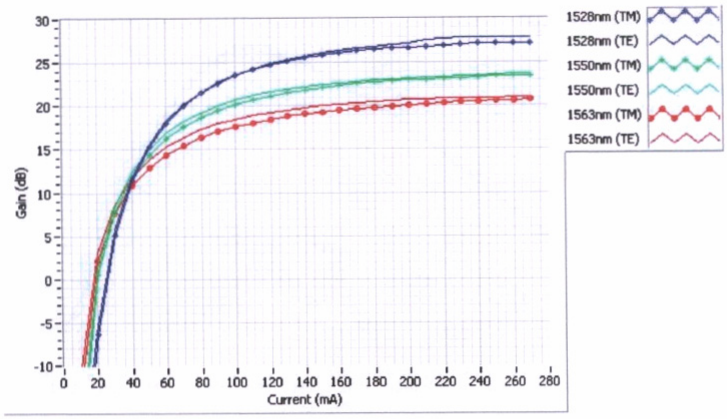

Gain vs Output Power

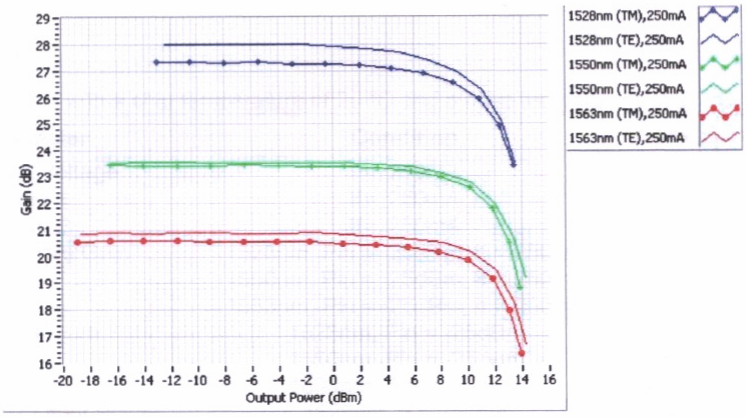

Noise Figure vs Forward Current

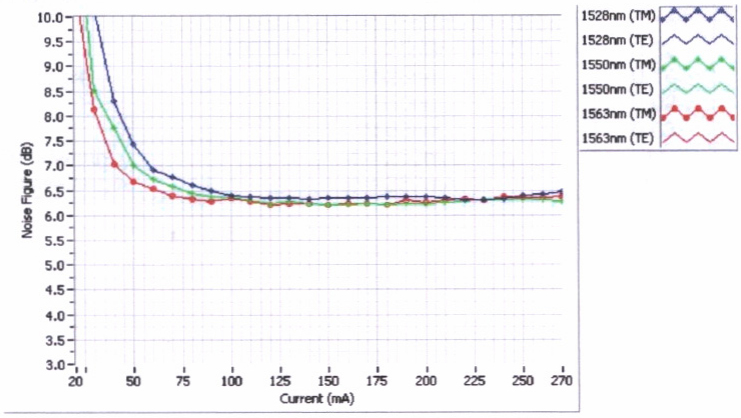

ASE Profile

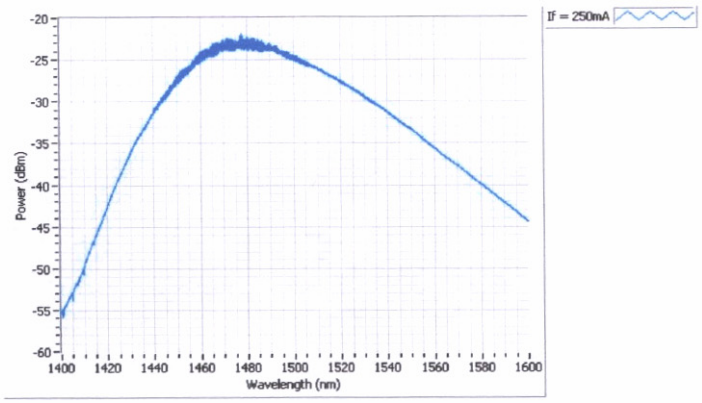

Test Summary

All tests performed with a chip temperature of 20 °C and a case temperature of 25 °C.

Parameter	Condition	Value	Units
Forward Voltage	If= 250mA	1.72	V
Fibre 1	If= 250mA	10.13	mW
Fibre 2	If= 250mA	10.77	mW
Fibre to Fibre Gain	1528nm, Pin = -25dBm, If = 250mA	27.57	dB
	1550nm, Pin = -25dBm, If = 250mA	23.40	dB
	1563nm, Pin = -25dBm, If = 250mA	20.65	dB
Noise Figure	1528nm, Pin = -25dBm	6.54	dB
	1550nm, Pin = -25dBm	6.40	dB
	1563nm, Pin = -25dBm	6.34	dB
Saturation Output Power	1528nm, If = 250mA	12.66	dBm
	1550nm, If = 250mA	13.50	dBm
	1563nm, If = 250mA	13.63	dBm
Polarisation Dependent Gain	1528nm, Pin = -25dBm, If = 250mA	0.71	dB
	1550nm, Pin = -25dBm, If = 250mA	0.14	dB
	1563nm, Pin = -25dBm, If = 250mA	0.32	dB
Gain Ripple	1528nm	0.14	dB
	1550nm	0.02	dB
	1563nm	0.03	dB
3dB Bandwidth	If = 250mA	44	nm
Centre Wavelength	If = 250mA	1477	nm

Device #02895

Centre for Integrated Photonics

SOA

Measured device results on fully packaged device. Results are provided for both linear and non-linear operation .

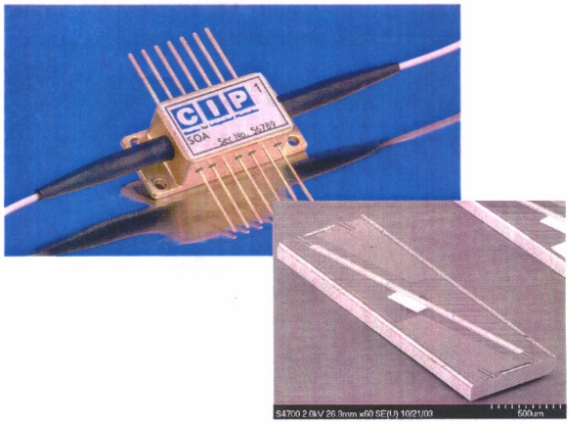

Unsaturated Results Summary

Device tested at 200mA and 20°C at 3 wavelengths in the C-band (1535 nm, 1550nm & 1560nm) for small signal input power of -30dBm. Tabulated results shown below.

Fibre coupling loss - input facet 1.6dB, output facet 1.5dB.

Parameter	1535nm	1550nm	1560nm
Gain	30.3dB	32.3dB	33.1dB
PDG	1.5dB	1.6dB	2.5dB
NF	8.6dB	8.0dB	7.4dB
Psat	8.6dBm	9.3dBm	9.5dBm

Saturated Polarisation dependent gain

Device tested at Pin=0dBm, 300mA and 20°C at 3 wavelengths in the C-band (1535 nm, 1550nm & 1560nm)

Parameter	1535nm	1550nm	1560nm
Saturated PDG	0.4dB	0.4dB	0.3dB

CIP Device Results Sheet

Device #02895

Centre for Integrated Photonics

Amplified spontaneous emission

Device tested at 20°C at 200mA drive current.

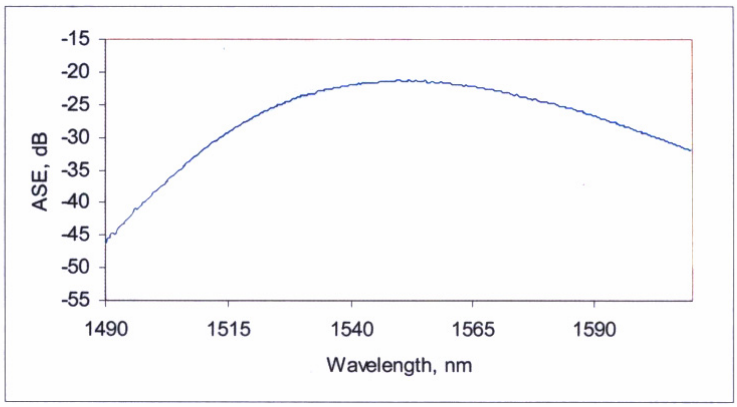

Non-Linear Results Summary

Device tested at 20°C at 300mA drive current. Pump/probe sampling measurements taken with:

Input 1550nm CW signal of 3.0dBm

Pulses (3ps) @ 2.5GHz and a wavelength of 1539nm

1/e recovery time is 14.0ps.

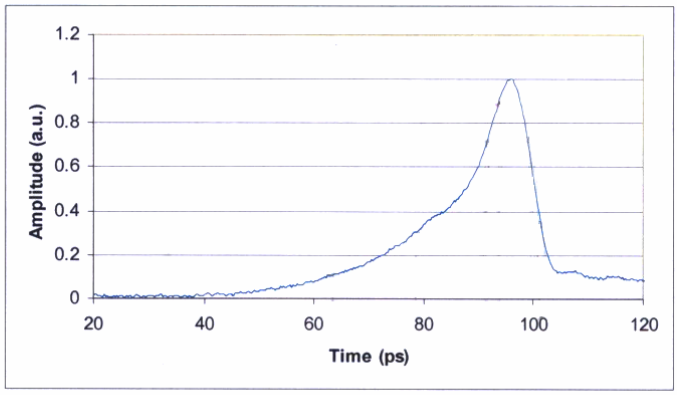

CIP Device Results Sheet

Centre for Integrated Photonics

SOA-NL-OEC-1550 - 1.55µm Non-Linear Semiconductor Optical Amplifier (SOA)

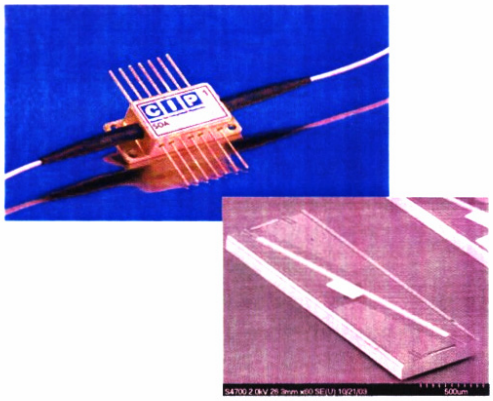

Features

- 1.55µm operation
- High gain (30dB)
- Low saturation output power
- Fast gain recovery times
- Low saturated PDG
- InP Buried Heterostructure design
- TEC cooled
- Available as packaged device or chip-on-carrier
- APC connectors provided

Application Examples

- All optical processing
- Wavelength conversion
- Cross-phase modulation
- Cross-gain modulation
- Four-wave mixing

Description

The non-linear SOA is a high confinement factor device optimised for high gain and fast gain recovery providing fast optical switching speeds. It utilises CIPs proprietary InP buried heterostructure design and is available in either a 14-pin butterfly package with a thermistor, thermo-electric cooler and single mode fibre pigtails or as a custom chip-on-carrier product including chip arrays.

The product is appropriate in wavelength converter or four wave mixing applications and is used in CIP's hybrid integrated regenerator/wavelength converter product (40G-2R-ORP). Custom specification variants may be defined as appropriate for other non-linear applications. Arrays of non-linear SOAs are also available either packaged or as chip-on-carrier.

Optical and electrical specifications

All measurements are at 20°C & 1535-1560nm unless stated otherwise.
I=bias current P_{IN}= Input optical power

Item	Test condition	Min.	Typ.	Max.	Unit
Small signal Gain	I = 200-300mA	25		34	dB
Polarisation Dependent Saturated Gain (PDG)	I = 300mA, P_{in}>0dBm		0.5	1	dB
Saturated Output Power (SOP)	I = 200mA	6			dBm
Gain Peak	I = 200mA	1550		1570	nm
Saturated Gain Recovery Time (1/e)	I = 300mA, P_{in}>0dBm, 1555nm			25	ps

APPENDIX III – LIST OF PUBLICATIONS ARISING FROM THIS WORK

Referred Journals

Performance Analysis of a Simple SOA Wavelegth Converter based on XPM and Shifted Filtering up to 80 Gbit/s

G. Girault, A.M Clarke, C. Guignard, P. Anandarajah, D. Reid, L. Bramerie, L.P. Barry, J.-C. Simon, and J. Harvey.

J. Lightwave Technol., to be published.

Investigation of Noise Suppression, Pulse Intensity and Chirp of an Actively Mode-Locked Semiconductor Fiber Ring Laser

I. Evans, C. O'Riordan, M.J. Connelly, L.P. Barry, A.M. Clarke, and P. Anandarajah.

Optics Commun., to be published.

Experimental Investigation of the Impact of Optical Injection on Vital Parameters of a Gain-Switched Pulse Source

C. Guignard, P.M. Anandarajah, A. Clarke, L.P. Barry, O. Vaudel, and P. Besnard.

Optics Commun., vol. 277, pp. 150-155, Apr. 2007.

System Performance Analysis of Optimized Gain Switched Pulse Source Employed in 40 and 80 Gb/s OTDM Systems

P.M. Anandarajah, A.M. Clarke, C. Guignard, L. Bramerie, L.P. Barry, J.D. Harvey, and J.C. Simon.

J. Lightwave Technol., vol. 25, pp. 1495-1502, June 2007.

80-Gb/s OTDM System Analysis of a Vertical Microcavity-Based Saturable Absorber for the Enhancement of Pulse Pedestal Suppression

A.M. Clarke, P.M. Anandarajah, L. Bramerie, C. Guignard, R. Maher, D. Massoubre, A. Shen, J.L. Oudar, L.P. Barry, and J.C. Simon.

IEEE Photonics Technol. Lett., vol. 19, pp. 321-323, Mar. 2007.

Optimized Pulse Source Employing an Externally Injected Gain-Switched Laser Diode in Conjunction with a Nonlinearly Chirped Grating

P.M. Anandarajah, C. Guignard, A. Clarke, D. Reid, M. Rensing, L.P. Barry, G. Edvell, and J.D. Harvey.

IEEE J. Sel. Top. Quantum Electron., vol. 12, pp. 255-264, Mar/Apr. 2006.

Optimized Pulse Source for 40-Gb/s Systems based on a Gain-Switched Laser Diode in Conjunction with a Nonlinearly Chirped Grating

A. Clarke, P.M. Anandarajah, D. Reid, G. Edvell, L.P. Barry, and J.D. Harvey.

IEEE Photonics. Technol. Lett., vol. 17, pp. 196-198, Jan. 2005.

Investigation of Pulse Pedestal and Dynamic Chirp Formation on Picosecond Pulses after Propagation Through an SOA

A.M. Clarke, M.J. Connelly, P. Anandarajah, L.P. Barry, and D. Reid.

IEEE Photonics Technol. Lett., vol. 17, pp. 1800-1802, Sept. 2005.

Generation of Widely Tunable Picosecond Pulses with large SMSR by Externally Injecting a Gain-Switched Dual Laser Source

A.M. Clarke, P.M. Anandarajah, and L.P. Barry.

IEEE Photonics Technol. Lett., vol. 16, pp. 2344-2346, Oct. 2004.

Self-Seeding of a Gain-Switched Integrated Dual-Laser Source for the Generation of Highly Wavelength-Tunable Picosecond Optical Pulses

P. Anandarajah, P.J. Maguire, A. Clarke, and L.P. Barry.

IEEE Photonics Technol. Lett., vol. 16, pp. 629-631, Feb. 2004.

Conference Papers

FROG Characterisation of a Turbo-Switch Wavelength Converter

X. Yang, A.M. Clarke, R. Maher, R.P. Webb, R.J. Manning, and L.P. Barry.

33rd European Conf. Optical Commun. (ECOC'07), to be published, Berlin, Germany, 16-20 Sep. 2007.

Numerical Analysis of Picosecond Pulse Propagation in a Tensile-Strained Semiconductor Optical Amplifier with Parameter Extraction using Frequency Resolved Optical Gating

M.J. Connelly, A.M. Clarke, P.M. Anandarajah, and L.P. Barry.

Euro. Conf. on Integrated Optics (ECIO 2007), paper P6, Copenhagen, Denmark, Apr. 2007.

FROG Characterisation of SOA-based Wavelength Conversion using XPM in Conjunction with Shifted Filtering up to Line Rates of 80 GHz

A.M. Clarke, G. Girault, P. Anandarajah, C. Guignard, L. Bramerie, L.P. Barry, J.C. Simon, and J. Harvey.

IEEE Lasers and Electro-Optics Society 19th Annual Meeting (LEOS), paper MP2, Montreal, Canada, Oct/Nov 2006.

Performance of Pulse Source Consisting of an Externally Injected Gain-Switched Laser followed by a Non-Linearly/Linearly Chirped Grating in an 80 Gb/s OTDM System

R. Maher, P. Anandarajah, A. Clarke, C. Guignard, L.P. Barry, L. Bramerie, and J. Harvey.

IEEE Lasers and Electro-Optics Society 19th Annual Meeting (LEOS), paper ThX3, Montreal, Canada, Oct./Nov. 2006.

Optimized Pulse Source for use in Broadband Photonic Communication Systems

P.M. Anandarajah, A. Clarke, C. Guignard, L.P. Barry, D. Reid, and J.D. Harvey.

China-Ireland International Conference on Information and Communications Technologies 2006, CIICT06, paper 134, Hangzhou, China, 18-19 Oct. 2006.

Enhancement of System Performance in 80 Gb/s OTDM Systems by using a Vertical Microcavity based Saturable Absorber

A.M. Clarke, P.M. Anandarajah, L. Bramerie, C. Guignard, D. Massoubre, A. Shen, J.L. Oudar, L P. Barry, and J.C. Simon.

32nd European Conf. Optical Commun. (ECOC'06), paper Th. 1.4.6, Cannes, France, 24-28 Sep. 2006.

Performance of 80 Gb/s OTDM system Employing Gain-Switched Pulses Compressed by a Linearly and a Nonlinearly Chirped Grating

P. Anandarajah, A. Clarke, C. Guignard, L. Bramerie, L. Barry, J.D. Harvey, and J.C. Simon.

32nd European Conf. Optical Commun. (ECOC'06), paper Th. 3.5.3, Cannes, France, 24-28 Sep. 2006

Shaping of Externally Injected Gain-Switched Pulses using a Tailor Made Non-Linearly Chirped Fibre Bragg Grating

P.M. Anandarajah, A. Clarke, C. Guignard, and L.P Barry.

4th International Symposium on Materials and Devices for Nonlinear Optics (ISOPL 2006), vol. 1 pp. 67, Dingle, Ireland, 27-30 June 2006.

FROG Characterisation of SOA-based Wavelength Conversion at 80 Gb/s using Bandpass Filtering

A. Clarke, G. Girault, L.P. Barry, and J.C. Simon.

4th International Symposium on Materials and Devices for Nonlinear Optics (ISOPL 2006), vol. 1, pp. 47-48, Dingle, Ireland, 27-30 June 2006.

Investigation of SOA-based Wavelength Conversion at 80 Gb/s using Bandpass Filtering

L. Bramerie, A. Clarke, G. Girault, S. Lobo, M. Gay, C. Guignard, V. Roncin,, B. Kennedy, P. Maguire, S. Feve, B. Clouet, F. Ginovert, L.P. Barry, and J.C. Simon.

Conf. Lasers and Electro-Optics (CLEO'06), paper CMT7, Long Beach, USA, 15-19 May 2006.

Pulse Source for 80 Gb/s Systems using a Gain-Switched Laser Diode followed by a Nonlinearly Chirped Grating

A. Clarke, M. Rensing, P. Anandarajah, L.P. Barry, J.D. Harvey, D. Reid, G. Edvell, and C. Guignard.

IEEE Lasers and Electro-Optics Society 18th Annual Meeting (LEOS), pp. 988-989, Sydney, Australia, 22-28 Oct. 2005.

80 Gb/s Optimised Pulse Source using a Gain-Switched Laser Diode in Conjunction with a Nonlinearly Chirped Grating

A.M. Clarke, M. Rensing, D. Reid, P. Anandarajah, L.P. Barry, J.D. Harvey, and G. Edvel

31st European Conf. Optical Commun. (ECOC'05), paper Th. 1.3.5, Glasgow, Scotland, 25-29 Sep. 2005.

Numerical Analysis of Pulse Pedestal and Dynamic Chirp Formation on Picosecond Modelocked Laser Pulses after Propagation through a Semiconductor Optical Amplifier

M.J. Connelly, A.M. Clarke, P.M. Anandarajah, and L.P. Barry

5th International Conf. on Numerical Simulation of Optoelectronic Devices (NUSOD '05), pp. 129-130, Berlin, Germany, 19-22 Sep. 2005.

80 Gb/s Optimised Pulse Source using a Gain-Switched Laser Diode in Conjunction with a Nonlinearly Chirped Grating

A. Clarke, M. Rensing, P. Anandarajah, L. Barry, J. Harvey, and G. Edvell

7th International Conf. on Transparent Optical Networks, (ICTON '05), vol. 2, pp. 337-340, Barcelona, Spain, 3-7 July 2005.

Characterisation of Picosecond Optical Pulses Propagating through a Semiconductor Amplifier using Frequency Resolved Optical Gating

A. Clarke, D. Reid, P. Anandarajah, and L.P. Barry

SPIE OptoIreland, pp. 5825-49, Technical Proceedings, Dublin, Ireland, 4-6 Apr. 2005.

Optimized Pulse Source Based on a Gain-Switched Laser Diode in Conjunction with a Non-Linearly Chirped Grating for 40 Gbit/s Systems

A. Kazubowska, A, Clarke, D. Reid, G. Edvell, S. Roumieux, P.M. Anandarajah, L.P. Barry, and J.D. Harvey

IEEE Lasers and Electro-Optics Society 17th Annual Meeting (LEOS), vol. 2, pp. 687-688, Peurto Rico, 7-11 Nov. 2004.

Wavelength-Tunable Transform-Limited Optical Pulse Generation using External-Injection of Two Fabry-Perot Gain-Switched Laser Diodes at 10GHz

P.J. Maguire, A.M. Clarke, C. Mulligan, P.M. Anandarajah, and L.P. Barry

Emerging Technology in Optical Sciences (ETOS'04), University College Cork, Ireland, 26-29 June 2004.

Characterisation of Picosecond Pulses Propagating through a Semiconductor Optical Amplifier using Frequency Resolved Optical Gating

A.M. Clarke, P. Anandarajah, L.P. Barry, and D.A. Reid

Emerging Technology in Optical Sciences (ETOS'04), University College Cork, Ireland, 26-29 June 2004.

External Injection of a Gain Switched Integrated Dual Laser Source for the Generation of Widely Tunable Picosecond Pulses with Large SMSR

A.M. Clarke, P. Anandarajah, P.J. Maguire, and L.P. Barry

Conf. Lasers and Electro-Optics (CLEO'04), paper CTuN2, San Francisco, USA, 16-21 May 2004.

Generation of Widely Tunable Picosecond Pulses With Large SMSR by Externally Injecting a Gain-Switched Dual Laser Source

A. M. Clarke, P. M. Anandarajah, and L. P. Barry

***Abstract*—The authors demonstrate a procedure of generating picosecond optical pulses that are tunable over a wide wavelength range (65 nm) and have very high spectral purity side-mode suppression ratio [(SMSR)$>$ 60 dB]. The large tuning range is obtained by employing external injection into a gain-switched source containing two Fabry–Pérot lasers. The use of a widely tunable Bragg grating at the output improves the SMSR such that it exceeds 60 dB over the entire tuning range.**

***Index Terms*—External injection, optical fiber communications, optical pulse generation, semiconductor laser, wavelength tunable source.**

I. Introduction

As THE demand for high-speed communications applications such as wavelength-division multiplexing (WDM) and optical time-division multiplexing (OTDM) continues to grow, there will be an increasing need to develop optical pulse sources suitable for these systems. Current trends may result in the operation of optical communication systems at line rates of 40 Gb/s and beyond, thereby making it more likely that return-to-zero coding be used for data transmission, as it is easier to compensate for dispersion and nonlinear effects in the fiber [1]. Furthermore, next-generation WDM systems that employ dynamic provisioning with the use of wavelength tunability are attracting a lot of interest. Thus, the key requirements on picosecond pulse sources to be used in high-speed communications applications will include broad wavelength tuning range, a high side-mode suppression ratio (SMSR), variable repetition rates, low timing jitter, and small frequency chirp [2]–[4].

Picosecond pulse generation can be accomplished through various methods, such as external modulation of a continuous-wave (CW) light signal [4], mode locking [5], and gain switching [6]. Gain switching of a semiconductor laser diode is probably one of the most reliable methods to generate optical pulses, and by employing self seeding [7] of a gain-switched Fabry–Pérot (FP) laser, it is possible to obtain high-quality wavelength tunable single-mode pulses which have low timing jitter and good spectral purity. Nonetheless, a major disadvantage with the self-seeded gain-switched (SSGS) scheme is that the length of the external cavity has to be continuously tuned so that the pulse repetition frequency is an integer multiple of the cavity round-trip frequency. An alternative technique entails external injection of light from a CW source into a gain-switched laser [8]–[10]. No adjustment of the repetition frequency or external cavity length is required in this case. Thus, external injection provides a more stable operation, even though a CW tunable laser is commonly required. Recent work has established that as the number of channels in a WDM system using SSGS pulse sources increases, the specifications on the required SMSR due to cross-channel interference may become very stringent [3]. Thus, if externally injected gain-switched lasers are to be used in future high-speed systems, it will be necessary to improve the SMSR of these sources to beyond 30 dB.

In this letter, we build on recent research we have undertaken which involved self-seeding of a gain-switched dual laser source [11]. This article demonstrates the use of external injection into a gain-switched transmitter comprising of two FP lasers to generate picosecond pulses that are tunable over 65 nm, with SMSRs in excess of 60 dB over the entire tuning range. This is the largest tuning range and SMSR that has ever been achieved for an optical pulse source based on gain-switched laser diodes.

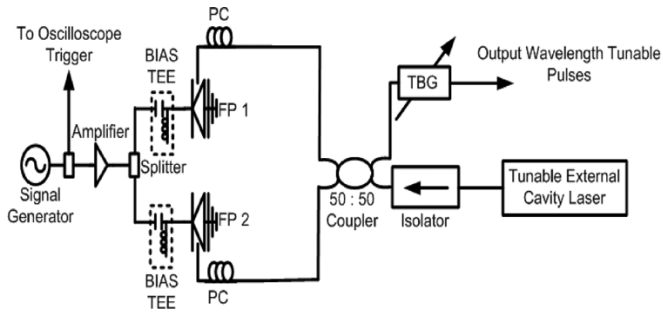

Fig. 1. Experimental setup for the generation of widely tunable externally injected gain-switched pulses.

II. Experimental Setup

The experimental setup is illustrated in Fig. 1. The lasers FP1 and FP2 are commercial 1.5-μm InGaAsP devices, with threshold currents of 19 and 26 mA, respectively. The lasers were chosen so that their gain profiles provided only a small overlap, which corresponds to the maximum wavelength of FP1, and the minimum wavelength of FP2, at which we can achieve

Manuscript received February 13, 2004; revised June 15, 2004. This work was supported by the Science Foundation Ireland Investigator Programme.

The authors are with the Research Institute for Networks and Communications Engineering, School of Electronic Engineering, Dublin City University, Dublin 9, Ireland (e-mail: liam.barry@eeng.dcu.ie).

Digital Object Identifier 10.1109/LPT.2004.834523

suitable SMSRs using the external injection configuration. Continuous wavelength tuning of the laser modes over the gain profiles of the two devices can be achieved by temperature controlling the diodes. The gain-switching process involves applying a sinusoidal modulation signal (peak-to-peak current ∼200 mA; frequency ∼2.5 GHz) to both lasers, in addition to dc bias currents of 15 and 26 mA for FP1 and FP2, respectively. The optical signal from both lasers is then coupled into fiber using a GRIN lens fiber pigtail. External injection requires injecting CW light from a tunable external cavity laser (ECL) into one of modes of the two FP lasers via an isolator, a 3-dB coupler, and a polarization controller (PC). The PC is varied in order to ensure optimum coupling of the injected light from the ECL into the selected FP laser cavity, which in turn optimizes the SMSR of the laser output. The output power of the CW source is set at −3 dBm, however, taking into account various losses, we estimate the injection level into the gain-switched sources to be about −13 dBm. The resulting single-mode output obtained after external injection into one of the FP lasers, together with the gain-switched signal from the FP laser that is not affected by the external injection (because the signal injected from the ECL does not lie within the gain curve of this FP diode), is then passed through a tunable Bragg grating (TBG) filter. The TBG has a bandwidth of 0.23 nm, a wavelength tuning range of 1460–1575 nm, and an insertion loss of 5 dB. The filter is used to eliminate the optical output from the gain-switched FP laser that is not influenced by the external injection, and also to enhance the SMSR of the generated pulses. The output pulses are characterized using a 50-GHz photodiode in conjunction with a 50-GHz oscilloscope, and an optical spectrum analyzer (OSA) with a 0.05-nm (6 GHz) resolution.

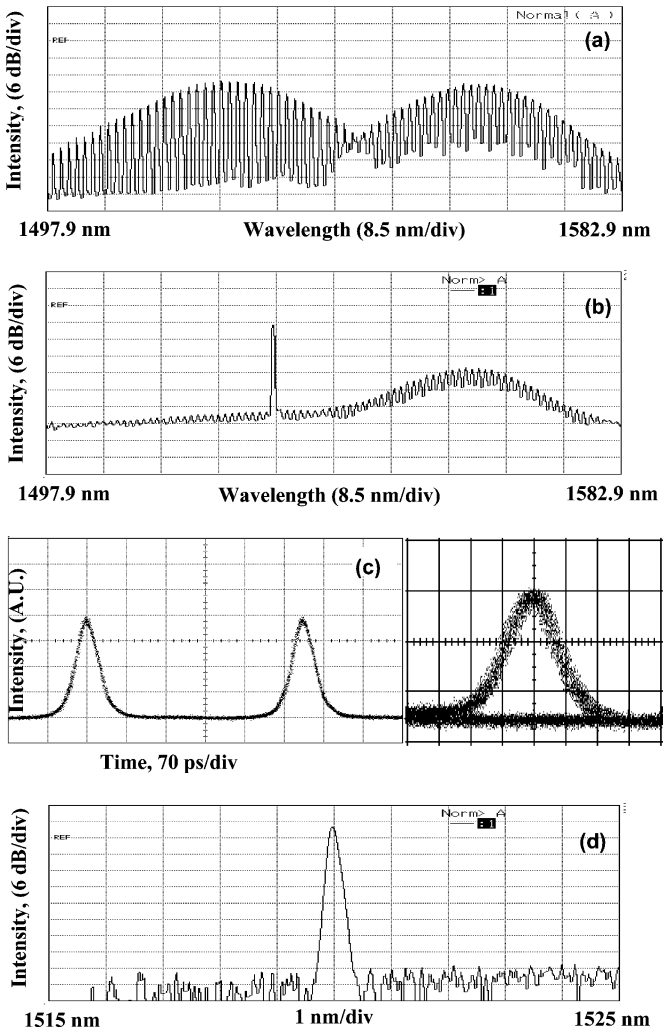

Fig. 2. (a) Optical spectrum of dual gain-switched source, (b) spectrum before the filter at 1519.9 nm, (c) pulse at 1519.9 nm (with inset showing extinction ratio), and (d) spectrum after the filter at 1519.9 nm.

III. Results and Discussion

The optical spectrum of the dual wavelength signal from the gain-switched lasers, without external injection, is shown in Fig. 2(a). It can clearly be seen that by combining the output of the gain-switched lasers in the wavelength domain, the composite span of the laser profiles that could be used for seeding has been greatly increased. The peak of the spectrum for FP1 is at 1524 nm, while the peak of the spectrum for FP2 is at 1561 nm. As we can see from the composite spectra of the two gain-switched lasers, the spectra from the individual gain-switched devices overlap at about 16 dB down from the peak of the spectra.

Different longitudinal modes of each FP laser were selectively excited when the seeding wavelength from the ECL was tuned near the center of any desired mode. Fig. 2(b) displays the resulting spectral output before the optical filter showing good SMSR for the seeded gain-switched diode. With the addition of the filter, the optical output from the unseeded FP laser is eliminated, and the SMSR of the output pulses is improved such that it becomes almost impossible to detect the side-modes above the noise floor of the OSA. The resulting SMSR is around 60 dB for the entire wavelength tuning range that can be achieved with this setup. Examples of the temporal (nonaveraged) and spectral profile of the output pulse (at 1520 nm) are shown in Fig. 2(c) and (d), and we can clearly see the excellent temporal and spectral purity of the pulse source. The pulse duration was about 28 ps while the spectral width was approximately 20 GHz (this spectral width is clearly not limited by the bandwidth, 29 GHz, of the optical filter), resulting in a time-bandwidth product of 0.56 (slightly larger than that for transform-limited Gaussian pulses). The extinction ratio of the generated pulses was measured to be 25 dB, and the timing jitter was estimated to be less than 1 ps. The timing jitter was measured to be 1 ps by using histogram analysis on an Agilent Digital Communications Analyzer, however, given that 1 ps is the lower limit on this measurement, we conclude that the jitter is actually less than 1 ps.

Fig. 3 illustrates the SMSR as a function of wavelength, across the tuning range of the pulse source. We obtain values greater than 60 dB over the complete wavelength span. It is important to note that the use of the filter in this setup is dependent on achieving a suitably high SMSR from the gain-switched externally injected laser before the filter (we have verified that this value remains above 30 dB in our work). If this is not the case then mode-partition-noise could seriously affect the temporal quality of the pulse source (from Fig. 2(c), this is clearly not the

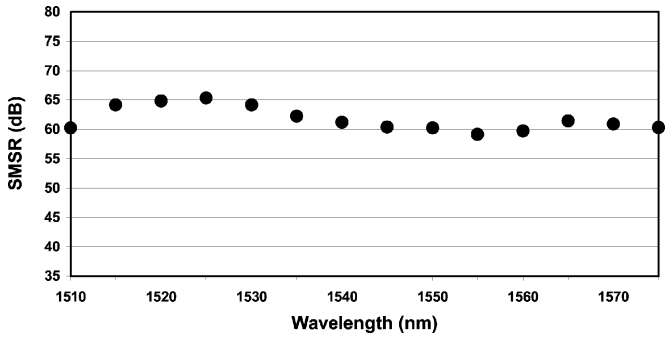

Fig. 3. SMSR of output pulses as a function of wavelength.

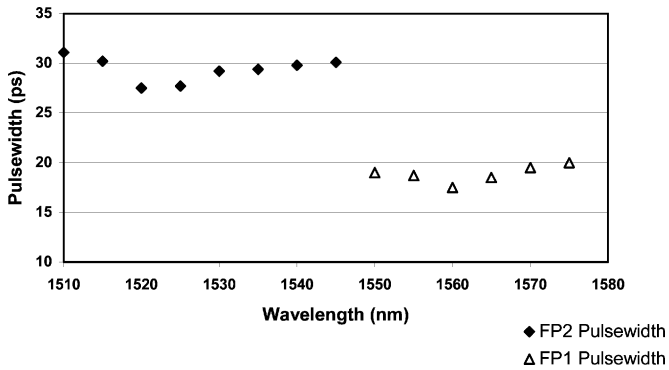

Fig. 4. Pulsewidths of optical output pulses as a function of wavelength tuning range.

case). Fig. 4 shows the variation in pulsewidth over the tuning range. The variation in pulsewidth around 1545 nm is due to the external injection from the ECL changing from seeding FP1 to seeding FP2. Differences in various physical parameters (e.g., gain) of the two lasers are responsible for the variation in output pulsewidth. In addition, the output spectral width from the higher wavelength laser (FP2) is slightly increased (from 20 to 29 GHz), and in this case, does become limited by the bandwidth of the output filter. Our experimental results exhibited very stable operation even at the crossover section from operation with FP1 to FP2. This is achieved because there is no overlap between the modes from the two different FP lasers, and thus, we never inject light into the same mode of both FP lasers at the same time.

IV. Conclusion

This experiment has demonstrated a simple and effective procedure of generating widely tunable ($\sim$65 nm) pulses with impressive SMSR ($>$60 dB) by using external injection into a source consisting of two gain-switched FP lasers. Such a source could play a vital part in ensuring the optimal performance of high-speed hybrid WDM/OTDM optical communication networks. It should also be noted that the tuning range could be expanded further by introducing a third FP laser with an appropriate spectral profile, and that by simultaneously injecting light into the FP lasers used, it may also be possible to develop a multiwavelength pulse source.

References

[1] R. Ludwig, U. Feiste, E. Dietrich, H. G. Weber, D. Breuer, M. Martin, and F. Küppers, "Experimental comparison of 40 Gbit/s RZ and NRZ transmission over standard single mode fiber," *Electron. Lett.*, vol. 35, pp. 2216–2218, 1999.

[2] C.-K. Chan, K. L. Sherman, and M. Zirngibl, "A fast 100-channel wavelength-tunable transmitter for optical packet switching," *IEEE Photon. Technol. Lett.*, vol. 13, pp. 729–731, July 2001.

[3] P. Anandarajah, L. P. Barry, and A. Kaszubowska, "Performance issues associated with WDM optical systems using self-seeded gain-switched pulse sources due to mode partition noise," *IEEE Photon Technol. Lett.*, vol. 14, pp. 1202–1204, Aug. 2002.

[4] S. Kawanishi, "Ultrahigh-Speed optical time division-multiplexed transmission technology based on optical signal processing," *IEEE J. Quantum Electron.*, vol. 34, pp. 2064–2079, Nov. 1998.

[5] J. E. Bowers, P. A. Morton, A. Mar, and S. W. Corzine, "Actively mode-locked semiconductor lasers," *IEEE J. Quantum Electron.*, vol. 25, pp. 1426–1439, June 1989.

[6] K. Y. Lau, "Gain-switching of semiconductor injection lasers," *Appl. Phys. Lett.*, vol. 52, pp. 257–259, 1988.

[7] D. Huhse, M. Schell, W. Utz, J. Kaessner, and D. Bimberg, "Dynamics of single-mode formation in self-seeded Fabry–Pérot laser diodes," *IEEE Photon. Technol. Lett.*, vol. 7, pp. 351–353, Apr. 1995.

[8] L. P. Barry, J. Debeau, and R. Boittin, "40 nm tunable source of picosecond pulses at 10 GHz by external injection into a gain switched FP laser," in *Proc. Eur. Conf. Optical Communications*, vol. 1, Florence, 1994, pp. 555–558.

[9] Y. Matsui, S. Kutsuzawa, S. Arahira, and Y. Ogawa, "Generation of wavelength tunable gain-switched pulses from FP MQW lasers with external injection seeding," *IEEE Photon. Technol. Lett.*, vol. 9, pp. 1087–1089, Aug. 1997.

[10] M. Zhang, D. N. Wang, H. Li, W. Jin, and M. S. Demokan, "Tunable dual wavelength picosecond pulse generation by the use of two Fabry–Pérot laser diodes in an external injection seeding scheme," *IEEE Photon. Technol. Lett.*, vol. 14, pp. 92–94, Jan. 2002.

[11] P. Anandarajah, P. J. Maguire, A. Clarke, and L. P. Barry, "Self-seeding of a gain switched integrated dual laser source for the generation of highly wavelength tunable picosecond optical pulses," *IEEE Photon. Technol. Lett.*, vol. 16, pp. 629–631, Feb. 2004.

80-Gb/s OTDM System Analysis of a Vertical Microcavity-Based Saturable Absorber for the Enhancement of Pulse Pedestal Suppression

A. M. Clarke, *Student Member, IEEE*, P. M. Anandarajah, *Member, IEEE*, L. Bramerie, C. Guignard, R. Maher, *Student Member, IEEE*, D. Massoubre, A. Shen, J. L. Oudar, L. P. Barry, *Member, IEEE*, and J. C. Simon

***Abstract*—In future high-speed optical time-division-multiplexed (OTDM) systems, an important factor that needs to be considered for optical pulse generation schemes is the impact of pulse pedestals on the overall system performance. The results presented in this letter are two-fold; first, the impact due to the height of pulse pedestals in an 80-Gb/s OTDM system are established. Second, a solution is provided to overcome these high pedestal levels through the use of a vertical microcavity saturable absorber, which can significantly reduce the pulse pedestal level and give enhanced system performance.**

***Index Terms*—Optical pulse shaping, optical time-division multiplexing (OTDM), pulse generation, saturable absorber (SA).**

I. Introduction

FUTURE high-speed communications systems are likely to employ optical time-division multiplexing (OTDM) due to simpler system configuration at increasing bit rates, relating to more cost-efficient systems [1]. One of the key components in such high-capacity OTDM systems is the picosecond optical pulse source, which should exhibit excellent temporal and spectral purity. One particular parameter of the optical pulse source which is important in OTDM systems is the extinction ratio (ER) [or temporal pedestal suppression ratio (TPSR)]. It has been shown in previous work that a 40-Gb/s OTDM system requires a TPSR of 30 dB [2] to prevent power penalties due to coherent interactions between the individual OTDM channels. The actual ER or TPSR required to prevent degradation of system performance will depend on the number of return-to-zero channels multiplexed together to obtain the overall OTDM signal, which in turn will be determined by the pulsewidth and repetition rate of the optical pulse source employed at the transmitter.

Considering the main pulse generation techniques available, namely, mode-locking, gain-switching, and use of electroabsorption modulators (EAMs), it is extremely difficult to achieve a TPSR in excess of 30 dB. In order to overcome this limitation of these sources, a number of techniques have been developed to improve the TPSR of optical pulses. These techniques include the use of an EAM [3], a nonlinear amplifying loop mirror (NALM) [4], or self-phase modulation in a semiconductor optical amplifier (SOA) in conjunction with shifted filtering [5]. The EAM can provide high TPSR values; however, it is an active and expensive component which may significantly increase the cost of the pulse source. The NALM is fiber-based, which makes it bulky, and suffers from instability problems, and the SOA scheme exhibits limited TPSR improvement ($\sim$7 dB). The limitation of these three ER enhancement techniques may be overcome by the use of a vertical microcavity-based saturable absorber (SA). This is a passive device that can be monolithically integrated with semiconductor laser sources. The SA is very efficient for ER enhancement and "space" noise attenuation. Furthermore, the efficiency of SA coupled with fiber or semiconductor techniques allowing "mark" fluctuations reduction has been demonstrated at 10 and 40 Gb/s [6], [7]. In [8], the authors have shown the enhancement of the ER of a 160-GHz optical pulse train by employing the microcavity-based SA. This improvement in ER is vital for OTDM systems. In this letter, we simulate and experimentally characterize the power penalties introduced by optical pulses with varying levels of TPSR in an 80-Gb/s OTDM system. We then present the TPSR improvement obtained using the SA ($>$15 dB) for different input TPSR levels, and subsequently demonstrate the improvement in system performance (3.3 dB), which is obtained as a result of the increased TPSR, in an 80-Gb/s OTDM system using bit-error-rate (BER) measurements.

II. Experimental Setup

A. Characterization of the Pulses Before and After the SA

The experimental setup used to introduce the pulse pedestals with varying levels, and subsequently reduce the pedestal height using the SA, is shown in Fig. 1. An actively mode-locked semiconductor laser that generates 2.1-ps pulses with a time-bandwidth-product (TBP) of 0.35. These pulses were split by a 3-dB coupler; one arm (for pedestal generation) was delayed by around 8 ps with respect to the main pulse, and attenuated via a variable optical attenuator (VOA). The pedestal delay of 8 ps was chosen as this delay corresponded to the point where the penalty due to the introduced pedestal level becomes significant. As the delay is increased, the penalty correspondingly increases for the same TPSR as the power

Manuscript received September 22, 2006; revised December 19, 2006. This work was supported in part by the Science Foundation Ireland Investigator Program and in part by the Enterprise Ireland Development Project.

A. M. Clarke, P. M. Anandarajah, C. Guignard, R. Maher, and L. P. Barry are with RINCE, School of Electronic Engineering, Dublin City University, Dublin 9, Ireland (e-mail: liam.barry@dcu.ie).

L. Bramerie and J. C. Simon are with ENSSAT, PERSYST Platform, UMR FOTON, 22300 Lannion, France (e-mail: Laurent.bramerie@persyst.fr).

D. Massoubre and J. L. Oudar are with LPN-CNRS, 91460 Nozay, France (e-mail: jean-louis.oudar@lpn.cnrs.fr).

A. Shen is with Alcatel-Thales III-V Lab, 91767 Palaiseau, France (e-mail: alexandre.shen@3-5lab.fr).

Digital Object Identifier 10.1109/LPT.2007.891594

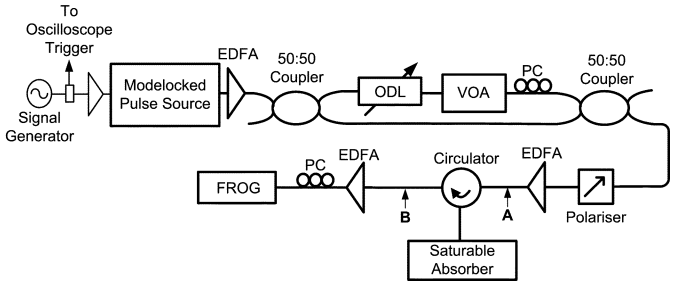

Fig. 1. Experimental setup used to introduce pedestals and SA to the pulse source.

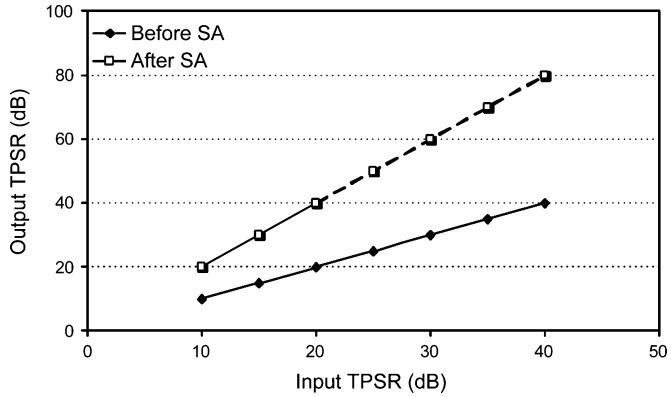

Fig. 2. Graph of input and output TPSR to the SA measured at Point A and B, respectively, by the FROG. The TPSR values are extrapolated at values greater than 40 dB (represented by a dashed line) as the FROG is limited by the noise floor of the system.

overlap between the next pulse and pedestal increases until it reaches the bit slot duration (12.5 ps). The increase in pulse and pedestal overlap leads to a larger generation of interferometric noise. The main pulse and pedestal were then recombined via a second coupler. A polarization controller and a polarizer were used to match the polarization of the main pulse with the pedestal so that an accurate measurement of the TPSR could be taken by using the technique of frequency-resolved optical gating (FROG) [9].

An SA was then introduced via a circulator. The SA used is a seven-quantum-well structure (InGaAs–InAlAs) in a resonant microcavity with a dielectric mirror ($2x[TiO_2–SiO_2]$) as the front mirror, and a broadband high-reflectivity metallic-based mirror ($Ag+SiO_2$) as the back mirror [10]. A heavy-ion-irradiation shortens the absorption recovery time down to 1.5 ps, which is short enough for the SAs to be employed in 160-Gb/s OTDM systems.

By varying the VOA, the height of the pedestal can be set to different values, and then measured using the FROG before (Point A) and after the SA (Point B), as shown in Fig. 2. The TPSR is improved by around 10 dB (to 20 dB) when its input value to the SA is 10 dB. As the input pedestal level decreases, the improvement in TPSR at the SA output increases due to the nonlinear transmission curve of the SA (Fig. 2). The FROG accurately measured TPSR values up to 40 dB for pulses with high signal-to-noise ratio (SNR). Thus, to demonstrate the nonlinear response of the SA, TPSR values greater than 40 dB were extrapolated and are represented by the dashed line in the figure.

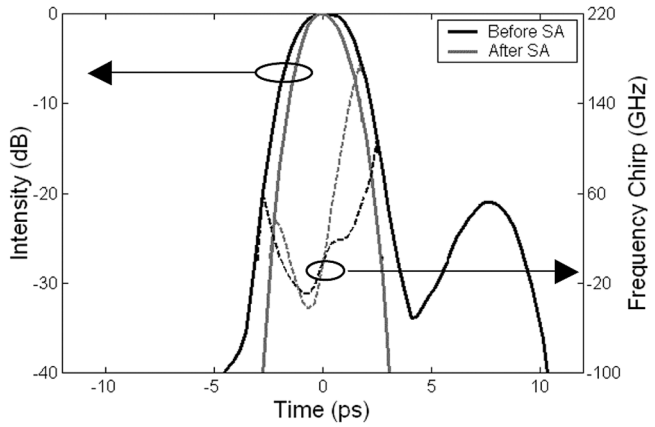

Fig. 3. Temporal and chirp profile of the pulse with 20-dB pedestal before and after the SA.

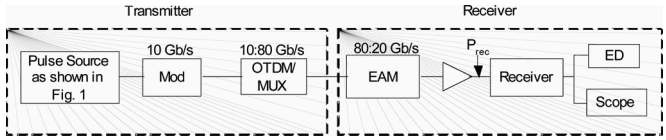

Fig. 4. An 80-Gb/s OTDM test-bed to characterize the performance of picosecond pulses with varying TPSR before and after the SA.

Fig. 3 displays the intensity and chirp profile of the pulse before and after the SA, with an input TPSR of 20 dB. This figure demonstrates that the SA reduces the pedestal level to greater than 40 dB, and also has very little effect on the frequency chirp of the pulse, an additional benefit of the device. Furthermore, it can be seen that the nonlinear response of the SA slightly compresses the pulse to 1.8 ps, with a corresponding TBP to 0.33.

B. 80-Gb/s OTDM System Performance Experiment and Simulation

To test the back-to-back performance of the optical pulse source with and without the SA, and with varying TPSR levels, in an 80-Gb/s OTDM system, we used the experimental test-bed presented in Fig. 4. The pulses as generated in Fig. 1 are modulated using a 10-Gb/s modulator and passively multiplexed up to 80 Gb/s. BER measurements were taken by initially demultiplexing down to 20 Gb/s using an EAM, and then by electrically demultiplexing from 20 to 10 Gb/s.

We initially examined the effect of pulses with varying input TPSR values and measured the power penalties introduced, which are displayed in Fig. 5. This plot clearly displays the effect of TPSR on the performance of an 80-Gb/s OTDM system. TPSR values of 15 and 20 dB exhibit power penalties of 3 and 1 dB, respectively, at a BER $1e^{-9}$, compared to a TPSR of 30 dB (which results in negligible system degradation).

To verify the experimental results, we simulated the above system using Virtual Photonics Incorporated (VPI) software, and measured the power penalties as a function of varying TPSR values. In the simulation, a sech squared pulse source was used. The pedestal was introduced in a similar manner to the experimental setup as were the demultiplexing stages. As can be seen

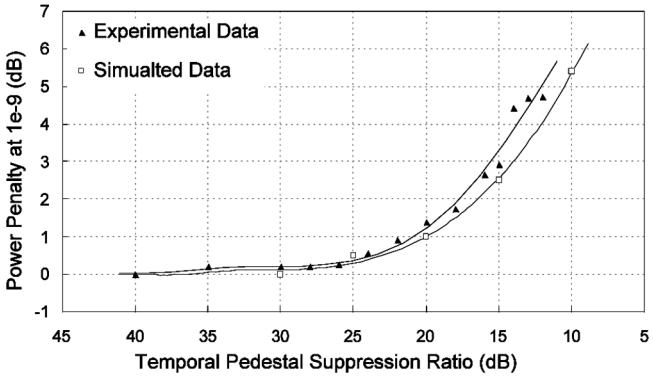

Fig. 5. Experimental and simulated results displaying induced power penalties by varying pulse TPSR values in an 80-Gb/s OTDM system.

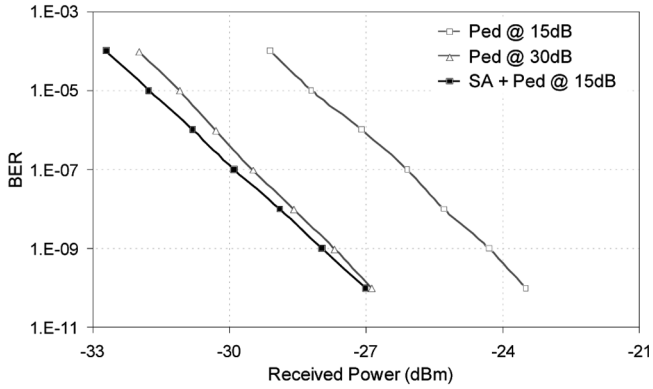

Fig. 6. BER versus received power for 1) pulse source with 15-dB TPSR, 2) this pulse source after the SA, showing TPSR improvement to 30 dB, and 3) a mode-locked pulse source.

from Fig. 5, the simulation results (grey line) match the experimental results reasonably well, confirming that pulse sources designed for high-speed OTDM systems require a high TPSR.

We then investigated how the introduction of the SA to increase the TPSR of the pulse source improved the performance of the 80-Gb/s OTDM system. For this work, we used a pulse source with an initial TPSR of 15 dB (which is improved to 30 dB after the SA). Fig. 6 displays the BER versus received power when using 1) the pulse source with TPSR of 15 dB, 2) this pulse source followed by SA, which improves TPSR to 30 dB, and 3) a mode-locked pulse source with TPSR set to 30 dB. Our results show how the SA improves the system performance by 3.3 dB. It is also important to note that the introduction of the SA improves the performance by 0.3 dB greater than what would be expected due to the increase in TPSR alone. This additional improvement is due to the narrowing of the main pulse which improves the overall sensitivity of the OTDM system.

III. Conclusion

We have presented the importance for pulse sources to have a high TPSR when used in high-speed OTDM systems. A 3-dB improvement in performance was obtained when the TPSR values were improved from 15 to 30 dB. For pulse sources that display poor pedestal suppression, the detrimental effects of poor TPSR values can be overcome by the introduction of a vertical microcavity-based SA, which has the potential to be integrated with a semiconductor-based pulse source. We demonstrated that with an initial TPSR of 15 dB, the SA can increase this level to 30 dB, and improve the overall system performance by 3.3 dB when these pulses are used in an 80-Gb/s OTDM system.

References

[1] D. M. Spirit, A. D. Ellis, and P. E. Barnsley, "Optical time division multiplexing: Systems and networks," *IEEE Commun. Mag.*, vol. 32, no. 12, pp. 56–62, Dec. 1994.

[2] P. L. Mason, A. Wonfor, D. D. Marcenac, D. G. Moodie, M. C. Brierley, R. V. Penty, I. H. White, and S. Bouchale, "The effects of pedestal suppression on gain-switched laser sources for 40 Gbit/s OTDM transmission," in *Proc. IEEE Lasers and Electro-Optics Society Annual Meeting*, Nov. 1997, vol. 1, pp. 289–290, Paper TuS2.

[3] P. Gunning, J. K. Lucek, D. G. Moodie, K. Smith, R. P. Davey, S. V. Chernikov, M. J. Guy, J. R. Taylor, and A. S. Siddiqui, "Gainswitched DFB laser diode pulse source using continous wave light injection for jitter suppression and an electroabsorption modulator for pedestal suppression," *Electron. Lett.*, vol. 32, pp. 1010–1011, 1996.

[4] M. C. Gross, M. Hanna, K. M. Patel, and S. E. Ralph, "Reduction of power fluctuations in ultrafast optically time-division-multpilexed pulse trains by use of a nonlinear amplifying loop mirror," *IEEE Photon. Technol. Lett.*, vol. 14, no. 5, pp. 690–692, May 2002.

[5] Z. Hu, M. Davanco, and D. J. Blumenthal, "Extinction ratio improvement by strong external injection and SPM in an SOA for OTDM pulse using a DBR laser diode," *IEEE Photon. Technol. Lett.*, vol. 15, no. 10, pp. 1419–1421, Oct. 2003.

[6] M. Gay, L. Bramerie, J. C. Simon, A. O'Hare, D. Massoubre, J. L. Oudar, and A. Shen, "Cascadability and wavelength tunablility assessment of a 2R regeneration device based on a saturable absorber and a semiconductor optical amplifier," in *Proc. Optical Fiber Communications Conf.*, Annaheim, CA, Mar. 2006, Paper OThB1.

[7] D. Rouvillain, F. Seguineau, L. Pierre, P. Brindel, H. Choumane, G. Aubin, J. L. Oudar, and O. Leclerc, "40 Gbit/s optical 2R regenerator based on passive saturable absorber for WDM long-haul transmissions," in *Proc. Optical Fiber Communications Conf.*, Annaheim, CA, Mar. 2002, pp. FD11-1–FD11-3.

[8] D. Massoubre, J. L. Oudar, J. Fatome, S. Pitios, G. Millot, J. Decobert, and J. Landreau, "All-optical extinction-ratio enhancement of a 160 GHz pulse train by a saturable-absorber vertical microcavity," *Opt. Lett.*, vol. 31, pp. 537–539, Feb. 2006.

[9] R. Trebino, K. W. DeLong, D. N. Fittinghoff, J. N. Sweerser, M. A. Krumbugel, and B. A. Richman, "Measuring ultrafast laser pulses in the time-frequency domain using frequency resolved optical gating," *Rev. Sci. Instrum.*, vol. 68, pp. 3277–3295, May 1997.

[10] D. Massoubre, J. L. Oudar, J. Dion, and J. C. Harmand, "Scaling of the saturation energy in microcavity saturable absorber devices," *Appl. Phys. Lett.*, vol. 88, no. 1535 13, pp. 1–3, Apr. 2006.

Optimized Pulse Source for 40-Gb/s Systems Based on a Gain-Switched Laser Diode in Conjunction With a Nonlinearly Chirped Grating

A. Clarke, P. M. Anandarajah, D. Reid, G. Edvell, L. P. Barry, and J. D. Harvey

***Abstract*—The authors demonstrate the generation of short optical pulses, which display spectral sidemode suppression ratio, and temporal pedestal suppression ratio, well in excess of 30 dB. The exceptional spectral and temporal characteristics exhibited by these pulses are attained by employing a novel technology, based on an externally injected gain-switched laser in conjunction with a nonlinearly chirped grating. Using this technique, near transform limited 7-ps optical pulses, exhibiting a time bandwidth product of 0.49, are generated.**

***Index Terms*—Gratings, optical fiber communication, optical pulse compression, optical pulse generation, semiconductor lasers.**

I. Introduction

With THE massive growth in demand for bandwidth showing no sign of declining in the coming decade, it will be necessary to further increase the overall capacity of the existing telecommunication networks. This goal of developing future terabit all-optical communication systems may be achieved by a reduction in channel spacing of wavelength-division-multiplexed (WDM) systems, an increase in the per-channel data rate by exploiting optical time-division multiplexing (OTDM) or by using a combination of these two methods as in hybrid WDM/OTDM systems.

The base data rate in high-speed optical networks for several years has been 10 Gb/s. Generally, such systems have tended to employ nonreturn-to-zero (NRZ) coding at the transmitter. However, current research has brought tremendous advances in the development of optical systems operating at 40 Gb/s and beyond [1]. In order to achieve line rates of 40 Gb/s and higher, it may become necessary to use return-to-zero (RZ) coding. RZ (pulse) modulation formats offer a number of advantages over NRZ modulation schemes [2]. First, for high-speed long-haul systems, RZ modulation maintains signal integrity over longer distances as it travels through the network. Moreover, RZ formatting has a lower bit-error rate and is far less susceptible to nonlinearity and dispersion effects in the transmission fiber that can cause the signal to spread (thus, rendering it unintelligible at the receiver) [3].

One of the major problems associated with the reduced channel spacing and increased line rate is the more stringent measures that are imposed on the transmitter performance. Hence, the design of an optical transmitter capable of generating pulses with adequate temporal and spectral purity for acceptable operation in high-speed optical communication systems is crucial. There are many techniques available to generate picosecond optical pulses [4], and it is readily recognized that the gain-switching technique is among the simplest of these. While the advantages in employing this technique are numerous, one of its major drawbacks is the spectral purity of the generated pulses. The direct modulation of the laser diode causes a time-varying carrier density in the active region of the device, which in turn causes a variation in the output wavelength from the laser during the emission of the optical pulse. This results in a frequency chirp across the pulse, which degrades the performance of these pulses when used in practical optical communication systems. It has been reported how this chirp can be used to compress the pulses using dispersion-compensating fiber [5] or linearly chirped gratings [6] to obtain near transform limited pulses. However, due to the chirp being nonlinear across the pulse, this compression typically results in pedestals on either side of the pulses that make them unsuitable for use in practical systems. By using more complex arrangements involving nonlinear loop mirrors or external modulators, after the linearly compressed pulse, it is possible to greatly reduce the pedestal [7].

In this letter, we report a simple yet systematic approach to design an optimized source of picosecond optical pulses, which exhibit excellent temporal and spectral purity. The procedure is based on an initial complete intensity and chirp characterization of pulses, from an externally injected gain-switched laser, using the technique of frequency-resolved optical gating (FROG). This characterization yields the parameters that are required for the design of a nonlinearly chirped fiber Bragg grating (NC FBG) with a chirp profile that is opposite to that measured across the pulse. By employing the tailor-made NC FBG after the gain-switched laser, we can achieve direct compression of the gain-switched pulses to obtain pedestal-free, near transform-limited, 7-ps pulses.

II. Experimental Setup

The experimental setup employed in this work is shown in Fig. 1. A 2.5-GHz sine wave is amplified with the aid of

Manuscript received June 23, 2004; revised August 26, 2004. This work supported in part by Enterprise Ireland (Proof of Concept) and Science Foundation Ireland (Investigator Program).

A. Clarke, P. M. Anandarajah, and L. P. Barry are with RINCE, School of Electronic Engineering, Dublin City University, Dublin 9, Ireland (e-mail: liam.barry@dcu.ie).

D. Reid and J. D. Harvey are with the Physics Department, Auckland University, Auckland, New Zealand.

G. Edvell is with the Redfern Optical Components, Eveleigh NSW 1430, Australia.

Digital Object Identifier 10.1109/LPT.2004.838624

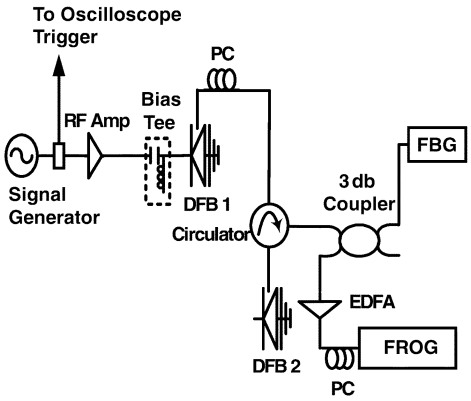

Fig. 1. Experimental setup for the generation of compressed externally injected gain-switched optical pulses.

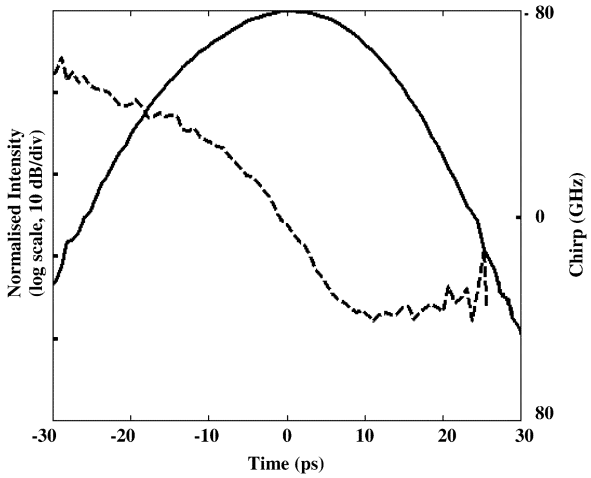

Fig. 2. Intensity and chirp of optical pulses from the externally injected gain-switched laser.

a high-power radio-frequency amplifier. A bias tee was then used to combine the electrical signal (∼25 dBm) with a dc bias (11.3 mA) to enable gain switching of a commercially available distributed feedback (DFB) laser contained within a hermetically sealed high-speed package. The resulting pulses generated were at a wavelength of 1549.35 nm. Wavelength tunablility of the laser mode could be achieved by temperature controlling the diode.

To overcome the poor sidemode suppression ratio (SMSR ∼15 dB) and timing jitter (4 ps) of the gain-switched pulses, we use external injection from a second DFB (2) laser (via an optical circulator) biased at 23.5 mA. A polarization controller was also used to ensure that the light being fed back was aligned with the optical axis of the laser. The injected power was measured to be about 13 dBm after taking into account the losses incurred in the optical injection path. The external light injection improves the SMSR to around 30 dB and reduces the timing jitter to $<$1 ps (as measured using an Agilent Digital Communications Analyzer). The generated pulses can then be characterized using an optical spectrum analyzer, a high-speed oscilloscope in conjunction with a 50-GHz p-i-n detector, and also a FROG measurement system [8]. From the FROG measurement, we can accurately characterize the intensity and chirp profile across the optical pulses from the gain-switched laser with external

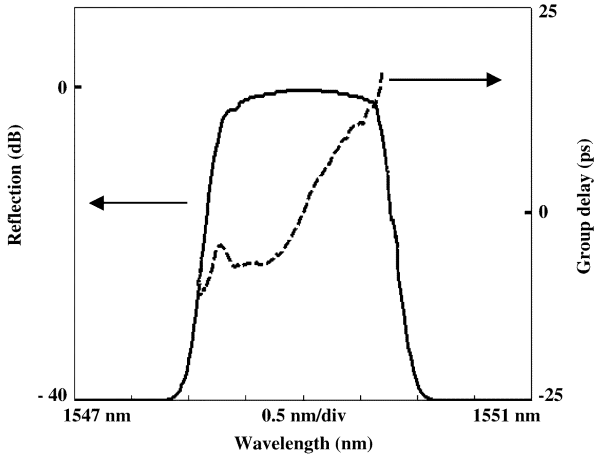

Fig. 3. Reflection and group delay profiles of nonlinearly chirped fiber grating.

injection (as shown in Fig. 2). We can clearly see how the frequency chirp becomes nonlinear in the wings of the 16-ps pulse generated, due to the gain-switching mechanism.

We subsequently use the measured nonlinear chirp across the pulse to design and fabricate an NC FBG with a chirp profile opposite to that measured across the pulse. The reflective and group delay profiles of the fabricated filter are shown in Fig. 3. We also fabricated a linearly chirped fiber grating which had a chirp profile that was opposite to a linear approximation of the chirp across the gain-switched pulse. By placing the fiber gratings after the gain-switched laser (with external injection), we subsequently characterize the pulse compression in the fiber gratings using the FROG measurement technique.

III. Results and Discussion

Fig. 4(a) and (b), respectively, shows the measured intensity and chirp profile of the gain-switched optical pulses after compression with the linearly and nonlinearly chirped fiber gratings. In both cases, we can see that the gratings have eliminated any frequency chirp across the center of the pulses. However, when the linearly chirped grating is used, we can clearly see how the nonlinearity of the chirp directly from the gain-switched laser results in significant pedestals on the leading and trailing edge of the pulse. These pedestals, which are around 23 dB down from the peak of the pulse, would clearly pose significant problems (through intersymbol interference) for the use of these pulses in 40-Gb/s OTDM systems [9].

When the nonlinearly chirped fiber grating is employed, the pedestal is completely eliminated on one side of the pulse and reduced to around 32 dB down from the peak of the pulse on the other side. The slight imperfection in the compression can be attributed to the fabricated nonlinearly chirped grating not being a perfect match to compensate the chirp of the gain-switched pulse. In both cases (linear and nonlinear grating), the duration of the compressed pulse is around 7 ps, compared with 16-ps pulsewidth directly from the gain-switched source. However, the nonlinearly chirped grating is vital for ensuring a high level of pedestal suppression.

The spectrum of the generated optical pulses as measured using an optical spectrum analyzer, in addition to the nonaveraged oscilloscope trace of the detected pulse (after the nonlinear

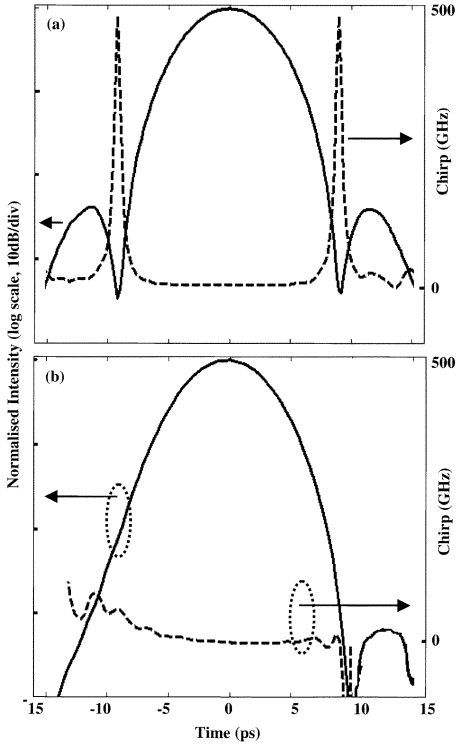

Fig. 4. Intensity and chirp of externally injected gain-switched pulses after (a) linearly chirped and (b) nonlinearly chirped gratings.

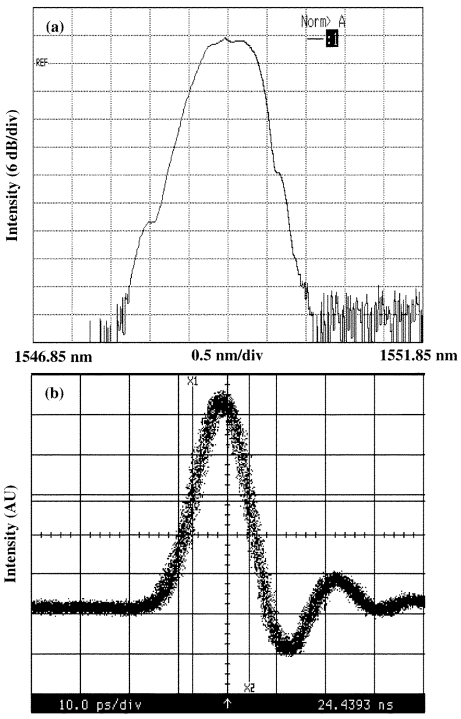

Fig. 5. (a) Optical spectrum and (b) oscilloscope trace of compressed pulse after nonlinearly chirped gratings.

grating), are shown in Fig. 5(a) and (b), respectively. The spectrum, which is in excellent agreement with the pulse spectrum obtained from the FROG measurement, shows that the spectral width is around 0.56 nm (70 GHz), thus giving a time bandwidth product of around 0.49. The low temporal jitter on the generated pulses is clear from the nonaveraged oscilloscope trace, and the ringing in the detected pulse is due to the pulse duration being a lot shorter than the response time of the detector ($\sim$10 ps).

This pulse generation/compression scheme exhibits excellent repeatability and stability over long periods of time, within laboratory conditions. This could be mainly attributed to the bias current and temperature of the two DFB (modulated and seeding) lasers being controlled with the aid of profile current/temperature controllers. Hence, drifts in wavelength of the lasers, due to current or temperature variations, were negligible. Furthermore the wavelength variation with temperature of the fabricated FBGs being relatively small ($\sim$0.009 nm/°C) also leads to the stable generation of optimized pulses over very long periods in time.

IV. Conclusion

We have demonstrated the use of nonlinearly chirped fiber gratings for optimum compression of optical pulses generated from a gain-switched laser diode. A nonlinearly chirped fiber grating is required to correctly compensate for the nonlinear chirp across the gain-switched pulse. This is vital for ensuring sufficient temporal pedestal suppression of the compressed gain-switched pulses. The resulting 7-ps pulse source comprising of gain-switched laser followed by nonlinearly chirped fiber grating would be suitable for use in 40-Gb/s transmission systems.

References

[1] A. Belahlou, S. Bickham, D. Chowdhury, P. Diep, A. Evans, J. M. Grochocinski, P. Han, A. Kobyakov, S. Kumar, G. Luther, J. C. Mauro, M. Yihong, M. Mlejnek, M. S. K. Muktoyuk, M. T. Murtagh, S. Raghavan, V. Ricci, A. Sevian, N. Taylor, S. Tsuda, M. Vasilyev, and L. Wang, "Fiber design considerations for 40 Gb/s systems," *J. Lightw. Technol.*, vol. 20, no. 12, pp. 2290–2305, Dec. 2002.

[2] R. Ludwig, U. Feiste, E. Dietrich, H. G. Weber, D. Breuer, M. Martin, and F. Küppers, "Experimental comparison of 40 Gbit/s RZ and NRZ transmission over standard single mode fiber," *Electron. Lett.*, vol. 35, pp. 2216–2218, 1999.

[3] A. Hasegawa, "Soliton-based optical communications: An overview," *IEEE J. Sel. Topics Quantum Electron.*, vol. 6, pp. 1161–1172, Nov./Dec. 2000.

[4] M. Saruwatari, "All optical signal processing for terabit/second optical transmission," *IEEE J. Sel. Topics Quantum Electron.*, vol. 6, pp. 1363–1374, Nov./Dec. 2000.

[5] K. A. Ahmed, H. F. Liu, N. Onodera, P. Lee, R. S. Tucker, and Y. Ogawa, "Nearly transform limited pulse (3.6 ps) generation from gain-switched 1.55 μm distributed feedback laser by using fiber compression technique," *Electron. Lett.*, vol. 29, pp. 54–56, 1993.

[6] B. J. Eggleton, P. A. Krug, L. Poladian, K. A. Ahmed, and H. F. Liu, "Experimental demonstration of compression of dispersed optical pulses by reflection from self-chirped optical fiber bragg gratings," *Opt. Lett.*, vol. 19, pp. 877–879, 1994.

[7] P. Gunning, J. K. Lucek, D. G. Moodie, K. Smith, R. P. Davey, S. V. Chernikov, M. J. Guy, J. R. Taylor, and A. S. Siddiqui, "Gain-switched DFB laser diode pulse source using continuous wave light injection for jitter suppression and an electroabsorption modulator for pedestal suppression," *Electron. Lett.*, vol. 32, pp. 1010–1011, 1996.

[8] R. Trebino, K. W. DeLong, D. N. Fittinghoff, J. N. Sweetser, M. A. Krumbugel, and B. A. Richman, "Measuring ultrashort laser pulses in the time-frequency domain using frequency-resolved optical gating," *Rev. Sci. Instrum.*, vol. 68, pp. 3277–3295, 1997.

[9] P. L. Mason, A. Wonfor, D. D. Marcenac, D. G. Moodie, M. C. Brierley, R. V. Penty, I. H. White, and S. Bouchoule, "The effects of pedestal suppression on gain switched laser sources for 40 Gbit/s OTDM tranmission," in *10th Annu. Meeting IEEE LEOS*, vol. 1, 1997, pp. 289–290.

80 Gb/s Optimised Pulse Source using a Gain-Switched Laser Diode in Conjunction with a Nonlinearly Chirped Grating

A. M. Clarke (1), M. Rensing (1), D. Reid (2), P. M. Anandarajah (1), L. P. Barry (1), J. D. Harvey (2), and G. Edvell (3)

1 : RINCE, School of Electronic Eng., Dublin City University, Ireland, liam.barry@dcu.ie

2 : Physics Dept., Auckland University, j.harvey@auckland.ac.nz

3 : Redfern Optical Components, Australia, g.edvell@redferncomponents.com.au

Abstract *The authors demonstrate near transform limited 3.5 ps pulse generation with pedestal suppression around 35 dB suitable for use in 80-Gb/s systems. The novel technology is based on an externally injected gain-switched laser in conjunction with a nonlinearly chirped grating.*

Introduction

The development of picosecond optical pulse sources with excellent temporal and spectral properties is vital for future implementation of high capacity optical communications systems using OTDM and hybrid WDM/OTDM technologies [1]. These sources will be important for enabling optical communication systems operating at line rates of 40, 80, and 160 Gb/s, employing Return to Zero (RZ) coding. The RZ coding is far less susceptible to nonlinearity and dispersion effects in the transmission fibre [2]. The work we present here is a development on previous work, which exhibited 2.5 GHz pulse source using a Nonlinearly Chirped Fibre Bragg Grating (NC FBG) [3]. In this paper, the technique is improved, such that 3.5 ps pulses at a repetition rate of 10 GHz are generated and the technique optimises the output spectrum of the pulse. The output pulses generated are near transform limited and have pulse pedestals that are virtually eliminated to around 35 dB below the peak of the pulse. These pulse sources would be suitable for use in 80 Gb/s OTDM systems or in hybrid WDM/OTDM systems.

The pulse generation method involves gain-switching which has been readily recognised as one of the simplest techniques available. A disadvantage of gain-switching technique is that a large nonlinear frequency chirp is present across the wings of the pulse that could degrade the performance of systems that employ them. It has been reported how this chirp can be used to compress the pulses using dispersion compensating fibre [4] or linearly chirped gratings [5], to obtain near transform limited pulses. However, due to the chirp being nonlinear this compression typically results in pedestals on either side (wings) of the pulses thus rendering them unsuitable for use in practical systems. Hence we propose a simple and effective method, with the use of NC FBGs, which compensates for the chirp entirely across the pulse thus eliminating the pedestals and generating transform limited pulses.

Experiment

The experimental set-up employed in this work is shown in Figure 1. A high-speed 1550 nm DFB (1) laser is gain-switched at 10 GHz using a signal generator and a high power RF amplifier. External injection is provided to improve the side mode suppression ratio (SMSR) and temporal jitter of the gain-switched pulse from a second DFB (2) laser via the circulator. The temporal jitter of the resulting pulses is measured to be < 1ps and the SMSR is improved from 15 dB to 30 dB. The generated pulses before and after the grating were characterised using an optical spectrum analyser (OSA), a high-speed oscilloscope in conjunction with a 50 GHz pin detector, and also a Frequency Resolved Optical Gating (FROG) measurement scheme [6]. The FROG allows complete characterisation of the temporal and spectral characteristics of the pulse, including the chirp and group delay profiles.

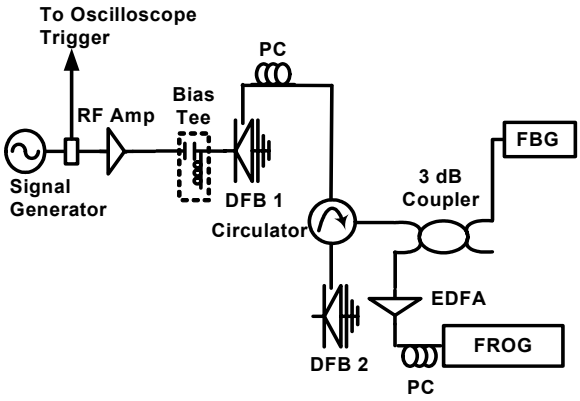

Fig .1 Experimental Set-up

With the external injection, the gain-switched pulses have a nonlinear chirp profile in the wings of the pulse as is shown in Figure 3. The gain-switched (input) pulse is characterised by the FROG and these parameters are used to design the NC FBG with a group delay profile that is opposite to that measured across the pulse. In addition, the reflection profile of the grating is made to ensure equalization in such a way that an optimised output Gaussian spectrum is

achieved (as shown in the reflection profile of the Bragg grating in Figure 2).

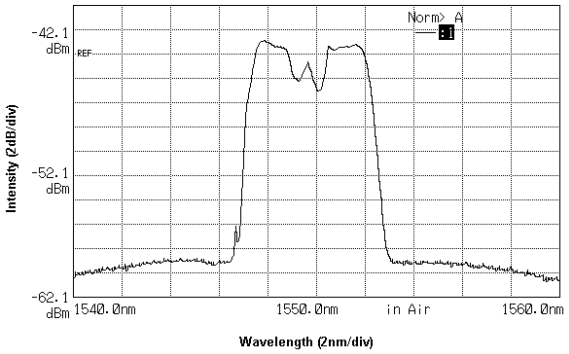

Fig. 2 Reflection profile of the NC FBG

Results and Discussion

The input and output pulses, and their corresponding chirp profiles are shown in Figure 3. The input pulse has a FWHM pulse width of about 10 ps. The nonlinear chirp has a large magnitude, thus resulting in the pulse having a time bandwidth product (TBP) of 1.5. The pulse is then passed to the grating via one arm of the coupler and the reflected output is characterised at the other arm of the coupler. The compression in the fibre grating results in a 3.5 ps FWHM pulse. The resultant chirp is very flat and has a very small order of magnitude across the pulse thus giving a TBP of 0.45. Also, an excellent Temporal Suppression Ratio (TSR >35 dB) is exhibited as can be seen in Figure 3 where the pedestals have almost been eliminated. Previous work has shown that the use of a linearly chirped FBG (fabricated by using a linear approximation of the pulse chirp profile) results in a TSR of about 23 dB that could lead to inter symbol interference in high-speed OTDM systems [7].

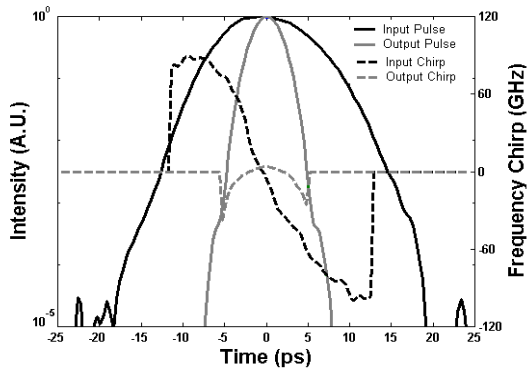

Fig. 3 Input and output pulse profile and their corresponding chirp profile to the NC FBG.

The spectra and the group delay of the input and output pulses are shown in Figure 4. It is clear that the group delay has been compensated for entirely by the NC FBG. The output spectrum is more Gaussian shaped and symmetric in comparison to the input, which is due to the compensation by the nonlinear reflection profile of the NC FBG.

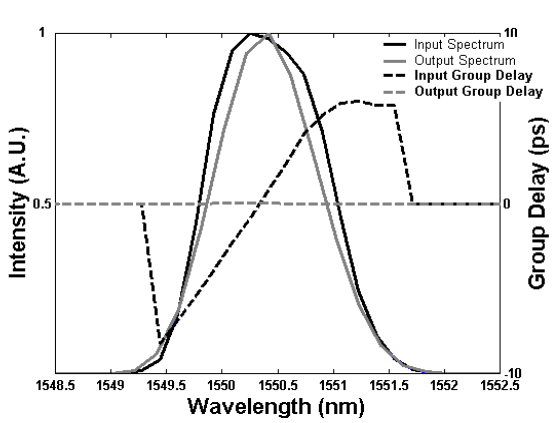

Fig. 4 Spectra and group delay of the input and output pulses to the nonlinear grating.

This pulse generation/compression scheme exhibits excellent repeatability and stability over long periods of time, within laboratory conditions. This could mainly be attributed to bias current and temperature of the two DFB lasers being controlled with the aid of current/temperature controllers. Hence, drifts in wavelength of the lasers, due to current or temperature variations, were negligible. Furthermore, the wavelength variation with temperature of the fabricated NC FGB being relatively small (~0.009 nm/±C) also leads to the stable generation of optimised pulses over long periods of time.

Conclusions

We have demonstrated the generation of near transform limited 3.5 ps gain switched pulses that exhibit an excellent TSR by using a NC FBG. The initial gain-switched pulses display a large nonlinear chirp across the wings of the pulse. The gratings are designed with a nonlinear group delay profile that is opposite to the group delay of the input pulse to compensate for the chirp, and the spectrum is optimised using a nonlinear reflection profile. The resultant output pulses display excellent temporal and spectral purity, which would make this pulse source ideal for use in 80 Gb/s OTDM systems.

References

1 M. Saruwatari, IEEE J. Sel. Top. Quantum Electron., vol. 6 (2000), pp. 1363-1374.

2 A. Hasegawa, IEEE J. Sel. Top Quantum Electron., vol. 6 (2000), pp. 1161-1172.

3 A. Clarke et al, IEEE Photon. Technol. Lett., vol. 17 (2005), pp. 196-198.

4 K. A. Ahmed et al, Electron. Lett., vol. 29 (1993), pp. 54-56.

5 B. J. Eggleton et al, Opt. Lett., vol. 19 (1994), pp. 877-879.

6 R. Trebino et al, Rev. Sci. Instrum, vol. 68 (1997), pp. 3277-3295.

7 P. L.Mason et al, LEOS 97, (1997), pp. 289-290.

System-Performance Analysis of Optimized Gain-Switched Pulse Source Employed in 40- and 80-Gb/s OTDM Systems

Prince M. Anandarajah, *Member, IEEE*, Aisling M. Clarke, *Student Member, IEEE*, Celine Guignard, Laurent Bramerie, Liam P. Barry, *Member, IEEE*, John D. Harvey, *Member, IEEE*, and Jean Claude Simon

***Abstract*—The development of ultrashort optical pulse sources, exhibiting excellent temporal and spectral profiles, will play a crucial role in the performance of future optical time division multiplexed (OTDM) systems. In this paper, we demonstrate the difference in performance in 40- and 80-Gb/s OTDM systems between optical pulse sources based on a gain-switched laser whose pulses are compressed by a nonlinearly and linearly chirped fiber Bragg grating. The results achieved show that nonlinear chirp in the wings of the pulse leads to temporal pedestals formed on either side of the pulse when using the linearly chirped grating, whereas with the nonlinearly chirped grating, pedestals are essentially eliminated. In an OTDM system, these pedestals cause coherent interaction between neighboring channels, resulting in intensity fluctuations that lead to a power penalty of 1.5 dB (40 Gb/s) and 3.5 dB (80 Gb/s) in comparison to the case where the nonlinearly chirped grating is used. Simulations carried out with the aid of Virtual Photonics Inc. verify the results achieved.**

***Index Terms*—Grating, optical communication, optical pulse generation, pulse compression.**

I. Introduction

ENHANCING the capacity of long-haul and metro-network photonic communication systems, without increasing the cost (by avoiding high-speed electronics), can be achieved by the use of optical time division multiplexing (OTDM) or hybrid wavelength division multiplexing/OTDM [1]. A key requirement in such high-capacity systems is a stable, compact, and low-cost source of picosecond optical pulses. However, the increased line rate and the reduced channel spacing place stringent requirements, such as a high repetition rate, narrow pulsewidth, low jitter, high side mode suppression ratio (SMSR), high temporal pedestal suppression ratio (TPSR), and small chirp, on the pulse source. For instance, a return-to-zero (RZ) optical transmitter designed to achieve satisfactory performance in a $\geq$ 40-Gb/s photonic communication system needs to be capable of generating pulses with repetition rates of at least 10 GHz [2], pulsewidths of $<$ 8 ps (duty cycle of $\sim$1/3) [3], SMSR of at least 30 dB [4], TPSR $>$ 30 dB [5], and a negligible chirp (transform-limited) [6]. Therefore, the design of an optical transmitter has to be optimized, in that it has to be capable of generating pulses with adequate temporal and spectral purity, for acceptable operation in high-speed lightwave communication systems.

The main types of picosecond optical pulse sources that have been used in recent OTDM-system demonstrations are mode-locked fiber ring lasers [7], tunable mode-locked semiconductor lasers (TMLL) [8], pulse shaping using external modulators [9], and gain-switched semiconductor laser diodes [10]. Relative to the rest of the aforementioned techniques, gain switching of a DFB laser is readily recognized to be an uncomplicated, robust, and reliable technique [11], [12]. Furthermore, the inherent simplicity brought about by being a direct modulation technique results in the gain-switched pulse source being cost-efficient, which proves to be of great practical significance with regard to market adoption. While the advantages in employing this method are numerous, it suffers from a few drawbacks such as a degraded SMSR and a relatively large temporal jitter exhibited by the generated pulses. However, these shortcomings could be overcome by externally injecting into a gain-switched laser [13], [14]. Yet, another problem associated with this technique is the spectral purity portrayed by the generated pulses. The large signal modulation applied directly to the laser diode causes a time varying carrier density in the active region of the device, which in turn causes a variation in the output wavelength from the laser during the emission of the optical pulse. This results in a frequency chirp across the pulse, which degrades the performance of these pulses when used in practical optical communication systems [15]. It has been reported how this chirp can be used to compress the pulses using dispersion compensating fiber [16] or linearly chirped fiber Bragg gratings (LC FBGs) [17] to obtain near transform-limited pulses. However, due to the chirp being nonlinear in the wings of the pulse, this compression typically results in pedestal formation on either side of the pulse [18]. By using more elaborate arrangements involving nonlinear amplifying loop mirrors [19], [20], external modulators [21], spectral windowing [22], or semiconductor optical amplifiers in conjunction with shifted

Manuscript received October 23, 2006; revised February 23, 2007. This work was supported in part by Enterprise Ireland Commercial Fund Technology Development Phase (CFTD/06/IT/315) and in part by the Science Foundation Ireland (Investigator Program).

P. M. Anandarajah, A. M. Clarke, C. Guignard, and L. P. Barry are with the Research Institute for Networks and Communications Engineering, School of Electronic Engineering, Dublin City University, Dublin 9, Ireland (e-mail: prince.anandarajah@dcu.ie; anandara@eeng.dcu.ie; clarkea@eeng.dcu.ie; guignard@eeng.dcu.ie; barryl@eeng.dcu.ie).

L. Bramerie and J. C. Simon are with the Centre National de la Recherche Scientifique Fonctions Optiques pour les Télécommunications–Ecole Nationale Supérieure des Sciences Appliquées et de Technologie (CNRS FOTON–ENSSAT), 22300 Lannion, France (e-mail: Laurent.bramerie@persyst.fr; Jean-Claude.Simon@enssat.fr).

J. D. Harvey is with the Physics Department, University of Auckland, Auckland 1020, New Zealand (e-mail: j.harvey@auckland.ac.nz).

Digital Object Identifier 10.1109/JLT.2007.896760

filtering [23] after the linearly compressed pulse, it is possible to greatly reduce the pedestal. The above-listed methods, to optimize the TPSR of the pulse source, leads to the source becoming more complex, bulky, and expensive. In previous work, we reported a simple, yet systematic approach to design a pulse source exhibiting excellent temporal and spectral purity with the aid of a nonlinearly chirped FBG (NC FBG) placed after an externally injected gain-switched laser diode [24]. This approach of using a tailor-made grating has an additional bonus in that it has the potential to be integrated with the gain-switched laser diode [25].

In this paper, we advance on our previous work by characterizing the performances of 40- and 80-Gb/s OTDM systems employing two gain-switched pulse sources: one compressed with an NC FBG that achieves an excellent TPSR ($>$ 40 dB) and the other with an LC FBG that achieves a poor TPSR ($\sim$20 dB). The degraded performance, in the case of the latter (power penalty of 1.5 dB in 40-Gb/s system and 3.5 dB in 80-Gb/s system), even though both sources generate pulses that are transform-limited, exhibit widths $<$ 30% of the 80-Gb/s bit slot and portray SMSRs of $>$ 30 dB, is attributed to the presence of pulse pedestals which cause coherent interactions between individual OTDM channels, thereby resulting in severe intensity fluctuations [19]. We define the TPSR (P_1/P_2) as the difference in power between the peak of the pulse (P_1) and the peak of the next highest pedestal (P_2). A commercially available TMLL pulse source was also used to benchmark the experimental system-performance characterization.

This paper is organized as follows. Section II describes the experimental realization of the two different pulse sources used in this paper. Section III focuses on the experimental performance characterization of 40- and 80-Gb/s OTDM test bed by employing the externally injected gain-switched pulse source followed by the NC FBG/LC FBG. In Section IV, we concentrate on the verification of the obtained experimental results by looking at simulations that were performed using a photonic design automation tool called Virtual Photonics Inc. (VPI). Finally, Section V presents a brief discussion on the achieved results.

II. Pulse Generation and Compression

The essential element in our proposed pulse source is an externally injected gain-switched DFB laser diode (EI GSLD). With the aid of the frequency-resolved optical gating (FROG) technique [26], [27], an accurate characterization of the intensity and chirp profile across the optical pulses generated from the EI GSLD is carried out. Fig. 1 shows that the generated pulses have a duration [full-width-half-maximum (FWHM)] of about 10.5 ps and that the frequency chirp (dashed line in the figure) becomes nonlinear in the wings, due to the gain-switching mechanism. The measured spectral width of the signal is about 140 GHz, yielding a time bandwidth product (TBP) of 1.5. We subsequently use the measured nonlinear chirp across the pulse to design and fabricate an NC FBG. This process involves the initial creation of the group-delay response for the FBG based on the group-delay data derived from the FROG measurements of the externally injected gain-switched pulse.

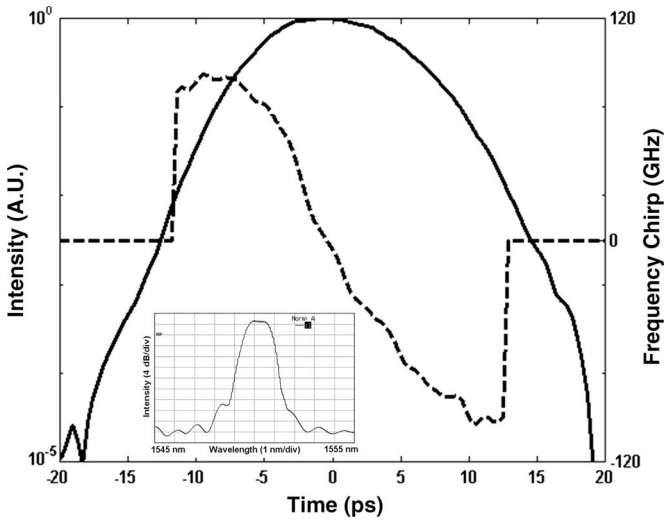

Fig. 1. Intensity (solid line) and chirp (dashed line) of optical pulses from the externally injected gain-switched laser. Inset: Corresponding pulse spectrum.

The FBG target group-delay response is simply selected as the inverse to the pulse group-delay response, which should result in the pulse having a constant group-delay profile over the pulse bandwidth after it has been reflected from the FBG. In addition to a constant group-delay profile across the pulse bandwidth, for an optimized pulse source, we also require the pulse to exhibit a Gaussian spectrum. Generally, gain-switched spectra tend to be more rectangular than Gaussian in shape. The reflection profile of the NC FBG is constructed as the difference between the spectral amplitude of the gain-switched output and a Gaussian profile, which should result in the compressed pulse portraying a Gaussian spectrum. Fig. 2 shows the reflection and group-delay profiles of the fabricated NC FBG. Since we aim to alter the group-delay profile only over the spectral range of the pulse, the group delay outside this spectral range rapidly falls off to zero.

Once the FBG target spectrum and group-delay profile are obtained, it is relatively straightforward to calculate an FBG design that can be implemented into the optical fiber by using an inverse scattering algorithm [28]–[30]. We also fabricated an LC FBG which had a chirp profile that was opposite to a linear approximation of the chirp across the gain-switched pulse. By employing the tailor-made NC FBG/LC FBG after the externally injected gain-switched laser (as shown schematically in Fig. 3), we achieve direct compression of the gain-switched pulses.

The pulse source consists of a commercially available high-speed 1550-nm DFB (1) laser that is gain-switched at a repetition rate of 10 GHz. External injection, from a second DFB (2) laser operating in continuous wave (CW) mode, is carried out to improve the SMSR and the temporal jitter of the gain-switched laser via a circulator. The temporal jitter is measured (with the aid of an oscilloscope characterized by a temporal resolution of 1 ps) to be $<$ 1 ps, and the SMSR is improved from 15 to 30 dB. The generated pulses are then spectrally shaped and temporally compressed by the specially fabricated gratings via another circulator.

Fig. 4 shows the compressed pulses after the NC FBG (bold black line) and the LC FBG (faint gray line). The measured

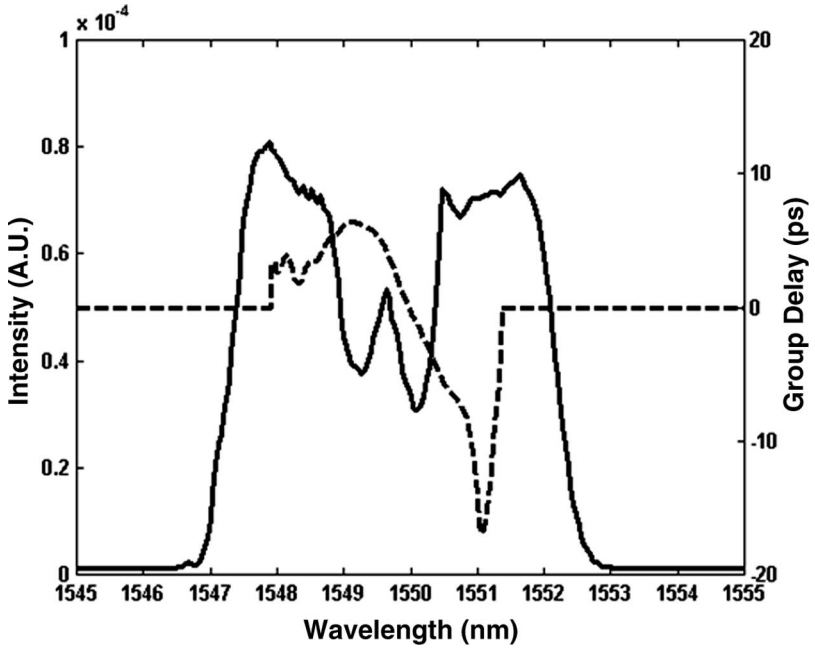

Fig. 2. Reflection (solid line) and group-delay (dashed line) profiles of the NC FBG.

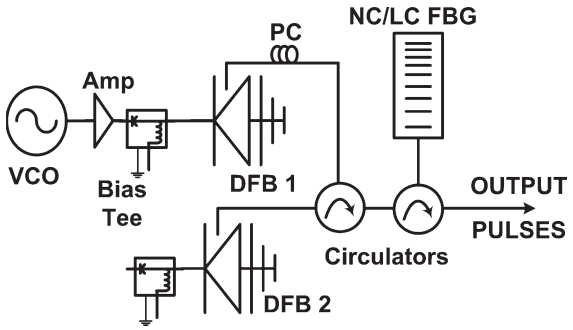

Fig. 3. Experimental setup for pulse generation.

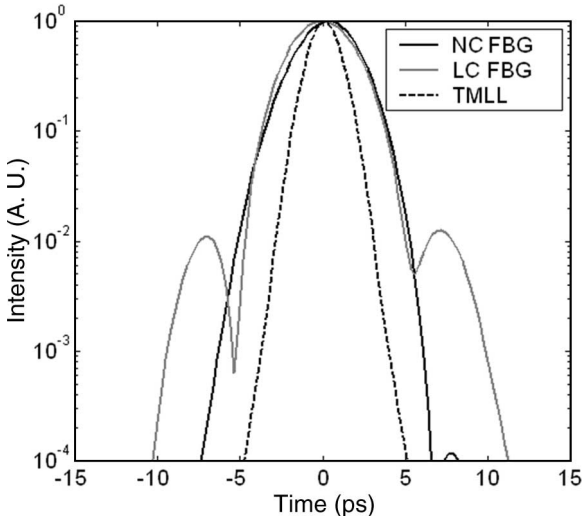

Fig. 4. Intensity of externally injected gain-switched pulses after (bold) NC FBG, (faint) LC FBG, and (dotted line) TMLL.

pulse widths (FWHM), which are characterized using FROG, are 3.5 and 3.6 ps respectively, while their associated TBPs are 0.45 and 0.47, respectively. The same figure also shows the

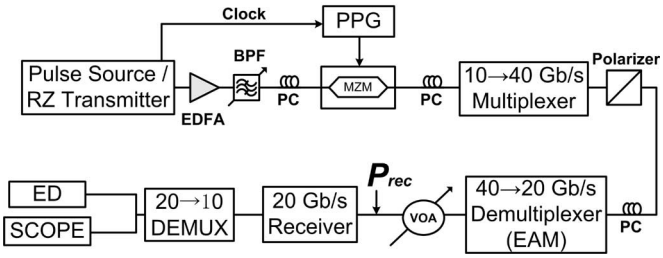

Fig. 5. The 40-Gb/s OTDM test bed.

pulses generated by the TMLL (commercial pulse source) that exhibited widths of about 2.1 ps (FWHM). The associated TBP of this pulse source is about 0.35.

As can be seen, the pulses compressed by the NC FBG exhibits a TPSR $>$ 40 dB, while that compressed by the LC FBG portray a TPSR of about 20 dB. The excellent TPSR, in the case of the NC FBG, is achieved by a combination of the fiber grating having the following: 1) a nonlinear group-delay profile that is the inverse of that across the gain-switched pulse directly from the laser and 2) a specially adapted reflection profile (transfer characteristic). However, when the LC FBG is used, the uncompensated nonlinear chirp directly from the gain-switched laser results in significant pedestals on the leading and trailing edges of the pulse.

III. Performance Characterization of 40- and 80-Gb/s OTDM Systems

The experimental set-up employed to realize the 40-Gb/s OTDM test bed is shown in Fig. 5. Three different pulse sources were employed alternatively as the RZ transmitter block (as in Fig. 4) in the 40-Gb/s OTDM test bed. In the first instance of system-performance characterization, the EI GSLD employing an NC FBG was used, after which, it was replaced by the LC FBG. They both gave out near transform-limited

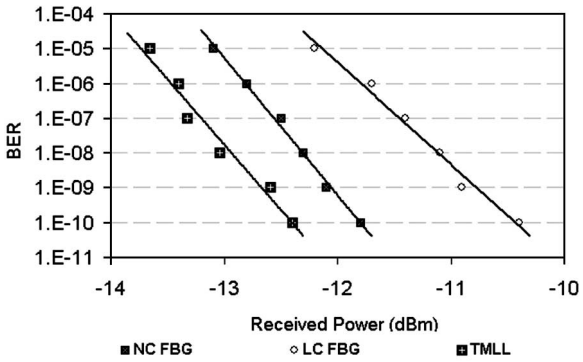

Fig. 6. BER versus received optical power for TMLL, NC FBG, and LC FBG employed in a 40-Gb/s OTDM test bed.

pulses with widths of 3.5 and 3.6 ps, depending on whether the NC FBG or LC FBG, respectively, is used for the compression. Once both versions of compression of the externally injected gain-switched pulses were characterized, the TMLL pulse source was used to replace them, mainly to act as a reference.

A pseudorandom binary sequence of length $2^7 - 1$ from a pulse pattern generator was used to modulate the 10-GHz pulse train with the aid of a Mach–Zehnder modulator. The resultant 10-Gb/s RZ optical signal is then passed into a passive fiber-based interleaver and multiplexed up to 40 Gb/s. The same state of polarization is maintained on all the tributaries by initially ensuring that the PC is optimized to maximize the amplitude of the 10-Gb/s signal passing through the multiplexer and the polarizer (all stages of the mux shut). Subsequently, as each stage of multiplexing is opened, the PC (available at each stage on the mux) is optimized to ensure copolarization by equalizing the power in all the tributaries.

In order to test the performance of the two sources when employed in the 40-Gb/s OTDM test bed, the signal is initially demultiplexed (stage 1) down to 20 Gb/s with the aid of an electroabsorption modulator (EAM) that is driven with a 20-GHz sinewave to yield an 8 ps switching window. The 20-Gb/s signal after the EAM is then optically preamplified prior to being received with the aid of a photodetector, after which, it is demultiplexed (stage 2) back down to 10 Gb/s using an electrical demultiplexer. Bit-error-rate (BER) measurements are performed for a range of received optical powers (P_{rec} measured before the 20-Gb/s preamplified receiver stage). Each of the four tributaries can be selected using electrical delay lines (EDLs) in the setup. The total variation in performance, between these channels, was observed to be about 0.4 dB. Signal analysis is carried out with the aid of an error detector (ED) and a high-speed oscilloscope.

Fig. 6 displays the BER versus received power plots for one of the demultiplexed channels. It can be observed that to achieve a BER of 10^{-9}, a power penalty of 1.5 dB is incurred when the pulse source with the LC FBG is employed, compared with the case where the NC FBG is used. This degraded performance is due to the presence of the pedestals about 20 dB below the peak of the pulse. These pedestals deteriorate the extinction between the adjacent timeslots of the temporally multiplexed signal, thereby leading to intensity fluctuations that cause the BER degradation.

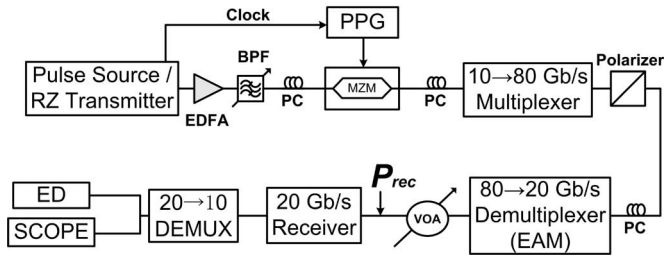

Fig. 7. The 80-Gb/s OTDM test bed.

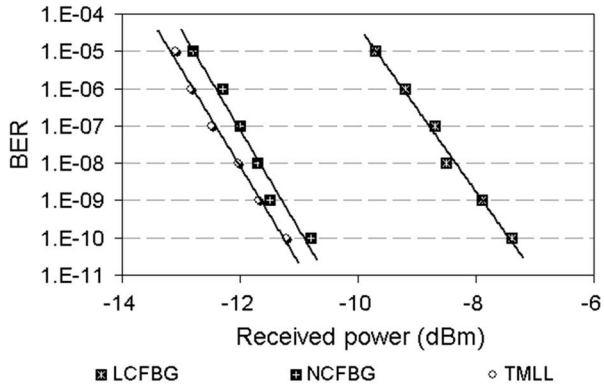

Fig. 8. BER versus received optical power for TMLL, NC FBG, and LC FBG employed in an 80-Gb/s OTDM test bed.

A difference of 0.5 dB was noticed in the case of the commercial TMLL and the optimized gain-switched pulse source employing an NC FBG. This variation could be attributed to the difference in pulsewidth, with the narrower pulsewidth leading to a slightly better sensitivity at the receiver.

The experimental setup used to realize the 80-Gb/s OTDM test bed is also shown in Fig. 7. Essentially, the setup and the sequence of performance characterization were the same as in the 40-Gb/s OTDM-system characterization. However, in this case, the modulated data at a base rate of 10 Gb/s were passively multiplexed up to an aggregate bit rate of 80 Gb/s. The demultiplexing was carried out in the same manner as described with the EAM used to demultiplex from 80 to 20 Gb/s prior to employing an electrical demultiplexer to go from 20 to the base rate of 10 Gb/s. Using the EDLs attached to the demux drive, each of the eight tributaries is selected (one at a time), and signal analysis is carried out with the aid of an ED and a high-speed oscilloscope.

Fig. 8 displays the BER versus received power curves for one of the demultiplexed channels. It can be observed that to achieve a BER of 10^{-9}, a power penalty of 3.5 dB is incurred in the case of the LC FBG when compared to the NC FBG. The degraded performance is once again due to the presence of the pedestals (poor TPSR), which results in ISI between the adjacent channels. Yet again, a difference of 0.5 dB was noticed in the case of the commercial TMLL and the optimized gain-switched pulse source employing an NC FBG. The slight difference in pulsewidth, as explained earlier, causes the marginal difference in the sensitivity at the receiver (shorter pulse exhibits better sensitivity).

The detected eye diagrams (shown at 20 Gb/s after the EAM demux stage) corresponding to received powers of -30.8

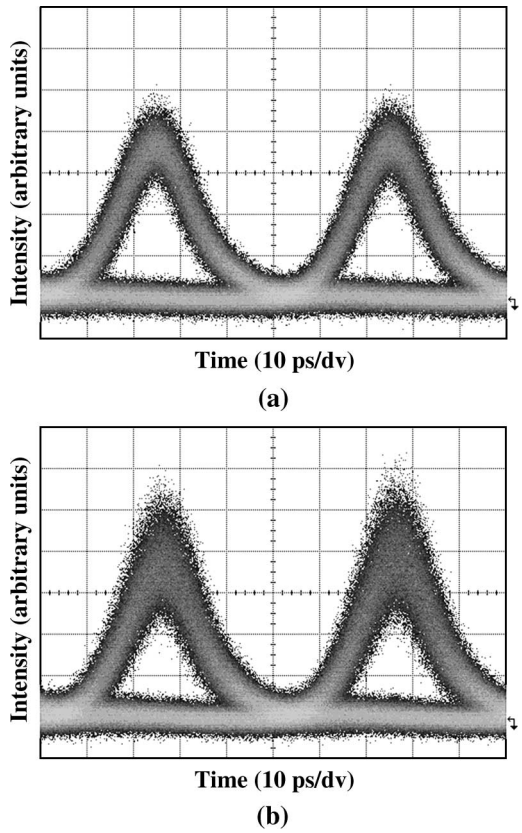

Fig. 9. Received eye diagrams at 20 Gb/s corresponding to the EI GSLD pulses compressed with the (a) NC FBG and (b) LC FBG when employed in an 80-Gb/s OTDM test bed.

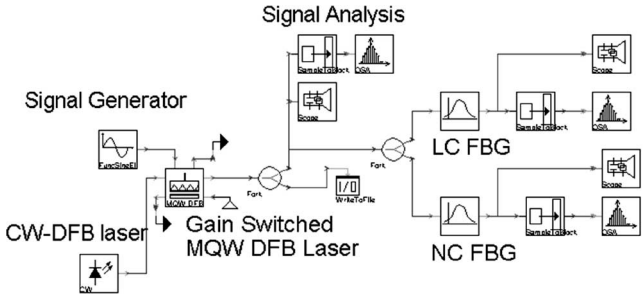

Fig. 10. Schematic of VPI simulation model used to realize EI GSLD pulse source.

and −29.7 dBm for the NC FBG and LC FBG are shown in Fig. 9(a) and (b), respectively. The increased level of noise (reflecting poorer performance) can be noticed in the case of the LC FBG [Fig. 9(b)], even though the received power level is higher than in the case where the NC FBG was used.

IV. Simulations

The system penalties introduced by a poor TPSR were characterized by carrying out simulations using VPI.

A. Pulse Generation and Compression

A schematic of the simulation model used to realize the externally injected gain-switched pulse source in conjunction with the NC FBG and LC FBG is shown in Fig. 10. A multiquantum-well DFB laser is gain-switched and subjected to external injection from another DFB laser that is operated in CW mode. The resulting pulses from the EI GSLD show widths (FWHM) of 9.8 ps, an SMSR of about 35 dB, and a TBP of about 1.27. The intensity and group-delay parameters are then extracted from the generated pulses and written to an output file.

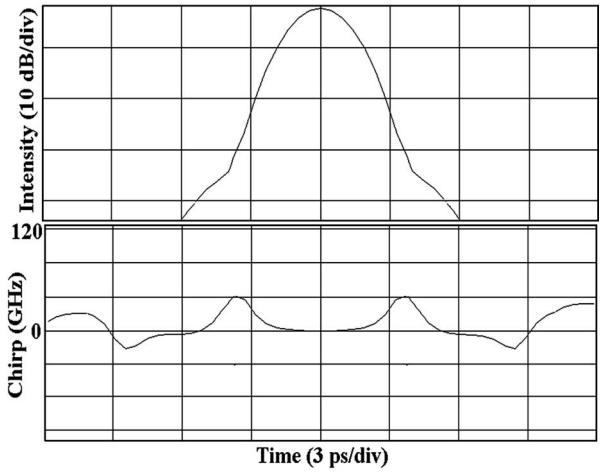

Fig. 11. Intensity and chirp profile of the EI GSLD pulse source employing an NC FBG for spectral shaping and temporal compression.

Temporal compressions using both the NC FBG and the LC FBG were simulated by using a measured optical filter in conjunction with the externally injected gain-switched laser. As in the experiment, the target reflection profile of these filters was set as the difference between the spectral amplitudes of a Gaussian profile and the EI GSLD output. Again, as in the experiment, the final group delay of the NC FBG and the LC FBG was obtained by selecting the following: 1) a group-delay response that is inverse to that measured across the EI GSLD pulse and 2) a group-delay profile opposite to a linear approximation of the pulse group-delay response, respectively.

Fig. 11 shows the pulse intensity and corresponding chirp when the EI GSLD pulses are compressed by the NC FBG. The resulting pulses portray a width of 2.9 ps (FWHM). Furthermore, it can be clearly seen that the resultant chirp has a negligible magnitude, thereby ensuing in an enhanced TPSR of about 35 dB. Fig. 12 shows the compressed pulses (3.1-ps width) and its corresponding chirp when the LC FBG is used. Here, the chirp in the central portion of the pulse can be seen to be flat and, hence, been compensated. However, the uncompensated nonlinear chirp in the wings of the pulse causes the formation of pedestals on the leading and trailing edges of the pulse and results in the pulses, exhibiting a TPSR of about 23 dB. The pulses from the TMLL pulse source were modeled by using a transform-limited Sech^2 pulse source that generated pulses with widths of 2.1 ps. The generated pulses and its equivalent chirp are shown in Fig. 13.

B. System-Performance Analysis of 80-Gb/s OTDM

Performance characterization of an 80-Gb/s OTDM system is carried out with each of these three different pulse sources employed alternatively.

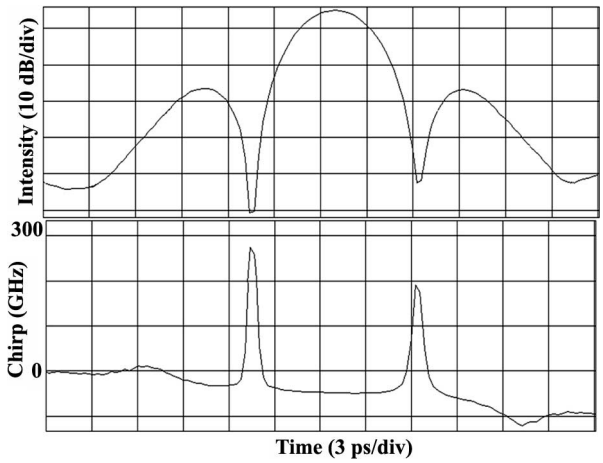

Fig. 12. Intensity and chirp profile of the EI GSLD pulse source employing an LC FBG for compression.

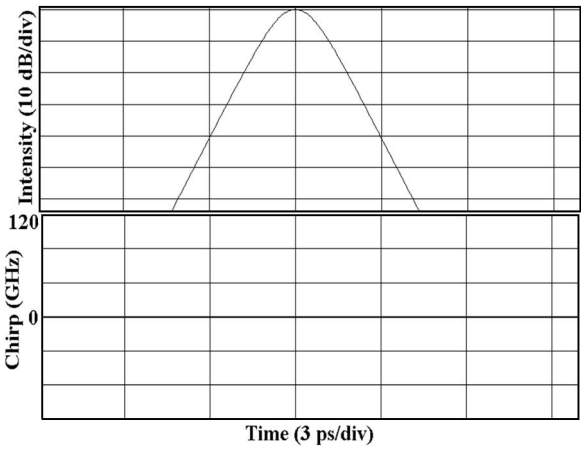

Fig. 13. Intensity and chirp profile of the TMLL pulse source.

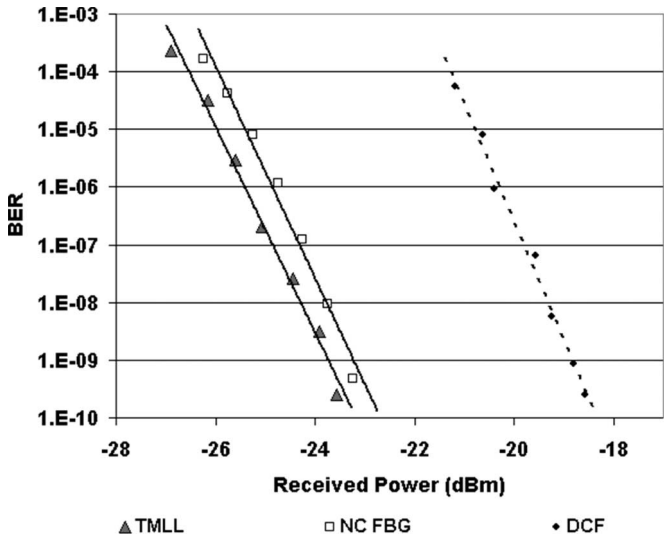

Fig. 14. BER versus received optical power for TMLL, NC FBG, and LC FBG employed in an 80-Gb/s OTDM test bed.

Fig. 14 displays the BER versus received power plots for one of the demultiplexed channels. It can be observed that to achieve a BER of 10^{-9}, a power penalty of 4 dB is incurred when the pulse source with the LC FBG is employed in comparison to the case where the NC FBG is used. This degraded performance is due to the presence of the pedestals about 23 dB below the peak of the pulse, as previously explained in the experimental case. In terms of the power penalty incurred, these simulation results achieved show a very good agreement with the experimental 80-Gb/s OTDM-system-performance characterization. The small difference in pulse width could be attributed to the minor difference (0.5 dB) in the sensitivities between the gain-switched pulses compressed by the NC FBG and the sech^2 pulses, as was noticed in the experimental section.

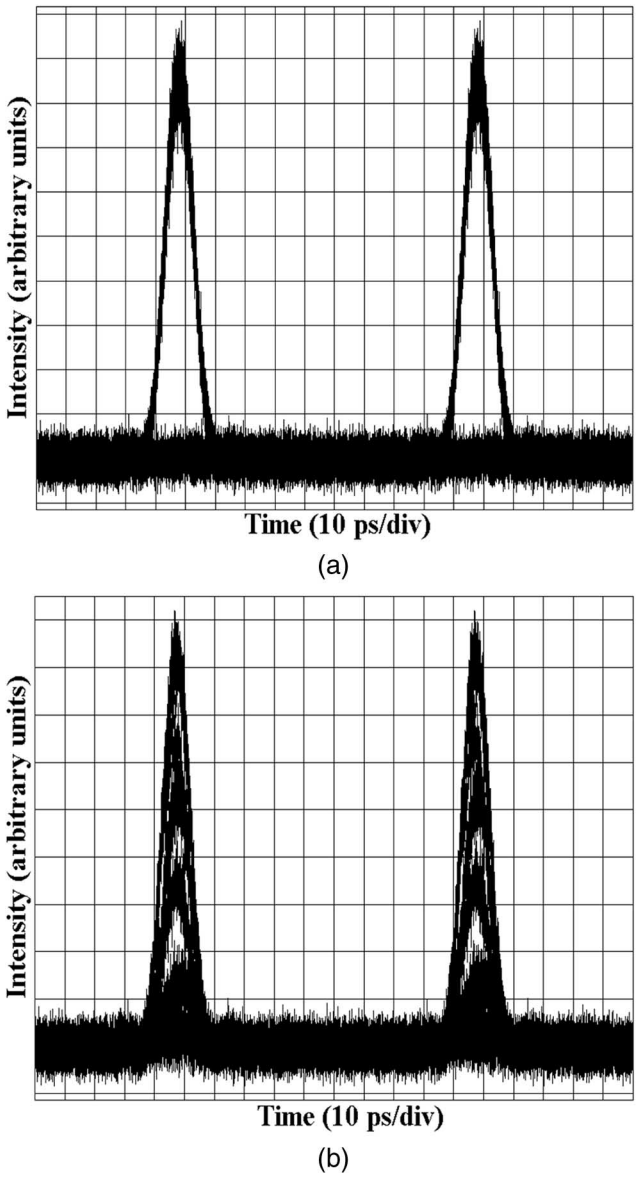

Fig. 15. Received eye diagrams at 10 Gb/s corresponding to the EI GSLD pulses compressed with the (a) NC FBG and (b) LC FBG when employed in an 80-Gb/s OTDM test bed.

The 10-Gb/s eye diagrams, corresponding to a power level of -23.24 dBm, are shown (Fig. 15) for the case of the EI GSLD pulses compressed by the NC FBG [Fig. 15(a)] and LC FBG [Fig. 15(b)]. The error free performance achieved by the pulses compressed by the NC FBG is reflected by the clean and open eye in the case of Fig. 15(a). On the other hand, the closed eye

[Fig. 15(b)] shows the degraded BER in the case of the pulses compressed by the LC FBG.

V. Discussion and Conclusion

OTDM is one of the techniques that could be used to realize high-capacity photonic communication systems. However, the fundamental component required to build such high-capacity OTDM systems is a cost-efficient source of short optical pulses that exhibits excellent temporal and spectral purity. An attractive solution to build such sources involves the use of a technique known as gain switching essentially due to its simplicity and reliability. The disadvantages that this technique suffers from could easily be overcome by employing external injection. The possibility of integrating the device used for external injection with a DFB laser [31] reduces the cost and footprint of the chosen solution.

Experiments performed show that pulses from an externally injected gain-switched source compressed by an LC FBG results in the formation of pedestals at a level of about 23 dB below the peak of the pulse. These pedestals occur as a result of the uncompensated nonlinear chirp in the wings of externally injected gain-switched pulse. BER measurements carried out show that these pedestals have a detrimental impact on the performance (1.5 dB) of a 40-Gb/s OTDM system. The penalty incurred goes up to 3.5 dB as the aggregate bit rate is doubled from 40 to 80 Gb/s. The increased interleaved bit rate leads to a reduction of the temporal slot allocated to each bit (25 ps for 40 Gb/s and 12.5 ps for 80 Gb/s). Hence, the coherent interactions between the adjacent OTDM channels (with poor TPSR) result in severe intensity fluctuations which in turn lead to the worsening system performance. Optimum system performance can be achieved by employing the tailor-made NC FBC. This grating not only portrays a nonlinear group delay (to compensate for the group delay of the gain-switched pulse) but also exhibits a nonlinear reflective profile (to compensate for the asymmetry of the pulse spectrum). These characteristics enable the compensation of the entire chirp across the pulse, thereby suppressing the pedestals to a level of about 40 dB below the peak of the pulse. The experimental results achieved demonstrate the importance of optimizing all the vital parameters of a gain-switched pulse source to yield pulses with excellent temporal and spectral purity. The simulations carried out with the aid of VPI transmission maker software verify the experimental result achieved.

In conclusion, we have presented a cost-efficient technique of generating pulses and provided a simple yet systematic way of optimizing such a source. We have also demonstrated its excellent performance in 40- and 80-Gb/s OTDM systems.

References

[1] M. Saruwatari, "All-optical signal processing for terabit/second optical transmission," *IEEE J. Sel. Topics Quantum Electron.*, vol. 6, no. 6, pp. 1363–1374, Nov./Dec. 2000.

[2] V. Mikhailov, P. Bayvel, I. Lealman, and R. Wyatt, "Compact and fully packaged fibre grating laser-based RZ pulse source for 40 Gb/s OTDM transmission systems," in *Proc. Eur. Conf. Opt. Commun.*, Amsterdam, The Netherlands, Sep. 2001, vol. 3, pp. 336–337.

[3] D. M. Spirit, A. D. Ellis, and P. E. Barnsley, "Optical time division multiplexing: Systems and networks," *IEEE Commun. Mag.*, vol. 32, no. 12, pp. 56–62, Dec. 1994.

[4] P. Anandarajah, L. P. Barry, and A. Kaszubowska, "Performance issues associated with WDM optical systems using self-seeded gain switched pulse sources due to mode partition noise effects," *IEEE Photon. Technol. Lett.*, vol. 14, no. 8, pp. 1202–1204, Aug. 2002.

[5] P. L. Mason, A. Wonfor, D. D. Marcenac, D. G. Moodie, M. C. Brierley, R. V. Penty, I. H. White, and S. Bouchoule, "The effects of pedestal suppression on gain-switched laser sources for 40 Gb/s OTDM transmission," in *Proc. 10th Annu. Meeting IEEE LEOS*, Nov. 10–13, 1997, vol. 1, pp. 289–290.

[6] L. P. Barry, P. Guignard, J. Debeau, R. Boittin, and M. Bernard, "A high-speed optical star network using TDMA and all-optical demultiplexing techniques," *IEEE J. Sel. Areas Commun.*, vol. 14, no. 5, pp. 1030–1038, Jun. 1996.

[7] M. Nakzawa, "Solitons for breaking barriers to terabit/second WDM and OTDM transmission in the next millennium," *IEEE J. Sel. Topics Quantum Electron.*, vol. 6, no. 6, pp. 1332–1343, Nov./Dec. 2000.

[8] S. Arahira and Y. Ogawa, "160 Gb/s OTDM signal source with 3R function utilizing ultrafast mode-locked laser diodes and modified NOLM," *IEEE Photon. Technol. Lett.*, vol. 17, no. 5, pp. 992–994, May 2005.

[9] K. Taira and K. Kikuchi, "Subpicosecond pulse generation using an electroabsorption modulator and a double-stage pulse compressor," *IEEE Photon. Technol. Lett.*, vol. 15, no. 9, pp. 1288–1290, Sep. 2003.

[10] L. P. Barry, R. F. O'Dowd, J. Debeau, and R. Boittin, "Tunable transform limited pulse generation using self-injection locking of an FP laser," *IEEE Photon. Technol. Lett.*, vol. 5, no. 10, pp. 1132–1134, Oct. 1993.

[11] K. Y. Lau, "Gain switching of semiconductor injection lasers," *Appl. Phys. Lett.*, vol. 52, no. 4, pp. 257–259, Jan. 1988.

[12] H. F. Liu, S. Oshiba, Y. Ogawa, and Y. Kawai, "Method of generating nearly transform-limited pulses from gain-switched distributed-feedback laser diodes and its application to soliton transmission," *Opt. Lett.*, vol. 17, no. 1, pp. 64–66, Jan. 1992.

[13] D.-S. Seo, D. Y. Kim, and H.-F. Liu, "Timing jitter reduction of gain-switched DFB laser by external injection seeding," *Electron. Lett.*, vol. 32, no. 1, pp. 44–45, Jan. 1996.

[14] A. M. Clarke, P. M. Anandarajah, and L. P. Barry, "Generation of widely tunable picosecond pulses with large SMSR by externally injecting a gain switched dual laser source," *IEEE Photon. Technol. Lett.*, vol. 16, no. 10, pp. 2344–2346, Oct. 2004.

[15] J. M. Dudley, L. P. Barry, J. D. Harvey, M. D. Thomson, B. C. Thomsen, P. G. Bollond, and R. Leonhardt, "Complete characterization of ultrashort pulse sources at 1550 nm," *IEEE J. Quantum Electron.*, vol. 35, no. 4, pp. 441–450, Apr. 1999.

[16] K. A. Ahmed, H. F. Liu, N. Onodera, P. Lee, R. S. Tucker, and Y. Ogawa, "Nearly transform limited pulse (3.6 ps) generation from gain-switched 1.55 μm distributed feedback laser by using fibre compression technique," *Electron. Lett.*, vol. 29, no. 1, pp. 54–56, Jan. 1993.

[17] B. J. Eggleton, P. A. Krug, L. Poladian, K. A. Ahmed, and H. F. Liu, "Experimental demonstration of compression of dispersed optical pulses by reflection from self-chirped optical fibre Bragg gratings," *Opt. Lett.*, vol. 19, no. 12, pp. 877–879, Jun. 1994.

[18] A. Clarke, P. M. Anandarajah, D. Reid, G. Edvell, L. P. Barry, and J. D. Harvey, "Optimized pulse source for 40-Gb/s systems based on a gain switched-laser diode in conjunction with a nonlinearly chirped grating," *IEEE Photon. Technol. Lett.*, vol. 17, no. 1, pp. 196–198, Jan. 2005.

[19] M. C. Gross, M. Hanna, K. M. Patel, and S. E. Ralph, "Reduction of power fluctuations in ultrafast optically time-division-multiplexed pulse trains by use of a nonlinear amplifying loop mirror," *IEEE Photon. Technol. Lett.*, vol. 14, no. 5, pp. 690–692, May 2002.

[20] D. Mechin, E. Le Cren, D. A. Reid, D.-K. Lee, B. C. Thomsen, and J. D. Harvey, "Picosecond and nanosecond sources generation of a 2.5 ps pedestal-free optical pulse using a 10 GHz gain-switched laser and a compressing nonlinear amplifying loop mirror," in *Proc. Conf. Laser Electro Opt.*, Long Beach, CA, May 2006, vol. 3, pp. 105–106.

[21] P. Gunning, J. K. Lucek, D. G. Moodie, K. Smith, R. P. Davey, S. V. Chernikov, M. J. Guy, J. R. Taylor, and A. S. Siddiqui, "Gain-switched DFB laser diode pulse source using continuous wave light injection for Jitter suppression and an electroabsorption modulator for pedestal suppression," *Electron. Lett.*, vol. 32, no. 11, pp. 1010–1011, May 1996.

[22] K. Iwatsuki, K. Suzuki, and S. Nishi, "Generation of transform limited gain-switched DFB-LD pulses < 6 ps with linear fibre compression and spectral window," *Electron. Lett.*, vol. 27, no. 21, pp. 1981–1982, Oct. 1991.

[23] Z. Hu, M. Davanco, and D. J. Blumenthal, "Extinction ratio improvement by strong external light injection and SPM in an SOA for OTDM pulse source using a DBR laser diode," *IEEE Photon. Technol. Lett.*, vol. 15, no. 10, pp. 1419–1421, Oct. 2003.

[24] P. M. Anandarajah, C. Guignard, A. Clarke, D. Reid, M. Rensing, L. P. Barry, G. Edvell, and J. D. Harvey, "Optimised pulse source employing an externally injected gain-switched laser diode in conjunction with a non-linearly chirped grating," *IEEE J. Sel. Topics Quantum Electron.*, vol. 12, no. 2, pp. 255–264, Mar./Apr. 2006.
[25] V. Mikhailov, P. Bayvel, I. Lealman, and R. Wyatt, "Fibre grating laser-based RZ pulse source for 40 Gb/s OTDM transmission systems," *Electron. Lett.*, vol. 37, no. 14, pp. 909–910, Jul. 2001.
[26] J. M. Dudley, F. Gutty, S. Pitois, and G. Millot, "Complete characterization of terahertz pulse trains generated from nonlinear process in optical fibers," *IEEE J. Quantum Electron.*, vol. 37, no. 4, pp. 587–594, Apr. 2001.
[27] R. Trebino, K. W. DeLong, D. N. Fittinghoff, J. N. Sweetser, M. A. Krumbugel, and B. A. Richman, "Measuring ultrashort laser pulses in the time-frequency domain using frequency-resolved optical gating," *Rev. Sci. Instrum.*, vol. 68, no. 9, pp. 3277–3295, May 1997.
[28] A. Rosenthal and M. Horowitz, "Inverse scattering algorithm for reconstructing strongly reflecting fiber Bragg gratings," *IEEE J. Quantum Electron.*, vol. 39, no. 8, pp. 1018–1026, Aug. 2003.
[29] J. Skaar and O. H. Waagaard, "Design and characterization of finite-length fiber gratings," *IEEE J. Quantum Electron.*, vol. 39, no. 10, pp. 1238–1245, Oct. 2003.
[30] R. Feced, M. N. Zervas, and M. A. Muriel, "An efficient inverse scattering algorithm for the design of non-uniform fibre Bragg gratings," *IEEE J. Quantum Electron.*, vol. 35, no. 8, pp. 1105–1115, Aug. 1999.
[31] U. Troppenz, J. Kreissl, W. Rehbein, C. Bornholdt, T. Gaerner, M. Radziunas, A. Glitzky, U. Bandelow, and M. Wolfrum, "40 Gb/s directly modulated InGaAsP passive feedback DFB laser," in *Proc. Eur. Conf. Opt. Commun.*, Cannes, France, Sep. 2006, vol. 6, pp. 61–62.

Prince M. Anandarajah (S'00–M'04) received the B.Eng. degree in electronic engineering from the University of Nigeria, Nsukka, Nigeria, in 1992 and the M.Eng. and Ph.D. degrees from Dublin City University, Dublin, Ireland, in 1998 and 2003, respectively.

From 1993 to 1997, he was an Instructor/Maintenance Engineer with the Aeronautical Telecommunications Department, Nigerian College of Aviation Technology, Zaria, Nigeria. Since September 2003, he has been a Postdoctoral Researcher with the Radio and Optical Communications Laboratory, Research Institute for Networks and Communications Engineering, Dublin City University. His major areas of research interests include generation and optimization of short optical pulses, all-optical signal processing using semiconductor optical amplifiers, radio-over-fiber distribution systems, and wavelength packet switching.

Aisling M. Clarke (S'03) received the B.Eng. degree in electronic engineering in 2002 from Dublin City University, Dublin, Ireland, where she is currently working toward the Ph.D. degree in optical communications. The main topic of her research is high-speed all-optical processing using semiconductor optical amplifiers.

Celine Guignard received the Eng. degree in optronics in 2001, the Masters degree in sciences and techniques of communications (D.E.A.) in optics communications, also in 2001, and the Ph.D. degree in optronics in 2005 from the University of Rennes I, Rennes, France.

Since April 2005, she has been a Postdoctoral Researcher with the Radio and Optical Communications Laboratory, Research Institute for Networks and Communications Engineering, Dublin City University, Dublin, Ireland. Her principal research interests include optical pulse generation with semiconductor lasers and optical injection.

Laurent Bramerie received the optoelectronic engineering degree from ENSSAT, University of Rennes I, Rennes, France, in 1999, and the Ph.D. degree in 2004.

He worked in France as a Technical Expert on ultralong haul 40-Gb/s dense-wavelength-division-multiplexing systems for two years with the Corvis Algety, Lannion, France. In 2003, he joined Centre National de la Recherche Scientifique Fonctions Optiques pour les Télécommunications–Ecole Nationale Supérieure des Sciences Appliquées et de Technologie (CNRS FOTON–ENSSAT), where he is currently a Research Engineer on the PERSYST platform, independent public research, and test facilities, offering a test bed for 40- and 10-Gb/s optical telecommunications systems open to private companies and university teams.

Liam P. Barry (M'98) received the B.E. degree in electronic engineering and the M.Eng.Sc. degree in optical communications from the University College Dublin, Dublin, Ireland, in 1991 and 1993, respectively, and the Ph.D. degree from the University of Rennes, Rennes, France.

From February 1993 to January 1996, he was a Research Engineer with the Optical Systems Department, France Telecom's Research Laboratories, Lannion, France. In February 1996, he was with the Applied Optics Centre, University of Auckland, Auckland, New Zealand, as a Research Fellow. In March 1998, he took up a lecturing position with the School of Electronic Engineering, Dublin City University, where he has since developed the Radio and Optical Communications Laboratory.

John D. Harvey (M'76) received the B.Sc. and M.Sc. degrees from the University of Auckland, Auckland, New Zealand, in 1965 and 1967, respectively, and the Ph.D. degree from the University of Surrey, Surrey U.K., for his work in theoretical nuclear physics.

Since 1970, he has been working at the University of Auckland, where he currently holds a Chair in the Physics Department. In recent years, his research has been concentrated in the areas of nonlinear fiber optics, ultrafast processes, and mode-locked lasers.

Prof. Harvey is a Fellow of the New Zealand Institute of Physics and is a member of the Optical Society of America and the Australian Optical Society.

Jean Claude Simon received the Ph.D. degree from the University d'Orsay, Orsay, France, in 1975 and the "Doctorat d'Etat" degree from the University of Nice, Nice, France, in 1983.

In 1972, he joined France Telecom's Research Laboratories (CNET), Lannion, France, which is the Research Center of the French PTT (now France Telecom), for his thesis work. In 1973, he was with CNET as a Research Scientist in the field of optical communication, particularly on the subject of optical amplifiers. From 1983 to 1997, he was Leader of a group in the field of semiconductor optical amplifiers and their applications for nonlinear optical devices. Since 1997, he has been responsible for the management of several research projects. Recently, he has moved to the University of Rennes, Rennes, France, where he is currently chairing a Professor position.

Investigation of Pulse Pedestal and Dynamic Chirp Formation on Picosecond Pulses After Propagation Through an SOA

A. M. Clarke, M. J. Connelly, P. Anandarajah, L. P. Barry, and D. Reid

***Abstract*—The authors investigate the propagation of picosecond pulses through semiconductor optical amplifiers using the measurement technique of frequency resolved optical gating. The work shows the generation of significant pulse pedestals and frequency chirp across the optical pulses, which initially have a duration of 2 ps. As the input peak power of the optical pulses is increased from 2.4 to 80 mW, the pulse pedestals increased by 20 dB and the chirp became significantly more nonlinear. The generated pedestals and the nonlinear output chirp may cause serious degradation in high-speed communications systems employing wavelength-division-multiplexing and optical time-division-multiplexing techniques.**

***Index Terms*—Frequency chirp, optical communications, optical pulse measurements, semiconductor optical amplifier (SOA).**

I. Introduction

SEMICONDUCTOR optical amplifiers (SOAs) are attracting a lot of interest in the field of telecommunications due to their high gain, small size, and opportunities for integration and low cost [1]. As telecommunication systems move toward higher capacities, it is essential to examine the operation of SOAs in high bit rate communication systems. Specifically, it is vital to investigate the effect of SOAs on picosecond optical pulses that may be employed in photonic systems operating at line rates of 40, 80, and 160 Gb/s. Presently, picosecond pulse sources [2] can generate high-quality pulses that have minimal chirp and jitter, and high (>30 dB) temporal and spectral purity as determined by the temporal extinction ratio, and the sidemode suppression ratio, respectively. These are required parameters for the practical use of these pulse sources in high-speed optical time-division-multiplexed (OTDM) transmission systems [2]. If future OTDM communication systems are going to employ SOAs, it is, thus, necessary to investigate the effects on picosecond pulses as they propagate through SOAs. This work focuses on the effects of SOA propagation and amplification on 2-ps pulses generated by a mode-locked laser source that may be suitable for OTDM systems operating at data rates from 40 to 160 Gb/s. We also explore the temporal shape of the induced chirp by the SOA, which will also be of vast importance for SOA-based interferometers used as all-optical switches.

Pulse propagation through SOAs has been experimentally investigated previously by traditional methods of autocorrelation, cross correlation, and optical spectrum analysis [3], [4]. However, the relatively new measurement scheme of frequency resolved optical gating (FROG) [5] may be used to overcome the limitations of traditional methods and provides complete characterization in the spectral and temporal domains with corresponding phase information. Previous work using FROG to characterize pulse propagation in SOAs has examined pulse distortion for pulsewidths around 200–300 fs in the absorption, transparency and gain regimes [6], and has examined nonlinear gain dynamics in the picosecond regime [7]. However, the pulse sources used in these works are not suitable for practical high-speed communications systems based on OTDM. In this letter, we present a complete analysis of the effect of SOA amplification on 2-ps mode-locked pulses generated at repetition rates of 10 GHz, which would be suitable for multiplexing to 40–160-Gb/s data rates. Our results are concerned primarily with the frequency chirp induced on the pulses by the SOA (an area that has seen extensive theoretical studies [8], [9]), and the introduction of temporal pedestals after pulse amplification in the SOA. We have characterized both of these effects (frequency chirp and temporal pedestals) for input pulse peak powers to the SOA ranging from 2.4 to 80 mW. Our results show the exact profile of the frequency chirp induced by the SOA for the range of optical input powers, and also an increase in the temporal pulse pedestal, induced by the SOA, of 20 dB as the input pulse peak power is increased. We also present results showing how a filter can be used to enhance the performance of SOAs for use in an OTDM system.

II. Experiment

The experimental setup is shown in Fig. 1. The pulses were generated using a commercially available mode-locked laser generating 5-ps pulses at a repetition rate of 10 GHz, and operating at a wavelength of 1534 nm. The pulses from the mode-locked laser have a significant linear frequency chirp, which is used to compress the pulses down to duration of 1.8 ps using dispersion-compensating fiber. The resultant Gaussian optical pulses are nearly transform limited, exhibiting a time bandwidth product of 0.5. A variable optical attenuator is then used to vary the input power of the optical pulses injected

Manuscript received February 24, 2005; revised May 9, 2005. This work was supported by Science Foundation Ireland Investigator Grant 02/IN1/I42.

A. M. Clarke, P. Anandarajah, and L. P. Barry are with RINCE, School of Electronic Engineering, Dublin City University, Dublin 9, Ireland (e-mail: liam.barry@dcu.ie).

M. J. Connelly is with the Department of Electronic and Computer Engineering, University of Limerick, Limerick, Ireland.

D. Reid is with the Physics Department, Auckland University, Auckland 1020, New Zealand.

Digital Object Identifier 10.1109/LPT.2005.852324

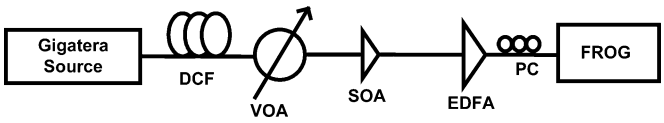

Fig. 1. Experimental setup.

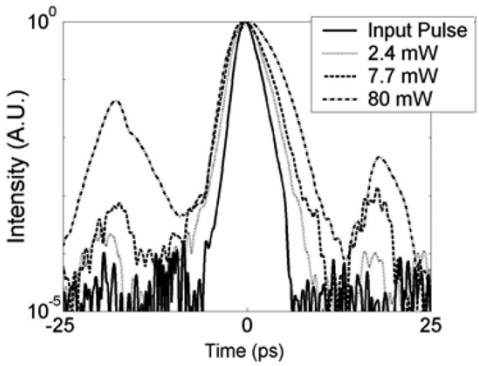

Fig. 2. Temporal profile of the input pulse and the pulse after the SOA with an input peak power of 2.4, 7.7, and 80 mW.

into the SOA. The SOA (from Kamelian) has an unsaturated fiber-to-fiber gain of 25 dB at an operating current of 250 mA.

Analysis of the pulses is carried out before and after amplification using a second-harmonic generation FROG with a spectral resolution of 0.05 nm (6 GHz). The FROG generates a spectrogram, which is a three-dimensional plot of intensity as a function of wavelength and time. A phase retrieval program is then applied to the generated spectrogram to reconstruct the electric field of the optical pulse giving complete spectral and temporal characterization of the measured pulse. To obtain good signal-to-noise ratio (SNR) in the FROG measurements, and to minimize the time taken to acquire the results, an erbium-doped fiber amplifier (EDFA) is employed to amplify the input pulses to the FROG to a peak power of around 500 mW. The EDFA used is designed specially for operation with 2-ps optical pulses, and it is operated in the linear gain regime such that it does not alter the phase of the optical pulses being characterized by the FROG. Frog errors below $\sim$0.004 were recorded for the retrieved pulses indicating accurate retrievals [5].

III. Results and Discussion

In this work, we initially analyze the physical effects on the pulse as it propagates through the SOA. The pulse pedestals and the frequency chirp induced on the optical pulses after amplification with the Kamelian SOA were examined as a function of input peak power to the amplifier. Fig. 2 displays the intensity profile of the input optical pulse and the temporal profile of the pulse after amplification by the SOA as the input peak power is varied from 2.4 to 80 mW, at a bias current of 200 mA. Fig. 2 shows that the pulsewidth increases from 1.8 to 4.2 ps. We can also see a dramatic increase in the pedestals on the leading and trailing edge of the pulse. For the pulses at the input to the SOA, the pedestals cannot be seen as they are below the noise level of our measurement system. At the output of the SOA, the pulse pedestals increase from approximately 40–15 dB below the peak of the pulse, as the input pulse peak power is increased. The

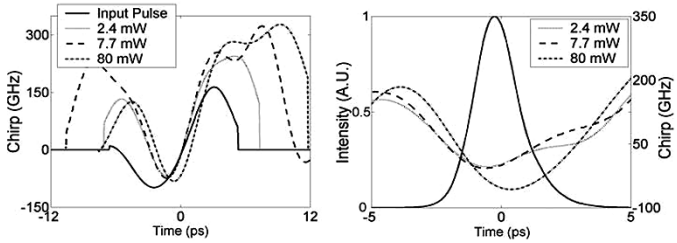

Fig. 3. (a) Chirp before and after the SOA and (b) the chirp induced by the SOA across the temporal profile of the pulse for input peak powers of 2.4, 7.7, and 80 mW.

reason for the decrease in the pulse pedestal suppression ratio is that the pulse pedestal present on the leading edge of the input pulse is amplified by the SOA as it sees a high linear gain. This partially saturates the amplifier gain leading to a reduced amplification of the main pulse. The high power main pulse then drives the SOA further into saturation. This is the reason for the asymmetric shape of the pulse outputted from the SOA, as the leading edge saturates the amplifier and the gain available for the trailing edge is reduced [8], [9]. The gain partially recovers for the trailing pedestal and it is, thus, also amplified relative to the main pulse. The central component of the 80-mW input pulse experiences higher gain saturation than is the case for the lower input power pulses. This implies that the relative intensity differences between the leading and trailing pedestals, and the main pulse, is less than is the case for lower power input pulses, which is shown from our results. For all of the input pulse powers, there is partial recovery of the gain after the main pulse but not as much as for the leading edge. This explains the observation that the relative effect of changing from 7.7 to 80 mW is larger than the effect of changing from 2.4 to 7.7 mW in the case of the leading pedestal. It should be noted that for the FROG measurements of the weak pedestals (>35 dB below pulse peak), the SNR of these pulses is such that there will be uncertainty as to the exact level of the weak pedestals. There is, however, no uncertainty in the large increase in these pedestals, which would clearly pose significant problems (through intersymbol interference) for the use of these pulses in high-speed OTDM systems [10].

Pulse chirp is an essential parameter used in the analysis of pulses in transmission systems as it determines the propagation distance of the pulse and it can give information about the pulse structure. It is important not only to know its peak-to-peak value but also its profile across the pulse, especially SOA-induced chirp as it has a nonlinear structure. Fig. 3(a) displays the profile of the frequency chirp across the pulses at the input and output of the SOA (for a range of input powers), and it is clear that the chirp becomes more nonlinear as the input power to the SOA is increased. The chirp ends abruptly close to the edges of the main pulse, as when the intensity level is close to zero, it is not possible to correctly measure the chirp (thus, it is set to zero at these levels). Fig. 3(b) displays the actual chirp induced by the SOA across the pulse. This chirp can be calculated by subtracting the input chirp of the compressed mode-locked laser pulses, from chirp at the output of the SOA [8]. The associated spectra of the optical pulses are illustrated in Fig. 4. Fig. 4(b) displays the spectrum of the amplified pulses from the FROG measurement,

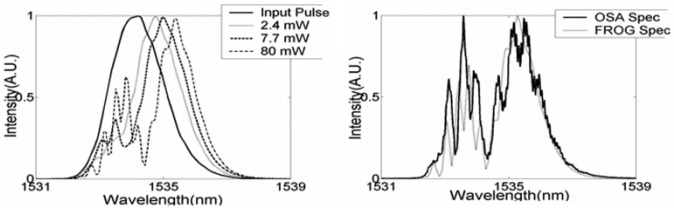

Fig. 4. (a) Spectra generated by the FROG for the input and output at input peak powers of 2.4, 7.7, and 80 mW and (b) a comparison of the spectrum generated by the FROG and the OSA at 80-mW input pulse peak power.

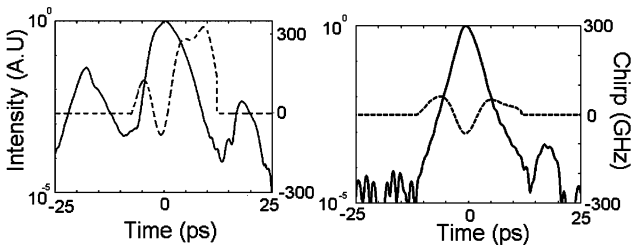

Fig. 5. Comparison of the temporal profile and the chirp output from the SOA (a) before and (b) after the simulated filter.

and that measured using an optical spectrum analyzer (OSA) when the input peak power to the SOA is 80 mW. These traces show reasonably good agreement, indicating the accuracy of the FROG technique.

The chirp across the leading edge of the pulse has a negative slope, which corresponds to the main peak of the spectrum shifting to longer wavelengths (often referred to as red-shifting). The chirp across the trailing edge has a positive slope. The second less dominant peak in the spectrum corresponds to the wings of the pulse and the pulse pedestals. The increase in the blue-shifted peak of the spectrum increases in line with the increases in pulse pedestals. These effects in the chirp are caused by self-phase modulation (SPM) induced by gain saturation caused by carrier depletion and carrier heating due to effects of stimulated emission, free carrier absorption, and in particular two-photon absorption [9], [11]. An additional contribution to SPM originates from the instantaneous nonlinear index [9]. The nonlinear effects are particularly important for pulsewidths below 2 ps [9]. Together all these effects result in gain suppression and a corresponding change in phase through the process of SPM.

It has been shown that by filtering out the unwanted blue-shifted component of the spectrum, the pulse from the SOA can be recovered to nearly its original form and the extinction ratio can be improved [12]. To demonstrate this, we used a theoretical simulation to apply an ideal bandpass filter with a bandwidth of 4 nm to the electric field produced by the FROG to remove the short wavelength components. The results illustrated in Fig. 5 show the reduction of the pulse pedestals to 30 dB below the peak and the pulsewidth reduced to a full-width at half-maximum of 2 ps. The nonlinear chirp is reduced, however there is some residual nonlinear chirp on the filtered pulse.

IV. Conclusion

This letter has investigated the effect of SOA amplification on 2-ps optical pulses using the FROG measurement technique. We have investigated in detail the reduction in pulse pedestal suppression ratio as the input power to the SOA is increased. We have also accurately measured the chirp after the SOA and the chirp induced by the SOA. Our results show that if SOAs are to be employed in high-speed optical communication systems, then it will be vital to optimize their operating characteristics in order to minimize the degradation in system performance that they may cause.

References

[1] M. J. Connelly, *Semiconductor Optical Amplifiers*. Boston, MA: Kluwer, 2002.

[2] D. Cotter, J. K. Lucek, and D. D. Marcenac, "Ultra-high-bit-rate networking: From the transcontinental backbone to the desktop," *IEEE Commun. Mag.*, vol. 35, no. 4, pp. 90–95, Apr. 1997.

[3] T. Saitoh and T. Mukai, "Gain saturation characteristics of travelling-wave semiconductor laser amplifiers in short optical pulse amplification," *IEEE J. Quantum Electron.*, vol. 26, no. 12, pp. 2086–2094, Dec. 1990.

[4] R. S. Grant and W. Sibbett, "Observations of ultrafast nonlinear refraction in an InGaAsP optical amplifier," *Appl. Phys. Lett.*, vol. 58, pp. 1119–1121, 1991.

[5] R. Trebino, K. W. Long, D. N. Fittinghoff, J. N. Sweetser, M. A. Krumbugel, and B. A. Richman, "Measuring ultrashort laser pulses in the time-frequency domain using frequency resolved optical gating," *Rev. Sci. Instrum.*, vol. 68, pp. 3277–3295, 1997.

[6] F. Romstad, P. Borri, W. Langbein, J. Mork, and J. M. Hvam, "Measurement of pulse amplitude and phase distortion in a semiconductor optical amplifier: From pulse compression to breakup," *IEEE Photon. Technol. Lett.*, vol. 12, no. 12, pp. 1674–1676, Dec. 2000.

[7] P. J. Delfyett, H. Shi, S. Gee, I. Nitta, J. C. Connolly, and G. A. Alphonse, "Joint time-frequency measurements of mode-locked semiconductor diode lasers and dynamics using frequency-resolved optical gating," *IEEE J. Quantum Electron.*, vol. 35, no. 4, pp. 487–500, Apr. 1999.

[8] G. P. Agrawal and N. A. Olsson, "Self-phase modulation and spectral broadening of optical pulses in semiconductor laser amplifiers," *IEEE J. Quantum Electron.*, vol. 25, no. 11, pp. 2297–2306, Nov. 1989.

[9] M. Y. Hong, Y. H. Chang, A. Dienes, J. P. Heritage, and P. J. Delfyett, "Subpicosecond pulse amplification in semiconductor laser amplifiers: Theory and experiment," *IEEE J. Quantum Electron.*, vol. 25, no. 4, pp. 2297–2306, Apr. 1989.

[10] P. L. Mason, A. Wonfor, D. D. Marcenac, D. G. Moodie, M. C. Brierley, R. V. Penty, I. H. White, and S. Bouchoule, "The effects of pedestal suppression on gain switched laser sources for 40 Gbit/s OTDM transmission," in *Proc. 10th Annu. Meeting IEEE LEOS*, vol. 1, 1997, pp. 289–290.

[11] J. M. Tang and K. A. Shore, "Amplification of strong picosecond optical pulses in semiconductor optical amplifiers," *Proc. IEEE, Optoelectron.*, vol. 146, no. 1, pp. 45–50, Feb. 1999.

[12] M. L. Neilson, B. Olsson, and J. Blumenthal, "Pulse extinction ratio improvement using SPM in an SOA for OTDM systems applications," *IEEE Photon. Technol. Lett.*, vol. 14, no. 2, pp. 245–247, Feb. 2002.

FROG characterisation of SOA-based wavelength conversion using XPM in conjunction with shifted filtering up to line rates of 80 GHz

A.M. Clarke[1], G. Girault[2], P. Anandarajah[1], C. Guignard[1], L. Bramerie[2], L.P. Barry[1], J. C. Simon[2] and J. Harvey[3]
[1]RINCE, School of Electronic Eng., Dublin City University, Ireland (email: liam.barry@dcu.ie).
[2] FOTON-ENSSAT / PERSYST Platform, 6 rue de Kérampont, BP 80518 22305 Lannion Cedex, France.
[3] Physics Dept. Auckland University, New Zealand.

Semiconductor Optical Amplifiers (SOAs) are ideal candidates for use as all-optical processing devices such as wavelength conversion [1]. Their attraction comes from their small size, low energy consumption, highly nonlinear response and possibilities for monolithic integration. The work we present here builds on recent work where we obtained 80 Gb/s error free performance using cross phase modulation (XPM) in an SOA in conjunction with a blue shifted bandpass filter [2]. Here we present a detailed characterisation of this wavelength conversion scheme using a Frequency Resolved Optical Gating (FROG) measurement scheme for both red and blue shifted filtering. This characterisation is important as it measures the exact temporal profile of the wavelength converted pulses and its corresponding output chirp as a function of input line rate from 10-80 GHz. Thus the patterning effect and the gain dynamics resulting from red and blue shifted filtering can be examined in detail. The FROG measurement scheme is advantageous over other pulse measurement schemes such as bandwidth limited oscilloscopes and traditional autocorrelation methods as it retrieves intensity and corresponding phase information [3].

The wavelength conversion scheme presented here uses a very simple technique, which exhibits low polarisation dependence and retains the polarity of the input pulse in comparison to other similarly published wavelength conversion schemes [4]. The experimental set-up is shown in Figure 1. Mode-locked pulses with a FWHM of 2.3 ps were generated at a repetition rate of 10 GHz at a wavelength of 1545 nm. The pulses were amplified and passively multiplexed at rates ranging from 10-80 GHz. This pulse train was coupled with a continuous wave (CW) probe signal and were injected into a commercially available SOA. The measured slow gain recovery time of this SOA was 50 ps. The pulse energy was kept constant for each line rate at 12 fJ and the probe average power was 2.5 dBm. To obtain optimised red and blue shifted filtering the probe signal was set at a wavelength of 1551.91 nm and 1558.6 nm respectively. The probe signal was tuned as a fixed Fibre Bragg Grating Filter was used following the SOA. This filter had a 3dB bandwidth of 5 nm and a sharp band edge, which was used to reject the original pump signal and to significantly reduce the CW portion of the probe. A second 3 nm tunable Gaussian filter was used to suppress further the CW signal and thus give an improved extinction ratio (ER). The intermediate EDFA (EDFA2) was used to overcome the high insertion loss due to the shifted filters. The wavelength converted pulses were then analysed using the FROG at line rates of 10, 20, 40, and 80 GHz. An EDFA was required before the FROG to obtain the maximum SNR of the measurement scheme.

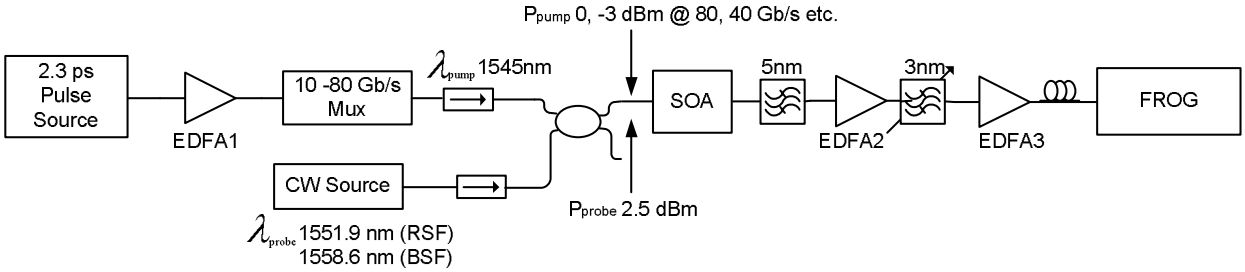

Figure 1: Experimental set up for the bandpass shifted filtering wavelength conversion scheme

The intensity profiles of the wavelength converted pulses for red and blue shifted filtering are shown in Figure 2. By placing the filter on the red shifted side of the original probe spectrum we obtain very short pulses as shown in Figure 2(a). This is due to the very fast response caused by the depletion of carriers which induces an equally fast red chirp. A small portion of blue chirped spectral components, which are not fully rejected by the filters, is the cause of the tail present on the trailing edge of the pulses. As is clearly evident, patterning effects are very prominent in red shifted wavelength conversion schemes, as the amount of carriers depleted dictates the size of the chirp and as the bit rates increase, fewer carriers have recovered. This leads to a reduction in red chirp and thus a reduction in output power. However, for the blue shifted filtering we can obtain error free performance up to 80 Gb/s [2] as the patterning effects are not as substantial as displayed in Figure 2(b), as blue shifted filtering is less dependent on the

input line rate. The leading edges of the blue shifted wavelength converted pulses have a very sharp slope. This is the result of the fast gain recovery of the SOA, which is related to intraband effects occurring on a timescale of approx 1-2ps. The structure at the centre of the pulse is due to a combination of the filter shape and the point where the slow gain recovery begins to take effect. The trailing edge of the pulse is determined by the shape of the filter profile.

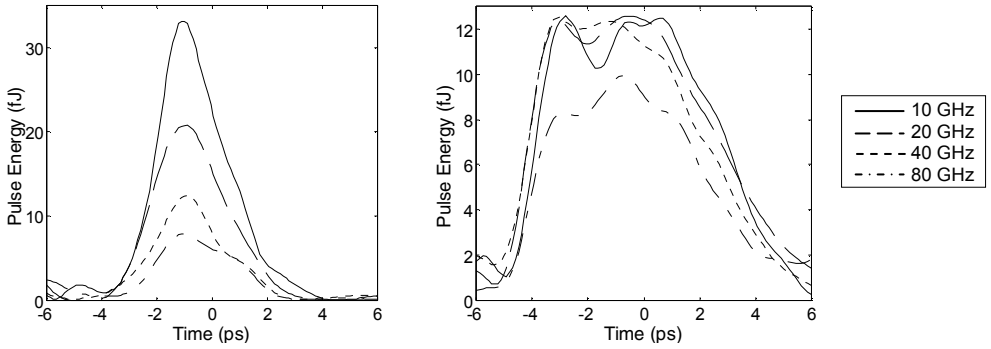

Figure 2 (a) and (b): Intensity profiles for red and blue shifted filtering respectively in conjunction with XPM in an SOA at line rates of 10, 20, 40 and 80 GHz.

In Figure 3 we show the wavelength converted pulses normalised and their corresponding output chirp. The output pulses have a pulse width of 2.5-3.6 ps and 7-6.3 ps for respective red and blue shifted converted pulses. The chirp in particular for the blue shifted pulses is approximately linear across the pulse. This is to be expected as the induced phase by the SOA is converted into amplitude modulation by the shifted filter. This linear chirp with an approximate magnitude of 200 GHz could be used to compress the blue-shifted converted pulses to 3.5 ps. The small ripple on the output chirp is due to an uneven filter profile. Enhanced performance could be achieved by using a filter with a smoother profile and pulse compression could be obtained with a filter that has a linear chirp opposite to the wavelength converted pulses.

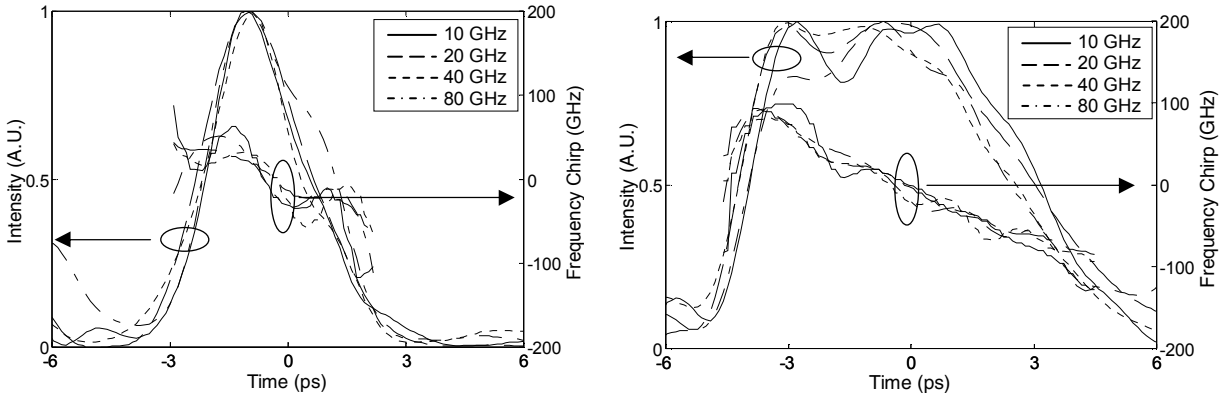

Figure 3 (a) and (b): Intensity and corresponding chirp profiles for red and blue shifted filtering respectively in conjunction with XPM in an SOA at line rates of 10, 20, 40 and 80 GHz.

In conclusion a full characterisation of a popular wavelength conversion scheme which uses XPM in an SOA in conjunction with bandpass shifted filtering is provided. This type of characterisation has not been provided before to the best of the authors knowledge and is an important analysis firstly to achieve a full understanding of the gain and phase dynamics exploited by the wavelength conversion scheme presented and secondly to design a filter so that an optimum performance can be obtained.

Acknowledgements: This work was supported in part by Science Foundation Ireland (Investigator Program), the French Research Ministry, Europe (FEDER) and Britanny Region.

[1] T. Durhuus et al., *IEEE J. of Lightwave Technol.,* vol. 14, pp. 942-954, 1996.
[2] L. Bramerie et al., CLEO 2006, CMT7, 2006.
[3] R. Trebino, et al., *Rev. Sci. Instrum.,* vol. 68, pp. 3277-3295, 1997.
[4] Y. Liu, et al., *IEEE J. of Lightwave Technol.,* vol. 24, pp. 230-236, 2006.

Performance Analysis of a Simple SOA Wavelength Converter based on XPM and Shifted Filtering up to 80 Gbit/s

G. Girault, A. M. Clarke, *Student Member, IEEE,* C. Guignard, P. Anandarajah, *Member, IEEE,* D. Reid, L. Bramerie, L. P. Barry, *Member, IEEE,* J-C. Simon, and J. Harvey, *Member, IEEE*.

***Abstract*— This paper provides a full analysis of a semiconductor optical amplifier (SOA)-based wavelength conversion scheme, which exploits cross phase modulation (XPM) in an SOA in conjunction with shifted filtering. The analysis includes an experimental measurement of the back-to-back system performance as well as a frequency-resolved optical gating (FROG) characterisation for both red and blue shifted filtering. The placement of the filter to undertake blue shifted filtering (BSF) shows optimum performance in comparison to red shifted filtering (RSF). Simulation work is carried out to examine the performance of this wavelength conversion scheme following transmission in 50 km of dispersion compensated fiber span.**

***Index Terms*—All-optical switch, Frequency-resolved optical gating, Semiconductor optical amplifier, Shifted bandpass filtering, Wavelength conversion, Ultrafast.**

I. Introduction

With ever increasing demand for high-bandwidth applications, the growth towards implementing Tbit/s optical networks continues. Wavelength division multiplexing (WDM) is currently the optical multiplexing technique of choice in order to exploit the large bandwidth capabilities provided by optical fiber. As individual line rates increase, all-optical processing techniques will be required, to provide simple network management.

In particular, wavelength converters will be key elements of optical networks, in that they enable simpler network operation and provide dynamic provisioning in order to make full use of the available bandwidth [1], [2]. Presently individual channel rates are operating up to line rates of 40 Gbit/s, limited typically by the speed of electronics. However the bit rate of each individual line rate is set to increase to even greater capacities. Therefore there is a need to design and develop all-optical wavelength converters that can perform at line rates greater than 40 Gbit/s.

Future all-optical wavelength converters must meet certain criteria such as simple and stable operation, cost effectiveness and low energy consumption. A semiconductor optical amplifier (SOA) is one such candidate which meets all of the above criteria [3]. In addition these components have a small footprint, hold possibilities for monolithic integration [4], polarisation insensitivity [5], and exhibit high nonlinearities for low input powers (compared to nonlinearities in fibers). Thus SOAs are ideal candidates for use as ultrafast wavelength converters [6], [7].

One method of implementing wavelength conversion with SOAs is to use cross gain modulation (XGM). However the main disadvantages of this process are the polarity inversion of the output data in comparison to the input signal, the poor output extinction ratio and the bit rate limitation due to the SOA gain recovery time which can typically vary from 40-100's ps for different SOAs [8]. A solution to overcome these disadvantages is to use cross phase modulation (XPM) in a SOA in conjunction with an interferometer [9]-[11]. However such schemes are often complicated and generally display problems with stability for example due to polarisation sensitivity. A more simple technique is to use a shifted bandpass filter (BPF) following the SOA which was first proposed by Ellis *et al.* [12] and which has recently shown to operate at very high bit rates by Liu *et al.* [13]. This solution overcomes the limitation due to the slow gain recovery time of SOAs and improves the extinction ratio in comparison with simple XGM. However the output data polarity is still inverted and the extinction ratio is insufficient. Cho *et al.* [14] have presented a similar scheme but the proposed scheme retains the polarity of the input data by spectrally shifting the filter further from the continuous wave probe signal, thus primarily exploiting XPM in the SOA, in the same way as using phase modulation in a fiber associated with a shifted filter [15], [16]. This kind of device gives an enhanced extinction ratio and has

Manuscript received April, 2007. This work was supported in part by the Enterprise Ireland, Science Foundation Ireland, the Research Ministry of France, the Britanny Region and the European Commission (FEDER).

G. Girault, L. Bramerie and J-C. Simon are with PERSYST platform from CNRS FOTON-ENSSAT, 6 rue de Kerampont BP 80518 LANNION CEDEX France.

Corresponding author: G. Girault (girault@enssat.fr).

A. M. Clarke, P. Anandarajah, D. Reid and L. P. Barry are with the Research Institute for Networks and Communications Engineering (RINCE), School of Electronic Eng., Dublin City University, Ireland (liam.barry@dcu.ie).

C. Guignard was with the Research Institute for Networks and Communications Engineering, School of Electronic Eng., Dublin City University, Ireland.

J. Harvey is with Physics Dept. Auckland University, New Zealand.

enabled operation at high data rates [17]. Fu *et al.* [18] have experimentally characterised the evolution of the wavelength converted pulse shape as the filter is shifted from blue to red wavelengths at a data rate of 10 Gbit/s. At this bit rate, Chayet *et al.* [19] have demonstrated the regenerative properties of such a scheme based on a high wavelength (red shifted) filtering. Vázquez *et al.* [20] have proposed the use of genetic algorithms to achieve the optimum filter shape. However these papers do not consider the changing shape of the wavelength converted pulses as a function of the input data pattern to the SOA and transmission of the wavelength converted signal at very high bit rates has not yet been examined.

In this paper we present an analysis of a wavelength converter which primarily exploits XPM in an SOA in conjunction with a shifted BPF. This scheme offers the advantages of simplicity, polarisation insensitivity, stability, polarity preservation and large output extinction ratio. The analysis investigates the scheme in terms of performance up to line rates of 80 Gbit/s and examines the output pulse and chirp profiles dependent on the repetition rate of the wavelength converted pulses. The analysis examines placement of the shifted filter to conserve either red or blue spectral components.

The paper is organized as follow: Section II describes the principle of the studied wavelength converter. Section III presents the back-to-back bit error rate (BER) performance of the wavelength conversion scheme and analyses their temporal and chirp output profiles using frequency-resolved optical gating (FROG) measurements at increasing line rates up to 80 GHz. Finally, in Section IV a numerical study is implemented to investigate the behaviour of the converted pulses in a transmission link.

II. Principle of the Wavelength Converter

The principle of the SOA and filter-based wavelength converter, which is illustrated in Fig. 1, consists of injecting two signals into the SOA: The data signal and a simple continuous wave (CW), called a “probe”, at the required conversion wavelength.

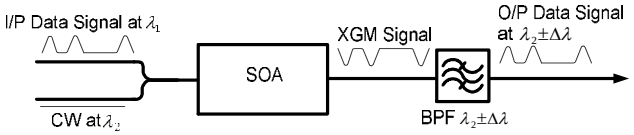

Fig. 1. Principle of wavelength converter based on cross phase modulation (XPM) in a SOA associated with a shifted bandpass filter (BPF).

The input data signal modulates the gain in the SOA due to gain saturation. In the same way the refractive index and thus the phase of the probe are also modulated. This process of XPM causes a shift of the probe spectral components firstly to longer wavelengths, known as red-shifting and then to lower wavelengths known as blue-shifting. Fig. 2 is an illustrative view of the corresponding temporal effects between an input pump pulse, the dynamic SOA gain compression and the frequency shift induced in the SOA, *i.e.* the SOA ‘chirp’.

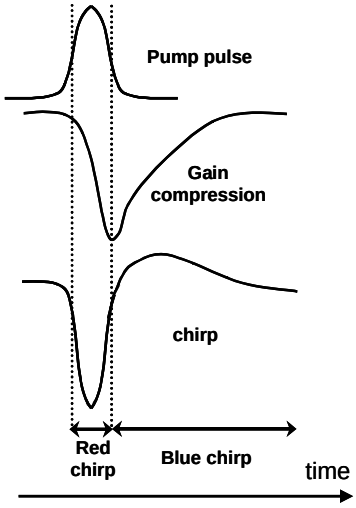

Fig. 2. Time correspondences between input pump pulse, SOA gain compression and induced SOA chirp.

Generally a BPF is placed after the SOA, to reject the original input data signal. By shifting this filter off centre to retain the lower wavelengths or the blue-shifted spectral components of the probe signal, the limitations typically governed by the slow gain recovery time of the SOA can be overcome, taking advantage of the short time scale on which the chirp occurs [21]. If the filter is placed further to longer or shorter wavelengths so as to suppress the DC component of the probe, the phase modulation of the probe signal can be converted to intensity modulation and thus the polarity of the input signal can be preserved [15],[17]. This can be explained in further detail: When a ‘0’ is input to the SOA, there is no saturation of the SOA gain and thus there is no corresponding wavelength shift of the probe spectral components. Thus the filter rejects the CW signal. On the contrary when a ‘1’ is input to the SOA, there is a shift of the probe spectral components to first the longer wavelengths (red shift) and then to lower wavelengths (blue shift). Thus depending on the placement of the filter either the red or blue shifted spectral components are maintained while the remaining probe signal (including the DC component) is suppressed.

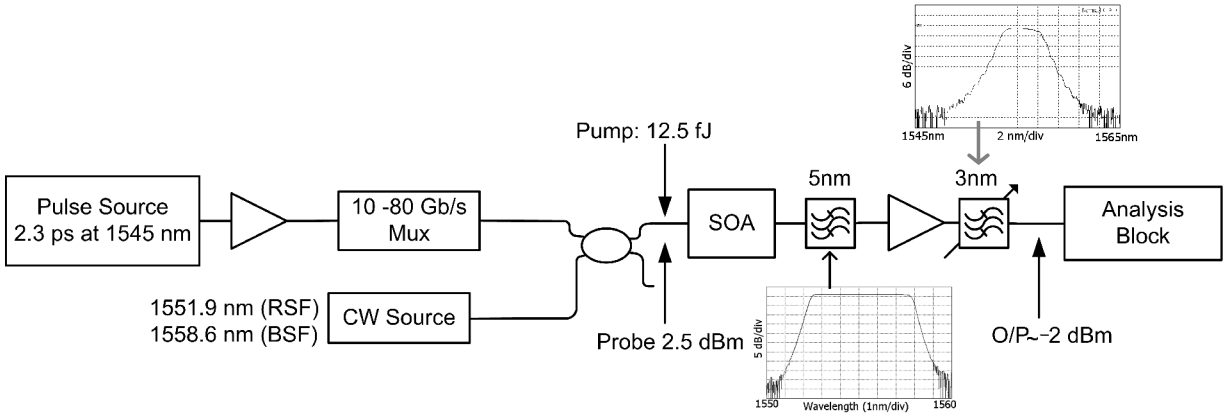

Fig. 3. Experimental set-up

The power efficiency of this technique increases as the amount of induced spectral broadening (*i.e.* 'chirp') becomes larger. Therefore the shorter and more energetic the input pulses are, the more efficient the process is, particularly thanks to intra-band effects [22]. In addition the more suppressed the DC component of the probe is, the larger the output extinction ratio.

III. Experimental analysis

The aim of the following experimental study is the analysis of the behaviour of such a wavelength converter in the case of both blue-shifted filtering (BSF) and red-shifted filtering (RSF). The analysis consists of BER measurements as a function of power received and a pulse and chirp characterisation of the wavelength converted pulses at different line rates up to 80 GHz (10, 20, 40 and 80 GHz) to explore the wavelength converted signal dependence on its preceding pattern.

A. Experimental set up

The experimental set up is shown in Fig. 3. Mode-locked pulses with a full width half maximum (FWHM) of 2.3 ps are generated at a repetition rate of 10 GHz and at a wavelength of 1545 nm. The pulses are amplified using an erbium doped fiber amplifier (EDFA) and passed through a Mach-Zehnder intensity modulator to obtain a RZ-PRBS of 2^7-1. The data signal was then passively multiplexed to the required line rate of 10, 20, 40, or 80 Gbit/s. At 80 Gbit/s the average pulse power is 0 dBm (energy = 12.5 fJ,) and was reduced by 3 dB as the data rate was decreased by half to maintain a constant pulse energy. The wavelength conversion scheme consists of injecting a CW signal coupled with the pump signal into an SOA. The probe power measured at the input to the SOA is 2.5 dBm.

The measured slow gain recovery time of this SOA is 55 ps at a bias current of 250 mA. Two filters and an EDFA were employed after the SOA. The first filter is a fixed filter, so to implement either RSF or BSF we change the probe wavelength rather than the position of the filter. Therefore to obtain optimised red and blue shifted filtering the probe signal is set at a wavelength of 1551.91 nm and 1558.6 nm respectively. This first filter has a sharp band edge, which is used to reject the original pump signal and to significantly reduce the CW portion of the probe. The second 3 nm tunable Gaussian filter is used to suppress further the CW signal and thus give an improved extinction ratio. An intermediate EDFA between the two filters is required to overcome the high insertion loss due to the shifted filtering. The average power at the output of the wavelength converter is measured at approximately -2 dBm at 80 Gbit/s. Fig. 4 shows the signal spectra at the input of the wavelength converter, at the output of the SOA and after RSF and BSF.

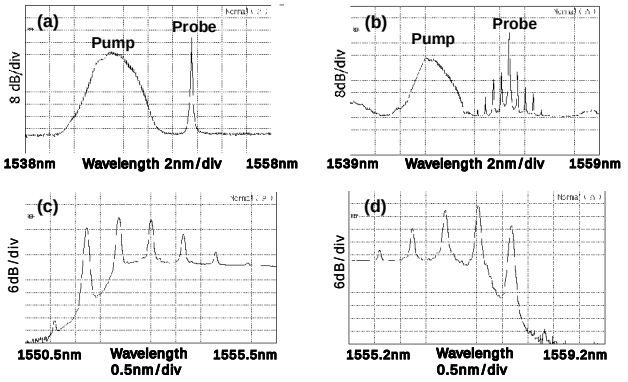

Fig. 4. Signal spectra at different points of the wavelength conversion process at 80 GHz: at the SOA input (a), at the SOA output (b), wavelength converted signal after RSF (c), wavelength converted signal after BSF (d).

B. Bit Error Rate Measurements

To measure the BER the signal was demultiplexed from 80 Gbit/s to 20 Gbit/s optically via two electro-absorption modulators and was then electrically demultiplexed to 10 Gbit/s. The power received level was measured at 20 Gbit/s just before the photodiode preceding the electrical demultiplexer. The BER measurements for both BSF and RSF at 80 Gbit/s are displayed in Fig. 5, in addition to a back-to-back measurement without wavelength conversion.

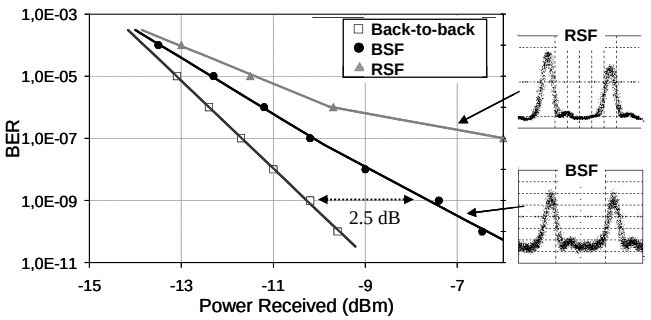

Fig. 5. BER measurements at 80 Gbit/s versus the received power for each case of filtering (BSF or RSF) and associated oscilloscope traces for a pattern of 00001010 (only the four last symbols are displayed).

Error free performance has been obtained at 80 Gbit/s with BSF as previously presented in [23]. By comparison with the back-to-back curve, a penalty of 2.5dB has been measured. However for the RSF technique error free performance has only been achieved at 40 Gbit/s. As can be seen in Fig. 5 an error floor is observed at a BER of 10^{-7} for 80 Gbit/s.

The error floor present for the RSF technique is due to patterning effects as a consequence of the incomplete gain recovery of the SOA. These patterning effects are clearly seen in the oscilloscope trace shown in Fig. 5. These oscilloscope traces were measured by applying a pattern of 00001010 to the wavelength conversion scheme which shows that in the RSF case patterning effects lead to a significant reduction in the power of the second '1'. This is because the magnitude of the red chirp corresponds to the gain saturation by the pulse as shown in Fig. 2. Thus the amount of chirp in RSF technique is dependent on how well the gain has recovered. We can note that these patterning effects are significantly reduced (almost negligible) in the case of BSF as observed in Fig. 5. This is explained in more detail in section C with the aid of FROG characterisation.

As shown in Fig. 6, these patterning effects lead to a small eye opening for the RSF case, while the BSF case retains a large eye opening, thus 80 Gbit/s error free performance is obtainable.

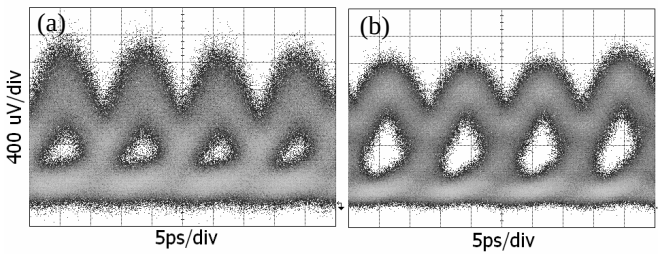

Fig. 6. Eye diagrams of the wavelength converted signal at 80 Gbit/s following (a) RSF and (b) BSF for a power received of -7.5 dBm relating to a BER of ~10^{-7} and 10^{-9} for RSF and BSF respectively.

C. FROG characterisation

The converted pulses after each type of filtering and at each line rate of 10, 20, 40 and 80 GHz are now analyzed by the FROG technique [24]. The FROG setup is comprised of a second harmonic generation (SHG) autocorrelator followed by a high resolution spectrometer. For SHG, we used a LiNbO3 crystal with an estimated interaction length of 250 µm. The SHG signal was spectrally resolved using a spectrometer with a charged coupled detector (CCD) array mounted on the output. The resulting spectrograms, which were obtained from the experimental FROG set-up, were then used to retrieve the pulse intensity and phase using the FROG phase retrieval algorithm of generalized projections (GP) [25]. For all the experimental results reported below, the standard checks on the quality of the data were made, including inspection of the FROG frequency and delay marginals, and comparing the spectrum and autocorrelation derived from the retrieved field with those directly measured. Pulse retrieval for the characterisation carried out in this work, routinely gave low retrieval errors < 0.005 [25] with a 128x128 grid (i.e. 128 spectral and temporal points). This FROG measurement scheme overcomes the limitations of other pulse measurement schemes (such as autocorrelation or a photodiode in conjunction with an oscilloscope) which must make assumptions about the pulse shape and render no phase information.

The experimental set-up remained the same as described above (in Fig. 3) however no data was applied to the intensity modulator, to obtain optimum pulse characterisation using the FROG technique. The FROG characterisation was carried out before any demultiplexing stage. Thus the analysis block comprises the SHG FROG preceded by an EDFA in order to obtain maximum sensitivity of the measurement scheme. This EDFA is designed specifically for short pulse amplification such that it does not introduce any chirp or alter the pulse shape.

The temporal profile of the pulses as measured by the FROG after red and blue shifted filtering at line rates of 10, 20, 40, and 80 GHz are displayed on Fig. 7, to examine how the preceding pattern can affect the output pulse shape and chirp of the two wavelength conversion schemes [26].

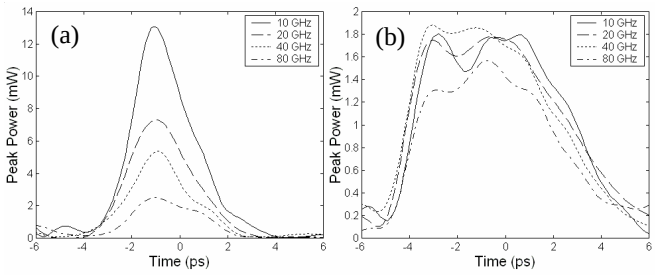

Fig. 7. Temporal pulse profiles at different line rates after (a) RSF and (b) BSF.

While these four pulses do not represent all the possible pulse variations that may be generated by patterning, it is a reasonable assumption that all the wavelength converted pulses will be the same as or lie somewhere in-between these four pulses. This is because the 80 GHz pulse represents the case when the SOA's gain is maximally depleted, the 10 GHz

pulse represents the case where the gain has sufficient time to completely recover between pulses while both 20 GHz and 40 GHz pulse represent two cases between these extremes.

RSF pulses depend on the fast gain saturation effect that occurs approximately over the pulse width of the input pulse (2 ps). Due to this fast depletion of carriers the corresponding red chirp, which occurs over the same time scale, causes the spectral components of the wavelength converted probe signal to shift to longer wavelengths. This allows only these spectral components to pass through the filter thus outputting a very short pulse as can be seen in Fig. 7(a). This short pulse width looks promising and in Ref. [18], it has been shown that RSF gives optimum performance. However, this study does not take into account the red chirp dependence on the carrier density and thus on the carrier lifetime. Consequently, if there is not complete gain recovery before the onset of the next pulse there is a smaller red shift of the probe and thus there is less power output from the filter. Therefore the major drawback of RSF is the patterning effects resulting from going to higher bit rates as is evident from the FROG traces taken with different input repetition rates and the previous BER measurements.

Furthermore one can note a double slope in the trailing edge of the RSF pulses. This is a consequence of two factors which determine the output pulse intensity; firstly the proportion of the probe transmitted through the shifted filter which is a function of the chirp imparted on probe by the SOA and secondly the level of gain saturation in the SOA. From Fig. 2 it can be seen that at the point of greatest red chirp the gain has only been depleted by half. After this point the output pulse intensity falls because the decreasing red chirp reduces filter transmission and also due to the gain saturating further. This corresponds to the initial fast fall of the trailing edge. When the gain saturates to its greatest extent and starts to recover the frequency chirp is still shifting towards the blue. At this point the filter transmission is still decreasing but the gain is recovering. This leads to the second slower fall-off in the trailing edge of the pulse. It can also be noted that the change of slope appears earlier as the bit rate increases. This can be explained because generation of red-chirped components is reduced as the bit rate increases, therefore the probe component returns earlier to its original wavelength which reduces the first part of the trailing edge of the pulses. There is the possibility that this double sloping could be removed by using an optimized filter, especially designed for this application.

In the case of BSF, illustrated in Fig. 7(b) the wavelength converted pulses are much broader, however the impact of patterning effects is far less evident as shown by the pulses being more independent of repetition rate. BSF takes advantages of intra-band effects which decrease nonlinear patterning dependence [22]. Furthermore the blue chirp is smaller than the red chirp, because the phase recovers over a longer timescale. The dominant parameters in determining the pulse shape are, as for the RSF case, the gain recovery slope and, in this BSF case, the filter shape instead of the SOA chirp profile. The leading edge of the pulse has a sharp edge due to the initial fast gain recovery and associated increase in the filter transmission. The probe wavelength returns much more slowly to its original wavelength as the gain recovers, resulting in a pulse with a long trailing edge. The structure at the top of the pulses is due to a combination between the filter transmission and ultrafast gain phenomena such as intraband effects (for example carrier heating).

Due to the processes involved in each configuration, pulses after RSF are shorter than after BSF. The large pulse width around 7 ps after BSF may limit this type of wavelength conversion. Shorter pulses could be achieved by using a filter with a narrower bandwidth, however this would significantly deteriorate the optical signal to noise (OSNR) and thus could prevent from obtaining error free performance at bit rates greater than 80 Gbit/s.

The chirp following RSF and BSF is displayed in Fig. 8 and is overlaid on a normalized intensity profile (10 GHz). As expected, the resultant chirp is approximately linear as the changes in chirp after the SOA are converted into amplitude changes by the filtering. This is particularly evident for BSF where the magnitude of chirp is 200 GHz. This would allow for the pulses to be compressed by using linear dispersion compensating techniques.

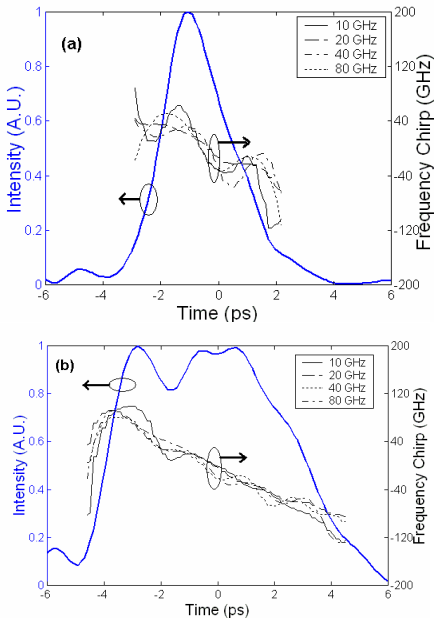

Fig. 8. Normalized intensity profile (10 GHz) and chirp profiles at different line rates in case of (a) RSF and (b) BSF.

Although we have shown 80 Gbit/s error free performance in a back-to-back measurement an analysis is required to show how well these BSF pulses will perform following further propagation in a transmission link. In particular, it is important to establish how the distorted pulse shape and its corresponding chirp could be detrimental to its overall performance. For the back-to-back measurements in (Section III-B) we believe that this pulse distortion does not add any induced penalty as the bandwidth resolution of the photodiode

placed before the error detector would lead to smoothing of the overall pulse shape. To investigate the impact of this pulse shape as it propagates in a transmission link, we simulate a simple 80 Gbit/s transmission system using Virtual Photonics Interface (VPI) software as is now discussed in Section IV.

IV. Numerical Analysis of Wavelength Converted Pulses Following Fiber Transmission

The FROG characterisation of the wavelength converted pulses has shown that while much better than the RSF case, the shape of the BSF wavelength converted pulses has a small dependence on the preceding data pattern. Thus in this section we simulate the propagation of each of these pulse shapes in a dispersion compensated fiber length of 50 km using VPI. The model used is shown in Fig. 9.

The FROG traces of the wavelength converted pulses at each channel rate from 10-80 GHz were interleaved to form an approximation to a pattern dependent PRBS signal of 2^7-1. If a pulse was directly preceded by another pulse then the 80 GHz measurement was used. If the most recent pulse was two bit slots earlier then the 40 GHz measurement was used and so on. The 10 GHz FROG trace was used to represent all pulses preceded by greater than 7 zeros as the SOA gain will have fully recovered in this time, thus the wavelength converted pulse shape will remain unchanged. This is an approximation because only four of the number of possible pulse shapes have been used. However the four pulses are a good representation of the range of possible pulses and by interleaving them in this way they appear in the correct proportion. It is a reasonable assumption that all the wavelength converted pulses will be the same as or lie somewhere in-between these four pulses, as explained previously. Noise and 300 fs of jitter were added to the system model to obtain an OSNR as measured in the experimental set-up which generates an eye diagram as shown in Fig. 6 (b). The wavelength converted eye directly following the BSF wavelength conversion scheme is shown in Fig. 10 (a) and has a quality of Q = 9.46. This eye diagram is a combination of the wavelength converted signals obtained using the wavelength converted pulse shapes measured by the FROG at 10, 20, 40 and 80 GHz. The noise seen in the one level is due largely to the patterning effects in the wavelength converter.

These pulses were initially transmitted over 50 km of single mode fiber (SMF), which has a chromatic dispersion coefficient of -16 ps/km.nm, an attenuation parameter of 0.2 dB/km, a dispersion slope of -0.086 ps/nm^2/km and a polarization mode dispersion parameter of zero. The nonlinear refractive index of the fiber was $2.6\text{x}10^{-20}$ m^2/W. Before the receiver an ideal amplifier was added to overcome fiber loss and a fixed dispersion compensating module (DCM) to overcome the transmission fiber dispersion was included. The DCM had a chromatic dispersion coefficient of 800 ps/km and a dispersion slope of 2.8 ps/nm^2.

The wavelength converted eye following propagation is shown in Fig. 10(b) and has a quality of Q = 8.13. Nonlinear effects were also found to be negligible when the pulses were launched with 1mW of average power. Although the residual dispersion (third order) leads to a small amount of eye closure, overall a large eye opening is still retained. The system's tolerance to uncompensated dispersion was evaluated by addition of a tunable dispersion compensation module before the receiver. The Q factor as a function of uncompensated dispersion is shown in Fig. 10(c). A Q factor above 6 was obtainable for dispersions from -4 ps/nm to +9 ps/nm. The slight bias to positive dispersion can be explained by the initial chirp on the pulses before transmission. This is seen in the optimal Q being obtained at +2 ps/nm of tunable dispersion and not 0 ps/nm.

While the different pulse shapes in the pattern are each affected differently by the residual dispersion, there is no large increase in noise due to patterning with propagation. Therefore this wavelength conversion scheme has the potential to be used in a real network as the structure evident on the measurements taken by the FROG technique does not lead to large distortions of the signal following transmission.

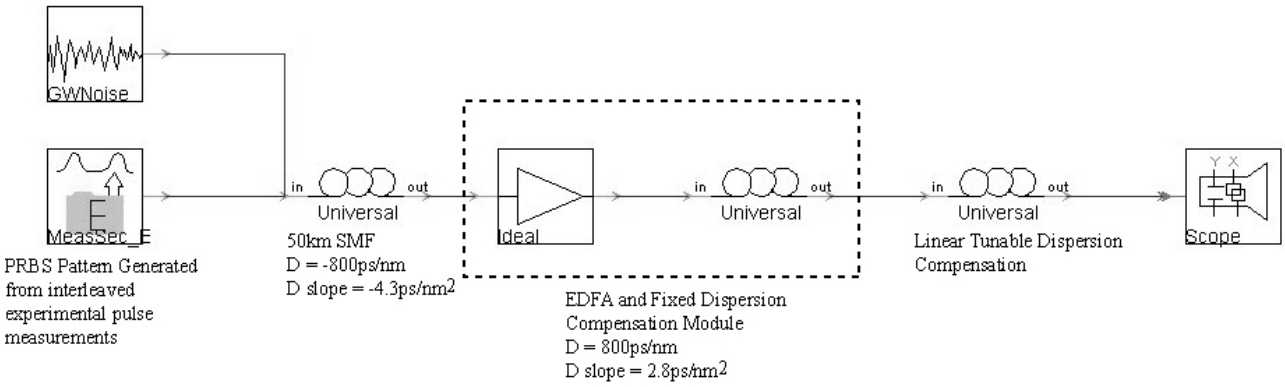

Fig. 9. The VPI model used to investigate the transmission properties of the wavelength converted pulses.

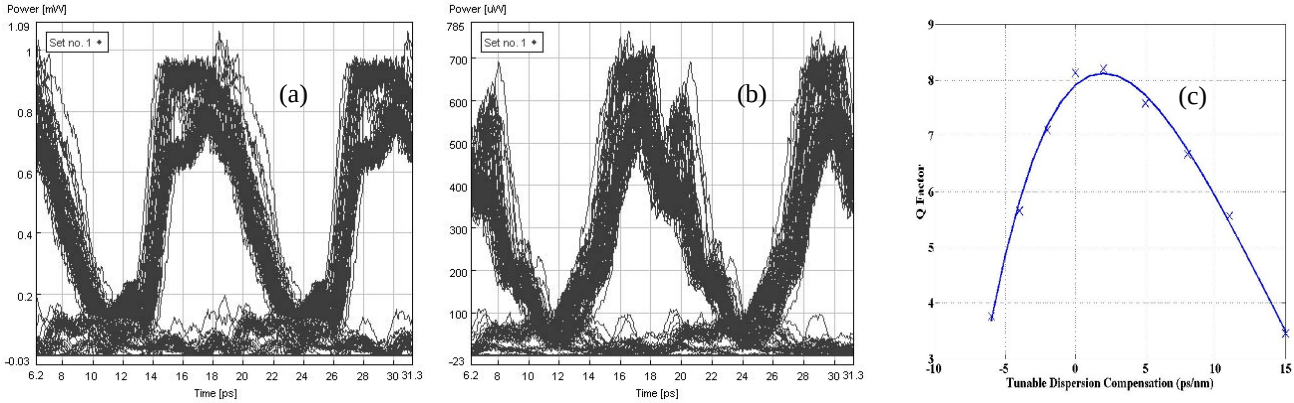

Fig.10. The 80 Gbit/s wavelength converted eye with BSF technique using FROG measurement and modelled by VPI simulation tool (a) before propagation and (b) following 50 km of dispersion compensated fiber span. The Q factor's dependence on residual dispersion (c).

V. Conclusion

In conclusion, we have presented a full analysis of an SOA-based shifted filtering wavelength conversion scheme. By placing a filter so as to suppress the CW signal of the probe following the SOA, polarity preserved wavelength conversion can be achieved. Back-to-back system performance was analyzed and it showed that placing the filter to retain the blue spectral components can give error free performance up to 80 Gbit/s. Characterisation of both the RSF and BSF was carried out using the FROG measurement technique, which showed that the pulse shape is largely dependent on the input data pattern. In the case of the RSF there is a large patterning due to the slow gain recovery time of the SOA, however for the BSF case patterning effects are reduced significantly. However the FROG results show that the BSF converted pulse shape is dependent on the input pattern, thus a simulation was carried out to determine the effect of this pattern dependent pulse shape following transmission. The simulation has shown that the eye remains open after a 50 km SMF transmission link which includes dispersion compensation.

Acknowledgment

G. Girault would like to thank O. Vaudel for helpful advice and fruitful discussions.

References

[1] S. J. B. Yoo, "Wavelength conversion technologies for WDM network applications," *J. Lightwave Technol.*, vol. 14, no 6, pp. 955-966, June 1996.

[2] M. Asghari, I. H. White, R. V. Penty, "Wavelength Conversion Using Semiconductor Optical Amplifiers," *J. Lightwave Technol.*, vol. 15, no 7, pp. 1181-1190, July 1997.

[3] N. Dutta and Q Wang (university of Connecticut, USA), "Semiconductor optical amplifiers", 312 p, Fev. 2006.

[4] C. Holtman, "Integration and applications of III-V semiconductor optical amplifiers," *European Conference on Optical Communication (ECOC'98)*, Madrid (Spain), September 1998.

[5] P. Doussière, P. Garabedian, C. Graver, D. Bonnerie, T. Fillion, E. Derouin, M. Monnot, J. G. Provost, D. Leclerc, M. Klenk, "1.55 µm Polarisation Independent Semiconductor Optical Amplifier with 25 dB Fiber to Fiber Gain," *IEEE Photon. Technol. Lett.*, vol. 6, no 2, pp. 170-172, February 1994.

[6] T. Durhuus, B. Mikkelsen, C. Joergensen, S. L. Danielsen, K. Stubkjaer, "All-optical wavelength conversion by semiconductor optical amplifiers," *IEEE J. Lightwave Technol.*, vol. 14, pp. 942-954, 1996.

[7] D. Nesset, T. Kelly, D. Marcenac, "All-Optical Wavelength Conversion Using SOA Nonlinearities," *IEEE Commun. Mag.*, pp.56-61, December 1998.

[8] P. B. Hansen, J. M. Wiesenfeld, G. Eisenstein, R. S. Tucker, G. Raybon, "Repetition-Rate Dependence of Gain Compression in InGaAsP Optical Amplifiers Using Picosecond Optical Pulses," *J. Quantum Electron.*, vol. 25, no 12, pp. 2611-2620, December 1989.

[9] Y. Ueno, S. Nakamura, J. Sasaki, T. Shimoda, A. Furukawa, T. Tamanuki, T. Sasaki, K. Tajima, "Ultrahigh-speed all-optical data regeneration and wavelength conversion for OTDM systems," *European Conference on Optical Communication (ECOC'01)*, Th.F.2.1, Amsterdam (Netherlands), September 2001.

[10] J. Leuthold, C. H. Joyner, B. Mikkelsen, G. Raybon, J. L. Pleumeekers, B. I. Miller, K. Dreyer, C. A. Burrus, "100 Gbit/s all-optical wavelength conversion with integrated SOA delayed-interference configuration," *Electron. Lett.*, vol. 36, no 13, pp. 1129-1130, June 2000.

[11] Y. Liu, M. T. Hill, E. Tangdiongga, H. de Waardt, N. Calabretta, G. D. Khoe, H. J. S. Dorren, "Wavelength conversion using nonlinear polarization rotation in a single semiconductor optical amplifier," *IEEE Photon. Technol. Lett.*, vol. 15, no 1, pp. 90- 92, January 2003.

[12] A.D. Ellis, A.E. Kelly, D. Nesset, D. Pitcher, D.G. Moodie, R. Kashyap, "Error free 100Gbit/s wavelength conversion using grating assisted cross-gain modulation in 2mm long semiconductor amplifier," *IEE Electron. Lett.*, vol. 34, pp. 1958-1959, 1998.

[13] Y. Liu, E. Tangdiongga, Z. Li, H. de Waardt, A. M. J. Koonen, G. D. Khoe, H. J. S. Dorren, X. Shu, I. Bennion, "Error-free 320 Gb/s SOA-based Wavelength Conversion using Optical Filtering", *OFC*, Postdeadline paper N° PDP28, USA, 2005.

[14] P. Cho, D. Mahgerefteh, J. Goldhar, G. L. Burdge, « RZ Wavelength Conversions with Reduced Power Penalty Using a Semiconductor-Optical-Amplifier/Fiber-Grating Hybrid Device », *IEEE Photon. Technol. Lett.*, Vol. 10, N° 1, pp. 66-68, January 1998.

[15] P. Mamyshev, "All-optical data regeneration based on self-phase modulation effects," *Proc. European Conference on Optical Communications (ECOC'98)*, Madrid (Spain), pp. 475-476, 1998.

[16] B-E. Olsson, P. Ohlen, L. Rau, D. Blumenthal, "A simple and Robust 40-Gb/s Wavelength Converter Using Fiber Cross-Phase Modulation and Optical Filtering", *Photon. Technol. Lett.*, vol. 12, no 7, July 2000.

[17] M. L. Nielsen, "Polarity-preserving SOA-based wavelength conversion at 40 Gbit/s using bandpass filter," *Electron. Lett.*, vol. 39, no 18, September 2003.

[18] S. Fu, J. Dong, P. Shum, L. Zhang, X. Zhang, and D. Huang, "Experimental demonstration of both inverted and non-inverted wavelength conversion based on transient cross phase modulation of SOA," *Optics Express*, vol. 14, no. 17, pp. 7587-7593, 2006.

[19] H. Chayet, S.B. Ezra, N. Shachar, S. Tzadok, S. Tsadka, J. Leuthold. "Regenerative all-optical wavelength converter based on semiconductor

optical amplifier and sharp frequency response filter";Optical Fiber Communication Conference, OFC, vol.2., Feb. 2004.
[20] J. M. Vazquez, Z. Li, Y. Liu, E. Tangdiongga, S. Zhang, D. Lenstra, G. D. Khoe, H. J. S. Dorren, "Optimiztion of Optical Band-Pass Filters for All-Optical Wavelength Conversion Using Genetic Algorithms," *IEEE J. Quentum Electron.*, vol. 43, no 1, January 2007.
[21] Y. Liu, E. Tangdiongga, Z. Li, S. Zhang, H. de Waardt, G. D. Khoe, H. J. S. Dorren, "Error-free all-optical wavelength conversions at 160 Gb/s using a semiconductor optical amplifier and an optical bandpass filter," *J. Lightwave Technol.*, vol. 24, no 1, pp. 230-235, January 2006.
[22] M. L. Nielsen, J. Mork, R. Suzuki, J. Sakaguchi, Y. Ueno, "Experimental and theoretical investigation of the impact of ultra-fast carrier dynamics on high-speed SOA-based all-optical switches," *Opt. Express.*, vol. 14, no 1, pp. 331-347, 2006.
[23] L. Bramerie, A. Clarke, G. Girault, S. Lobo, M. Gay, C. Guignard, V. Roncin, B. Kennedy, P. Maguire, S. Fève, B. Clouet, F. Ginovart, L. P. Barry, J.C. Simon, "Investigation of SOA-based wavelength conversion at 80 Gb/s using bandpass filtering," CLEO/QELS, oral session CMT7, Long Beach, California, USA, May 2006.
[24] R. Trebino, K. W. Long, D. N. Fittinghoff, J. N. Sweetser, M. A. Krumbugel, B. A. Richman, "Measuring ultrashort laser pulses in the time-frequency domain using frequency resolved optical gating," *Rev. Sci. Instrum.*, vol. 68, pp. 3277-3295, 1997.
[25] D.J. Kane, "Real-time measurement of ultrashort laser pulses using principal component generalized projections", *IEEE J. of Selected Topics in Quantum Electronics*, vol. 4, no 2, pp. 278-84, 1998.
[26] A. Clarke, G. Girault, P. Anandarajah, C. Guignard, L. Bramerie, L. Barry, J-C. Simon and J. Harvey, "FROG Characterisation of SOA-based Wavelength Conversion using XPM in Conjunction with Shifted Filtering up to Line Rates of 80 GHz", *LEOS*, oral MP 2, Montreal, Canada, November 2006.

G. Girault received the Engineer degree in optronics in 2003, the Master degree (D.E.A.) in sciences and techniques of communication the same year, and the PhD degree in optical communications and physics in 2007 from CNRS unity FOTON-ENSSAT, University of Rennes I, France. The main topic of her research is the study of semiconductor optical amplifier based optical functions for all-optical regeneration and optical system transmission. She is now research engineer on PERSYST platform, independent public research and test facility offering a testbed for 40Gb/s and 10Gb/s optical telecommunications systems open to private companies and university teams.

A. M. Clarke graduated from Dublin City University (DCU) with a B. Eng in Electronic Engineering in October 2002 and with a PhD degree in Optical Communications in 2007. The main topic of her research is All-Optical Processing techniques for High-Speed Networks, with a particular interest in Semiconductor Optical Amplifiers (SOAs).

C. Guignard received the Eng. degree in optronics in 2001, the Masters degree in Sciences and Techniques of Communications (D.E.A.) in optics communications, also in 2001, and the Ph.D. degree in optronics in 2005 from the ENSSAT, University of Rennes I, France. From April 2005 to September 2006, she was a Postdoctoral Researcher in the Radio and Optical Communications Laboratory, Research Institute for Networks and Communications Engineering (RINCE), Dublin City University, Dublin, Ireland. Her principal research interests included optical pulse generation with semiconductor laser, optical feedback and optical injection.

P. Anandarajah received the B. Eng (Electronic engineering) degree from Univrsity of Nigeria, Nsukka (UNN) in 1992. In 1993 he joined the Nigerian College of Aviation technology (NCAT), where he worked as an instructor / Maintenance Engineer on the Aeronautical Telecommunications department until 1997. On completion of his M. Eng (1998) in Electronic Systems at Dublin City University (DCU) he joined the Optical Communications Group, also at DCU, where he obtained his PhD degree (2003). The research work for his thesis was based on the generation and optimization of Pico-second optical pulses to be utilized in hybrid WDM / OTDM systems. Since September 2003, he has been working as a postdoctoral researcher with the Radio and Optical Communications Laboratory which is part of the Research Institute for Networks and Communications Engineering (RINCE).

D. Reid received his BTech (Optoelectronics) in 2000 then went on to complete an MSc (Physics) in 2002 at the University of Auckland. He is currently working towards completion of a PhD in Physics specializing in optical communications. His main area of research is in the development of techniques for the characterization of Ultra-Short optical pulses. In particular, the use of Frequency Resolved Optical Gating (FROG) and other linear spectrographic techniques for real time measurement of optical communication pulses.

L. Bramerie received the opto-electronic engineering degree from ENSSAT, University of Rennes I, France, in 1999 and the PhD degree in 2004. He worked, France as technical expert on ultra-long haul 40 Gb/s DWDM systems for 2 years in Corvis Algety in Lannion. In 2003 he has joined CNRS FOTON-ENSSAT where is now research engineer on PERSYST platform, independent public research and test facility offering a testbed for 40Gb/s and 10Gb/s optical telecommunications systems open to private companies and university teams.

L. P. Barry received his BE (Electronic Engineering) and MEngSc (Optical Communications) degrees from University College Dublin in 1991 and 1993 respectively. From February 1993 until January 1996 he was employed as a research Engineer in the Optical Systems Department of France Telecom's Research Laboratories (CNET) in Lannion, France. During this period his research involved the use of ultra short optical pulses in high capacity optical networks, and as a result of this work he obtained his PhD Degree from the University of Rennes in France. In February 1996 he joined the Applied Optics Centre in Auckland University, New Zealand, as a Research Fellow. His work in New Zealand was mainly concerned optical pulse generation and measurement, and the use of optical nonlinearities for high-speed all-optical switching in fiber networks. In March 1998 he took up a lecturing position in the School of Electronic Engineering at Dublin City University, where he has since developed the Optical Communications Research Laboratory.

J-C Simon received the Doctorat d'Etat degree from Université de Nice in 1983. From 1975 to 1998 he was with CNET, the research centre of the French PTT (now France Telecom R&D) as a researcher in the field of semiconductor optical amplifiers and non-linear optical signal processing, principally 2R and 3R all-optical regeneration. In 1999 he moved to ENSSAT, an engineering school, as a full professor in optoelectronics. He is director of Laboratoire d'Optronique, a research lab. associated with CNRS and Université de Rennes I. He has authored or co-authored approximately 160 journal and conference papers including some 25 invited presentations, 10 patents, and 3 book chapters. He has contributed to European research programs (RACE 1027, ESPRIT 3 MOSAIC and ACTS KEOPS). He is recipient of the Fabry-de Grammont award from the French Optical Society.

J. D. Harvey (M76) received the B.Sc. and M.Sc. degrees from the University of Auckland, Auckland, New Zealand, in 1965 and 1967, respectively, and the Ph.D. degree from the University of Surrey, U.K., for work in theoretical nuclear physics. Since 1970, he has worked at the University of Auckland where he now holds a Chair in the Physics Department. In recent years, his research has been concentrated in the areas of nonlinear fiber optics, ultrafast processes, and mode-locked lasers. Prof. Harvey is a fellow of the New Zealand Institute of Physics and is a member of the Optical Society of America and the Australian Optical Society.

FROG characterisation of a Turbo-Switch wavelength converter

X. Yang (1), A.M. Clarke (2), R. Maher (2), R.P. Webb(1), R.J. Manning (1), L.P. Barry (2)
1: Photonic Systems Group, Tyndall National Institute & Department of Physics, University College Cork, Ireland, x.yang@ucc.ie
2: RINCE, School of Electronic Eng., Dublin City University, Ireland, liam.barry@dcu.ie

Abstract *The FROG technique is used to characterise output pulses from a Turbo-Switch wavelength converter in different configurations. Results show low chip on the output pulses, a vital requirement in high-speed optical transmission systems.*

Introduction

Wavelength converters will be important components in future optical networks, as they will be required to avoid wavelength contention at nodes and render wavelength division multiplexed (WDM) systems more flexible [1]. Consequently, there is much interest in all-optical approaches to wavelength conversion for high bit rates. In this paper we characterise the all-optical Turbo-Switch wavelength converter, which has already shown error free performance up to 170Gb/s [2]. In particular the pulse shape and chirp of the wavelength converted signal are measured using the frequency-resolved optical gating (FROG) measurement scheme. We employ the FROG technique to optimise the Turbo-Switch configuration, including the position of the PM fibre of the interferometer, to obtain the best intensity and chirp profile of the output pulses. The optimised pulse has very low chirp, which is important for propagation through subsequent fibre transmission links

Experimental Set-up

The Turbo-Switch provides a much faster gain recovery in comparison to that of a single semiconductor optical amplifier (SOA), which helps to mitigate the nonlinear patterning effects associated with wavelength conversion schemes which exploit cross-phase modulation in one SOA alone [2]. An asymmetric Mach-Zehnder interferometer (AMZI) acts as a shaping filter for the wavelength converted pulses, and optimisation of the AMZI can lead to improvement of the extinction ratio and cancellation of the chirp of such pulses.

The wavelength conversion experimental set-up is shown in Fig. 1. The pump signal was generated by a 10.65 GHz tuneable mode-locked laser (TMLL), giving 3ps pulse trains at 1540nm. A modulator and passive multiplexer (up to x16) were used to give PRBS data rates ranging between 10.65Gb/s and 170.4Gb/s, with pattern length 2^7-1. The continuous wave (CW) probe signal was set at 1558nm. The two (Kamelian) SOAs both had 1490nm gain peaks at operating bias currents of 400mA. The filter employed was 4.5nm wide and blocked the pump pulses. A length of PM fibre, having a relative time-of-flight

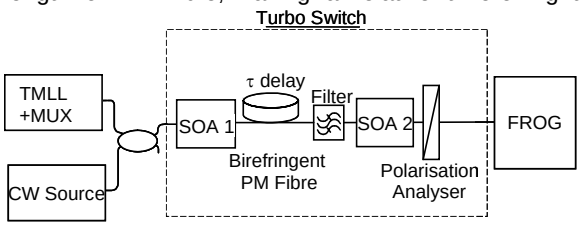

Fig. 1 Experimental Set-up

delay between fast and slow axes of τ~3ps, and a polariser, were used to form the AMZI. The PM fibre was placed either in the position shown in Fig 1, or after SOA2, in order to compare the wavelength conversion performance.

FROG Characterisation Results

The FROG scheme measures the temporal shape and phase profile of a pulse. The characteristics of the wavelength-converted pulse at data rates 10 - 170Gb/s and for different Turbo-Switch configurations were recorded using second harmonic generation FROG. The error for all FROG measurements was less than 10^{-5} for a 128x128 grid [3].

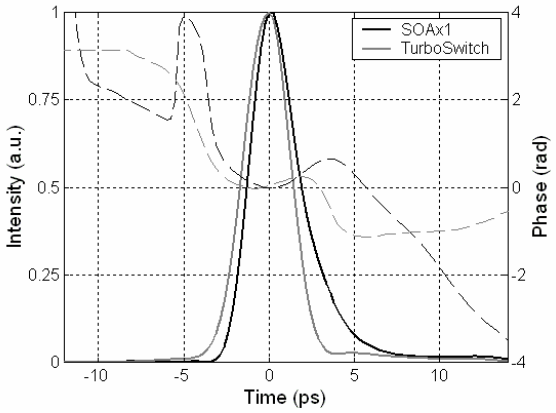

Fig.2 Intensity (solid) and phase (dashed) of the wavelength converted pulses, showing comparison between use of a single SOA and a Turbo-Switch.

Here we investigate the effects of the Turbo-Switch on the pulse shape and phase. Initially the wavelength converted pulses were measured directly

after just one SOA and AMZI, and then measured using the complete Turbo-Switch and AMZI, and the results are shown in Fig. 2. Note that although there are large phase variations in the wings of the pulses, they occur when the AMZI output is close to a null and the pulse energy is negligible. Whilst the AMZI primarily dictates the pulse width, this FROG characterisation shows that the improved phase cancellation in the interferometer due to the very high speed response of the Turbo-Switch leads to a pulse width reduction of ~0.5ps. It also results in a very small chirp across the pulse, and gives nearly transform limited pulses (time bandwidth product = 0.59).

In addition, changing the placement of the PM fibre of the AMZI results in a further optimisation of the pulse shape and chirp as displayed in Fig. 3.

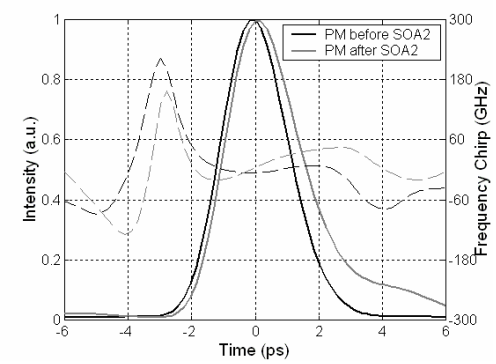

Fig. 3 Intensity (solid) and chirp (dashed) of wavelength converted pulses, showing comparison of configurations with PM fibre placed before and after SOA2.

If the PM fibre is placed in between the two SOAs of the Turbo-Switch as shown in Fig. 1, a more symmetric pulse and a near zero level of chirp can be achieved in comparison to placing the PM fibre after the second SOA.

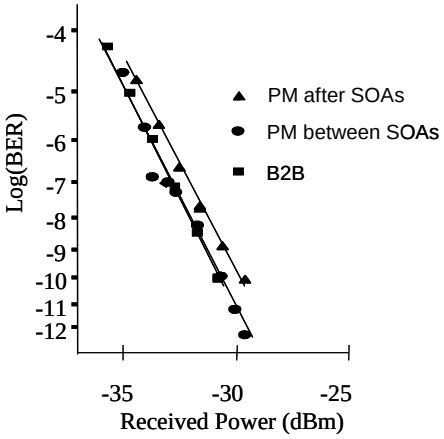

Fig.4. BER measurements of wavelength-converted output at 85Gbit/s, compared to back-to-back (B2B), when PM fibre is placed before and after SOA2.

This improvement in pulse quality is reflected in the corresponding bit error rates for the two configurations, as shown in Fig 4 for 85Gbit/s data, which indicate a 1dB penalty if the PM fibre is placed after the second SOA.

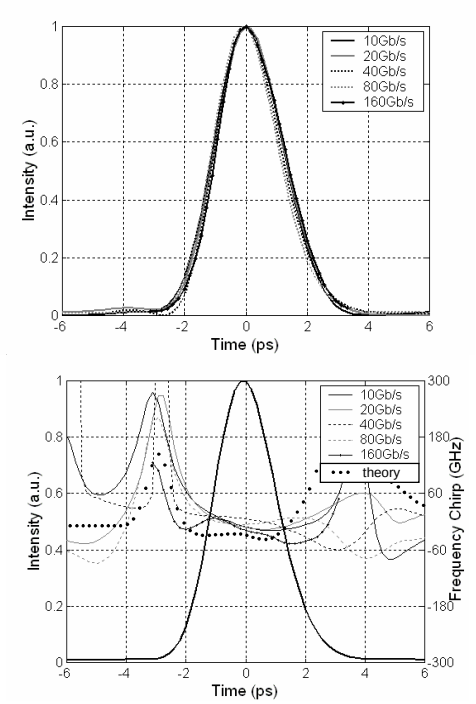

Fig. 5 (a) Intensity and (b) frequency chirp of wavelength converted pulses for input data rates 10 - 170Gb/s.

Finally we characterised the pulse shape and chirp as a function of data rate. Fig. 5 (a) shows that the pulse shape does not change for input data signal rates between 10-170Gb/s. Fig. 5 (b) shows the chirp for the same range of input data rates together with a theoretical curve, illustrating that the chirp across the wavelength converted pulses varies by less than 60GHz for all data rates up to 160 Gb/s. The pulses would therefore be suitable for propagation through fibre transmission links.

Conclusions

We have shown that wavelength converted pulses from the Turbo-Switch have very low chirp and are nearly transform limited. Placement of the PM fibre between SOAs is advantageous.

Acknowledgement

This work was supported by the Science Foundation Ireland under grant Nos. 03/IN.1/1340, 06/IN/I969 and 02/IN.1/142.

References

1 S.J.B. Yoo, J. Lightwave Technol., vol. 14 (1996), pp. 955-966.
2 R.J. Manning et al, OFC 2006, paper OWS8.
3 R. Trebino et al, Rev. Sci. Instrum., vol. 68 (1997), pp. 3277-3295